Atoms-In-a-Molecule-In-a High Intensity LASER: Dynamical Molecular Electron Densities

A thesis
submitted by

Nitin Kumar Singh

in partial fulfillment of
the requirements for the degree of

Doctor of Philosophy

Department of Chemical Sciences
Indian Institute of Science Education and Research, Mohali
Knowledge City, Sector-81, S.A.S Nagar, Manauli PO, Mohali,
Punjab-140306, India
February, 2024

Certificate of Examination

The work presented in this thesis has been carried out by me with **Dr. P. Balanarayan** at Indian Institute of Science Education and Research Mohali. This work has not been submitted in part or in full for a degree, a diploma, or a fellowship to any other university or institute. Whenever contributions of others are involved, every effort is made to indicate this clearly, with due acknowledgement of colloborative research and discussions. This thesis is a bona fide record of original work done by me and all sources listed within have been in the bibliography.

Nitin Kumar Singh
(Candidate)

In my capacity as the supervisor of the candidate's thesis work, I certify that the above statements by the candidate are true to the best of my knowledge.

Dr. P. Balanarayan
(Supervisor)

Acknowledgement

This thesis has resulted from efforts and support put in by many people, directly or indirectly. The very first and foremost person, my thesis supervisor, Dr. P. Balanarayan, is thankfully acknowledged for providing mentorship and guidance throughout my Ph.D. tenure. His support, ideas, and helps in the research work abled me to fetch INSPIRE fellowship and carry out the Ph. D works comfortably. I am thankful to my doctoral committee members - Dr. K. R. Shamasundar and Dr. Sugumar Venkatramani for timely checks on the research progress via yearly reports and presentations. The role of our research lab, the Quantum Mechanics group at IISER M has been immense, in sharing knowledge from the informal in-person discussion, group presentations, poster sessions and in conferences. Thanks! QM group! for providing a such a cordial space to make this Ph. D journey a memorable experience. My labmates, batchmates, seniors, juniors-turned friends (Dr. Prashant, Dr. Naveen, Dr. Mishu, Dr. Rajat, Prateek, Alkit, Taseng, Aman, Kirti, and Harwinder) are duly acknowledged for making the environment inside and outside the lab, a lively one, where we enjoyed each others companionship and camaraderie.

The in-house code ABELDYN, provided by Dr. Prashant Raj and Dr. P. Balanarayan, was essential to the work presented in this thesis because I used the output files obtained from the code further to calculate properties in the context of the present dissertation—my sincere thanks to them. Dr. Mishu Paul is thankfully acknowledged to have collaborated on the ABELDYNPROP project, where she worked on the momentum space properties. I thank Dr. Naveen Kumar for letting me help on the project - linearizing water in the presence of a circularly polarized laser. We have also collaborated with Professor S. S. V. Ramasastry, Professor Sanjay Singh, IISER Mohali, and Professor Naresh Patwari, IIT Bombay, on computational projects concerning the calculation of reaction mechanisms and the construction of potential energy curves of weakly binding complexes. The research works with them are acknowledged with sincerity and respect, imparting new skills and knowledge to me.

I am indebted to the Department of Science and Technology for providing financial help through the INSPIRE fellowship. I thank the former and present, Directors, Deans of Academics, Heads of the Department of Chemical Sciences, Computing Facility, and its committee members for providing the infrastructure, computing facility, and smooth documentation process throughout the Ph. D tenure.

A final note of thanks to my beloved family members, Maa, Papa, Didi, Bhaiya, and Bhabhi. They have always been supporting and patiently waiting to see me pass through this phase of life. I pay my respect to them for the care and concern for my physical and mental well being. My sister and brothers have always been there to hear out my experience in good and troubled times. They have been the guiding light in my choices and paths. I hope to make them proud through my endeavours and efforts in this journey.

Nitin Kumar Singh

List of Figures

List of Tables

Contents

Chapter 1

Dynamical Molecular Electron Densities in LASER Fields

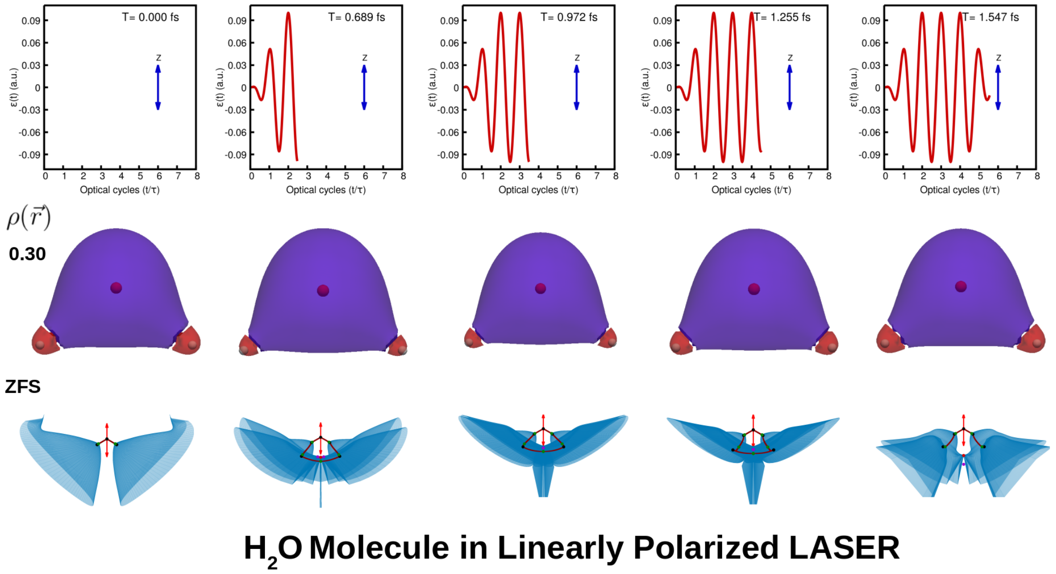

---

[1] Graphical abstract shows the atoms-in-molecule picture for the electron densities of water molecule in a linear polarized laser at different time steps of a laser pulse in the second row panel. The blue and red regions depict the electron density isosurfaces of the molecular subspace occupied by Oxygen and Hydrogen atomic basins respectively.The third-row panel depicts the time-varying zero-flux surfaces. The concepts to understand and evaluate these quantities would be explained in this introductory chapter.

Abstract

Current technologies in optics have grown to an extent where experiments are conducted on molecules in high intensity ($\sim 10^{14} - 10^{16}$ W/cm^2) and high-frequency LASER pulses in the timescales of femtoseconds (10^{-15} s) to attoseconds (10^{-18} s). These are the timescales where electronic motion happens, and the electric field intensities are much more significant than an atom's internal field strength ($\sim 10^3$ W/cm^2). Thus, specific frequency-tuned LASERs were used to gauge and control the dynamics of atoms and electrons in molecules. In the same context, time-resolved X-ray diffraction laser pulses have been studied for time-evolving electronic charge distributions. Using theoretical methods, obtaining the time-dependent wave function of atoms and molecules in external LASER fields became possible through the parallel development of theoretical methodologies. Therefore, this has enabled researchers to evaluate molecular densities and retrieve the electronic properties of atoms and molecules in the presence of external time-evolving fields. This thesis attempts to study the dynamics of molecular electron densities through their time-varying topographies, bond paths, zero-flux surfaces, and Atoms-In-a-Molecule properties in a LASER. Thus, Chapter 1 introduces the basics of the electronic structure of atoms and molecules, the standard solutions of time-independent and time-dependent Schrödinger equations to obtain the wave functions essential to evaluate electron densities and properties. The topological tools, such as gradient paths, critical points, bond paths, zero-flux surfaces, and Bader's quantum theory of Atoms-In-Molecules, are briefly explained, which will help understand features in the time-evolving electron density distributions. The final section of this chapter describes the plan for the thesis.

1.1 Preamble

Electron densities (ED) of molecular systems are routinely measured using X-ray scattering experiments to determine their equilibrium geometrical structure.[1] Using theoretical methods, it is also possible to compute ED using the electronic wavefunctions obtained from the solutions of the Schrödinger equation. The proof of the first Hohenberg-Kohn Theorem[2] in Density Functional Theory shows that the electron density of a system uniquely defines the Hamiltonian operator and all its properties. In turn, its unique potential is a functional of electron density. So, conceptually, any changes in the external potential of a system would result in the deformations in the newly formed electron densities and their properties. With the recent surge in state-of-the-art optics, it is now possible to alter the potentials of molecules and their properties using external electric fields, especially high-intensity, high-frequency light sources such as a **LASER** (Light Amplification by Stimulated Emission Radiation, working principle shown in Fig. [1.1]).

Nowadays, pulsed LASER fields can attain timescales ranging from a few femtoseconds (10^{-15} s) to attoseconds (10^{-18} s) in experiments. With X-rays, technological advancements in optics were able to achieve intense ultrashort laser pulses from X-ray sources called as X-ray free-electron lasers (XFELs).[3–5] Using XFEL sources, experiments with femtosecond time resolutions have been routinely performed. However, in recent past years, X-ray laser pulses with attosecond resolutions have also been generated, and experiments have been performed on molecules.[6, 7] Exceptional temporal resolution has been achieved using these ultrashort X-ray pulses.[8] An emerging method called time-resolved X-ray diffraction (TRXD) within a pump-probe configuration enables experimentalists to take snapshots of time-evolving electronic charge distribution in matter with spatiotemporal resolution on molecular and

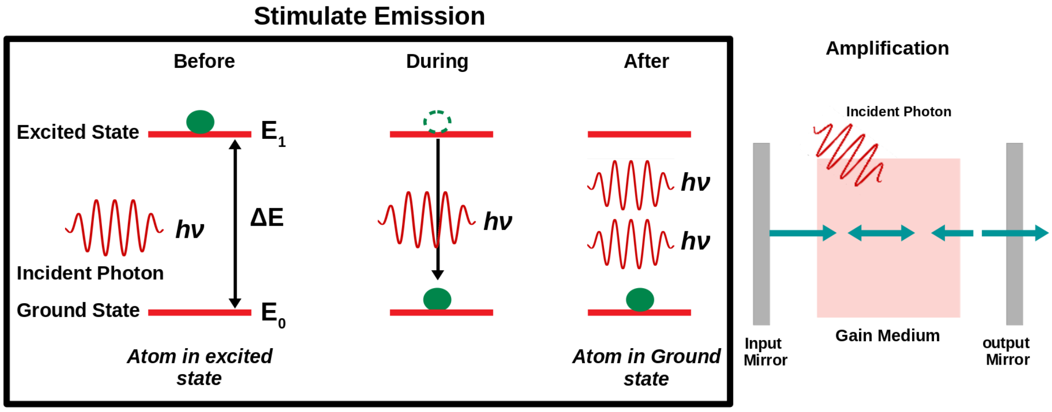

Figure 1.1: The picture shows the two princliples that are used to make LASERs. 1. Stimulated emission and 2. Amplification. The stimulate emission is achieved by the incident photons on the excited state which emits another photon while relaxing to the groud state. This processes is repeated to gain amplification of the emitted radiation.

electronic timescales.[9] Theoretical and computational work carried out by Santra and coworkers [10, 11] showed an electronic movie of ultrafast charge migration by putting the timed snapshots as a function of pump-probe delay time. All these have led to the development of a new kind of chemistry field called *femtosecond*,[12, 13] and *attosecond* chemistry[14, 15] which allowed gauging the timescales at which nuclear and electronic motions occur. Experiments at these timescales give insights into and gains control over nuclear and electronic dynamics in atoms, molecules, and reactions.[16–19] The different molecular processes occuring at various timescales are represented in Fig. [1.2].

Along with the experiments, the development of relevant theoretical models for solving time-dependent Schrödinger equation to study electronic dynamics have also been carried out. With the knowledge of LASER-dressed time-evolving electronic wavefunctions, the question we pose here is, "**How do dynamical electron densities behave in LASER fields?**" This thesis is an attempt to answer this questions.

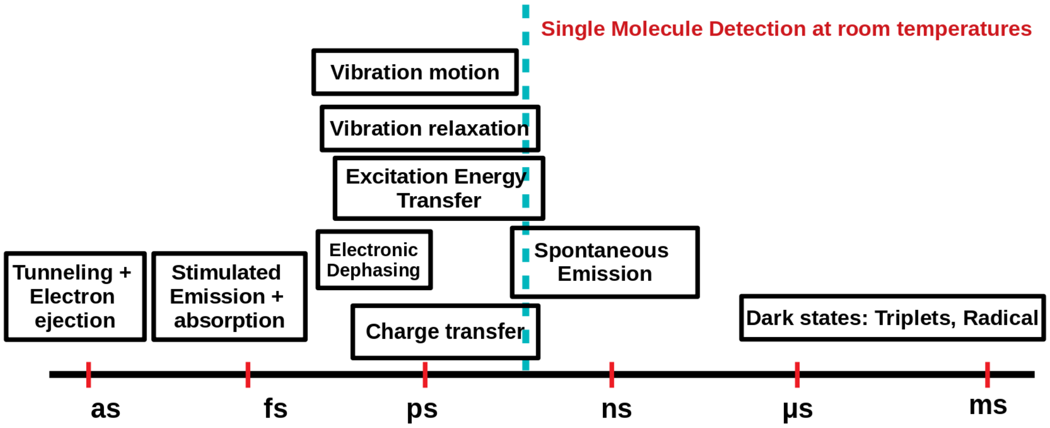

Figure 1.2: The timescales of various molecular processes are given. The single molecule detection at room temperature has a time resolution of few 100 ns. Femtosecond and attosecond timescales are the regimes of ultrafast timescales in molecular processes.[12–15]

The pioneering investigations from Bader and coworkers[20] studied the topology of electron densities obtained from theoretical calculations and X-ray scattering experiments on crystals for various simple and complex molecules. Different properties related to the chemistry of molecules, such as bond order,[20] bond polarity,[2] and bond ellipticity,[21] were formulated using the analysis from the topology of electron densities for small molecules. Employing the topological analysis of electron densities, they investigated the C_{2v} dissociative pathway for the ground state of water molecule.[22] Popelier and coworkers have used bond critical points analysis to study DNA and drug molecules, an extensively researched field by them.[129–131] They introduced a concept called *Quantum Molecular Similarity* using the value of electron density at bond critical point and bond lengths.[23–25] Using the gradients of electron densities, Eberhart and coworkers[29] conceptualized *gradient bundle analysis*. The gradient bundle analysis was applied to study the influence of interatomic boundary surfaces of electron density on chemical reactivity. Therefore, these examples reveal a wealth of information on structural parameters and reactivity patterns of atoms and molecules obtained from ED, its gradients, and topology.

Applying the concepts of topological analysis and information from the gradients of ED in molecules, Bader and coworkers' research led to the birth and development of *Quantum Theory of Atoms-In-Molecules* (QTAIM).[20] The theory states that atoms occupy mutually exhaustive subspaces in the whole molecular space. These subspaces are separated from one another by virtual surface boundaries. QTAIM's consequence was that the entire property of molecules would be a sum of all the individual atomic properties. For example, the total charge of a free-field ground state water molecule would be the sum of charges (called *Bader charges*) contained in each of the subspaces/basins (*called Bader atoms/volumes*). Identifying these atomic subregions in molecular space of electron density is a non-trivial problem. Hence, Bader,[20] Popelier,[26] Hennkelman,[27] Rodriguez,[28] and groups attempted to develop fast and robust algorithms to compute these properties in a computationally cost-efficient fashion. The foremost algorithm proposed by Bader and group[20] was based on identifying the interatomic surfaces (IAS) making it computationally expensive, while Popelier proposed serveral methods to integrate atoms-in-molecules without explicit representation of IAS.[26] Henkelman and coworkers[27] developed an fast and robust algorithm based on *steepest ascent search* in the electron density data. Rodriguez *et al.*[28] proposed an efficient grid-based scheme to evalute the QTAIM properties.

Using these concepts, Bader *et al.*[30] studied the transferability and additivity of methyl and methylene groups in various hydrocarbons. The concepts of QTAIM have been applied to reveal atom-atom interactions in covalent and non-covalent interactions in molecules, molecular clusters,[31, 32] small molecular crystals,[33] proteins,[34] DNA base pairing and stacking.[35] The primary goal of implementing QTAIM in literature has therefore been to explore molecular electron densities (MED) to study the nature of bonding in molecular systems.

In principle, the atomic and molecular electron densities (MED), their topology, and concepts of QTAIM could be applied and computed from electron densities obtained from either X-ray scattering experiments or theoretical methods like Hartree-Fock method, Møller-Plesset perturbation theory, (wavefunction based) or density functional theory (density based). The accuracy of calculated ED properties depends on the level of theory employed. Researchers have used these theoretical methods in literature to evaluate MED and properties mostly in **free-field scenarios**. However, In 1992, Mezey *et al.*[36] carried out studies of electron densities in static **external electric fields** (EEF) for homonuclear, heteronuclear, and triatomic molecules. Two directions of static EEF, one parallel and the other perpendicular to the molecular axis, were chosen. The results showed that low and high electron density regions have opposite behaviors with increasing electric field strengths. The electron density isocontours near the regions of nuclei contract by the applied field, while in the regions far from nuclei, the electron density contours spread out away.

The study of chemistry in EEF has emerged as a topic of relevance in the current century since it has enabled researchers to gauge and gain control of the electronic/nuclear dynamics of atoms and molecules in reactions, materials, or biological systems. It has involved an interplay between theoretical and experimental aspects. The *proof-of-concept* of this was shown by Shaik and coworkers,[37] who also extensively have studied atoms, molecules and reactions in intense EEF. They studied the Diels-Alder reaction, which involves simultaneous C-C bond breaking and formation, got it catalyzed in *oriented external electric fields*, thus achieving selectivity.[37] Another example where Shaik *et al.*[38] showed control in selectivity of Enzymatic-Like Bond Activations. EEF has been applied to investigate response of electron momentum densities (EMD) of small molecules.[39] The study revealed the EMD maxima rotating with a increasing electric field strengths. The intensity of the EEF can lead to changes in several fundamental physical and physicochemical phenomena, which are also experimentally detected. Stark effect in atoms and molecules, where splitting of energy levels is observed in the presence of intense EEF.[40] Atoms and molecules in EEF may experience ionization and activation of electrons,[41] proton transfers,[42] changes in geometrical parameters,[43] affecting the interatomic bonds and making chemical interactions feasible.[44]

In **strong field chemistry and physics**, the high-frequency and high-intensity LASER fields and their interaction with matter have led to several phenomena, such as metastable states, slow ionization rates, and quasi-bound states, which have been theoretically predicted and experimentally realized.[64] The works of Gavrila, Moiseyev and coworkers[46–49] showed that the atoms and anions could achieve stable states in high frequency regimes of LASERs. Here, the electron overcomes the binding potential and follows the to and fro motion about the classical turning points of the LASER. The results revealed the dichotomous states of electron in atoms and the electron density of atoms shows resemblance to that of a homonuclear diatomic molecule. Initially by Kramers in 1956,[50] and later Henneberger in 1968,[51] theorectically predicted the phenomenon in the case of high intensity and high frequency LASER fields. This concept got experimentally realized for gases of noble atoms such as neon, helium and argon.[52–55]

The investigations concerning the **time evolution of electron densities** are not rich in the literature. However, few reports have studied the QTAIM and topological analysis using the electron densities in quantum molecular dynamics. Rodrigo et al. [56] studied charge transfer using the topology of electron density in two types of systems: (1) reactive collision of $H^+ + H_2$ under different initial conditions and (2) photodissociation of LiF for either diabatic or adiabatic processes. Using the simple model systems proposed by

Shin and Meitu,[57] coupled nuclear-electron dynamics was performed with time-dependence of electron densities.[58–60] Using the geometries obtained from the trajectories of molecular dynamics, the time-dependent topological and atoms-in-molecule analysis of electron densities was performed to study allyl radicals and relocalization process in benzene by Chevreau.[61, 62] Another report by Chevreau and coworkers[63] studied electron relocalization process in S_2H_2 and $S_2H_2^-$ using time-dependent topological analysis of electron density and showed a possible hydrogen bonding motion in biological systems.

The present thesis attempts to study **dynamics of molecular electron densities in LASER-dressed fields, their dynamical topographies, and Atoms-in-A-Molecule-In-A-LASER**. For this study, a code-named *Ab-initio Electronic Dynamics Properties* (ABELDYNPROP) is developed to evaluate time-evolving MED and their properties. The ABELDYNPROP code is discussed in Chapter 2. The following chapters discusses application of ABELDYNPROP code on small molecules in linearly polarized lasers and their respective property analysis. Here, In Chapter 1, we shall discuss all the basics, concepts, equations, termonologies, and prerequisites required to understand the subsequent chapters better.

We start the next section 1.2 explaining the TDSE equations, and the role of potential in the Hamiltonain. The general solutions of TDSE are different for time independent and time-varying potentials. This is further elaborated in subsequent subsection using the Schrödinger, Heisenberg and Interaction Pictures. The perturbation in the potential of Hamiltonian of TDSE is solved showing the first and second order corrections to the wavefunctions. However, since, our problem deals with strong laser fields, therefore, this perturbative approach is not valid. Hence, a short description of strong field approximation is provided. Thereafter, the TDSE solutions for light-matter interactions, and its gauge transformations are discussed in related subsections are discussed. The numerical solutions to solve TDSE are also provided along with the RT-TDHF algorithm developed used to generate the wavefunctions.

The information on electronic wavefunctions or the molecular orbitals of a quantum system is the first and foremost fundamental quantity required to obtain any information and to evaluate molecular electron densities (our interest in this thesis). So, section 1.4 provides details of the methods used to solve the time-independent and time-dependent Schrödinger equations (TISE/TDSE). Section 1.4 starts with giving the definition and need to understand the **Ab-Initio Electronic Structure of Atoms and Molecules**. It briefs the history and the approximations used in solutions of the theoretical methods used in this section. An introduction to the molecular problem is in the following subsection 1.4.1. This subsection describes the basic construct of the molecular Hamiltonian for a system of N electrons and M nuclei. The following subsection 1.4.2 explains the **Born-Oppenheimer Approximation**, which is fundamental to the solutions obtained in later subsections. The approximation describes the separation of molecular Hamiltonian into nuclear and electronic parts, as the electronic motion is much faster than the nuclear motion. Therefore, the wave functions obtained from solving the TISE or TDSE would directly depend on the electronic coordinates and parametric dependence on the nuclear coordinates. This subsection is followed by subsection 1.4.3, giving details regarding the electronic wavefunctions, their forms, and their dependence on coordinates. The following subsection, 1.4.4, outlines the formalism of the time-independent Hartree-Fock (HF) Method. It describes the forms in constructing the Fock matrix and the solutions obtained afterward. The time-evolving wavefunctions would be obtained from the solutions of TDSE. Since, the work uses external electric fields specifically LASERs, the subsection 1.2.4, describes the form of TDSE for atoms and molecules in LASER-dressed fields and their approximations used in them. The basic definition of LASERs, are described in section 1.3.1.

The time-dependent topological properties are used to analyze the dynamics of molecular electron densities in LASER-dressed fields. The tools used to understand topology are provided in the section 1.5. The section starts with the formal definition of electron densitites and followed by the explanation of density distribution in atomic and molecular electron densities in the subsection 1.5.2. The next subsection 1.5.1 explains the conditions of critical points in a real-valued 3D scalar function for requied for its identification, their types, and terminology w.r.t MED. The subsection 1.5.3, discusses the gradient vector fields, bond paths and zero-flux surfaces with respect to electron densities. The theory of *quantum theory of atoms in molecule* is explained in the subsection 1.5.5. The last section 1.6 describes the plan of the thesis.

1.2 Time-Dependent Schrödinder Equation (TDSE)

In quantum mechanics, one needs the time-dependent wavefunction $\Psi(\vec{r}, t)$, which are the solutions obtained from time-dependent Schrödinder Equation (TDSE). Analogous to classical wave equation that involves second-order time derivate related to energy, while in TDSE, the energy is related to its first time-derivative. The general form of TDSE is provided in Eq. [1.1].

$$i\hbar\frac{\partial}{\partial t}\Psi(\vec{r}, t) = \hat{H}\Psi(\vec{r}, t) \tag{1.1}$$

where $\hbar$ is the Planck's constant and, $\Psi(\vec{r},t)$ represents the wave function solutions of TDSE, $\hat{H}$ is the Hamiltonian operator whose form is as follows,

$$\hat{H} = -\frac{\hbar^2}{2m}\nabla^2 + V \tag{1.2}$$

The first part of Hamiltonian in Eq. [1.2], $\nabla^2 = \frac{\partial^2}{\partial x^2} + \frac{\partial^2}{\partial y^2} + \frac{\partial^2}{\partial z^2}$ is the kinetic energy term for a 3D form of TDSE. The second term V, represent the potential energy function. In general, the potential function depends on both coordinates and time variables V=V($\vec{r}$,t).

Case1: When potential energy function is time-independent and purely depends on coordinate V($\vec{r}$), therefore the resultant Hamiltonian is time-independent $\hat{H}(\vec{r})$: Then the general solutions of the TDSE with a time-independent Hamiltonian is solved using separation of variables in position and time, that is $\Psi(\vec{r},t) = \psi(\vec{r})\chi(t)$. It is expressed in the terms of particular solutions as given in the following Eq. [1.3] and [1.4]

$$\Psi(\vec{r},t) = \sum_{n=1}^{\infty} a_n \psi_n(\vec{r}) e^{-\frac{i}{\hbar}E_n t} \tag{1.3}$$

$$\Psi(\vec{r},t) = \int_0^{\infty} a(E)\psi_E(\vec{r}) e^{-\frac{i}{\hbar}Et} \tag{1.4}$$

The Eq. [1.3] and [1.4] represents the discrete and continous solutions of the TDSE refered in Eq. [1.1].

Case 2: Potential energy function depends on both coordinates and time $V(\vec{r},t)$. In TDSE, not only the wavefunction solutions are time-dependent, but the Hamiltonian can also be time-dependent $\hat{H}$ $(\vec{r},t)$. Therefore, the time-dependence in TDSE can also be induced through time-varying potentials $V(\vec{r},t)$. The general solutions of TDSE, even valid with time-dependent Hamiltonian, involves an unitary operator called the evolution or propagator operator having the following form,

$$\hat{U}(t) = e^{-iHt/\hbar} \tag{1.5}$$

It is given the name evolution since it generates the evolution of the wave-function from $\Psi(x, t = 0)$ to $\Psi(x, t)$. Therefore, $e^{-iHt/\hbar}$ maps $\Psi(x, t = 0)$ to $\Psi(x, t)$. Alternative representations of TDSE is presented in the next section. These may not be the approximations, but the interaction picture discussed will provide an alternative starting point that is helpful in perturbation series expansion.

1.2.1 Schrödinger, Heisenberg and Interaction Pictures

Three kinds of pictures representing the of TDSE are possible,

1. Schrödinder picture: When the state operators are stationary (*Case 1: time-independent Hamiltonian*) but the state vectors Ψ evolves in time, and thus expectation values may also evolve in time. The solution of TDSE in this picture is

$$\Psi_S(t) = e^{-\frac{i}{\hbar}Ht}\Psi_S(0) \tag{1.6}$$

2. Heisenberg Picture: When the state operators are time-dependent (*Case 2: time-dependent Hamiltonian*) and the state vectors Ψ are constant in time.

$$\Psi_H(t) = e^{\frac{i}{\hbar}Ht}\Psi_S(t) \tag{1.7}$$

The time-independence of state vectors can be verified using Eq. [1.6] in [1.7]. Operators in Heisenberg picture, $\hat{A}_H$, are related to their Schrödinder picture by the relation

$$\hat{A}_H(t) = e^{\frac{i}{\hbar}Ht}\hat{A}e^{-\frac{i}{\hbar}Ht} \tag{1.8}$$

This results in getting the same expectation values of any operator in both Heisenberg and Schrödinder pictures.

3. Interaction Picture: When the total time-dependent Hamiltonian $\hat{H}$(t) can be partitioned into $\hat{H}(t) = \hat{H}_0 + \hat{V}$. Here the time evolution generated by $\vec{H}_0$ is known. The interaction picture wavefunction Ψ_I is defined in Eq. [1.9] and the interaction picture Hamiltonian, $\hat{H}_I$ is defined in Eq. [1.10],

$$\Psi_I(t) = e^{\frac{i}{\hbar}H_0t}\Psi_s(t) = e^{\frac{i}{\hbar}H_0t}e^{-\frac{i}{\hbar}Ht}\Psi_S(0) \tag{1.9}$$

$$\hat{H}_I = e^{\frac{i}{\hbar}H_0t}Ve^{-\frac{i}{\hbar}\hat{H}_0t} \tag{1.10}$$

Here, in the interaction picture, both the state vector and state operator contains the part of time evolution. The interaction picture appears as an intermediate between the Schrödinger picture and the Heisenberg picture.

In the practical cases, the term V in the total time-dependent Hamiltonian are mostly unknown. Therefore, to obtain at least the approximate solutions of TDSE, time-dependent perturbation theory can be applied when V is small compared to H_0.

1.2.2 Time-Dependent Perturbation Theory

The interaction picture described in the previous subsection is exact. Also, the time-dependent perturbation theory (TDPT) would use the similar partitioning of the total Hamiltonian $\hat{H}(t) = \hat{H}_0 + \hat{V}$, where $\hat{V}$ is the perturbation term and is very small in comparison to H_0, that is V $\ll H_0(t)$. The dynamics from TDPT are only useful if the dynamics under $\hat{H}_0(t)$ is known. If V is too large, the TDPT solutions do not converge.

Derivation from the interaction Picture:

Consider a time-dependent Hamiltonian, $H = H_0 + H_1$, where H_0 is time-independent and H_1 is time-dependent. The corrections to the evolution operator is found out using the interaction picture, which will be applied to zeroth order wavefunction $\Psi^0(t_0)$ to obtain corrections to the wavefunctions. The unperturbed Hamiltonian H_0 associated with the evolution operator $U^0(t, t_0)$, satisfying the TDSE,

$$i\hbar\frac{\partial}{\partial t}U^0(t, t_0) = H_0 U^0(t, t_0) \tag{1.11}$$

The interaction picture wavefunction from Eq. [1.9],

$$\Psi_I(t) = e^{\frac{i}{\hbar}H_0(t)}\Psi_S(t) = e^{\frac{i}{\hbar}H_0 t}e^{-\frac{i}{\hbar}Ht}\Psi_S(0) \tag{1.12}$$

The interaction picture evolution operator can also be defined as,

$$U_1(t, t_0) = e^{\frac{i}{\hbar}H_0(t-t_0)}e^{-\frac{i}{\hbar}H(t-t_0)} = U^{(0)\dagger}(t, t_0)U(t, t_0) \tag{1.13}$$

This evolution operator in Eq. [1.13] also satisfies a TDSE of the following form,

$$i\hbar\frac{\partial}{\partial t}U_1(t, t_0) = H_1 U_1(t, t_0) \tag{1.14}$$

where,

$$H_1(t) = e^{\frac{i}{\hbar}H_0 t} H_1(t) e^{-\frac{i}{\hbar}H_0 t} \tag{1.15}$$

The iterative solutions of the interaction picture Hamiltonian in Eq. [1.14] yields the following form,

$$U_1(t, t_0) = 1 + \sum_{n=1}^{\infty} U_1^{(n)}(t, t_0) \tag{1.16}$$

where the form of $U^{(n)}(t, t_0)$ is described by the Eq. [1.17]

$$\begin{aligned} U^{(n)}(t, t_0) = \frac{1}{(i\hbar)^n} \int_{t_0}^{t} d\tau_n \int_{t_0}^{\tau_n} d\tau_{n-1} \cdots \int_{t_0}^{\tau_2} d\tau_1 H_1(\tau_n) H_1(\tau_{n-1}) \cdots \\ H_1(\tau_1) U_1(\tau_1, t_0) \end{aligned} \tag{1.17}$$

The integral is performed with the constraint that $t > \tau_n > \tau_{n-1} > \cdots > \tau_1 > t_0$. The $U_1(\tau_1, t_0)$ is replaced with 1 in the construction of a perturbation series from Eqs. [1.16] and [1.17]. There it can be said that $H = H_0$. Substituting and using Eq. [1.13], the perturbation series for the Schrödinger picture propagator $U(t, t_0)$ can be written down as in Eq. [1.18],

$$U(t, t_0) = U^{(0)}(t, t_0) + \sum_{n=1}^{\infty} U^{(n)}(t, t_0) \tag{1.18}$$

where the $U^{(n)}(t, t_0)$ is given by Eq. [1.19],

$$\begin{aligned} U^{(n)}(t, t_0) = \frac{1}{(i\hbar)^n} \int_{t_0}^{t} d\tau_n \int_{t_0}^{\tau_n} d\tau_{n-1} \cdots \int_{t_0}^{\tau_2} d\tau_1 U^{0}(t, \tau_n) H_1(\tau_n) U^{(0)}(\tau_n, \tau_{n-1}) \\ \times H_1(\tau_{n-1}) \cdots U^{(0)}(\tau_2, \tau_1) H_1(\tau_1) U^{(0)}(\tau_1, t_0) \end{aligned} \tag{1.19}$$

these integrals are also subjected to the constraint that $t > \tau_n > \tau_{n-1} > \cdots > \tau_1 > t_0$. substituting the following evolution operator of Eq. [1.20],

$$U^{(0)}(t,t') = e^{-\frac{i}{\hbar}H_0(t-t')} \tag{1.20}$$

into Eq. [1.18] and [1.19] and applying this result to $\Psi^{(0)}(t_0)$, one can obtain the first and second order time-dependent perturbative corrections to the wavefunctions described in Eq. [1.21] and [1.22].

$$\Psi^{(1)}(t) = \frac{1}{i\hbar}\int_{t_0}^{t} dt' e^{-\frac{i}{\hbar}H_0(t-t')}\hat{H}_1(t')e^{-\frac{i}{\hbar}H_0(t-t')}\Psi^0(t_0) \tag{1.21}$$

$$\begin{aligned}\Psi^{(2)}(t) = \frac{1}{(i\hbar)^2}\int_{t_0}^{t} dt' \int_{t_0}^{t'} dt'' e^{-\frac{i}{\hbar}H_0(t-t')}\hat{H}_1(t')e^{-\frac{i}{\hbar}H_0(t'-t'')} \\ \hat{H}_1(t'')e^{-\frac{i}{\hbar}H_0(t''-t_0)}\Psi_0(t_0)\end{aligned} \tag{1.22}$$

Several spectroscopic techniques, such as infrared-spectroscopy and UV-spectroscopy, induce transitions between vibrational and electronic levels using a specific range of frequencies at intensities which are less than 10^{13} W/cm^2. Perturbation theory applies to the intensities which are less than 10^{13} W/cm^2. However, The work presented in the thesis uses **high intensities of laser pulses** (I $>$ 10^{14} W/cm^2). Since such high intensities become comparable or sometimes greater than the internal electric fields, this results in competition in the electronic dynamics between the coulomb binding potential and the external electric field. Therefore, TDPT formalism will not be valid in this case. Therefore, a strong field approximations is used to solve the TDSE.

1.2.3 Strong Field Approximation

Strong field approximations (SFA) are considered for non-perturbative external field interactions. These interactions are described by including the continuum-continuum interaction using perturbation. It is assumed that the high intensity fields moves the electrons very fast away from the vicinity of atomic potential such that the interaction with the binding potential becomes negligible. In 1964, Keldysh came up with an analytical form to calculate tunnel ionization for atoms in the presence of strong oscillating fields.[66] The time-evolution operator for the time-dependent Hamiltonian ($\hat{H} = \hat{H}_0 + \hat{H}_1$) in TDSE can be written as follows,

$$\hat{U}(t_f, t_i) = \hat{U}_0(t_f, t_i) - \frac{i}{\hbar} \int_{t_i}^{t_f} d\tau \hat{U}(t_f, \tau) \hat{H}_1(\vec{r}, t) \hat{U}_0(\tau, t_i) \tag{1.23}$$

In Eq. [1.23], $\hat{U}(t_f, t_i)$ is the time-evolution operator for time-independent Hamiltonian. The transition amplitude M_P is calculated using the initial bound state, $|\Psi_0(t)\rangle$ to a final continuum state, $|\Psi_P(t)\rangle$, shown in Eq. [1.24]

$$M_P = \lim_{t_f \to \infty, t_i \to -\infty} \langle \Psi_P(t_f) \mid \hat{U}(t_f, t_i) \mid \Psi_0(t_i) \rangle \tag{1.24}$$

Here in this Eq. [1.24], t_f and t_i corresponds to the initial and final end of the pulse. In order to describe SFA, use Eq. [1.23] in [1.24] to calculate the transition probability. The ionization probability equation is given as follows,

$$M_P = \lim_{t_f \to \infty, t_i \to -\infty} \langle \Psi_P(t_f) \mid [\hat{U}_0(t_f, t_i) - \frac{i}{\hbar} \int_{t_f}^{t_i} d\tau \hat{U}(t_f, \tau) \hat{H}_1(\vec{r}, t) \hat{U}(\tau, t_i)] \mid \Psi_0(t_i) \rangle \tag{1.25}$$

The first term in the time-evolution represents the free-field Hamiltonian, and the bound and continuum states are orthogonal. Therefore, the first term vanishes and transition amplitude is written as,

$$\begin{aligned} M_P &= -\frac{i}{\hbar} \lim_{t_f \to \infty, t_i \to -\infty} \int_{t_i}^{t_f} d\tau \langle \Psi_P(t_f) \mid \hat{U}(t_f, \tau) \hat{H}_1(\vec{r}, t) \hat{U}_0(\tau, t_i) \mid \Psi_0(t_i) \rangle \\ &= -\frac{i}{\hbar} \lim_{t_f \to \infty, t_i \to -\infty} \int_{t_i}^{t_f} d\tau \langle \Psi_P(t_f) \mid \hat{U}(t_f, \tau) \hat{H}_1(\vec{r}, t) \mid \Psi_0(t_i) \rangle \end{aligned} \tag{1.26}$$

It is assumed that after ionization, the electrons will not feel the binding potential. So, the the above Eq. [1.26], $\langle \Psi_P(t_f) \mid \hat{U}(t_f, \tau)$ is replaced by Wolkow states $\langle \Psi_P^{(V)}(\tau)$ [67] The SFA amplitude evaluated by Keldysh is shown in the following Eq. [1.27]

$$M_P = -\frac{i}{h} \lim_{t_f \to \infty, t_i \to -\infty} \int_{t_i}^{t_f} d\tau \langle \Psi_P^{(V)}(\tau) \mid \hat{H}_1(\vec{r}, t) \mid \Psi_0(t_\tau) \rangle \tag{1.27}$$

This can be used to properly describe external field related phenomenons such as high harmonic generation spectra, above threshold ionization occurring in the high intensity fields. However, The work presented in the thesis would only use the wavefunctions obtained from the solutions of TDSE in these high intensity fields. Since, the perturbation does not apply in the presence of high field, therefore, there is a need to get a better understanding of the TDSE for atoms and molecules in the presence of light to be described in the next section.

1.2.4 TDSE for Light-matter interaction: A Semi-Classical view

TDSE in the case of an atom interacting with light, for an electron of charge e, mass m and position $\vec{r}$ for an attractive potential $V(\vec{r})$ is given by the Eq. [1.28],

$$-i\hbar\frac{\partial}{\partial t}\psi(\vec{r},t) = \left[\frac{1}{2m}(-i\hbar\vec{\nabla} - e\vec{A})^2 + e\phi + \vec{V}(\vec{r})\right]\psi(\vec{r},t) \tag{1.28}$$

In this Eq. [1.28], $\vec{A}$ and ϕ are the vector and scalar potential, respectively. In quantum mechanics, the Eq. [1.28] is often specified in atomic units or Hartree units , where $\hbar$=1, mass of electron m, charge of electron e, time t = 0.0241 fs, length a_0 = 0.5292 Å, the dipole moment ea_0 is 1. The expansion of Eq. [1.28] in atomic units, is shown here as,

$$i\frac{\partial}{\partial t}\psi = \left[-\frac{1}{2}\hat{\nabla}^2 + \hat{V}(\vec{r}) + \frac{1}{2}(\hat{A}^2 - i\vec{\nabla}\cdot\vec{A} - i\vec{A}\cdot\vec{\nabla} + \phi)\right]\psi \tag{1.29}$$

The first two terms in the Eq. [1.29] defines the unperturbed Hamiltonian $\hat{H}_0$, which contains the kinetic energy of the electron and the attractive Coulombic potential energy operator $\hat{V}(\vec{r})$. The next four terms in Eq. [1.29] defines the Hamiltonian part, $\hat{H}_{int}$ as the interaction between atom and light.

The physical quantities which can be measured, for example, electric field $\vec{\epsilon}$ and magnetic field $\vec{B}$ can be evaluate using the vector potential $\vec{A}$ and scalar potential ϕ given by the following relations [1.30] and [1.31],

$$\vec{B} = \vec{\nabla}\times\vec{A} \tag{1.30}$$

$$\vec{\epsilon} = \vec{\nabla} \cdot \vec{A} - \frac{\partial \vec{A}}{\partial t} \tag{1.31}$$

If a gradient of a scalar function, for example $\chi(\vec{r}, t)$ is added to the vector potential $\vec{A}$ and $-\frac{\partial}{\partial t}\chi(\vec{r}, t)$ to the scalar potential ϕ, then the electric field and magnetic fields remain invariant. This is expressed in the following relations,

$$\vec{A} \longrightarrow \vec{A}' = \vec{A} + \vec{\nabla}\chi \tag{1.32}$$

$$\vec{B} = \vec{\nabla} \times \vec{A}' = \vec{\nabla} \times \vec{A} + \vec{\nabla} \times \vec{\nabla} \cdot \chi = \vec{\nabla} \times \vec{A} \tag{1.33}$$

In the same way when,

$$\phi \longrightarrow \phi' = \phi - \frac{\partial \chi}{\partial t} \tag{1.34}$$

and hence,

$$\vec{\epsilon} = -\vec{\nabla} \cdot \phi' - \frac{\partial \vec{A}'}{\partial t} \tag{1.35}$$

$$\vec{\epsilon} = -\vec{\nabla} \cdot \phi' + \vec{\nabla} \cdot \frac{\partial \chi}{\partial t} - \frac{\partial \vec{A}}{\partial t} - \vec{\nabla} \cdot \frac{\partial \chi}{\partial t} \tag{1.36}$$

$$\vec{\epsilon} = -\vec{\nabla} \cdot \phi' - \frac{\partial \vec{A}}{\partial t} \tag{1.37}$$

From the above equations, it shows that the vector potential $\vec{A}$ and scalar potential ϕ, does not uniquely determine electric and magnetic fields. It is also known as the choice of gauge.[68]. This could be shown through unitary transformation. Therefore, the unitary transformation of a wavefunction of the one shown in Eq. [1.36]

$$\tilde{\psi}(\vec{r},t) = exp(-i\chi)\psi(\vec{r},t) \tag{1.38}$$

It preserves the invariance of the Schrödinder equation under different gauges, and the different physical quantities do not change. To study the light-matter interaction under the dipole approximation, due to the interaction term (in Eq. [1.29]), the TDSE can be represented in different types of gauges, for example, velocity and length.

1.2.5 Gauge Transformation of TDSE

TDSE in dipole approximation: The wavelengths of the electromagnetic (EM) fields for IR, Visible, and UV radiations fall from micrometers to a few nanometers. For most cases, the atomic or molecular sizes are smaller when compared to the wave length of EM fields. The dipole approximation can be used[68, 69] for the variation in vector field $\vec{A}$ which is purely time-dependent and space-independent for atoms and molecules, that is, $\vec{\nabla} \cdot \vec{A} = 0$. The TDSE assuming the dipole approximation in atomic units is

$$i\frac{\partial\psi}{\partial t} = \left[-\frac{1}{2}\hat{\nabla}^2 + \hat{V}(\vec{r}) + \frac{1}{2}(\hat{A}^2 - i\vec{A}\cdot\vec{\nabla}) + \phi\right]\psi \tag{1.39}$$

TDSE in velocity gauge: The Eq. [1.39] can also be written in the velocity gauge when $\vec{A}$, and $\vec{\nabla}$ couple with each other.[69, 70] The chosen unitary transformation follows as shown in Eq. [1.40],

$$\hat{U} = \exp\left(-\frac{i}{2}\hat{A}^2)\right) \tag{1.40}$$

Here, $\hat{A}^2$ is a purely time-dependent term. Using the $\hat{U}$ from Eq. [1.40] to the Eq. [1.39] with the dipole approximation, Then, in the velocity gauge the TDSE equation becomes,

$$i\frac{\partial}{\partial t}\psi V(\vec{r},t) = \left[-\frac{1}{2}\hat{\nabla}^2 + \hat{V}(\vec{r} + \vec{A}\cdot\vec{\nabla})\right]\psi V(\vec{r},t) \tag{1.41}$$

TDSE in length gauge: This is the mostly used gauge to study the light-matter interaction.[68, 69] The unitary operator $\hat{U}$ is defined as,

$$\hat{U} = exp(-i\vec{A}\cdot\vec{r}) \tag{1.42}$$

Applying this unitary transformation (Eq. [1.42]) along with the dipole approximation and $\frac{\partial\vec{A}}{\partial t} = \vec{\epsilon}(t)$, then the length gauge TDSE becomes,

$$i\frac{\partial}{\partial t}\psi_L(\vec{r},t) = \left[-\frac{1}{2}\hat{\nabla}^2 + \hat{V}(\vec{r}) + \vec{\epsilon}(t)\cdot\vec{r}\right]\psi_L(\vec{r},t) \tag{1.43}$$

The term $\vec{\epsilon}\cdot\vec{r}$ describes the interaction between light and matter, which depicts the same classical dipole in the classical oscillating electric field.

TDSE in the absence of the oscillating field: When the $\vec{\epsilon}\cdot\vec{r}$ terms is omitted from the Eq. [1.43], the resultant TDSE is,

$$i\frac{\partial}{\partial t}\psi(\vec{r},t) = \left[-\frac{1}{2}\hat{\nabla}^2 + \hat{V}(\vec{r})\right]\psi(\vec{r},t) \tag{1.44}$$

Because the potential energy function $\hat{V}(\vec{r})$ is time-independent, therefore the eigenstates would be stationary waves. Thus, for a given eigenstate $\chi(\vec{r})$ of energy E, the time evolution of the probability density is defined as $\rho = \left[\chi(\vec{r}exp(-i\frac{Et}{\hbar}))\right]^* \chi(\vec{r})exp(-i\frac{Et}{\hbar}) = \mid \chi(\vec{r}) \mid^2$. This probability density does not change in time.[71, 72] The future time-step wave packet could be calculated for the time-independent potential. The case is not the same for time-dependent potentials. So, how do we determine the wave function $\psi(\vec{r},t)$ at time t, given the information at time t_0, where t>t_0. To solve this, an operator called time-displacement operator is required. This operator $\hat{U}$ operates on the wave packet at previous timestep t_0 and provides the wave packet at time t, given by the following Eq. [1.45],[70–74]

$$\psi(\vec{r},t) = \hat{U}(t,t_0)\psi(\vec{r},t_0) \tag{1.45}$$

The following properties are obeyed by time-evolution operator $\hat{U}(t,t_0)$ [71, 72]

1. Time evolution operator is an unitary operator: $\hat{U}^{\dagger}\hat{U} = 1$

2. For the time $t_2 > t_1 > t_0$, the evolution operator for time $t_0 \longrightarrow t_2$ is:

$$\hat{U}(t_2,t_0) = \hat{U}(t_2,t_1)\hat{U}(t_1,t_0) \tag{1.46}$$

3. If the final and initial time are same, then $\hat{U}(t,t) = 1$.

The goal is to find the expression for $\hat{U}$ operator. Using the Eq. [1.45] in Eq. [1.43], we get:

$$i\hbar\frac{d}{dt}\left[\hat{U}\psi(\vec{r},t_0)\right] = \hat{H}\left[\hat{U}\psi(\vec{r},t_0)\right] \tag{1.47}$$

In Eq. [1.47], $\hat{H}$ is the Hamiltonian operator. In the next subsection, we provide the details of the time-evolution operator $\hat{U}$ for the time-dependent Hamiltonian.

1.2.6 Numerical Methods to solve TDSE

The time-evolution operator for the time-independent potential energy is $\hat{U} = exp(i\frac{Et}{\hbar})$.[71, 72] Whereas, for the time-dependent potential energy, the solution of TDSE in length gauge from Eq. [1.43] is given by the following form[81–83]

$$|\psi(x)\rangle = |\psi(t_0)\rangle - i\int_{t_0}^{t} \hat{H}(t')|\psi(t')\rangle dt' \tag{1.48}$$

The main problem with the formultion of Eq. [1.48] is that the Hamiltonian does not commute at different time steps. In order to evaluate the right-hand side in Eq. [1.48], one needs to slice the time, $t_1 < t_2 < t_3 \cdots t_n$ such that $\lim_{n\longleftrightarrow\infty}(\frac{t_n-t_1}{n} = 0)$. The first iteration of Eq. [1.48] will be as follows[81–83]

$$|\psi(t_1) = |\psi(t_0)\rangle - i\int_{t_0}^{t_1} H(t')|\psi(t')\rangle dt' \tag{1.49}$$

For the next set of time steps $t_2, t_3, \cdots, t_\infty$,

$$\begin{aligned}|\psi(t)\rangle = |\psi(t_0)\rangle + \sum_{n=1}^{\infty}(-i)^n \int_{t_0}^{t_1} dt_n \cdots \int_{t_0}^{t_2} dt_1 \int_{t_0}^{t_1} H(t_n)|\psi(t_n)\rangle \cdots \\ H(t_2)|\psi(t_2)\rangle H(t_1)|\psi(t_1)\rangle dt.\end{aligned} \tag{1.50}$$

Hence, the time-evolution operator $\hat{U}$ is,

$$\begin{aligned}|\psi(t)\rangle = \hat{I} + \sum_{n=1}^{\infty}(-i)^n \int_{t_0}^{t_1} dt_n \cdots \int_{t_0}^{t_2} dt_1 \int_{t_0}^{t_1} H(t_n)|\psi(t_n)\rangle \cdots \\ H(t_2)|\psi(t_2)\rangle H(t_1)|\psi(t_1)\rangle dt\end{aligned} \tag{1.51}$$

The Eq. [1.51] can be further compacted into the following form,

$$\hat{U}(t,t_0) = \hat{\tau}\left[\sum_{n=0}^{\infty}\frac{(-i)^n}{n!}\left(\int_{t_0}^{t} dt'\hat{H}(t')\right)\right] \tag{1.52}$$

In this Eq. [1.52], the $\hat{\tau}$ is the time-ordering operator. The above expression can also be written as an exponential operator,

$$\hat{U}(t,t_0) = \hat{\tau}\left[exp\left(-i\int_{t_0}^{t_n} H(t')dt'\right)\right] \tag{1.53}$$

For a small increment in time δt, the Hamiltonian remains constant, the $\hat{U}$ is approximated as,

$$\hat{U}(t_0+\delta t,t_0) = exp\left[-i\int_{t_0}^{t_0+\delta t} H(t')dt'\right] \approx exp[-iH(t)\Delta t] \tag{1.54}$$

The evolution operator can be described as a sequence of successive operations of the previous evolution operators, written in the following fashion,

$$\hat{U}(t_n,t_0) = \hat{U}(t_n,t_{n-1})\cdots\hat{U}(t_2,t_1)\hat{U}(t_1,t_0) \tag{1.55}$$

There are different methods available to approximate the time-evolutions operators $\hat{U}$ given in Eq. [1.53], for studying nuclear and electronic dynamics. The numerical receipes available in literature are: Trotter-factorization,[72] (t,t′) method,[75–78] time-dependent configuration interaction singles (TD-CIS) method.[79, 80]

Since, the work presented deals with properties to be calculated in the presence of strong external fields, such as LASERs. We here briefly describe the light, formal definition of LASER and its polarization forms.

1.3 Light: The External Field

In modern physics, *light* has two nature descriptions. In the first description, light is said to contain or is made up of tiny particles called photons and travels linearly. In another definition, light is said to have a transverse wave-like nature, where it can bend and superimpose while traveling in any medium or space. Compton effect and photoelectric effect experiments confirm the particle nature of light while processes such as diffraction, interference and polarization confirm the wave nature of light.

Since, wave nature is fundamental to the description of quantum systems in quantum mechanics, we in the present thesis, on studying dynamical electron densities, focus our attention only to time-varying wave functions in the presence of light, specially LASERs. In the next subsection, we provide basic descriptions regarding the LASERs working principles, its mathematical form in polarization.

1.3.1 LASERs

Laser is a device to produce a coherent and monochromatic source of electromagnetic radiation. Laser is the acronym for *Light Amplification by Stimulated Emission of Radiations*.

The Working Principle:
Lasers are based on the principle of amplification of radiations generated by stimulated emissions.

To explain this, let us consider a two level system, one a ground state E_0, and other excited state E_1. There are three ways in which a resonant photon can interact with the system. The first one is a process, where a resonant photon excites electrons from ground state to the excited state. This processes is called absorption. The second process is called spontaneous emission, where electrons in excited state E_1 decays to the ground state E_0 with the emission of a photon in random direction with a random phase. Stimulate emission, is the thrid process and involved in the working of lasers. In stimulted emission, for a large population n_1 in the excited state E_1, gets to the ground state via relaxation achieved by the application of resonant electromagnetic radiation. This process can happen if there is an population inversion, that is, $n_1 > n_0$. To generate radiations from stimulated emission, the collision of one photon with the atom in excited state E_1 relaxes to the ground state. This generates a second photon of the same energy and phase in the same directions as that of the first photon. The second photon is made to collide with another excited state atom to generate a thrid photon. This processes is continued to amplify the intensity of the incident resonant radiation.[64, 65]

Fig. [1.1] depicts the working of a laser. The experimental step contains mainly three components, a pump, an optical cavity and a laser medium. The process of population inversion is achieved through the pump, which are devices such as electric discharges or flash lamps. The laser medium which amplifies the light can be solid, liquid or gas.

Theoretical Definitions:

Light is an electromagnetic radiations which can be defined using electric $\vec{E}$ and magnetic field $\vec{B}$ vectors. The set of Maxwell's equations for charge density ρ and a vector current density $\vec{J}$ as sources in a medium whose permittivity ϵ_0, is given by Eq. [1.56], [1.57], [1.58], and [1.59].

$$\vec{\nabla} \cdot \vec{E}(\vec{r}, t) = \frac{\rho}{\epsilon_0} \tag{1.56}$$

$$\vec{\nabla} \times \vec{E}(\vec{r}, t) = -\frac{\partial}{\partial t} \vec{B}(\vec{r}, t) \tag{1.57}$$

$$\vec{\nabla} \cdot \vec{B}(\vec{r}, t) = 0 \tag{1.58}$$

$$\vec{\nabla} \times \vec{B}(\vec{r}, t) - \frac{1}{c^2} \frac{\partial}{\partial t} \vec{E}(\vec{r}, t) = \mu_0 \vec{J} \tag{1.59}$$

The quantities ρ and $\vec{J}$ contains all the information regarding the material and source of charge. To derive an analytical form of the laser, one needs to use Maxwell equations without any sources. Therefore, in an space with no charges or currents with unbounded homogeneous vacuum, the Eq. [1.56], [1.57], [1.58], and [1.59] gets reduced to,

$$\vec{\nabla} \cdot \vec{E}(\vec{r}, t) = 0 \tag{1.60}$$

$$\vec{\nabla} \times \vec{E}(\vec{r}, t) = -\frac{\partial}{\partial t} \vec{B}(\vec{r}, t) \tag{1.61}$$

$$\vec{\nabla} \cdot \vec{B}(\vec{r}, t) = 0 \tag{1.62}$$

$$\vec{\nabla} \times \vec{B}(\vec{r}, t) - \frac{1}{c^2} \frac{\partial}{\partial t} \vec{E}(\vec{r}, t) = 0 \tag{1.63}$$

Using the Eq. [1.60], [1.61], [1.62] and [1.63], we arrive at the following differential equations,

$$-\vec{\nabla}^2 \vec{B}(\vec{r}, t) + \frac{1}{c^2} \frac{\partial^2}{\partial t^2} \vec{B}(\vec{r}, t) = 0 \tag{1.64}$$

$$-\vec{\nabla}^2\vec{E}(\vec{r},t)+\frac{1}{c^2}\frac{\partial}{\partial t^2}\vec{E}(\vec{r},t)=0 \tag{1.65}$$

The solutions to the above equations is complex and represent the plane waves,

$$\vec{E}(\vec{r},t)=E_0\hat{\epsilon}_e\exp[i(\vec{k}\cdot\vec{r}-\omega t)] \tag{1.66}$$

$$\vec{B}(\vec{r},t)=B_0\hat{\epsilon}_b\exp[i(\vec{k}\cdot\vec{r}-\omega t)] \tag{1.67}$$

In these equations, E_0 and B_0 are the field amplitudes, $\vec{k}$ is the propagation vector. The polarization vector for the electric field ϵ_e and polarization vector for the magnetic field ϵ_b are orthogonal and perpendicular to each other. Both the waves are linearly polarized in orthogonal planes. The frequency of other wave is represented by ω.

Laser polarization:

In general, the oscillations of the electric and magnetic field vectors are oriented randomly about the direction of propagation and, therefore, are considered unpolarized. However, suppose the direction of electric or magnetic field vector oscillations is made to orient along the particular choice of transverse plane, handedness, or shape. In that case, it is referred to as a polarized laser field.

Different types of polarized laser fields can be derived from the following Eq. [1.68], [1.69]. Considering two plane waves with phase constants ϕ_1 and ϕ_2

$$\vec{E}_1(\vec{r},t)=E_1\hat{\epsilon}_{e_1}\exp[i(\vec{k}\cdot\vec{r}-\omega t+\phi_1)] \tag{1.68}$$

$$\vec{E}_2(\vec{r},t) = E_2\hat{\epsilon}_{e_2}\exp[i(\vec{k}\cdot\vec{r} - \omega t + \phi_2)] \tag{1.69}$$

The total wavefunctions can be constructed using the forms of Eq. [1.68], and [1.69] which is as follows,

$$\vec{E}(\vec{r},t) = [E_1\hat{\epsilon}_{e_1}\exp(\phi_1) + E_2\hat{\epsilon}_{e_2}\exp(\phi_2)]\exp[i(\vec{k}\cdot\vec{r} - \omega t)] \tag{1.70}$$

The different types of polarization are,

1. A linearly polarized laser is constructed using the relation as $\phi_1 = \phi_2$ between the phases. The effective laser field is,

   $$\vec{E}(\vec{r},t) = (E_1^2 + E_2^2)^{\frac{1}{2}}\epsilon\hat{_{e_{12}}}^{\theta}\exp[i(\vec{k}\cdot\vec{r} - \omega t + \phi)] \tag{1.71}$$

   where $\theta = tan^{-1}\frac{E_1}{E_2}$

2. If $\phi_1 \neq \phi_2$ and $E_1 = E_2 = E_0$, then the total field is elliptically polarized. Now, if the phase difference for the elliptically polarized wave is $\pm\frac{\pi}{2}$ then it is this case is referred as a circularly polarized laser. The forms of these polarization are shown in Eq. [1.72], and [1.73].

   $$\vec{E}_{epl}(\vec{r},t) = E_0[\hat{\epsilon}_{e1}\exp(\phi_1) + \hat{\epsilon}_{e2}\exp(\phi_2)]\exp[i(\vec{k}\cdot\vec{r} - \omega t)] \tag{1.72}$$

   $$\vec{E}_{cpl}(\vec{r},t) = E_0[\hat{\epsilon}_{e1} + \hat{\epsilon}_{e2}\exp(\pm\frac{\pi}{2})]\exp[i(\vec{k}\cdot\vec{r} - \omega t)] \tag{1.73}$$

3. If the frequency of the two waves is in a certain ratio such that it is a whole number, with a phase difference of $\pm\frac{\pi}{2}$, then the polarized

field takes shapes like-fan lobes, often called foils. The number of lobes formed confirms the number of foils, called n-foils.

$$\begin{aligned}\vec{E}_{nPL}(\vec{r},t) = (&E_1\hat{\epsilon}_{e1}\exp[i(\phi_1-\omega_1)]\\ &+E_2\hat{\epsilon}_{e2}\exp[i(\phi_2-\omega_2)])\exp(i\vec{k}\cdot\vec{r})\end{aligned} \tag{1.74}$$

Different polarization fields change the wave functions such that the scalar field properties get deformed, and electron densities seem to orient along the polarization direction. The effect on molecular properties, specifically electron densities, will be discussed in later chapters of the thesis.

1.4 Ab-Initio Electronic Structure of Atoms and Molecules

The study of applying quantum mechanical principles to the system of atoms and molecules was termed quantum chemistry. In quantum chemistry, *ab-initio* electronic structure theory of atoms and molecules refers to the methods of solving Schrödinger equation using first principles in Born-Oppenheimer approximation. Robert Parr and coworkers, David Craig and the group were the first to introduce the term ab-initio in the context of quantum chemistry while carrying out semiempirical studies on the excited states of benzene.[86] The word *ab-initio* meant quantities derived *from first principle* or *from the beginning*, which implies only physical constants go as inputs in the calculation and no empirically or experimentally derived information. For the system of atoms and molecules, their charges, nuclear positions, and information on the number of electrons and nuclei are taken as inputs in the calculation to yield helpful information, such as energies, charges, electron densities, and many other system properties.

The *ab-initio* electronic structure methods use approximations to obtain many-electron functions from the solutions of electronic Schrödinger equation. The evaluated many-electron functions are often referred to as molecular wavefunctions in quantum chemistry. Furthermore, these molecular wavefunctions are fundamental quantities to evaluate electronic properties using their analytical or numerical forms.

The most famous theoretical methods are the semi-empirical methods, Hartree-Fock (HF), post-Hartree-Fock and density functional theory (DFT) methods. Since, the Hamiltonian constructed in these methods do not contain any time-dependent terms, therefore the solutions obtained from these methods only provide time-independent wavefunctions. On the other hand, the dynamics in wavefunctions through time-evolving wavefunctions are obtained from the solutions of methods solving time-dependent Schrödinger equation. Some of the popular methods which solve TDSE are Time-Dependent Hartree-Fock (TDHF), configuration interaction (CI) and DFT methods.

This thesis present results and discussions on the electronic properties, specially electron densities, using the time-evolving wavefunctions in laser-dressed fields. Therefore, in the following section we would discuss the general concepts of quantum chemistry, the Hartree-Fock formalism, and the method used to solve TDSE for atoms and molecules in the presence of polarized LASERs (specifically RT-TDHF).

1.4.1 The Molecular Problem

The central goal of quantum chemistry is to find solutions of the non-relativistic Schrödinger equation. This section provides a brief description of the methods used to obtain approximate results of the electronic properties of molecular system. Consider a molecular system with M nuclei and N electrons

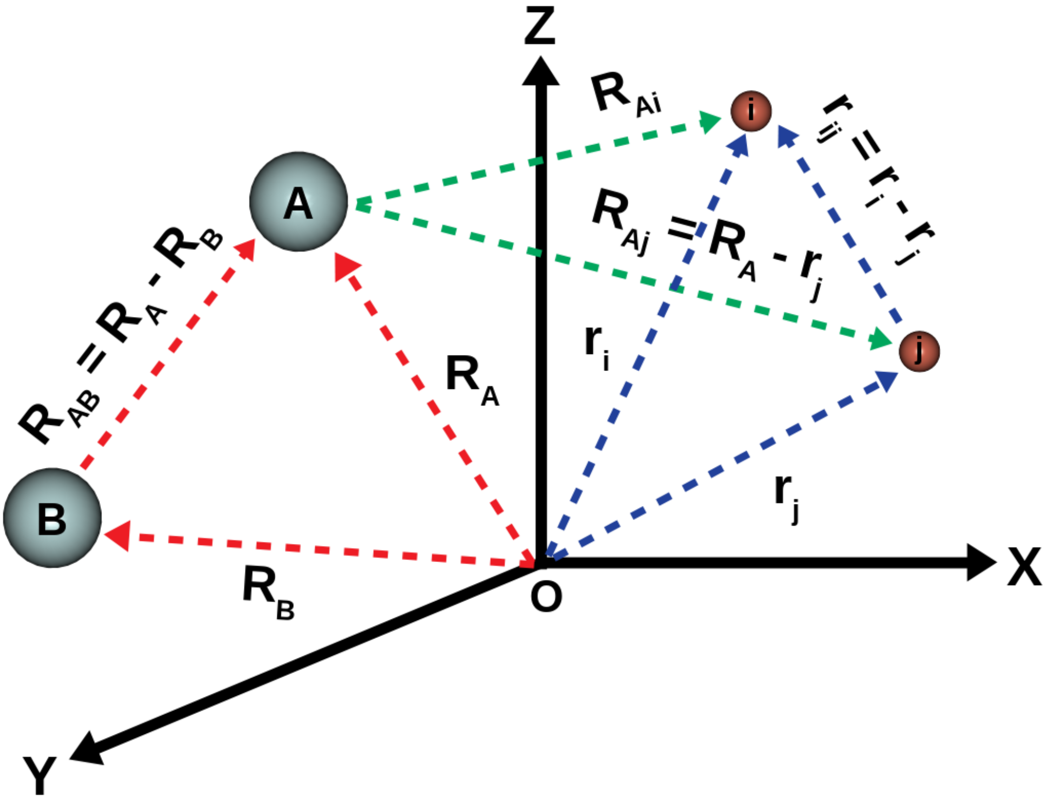

Figure 1.3: Representation of the molecular coordinate system for a collection of four particles: two nuclei A, B and two electrons i, j. The R_A, R_B, r_i, and r_j depict the position vectors of nuclei and electrons w.r.t the origin.

that can be represented in the coordinate system. The Time-Independent Schrödinger equation (TISE) for molecular wavefunctions $\Psi(\vec{r_i},\vec{R_A})$, is given by Eq. [1.75].

$$\hat{H}\Psi\left(\{\vec{r_i}\},\{\vec{R_A}\}\right) = E\Psi\left(\{\vec{r_i}\},\{\vec{R_A}\}\right) \qquad (1.75)$$

where $\hat{H}$ is the Hamiltonian operator for a system of M nuclei and N electrons, which is described by position vectors $\vec{R_A}$ and $\vec{r_i}$, respectively. A representative molecular coordinates system for two nuclei A and B, two electrons i and j is shown in Fig. [1.3]. r_{Ai}=$|\vec{r}_{Ai}|$=$|\vec{R}_A - \vec{r}_i|$, represents the distance between the i^{th} electron and A^{th} nucleus ; r_{ij}=$|\vec{r}_{ij}|$=$|\vec{r}_i - \vec{r}_j|$ represents the distance between the i^{th} and j^{th} electron, and R_{AB}=$|\vec{R}_{AB}|$=$|\vec{R}_A - \vec{R}_B|$ is the distance between the A^{th} and B^{th} nucleus. The Hamiltonian in atomic units ($\hbar$=m_e=e=k=1) for N electrons and M nuclei is shown in Eq. [1.76].

$$\begin{aligned}\hat{H} &= \Bigg[-\sum_{i=1}^{N}\frac{1}{2}\nabla_i^2-\sum_{A=1}^{M}\frac{1}{2M_A}\nabla_A^2-\sum_{i=1}^{N}\sum_{A=1}^{M}\frac{Z_A}{r_{iA}} \\ &\quad +\sum_{i=1}^{N}\sum_{j>i}^{N}\frac{1}{r_{ij}}+\sum_{A=1}^{M}\sum_{B>A}^{M}\frac{Z_AZ_B}{R_{AB}}\Bigg]\end{aligned} \tag{1.76}$$

In Eq. [1.75], M_A represents the ratio of mass of the nucleus A to the mass of an electron, and Z_A depicts the atomic number of nucleus A. ∇_i^2 and ∇_A^2 are the Laplacian operators which depict the differentiation with respect to the coordinates of the i^{th} electron and the A^{th} nucleus. The first term and second term of Eq. [1.76] is the operator for the kinetic energy of the electrons and nuclei respectively; the third term represents the coulomb attraction term formed between electrons and nuclei; the fourth and fifth terms represents the repulsion between electrons and between nuclei, respectively. The Eq. [1.76] can be written in a more generic fashion in this form, $\hat{H} = \hat{T}_e(\vec{r}) + \hat{T}_N(\vec{R}) + \hat{V}_{eN}(\vec{r},\vec{R}) + \hat{V}_{NN}(\vec{R}) + \hat{V}_{ee}(\vec{r})$. The 2^{nd} and 4^{th} terms represent the kinetic and potential energy operators purely dependent on Nuclei coordinates, while other terms rely on the electronic or electronic-nuclear coordinates. Therefore, in a fixed nuclear approximation, the Hamiltonian $\hat{H}$ can be represented as the sum of electronic and nuclear hamiltonian. This approximation is discussed in the next section.

1.4.2 Born Oppenheimer Approximation

The Born-Oppenheimer approximation (BOA) is important and relevant concept w.r.t. quantum chemistry. The discussion in this section will provide qualitative description of BOA. Since, mass of nuclei is much more than electrons, and this is the reason nuclei are considered to move very much slower than the electrons. Therefore, one can consider electrons moving in the fields of nuclei to be a fairly good approximation.[87, 88]

$$\hat{H}_{ele} = -\sum_{i=1}^{N}\frac{1}{2}\nabla_i^2 - \sum_{i=1}^{N}\sum_{A=1}^{M}\frac{Z_A}{r_{iA}} + \sum_{i=1}^{N}\sum_{j>i}^{N}\frac{1}{r_{ij}} \quad (1.77)$$

Within this approximation, the second term of Eq. [1.76], the kinetic energy of nuclei will be a small number close to zero and therefore, it can be neglected. The last term of Eq. 1.76 is the repulsion between fixed nuclei which can be considered to be a constant. If a constant is added to an operator, it adds only to operator eigenvalues and no effect on the operator eigenfunction. The first, third and fourth terms of Eq. [1.76] makeup the electronic hamiltonian Eq. [1.77], describing the motion of N electrons in the field of M fixed nuclei or point charges. The solution from the Schrödinger equation using electronic hamiltonian $\hat{H}_{ele}$ given in Eq. [1.78] is,

$$\hat{H}_{ele}\phi_{ele} = E_{ele}\phi_{ele} \quad (1.78)$$

The ϕ_{ele} is called the electronic wave function

$$\phi_{ele} = \phi_{ele}(\{\vec{r}_i\};\{\vec{R}_A\}) \quad (1.79)$$

which represents the function describing the motion of electrons in atom and molecules. The electronic wave function ϕ_{ele} explicitly depends on the electronic coordinates and depends parametrically on the nuclear coordinates (refer Eq. [1.79]). Also, the electronic energy depends parametrically on nuclear coordinates (refer Eq. [1.80]).

$$E_{ele} = E_{ele}(\{\vec{R}_A\}) \quad (1.80)$$

By the parametric dependence in ϕ_{ele}, it is meant that, for different orientations of the nuclei in system, ϕ_{ele} is a different function of electronic coordinates. Hence, explicit dependence of nuclear coordinates does not appear in ϕ_{ele}. The total energy for a fixed nuclei system should include the constant nuclear repulsion term.

$$E_{tot} = E_{ele} + \sum_{A=1}^{M} \sum_{B>A}^{M} \frac{Z_A Z_B}{R_{AB}} \tag{1.81}$$

Since, the motion of electrons much faster than the nuclei, in the Eq. [1.76] one can replace electronic coordinates by their average values, averaged over the electronic wave function. This defines the motion of nuclei experienced in the average field of electrons as nuclear Hamiltonian.

$$\hat{H}_{nuc} = -\sum_{A=1}^{M} \frac{1}{2M_A} \nabla_A^2 + E_{ele}(\{\vec{R}_A\}) + \sum_{A=1}^{M} \sum_{B>A}^{M} \frac{Z_A Z_B}{R_{AB}} \tag{1.82}$$

$$\hat{H}_{nuc} = -\sum_{A=1}^{M} \frac{1}{2M_A} \nabla_A^2 + E_{tot}(\{\vec{R}_A\}) \tag{1.83}$$

The total energy $E_{tot}(\{\vec{R}_A)$ is a function for nuclear motion. The nuclei move on the potential energy surface obtained by solving the molecular electronic problem in Born-Oppenheimer approximation.Thus, the solutions, ϕ_{nuc}, obtained from nuclear Schrödinger Eq. [4.3],

$$\hat{H}_{nuc} \phi_{nuc} = E \phi_{nuc} \tag{1.84}$$

describe the vibration, rotation, and translation of a molecule. E describes, the sum of electronic, vibrational, rotational and translational energy. The

Born-Oppenheimer approximation to the total wave function of Eq. [1.75] is by the following form in Eq. [1.85],

$$\phi(\{\vec{r}_i\};\{\vec{R}_A\}) \quad = \quad \phi_{ele}(\{\vec{r}_i\};\{\vec{R}_A\})\phi_{nuc}(\{\vec{R}_A\}) \tag{1.85}$$

The electronic properties code and related work in the thesis is done by using the electronic wave functions.

1.4.3 The Molecular Electronic Wave function

In quantum mechanics, wavefunctions are mathematical construct that describe a particle's quantum state in a quantum system. For the time-independent wavefunctions such as many-electron molecular systems $\Psi(\vec{R}_A, \vec{r}_i)$, would be described by a function dependent on the variables of nuclear $\{\vec{R}_A\}$ and electronic $\{\vec{r}_i\}$ coordinates. According to the BO approximation, as in Eq. [1.85], the molecular wavefunctions can be approximated. It can be separated into two components, one nuclear part $\Psi_{nuc}(\{\vec{R}_A\})$ - purely dependent on the nuclear coordinates, while the other electronic part $\Psi_{ele}(\{\vec{r}_i\};\{\vec{R}_A\})$ - depending on electronic coordinates along with parametric dependence of nuclear positions. The nuclear wave functions in the total Hamiltonian provide constants to the whole property of the system. At the same time, the coefficients of electronic wave functions are found using the standard electronic structure methods and contribute to the total energy such that error in the exact property values is minimized.

The Eq. [1.77] depicts the electronic Hamiltonian and shows its dependence only on the spatial coordinates of the electrons. However, including the spin coordinates $\{\alpha(\omega)$,$\beta(\omega)\}$ along with the spatial $\{\vec{r}_i\}$, completely describes the four-dimensional electronic coordinates collectively by x as,

$$x = \{\vec{r}_i, \omega\} \tag{1.86}$$

For a N-electron system, the wavefunction is a function of x_1, x_2, x_3, $\cdots$, x_N coordinates, that is, $\Phi_{ele}(x_1$, x_2, x_3, $\cdots$, $x_N)$. Since, the electronic Hamiltonian does not include any sort of spin operations, making the wavefunction include spin actually does not make any difference. However, if we make the electronic wave function antisymmetric w.r.t the interchange of the coordinate x (both space and spin) of any two electrons, that is,

$$\Phi_{ele}(x_1, \cdots, x_i, \cdots, x_j, \cdots, x_N) = -\Phi_{ele}(x_1, \cdots, x_j, \cdots, x_i, \cdots, x_N) \tag{1.87}$$

This condition, also called the antisymmetry principle and is the mathematical form of statements from the *Pauli exclusion principle*. Therefore, the exact wavefunction solutions should also be antisymmetric, apart from satisfying the Schrödinger equations. Imposing antisymmetry in wavefunctions is constructed using the form of Slater determinants. Thus, the wavefunctions for many-electron systems are either a single determinant or a linear combination of many Slater determinants.

The molecular orbital is a wavefunction for a single electron particle in a many-electron molecular system. The spatial molecular orbital $\psi_i(\vec{r})$ shows the spatial distribution of the i^{th} electron as a function of position vector $\vec{r}$. $|\psi_i|^2\ d^3r$. It is the probability of finding the electron in the volume element d^3r around $\vec{r}$. The set of $\{\psi_i(\vec{r})\}$ for a many-electron system are found such that they should be an orthonormal set which is $\int \psi_i(\vec{r})\psi_j^*(\vec{r}) = \delta_{ij}$. These molecular orbitals can be thought of as a set of basis functions which could be span the whole molecular space.

In most cases, molecular orbitals are evaluated as the summation, which are the linear combination the set of atomic orbitals, shown here in through Eq. [1.88] as

$$\psi_i(\vec{r}) = \sum_{k=1}^{N_{bas}} C_{k,i}\phi_k(\vec{r}) \tag{1.88}$$

where N_{bas} represents the total number of atomic basis functions used, $C_{k,i}$ **are the real valued coefficients obtained from the solutions of TISE** and Φ_k are the atomic orbitals. These atomic orbitals are usually constructed using **Gaussian-type functions**. For the case of time-dependence in molecular orbitals is introduced in the Eq. [1.88] via a variable of time t, as shown in Eq. [1.89]

$$\psi_i(\vec{r}, t) = \sum_{k=1}^{N_{bas}} C_{k,i}(t)\phi_k(\vec{r}) \tag{1.89}$$

Note that, in this equation, the time dependence in the molecular orbital is because of the complex-valued and time-varying coefficients $C_{k,i}(t)$. These time-dependent coefficients are obtained at each time step from the solutions of TDSE. Therefore, the time-dependent molecular orbital could be complex-valued.

The Gaussian-type function are used in the calculation of molecular properties because of their ease in providing analytical forms in molecular integrals and therefore minimizing the efforts of computational cost. The atomic orbitals $\phi_k(\vec{r})$ are evaluated from a summation of primitive Gaussian-type functions (GTFs). The form of atomic orbital in Eq. [1.90]

$$\phi_k(\vec{r}) = \sum_j a_j G(\alpha, R_A, \vec{l}) \tag{1.90}$$

In this Eq. [1.90], a_j's represent the contraction coefficients of the primitive GTFs, $G(\alpha, R_A, \vec{l})$. The primitive GTFs in the cartesian form[72] is represented by the following Eq. [1.91],

$$G(\alpha, R_A, \vec{l}) = (x - x_A)^l (y - y_A)^m (z - z_A)^n exp(-\alpha|\vec{R}_A|^2) \tag{1.91}$$

The symbols, α, depict the exponent of GFT, R_A the center of GFT, $\vec{l}$ represents the angular quantum number/index l, m, n. For example, an S-type gaussian will have values of l=0, m=0, n=0, while the l, m, n values for $P_x/P_y/P_Z$-type gaussian are 1, 0, 0, 0, 1, 0 and 0, 0, 1. The distance between the point $\vec{r}$ and center $\vec{A}$ is represented by the $R_A = |\vec{r} - \vec{A}|$.

1.4.4 The Hartree-Fock Formalism

The antisymmetric principle, which follows the relation discussed in Eq. [1.86], is imposed on the spin orbitals of the electronic coordinates by making them using either a Slater determinant or a combination of Slater determinants has been discussed in the earlier section. considering an atom of two electrons, in the $1s^2$ state, then this electronic state can be described by two wave functions

$$\psi_{1,2} = 1s(1)\alpha(1)1s(2)\beta(2) \tag{1.92}$$

$$\psi_{2,1} = 1s(2)\alpha(2)1s(1)\beta(1) \tag{1.93}$$

where the number in bracket indicates electron 1 and electron 2. The two possible combinations are,

$$\psi_A = \frac{1}{\sqrt{2}}[1s(1)\alpha(1)1s(2)\beta(2) + 1s(2)\alpha(2)1s(1)\beta(1)] \tag{1.94}$$

$$\psi_B = \frac{1}{\sqrt{2}}[1s(1)\alpha(1)1s(2)\beta(2) - 1s(2)\alpha(2)1s(1)\beta(1)] \tag{1.95}$$

Here, ψ_A is the symmetric wave function, while ψ_B is the antisymmetric wave function. The factor $1/\sqrt{2}$ from the normalization of the total wave function. The antisymmetric wave function can also be written in terms of matrix determinant,

$$\psi_B(1,2) = \frac{1}{\sqrt{2}}\begin{vmatrix} 1s(1)\alpha(1) & 1s(2)\alpha(2) \\ 1s(1)\beta(1) & 1s(2)\beta(2) \end{vmatrix} \tag{1.96}$$

It becomes much more convenient when determinant are used to describe the electronic wave functions, since both the Pauli's exclusion principle (the determinant becomes null or zero, if two electrons occupy the same spin-orbital) and antisymmetry principle (the determinant will change sign when any two electrons switch its the position for a set of spin orbitals) are satisfied.

The Eq. [1.96], can be generalized for a N-electron systems occupying N spin orbitals χ_1, χ_2, $\cdots$, χ_N as

$$\psi(x_1, x_2, \cdots, x_N) = \frac{1}{(N!)^{1/2}} \begin{vmatrix} \chi_1(x_1) & \chi_2(x_1) & \cdots & \chi_N(x_1) \\ \chi_1(x_2) & \chi_2(x_2) & \cdots & \chi_2(x_2) \\ . & . & & . \\ . & . & & . \\ \chi_N(x_N) & \chi_N(x_N) & \cdots & \chi_N(x_N) \end{vmatrix} \tag{1.97}$$

Thus, writing the wavefunction in the form described by Eq. 1.97 is called Slater's determinant. The short hand notation for writing the Eq. [1.97] is

$$\psi(x) = |\chi_1 \chi_2 \cdots \chi_N\rangle \tag{1.98}$$

In order to solve Schrödinger equation exactly (Eq. [1.78]) for any molecular system is still mathematically not possible, due to the electron-electron repulsive term between in the electronic Hamiltonian (Eq. [1.77]). An alternative is to find the approximate wave function solutions for the multi-electron molecular systems. D. R. Hartree and V. Fock proposed a method for calculating the electron structure of atoms and molecules. In the Hartree-Fock formalism, the interaction potential of the electrons is represented by a mean-field potential, while the electronic wave function is approximated by the Slater determinant.

The working of Hartree-Fock formalism is based on variational principle, which specifies that the best electronic wavefunction is the one corresponding to the lowest possible energy nearer to the exact energy, when the spin orbitals of the system are varied. This means to find the set of wave functions which minimizes the expectation value of $\langle\psi|\hat{H}_{ele}|\psi\rangle$.

According to the variational principle, the expectation value of the energy is always an greater than or equal to the exact state energy. The mathematical form of which is,

$$\langle\psi|\hat{H}_{ele}|\psi\rangle \geq E_{exact} \tag{1.99}$$

The electronic Hamiltonian can be separated into one and two electron integral contributions

$$\hat{H}_{ele} = \sum_{i=1}^{N} \hat{h}(i) + \sum_{i=j}^{N}\sum_{j>i}^{N} \hat{g}(i,j) \tag{1.100}$$

where, $\hat{h}(i)$ and $\hat{g}(i,j)$ are

$$\hat{h}(i) = -\frac{1}{2}\sum_{i=1}^{N} \nabla_i^2 - \sum_{A=1}^{M} \frac{Z_A}{r_{Ai}} \tag{1.101}$$

$$\hat{g}(i,j) = \frac{1}{r_{ij}} \tag{1.102}$$

When we define the energy functional $E_0[\chi_i]$ for the ground state, we get,

$$E_0[\chi_i] = \langle\psi|\hat{H}_{ele}|\psi\rangle \tag{1.103}$$

To find the best wavefunction for the systems, the functional $E_0[\chi_i]$ should be minimized so that the molecular spin orbitals must also be kept orthonormalized,

$$\langle\chi_i|\chi_j\rangle = \delta_{ij} \tag{1.104}$$

The expectation value of the energy in the ground state E_0 is given by,

$$E_0[\chi_i] = \sum_{i=1}^{N}\langle\chi_i|\hat{h}|\chi_i\rangle + \frac{1}{2}\sum_{i=1}^{N}\sum_{j=1}^{N}(\langle\chi_i\chi_j|\chi_i\chi_j\rangle - \langle\chi_i\chi_j|\chi_j\chi_i\rangle) \tag{1.105}$$

In order to minimize this functional, we will use Lagrange's indeterminate multipliers method. A functional $L[\chi_i]$ is minimized which minimizes the functional E_0, subjected to the constraint of orthonormalization (Eq. [1.104]). This is given by,

$$L[\chi_i] = E_0[\chi_i] - \sum_{i=1}^{N}\sum_{j=1}^{N}\lambda_{ij}(\langle\chi_i|\chi_j\rangle - \delta_{ij}) \tag{1.106}$$

where the coefficients λ_{ij} are the Lagrange's indeterminate multipliers.

By infinitesimally varying the spin-orbitals functions, we get,

$$\delta L[\chi_i] = \delta E_0[\chi_i] - \sum_{i=1}^{N}\sum_{j=1}^{N} \lambda_{ij}\delta(\langle\chi_i|\chi_j\rangle - \delta_{ij}) \tag{1.107}$$

Using Eq. [1.105] in Eq. [1.107] explicitly in the new functional for the ground state, we obtain,

$$\begin{aligned}\delta L[\chi_i] \quad = \quad & \sum_{i=1}^{N}\sum_{j=1}^{N}\langle\delta\chi_i|\hat{h}|\chi_j\rangle + \sum_{i=1}^{N}\sum_{j=1}^{N}\langle\delta\chi_i\chi_j|\chi_i\chi_j\rangle \\ & + \sum_{i=1}^{N}\sum_{j=1}^{N}\langle\delta\chi_i\chi_j|\chi_j\chi_i\rangle \\ & + \sum_{i=1}^{N}\sum_{j=1}^{N}\lambda_{ij}\langle\delta\chi_i|\chi_j\rangle + complexconjugate \end{aligned} \tag{1.108}$$

We introduce, the Coulomb ($\hat{J}_j$) and Exchange ($\hat{K}_j$) operators,

$$\hat{J}_j(x_1)\chi_i(x_1) = [\int \chi_j(x_2)\frac{1}{r_{12}}\chi_j(x_2)dx_2]\chi_i(x_1) \tag{1.109}$$

$$\hat{K}_j(x_1)\chi_i(x_1) = [\int \chi_j(x_2)\frac{1}{r_{12}}\chi_i(x_2)dx_2]\chi_j(x_1) \tag{1.110}$$

Using the Eq. [1.109] and [1.110] in [1.108] can be re-written as,

$$\begin{aligned}\delta L[\chi_i] = \sum_{i=1}^{N}\int \delta\chi_i^*(x_1)\{\hat{h}(x_1)\chi_i(x_1) + \sum_{i=1}^{N}[\hat{J}_j(x_1) - \hat{K}_j(x_1)]\chi_i(x_1) \\ - \sum_{j=1}^{N}\lambda_{ij}\chi_i(x_1)\}dx_1 + complexconjugate \end{aligned} \tag{1.111}$$

The Coulomb repulsion arising from all other $N-1$ electrons, distributed as probability density, which is represented by Coulomb operator. The spin correlation is accounted by exchange operator, that is, the same spin electrons tends to be avoided, therefore reduces the global coulomb potential between them.

In order for the functional $L[\chi_i]$ to be a minimum, a condition imposed such that $\delta L[\chi_i] = 0$ on Eq. [1.111], and considering that the variation $\delta\chi_i^*$, we have,

$$\{\hat{H}(x_1) + \sum_{j=1}^{N}[\hat{J}_j(x_1) - \hat{K}_j(x_1)]\}\chi_i(x_1) = \sum_{j=1}^{N}\lambda_{ij}\chi_i(x_1) \tag{1.112}$$

There will be a similar expression for the complex conjugate. The term in brackets in Eq. [1.112] is called the Fock operator.

$$\hat{f}(x_1) = \hat{h}(x_1) + \sum_{j=1}^{N}[\hat{J}_j(x_1) - \hat{K}_j(x_1)] \tag{1.113}$$

Therefore, the Hartree-Fock equations can be written as,

$$\hat{f}(x_1)\chi_i(x_1) = \sum_{j=1}^{N}\lambda_{ij}\chi_i(x_1) \tag{1.114}$$

The Eq. [1.114] can be converted into a canonical eigenvalue equation through a unitary transformation, since the Fock operator is invariant under any unitary transformation. Therefore, it can be written as,

$$\hat{f}(x_1)\chi_i(x_1) = \in_i \chi_i(x_1) \tag{1.115}$$

In the Eq. [1.115], the Lagrange multipliers were replaced by $\in_i$ to indicate that it represents the energy. The Eq. [1.115] represents the canonical Hartree-Fock equations.

To obtain the spin-orbital functions $\chi_i(x_1)$, the Eq. [1.114] must be solved. The Coulomb operator [1.109] shows that it is necessary to know all the other occupied spin-orbital functions to gather the operators $\hat{J}_j$ and $\hat{K}_j$, and therefore obtain $\chi_i(x_1)$.

To overcome the problem, an initial form of all the spin-orbital wave functions of an electron is defined. These are used to define the Coulomb and exchange operators, and solve the canonical Hartree-Fock equations. The calculations is repeated until the energies and the new spin-orbitals functions remain unaltered i.e gets converged.

This method of solving is known as the Hartree-Fock Self-Consistent Field Method (HF-SCF). The numerical solutions of Hartree-Fock equations, have an operation count of $N^4/8$, where N is the number of basis functions of the system. Therefore, as the number of atoms and molecules increases, the HF method becomes computationally expensive. Another problem encountered with the Hartree-Fock method is that it uses only a single Slater determinant and treats the electron-electron interaction in an average way. So, this does not taken into account the correlated movements of the electrons, which does not include the small fraction of the total energy of the system. The difference between the exact energy and the Hartree-Fock energy is called the correlation energy.

$$E_{corr} = E_{exact} - E_{HF} \tag{1.116}$$

Thus, the correlation energy is an important aspect, and several methods methods have been developed over the years and implemented in the calculations, are called post-Hartree-Fock methods.

The present Thesis Work, we use the time evolving electronic wave functions from an in-house code Ab-Initio Electron Dynamics (ABELDYN), solving Real Time Hartree-Fock (RTHF) using (t,t′) method.[78, 84, 85] The molecular orbital coefficients of this electronic wavefunction are used as an input at each time step for the calculation of electronic properties. In the next subsections, we provide the description and working of in-house ABELDYN code, which we have used to obtain time-dependent molecular orbital coefficients.

1.4.5 The Real Time Hartree-Fock (RTHF) method

The work presented in the next chapters uses the wave functions obtained from the in-house code ABELDYN. This code incorporates the effects of external oscillating electric fields in the electronic Hamiltonian. This code is made to measure the ionization effects, with a complex absorbing potential applied outside the interaction region.

The RTHF procedure provides solutions for a fixed-nuclear geometry. The algorithm of ABELDYN code involves block diagonalization procedure of a time-dependent Floquet-Fock Matrix. The time-dependent Fourier components of the TD charge density matrix are calculated at each time-step of the propagation. This is done using a numerical integration of all the previous density matrices propagated in time. Thus, the Fourier components of this density matrix is used to construct a new Floquet Fock matrix. To obtain new set of molecular orbitals from the previous MOs, the exponential of the new formed Floquet Fock matrix is evaluated.

One of the advantages of using RTHF method implement in ABELDYN is that it incorporates electron correlation effects by using an extra time-dependent coordinate t′ in the extended Hilbert space. The TD density matrices carries the information of previous matrices and therefore, it is also referred to as *memory* of previous matrices. The wave function evolution performed is done using the (t,t′) method.

In the numerical formalism for the RTHF using (t,t′) method, we form the time dependent Eq. [1.117] for the molecular orbitals in Floquet Fourier basis, where the hamiltonain is Floquet Fock type Fock operator,

$$i\frac{\partial \Phi_F^i(t)}{\partial t} = \hat{F}_F \Phi_F^i(t) \tag{1.117}$$

Where, the form of Fock operator $\hat{F}(t')$ is defined in Eq. [1.118],

$$\hat{F}(t') = \hat{F}(t') - i\frac{\hat{\partial}}{\partial t'} \tag{1.118}$$

and the Floquet molecular orbitals $\Phi_F^i(t)$ are written in terms of spatial basis functions χ_μ. In the Eq. [1.119], χ_μ are the set of atomic orbitals, usually constructed from cartesian Gaussian basis sets,

$$\Phi_F^i(t) = \sum_\mu c_{\mu,i}(t)\chi_\mu \tag{1.119}$$

The Floquet molecular orbitals $\Phi_F^i(t)$, can also be expanded in terms of time-dependent Fourier basis functions $e^{in\omega t'}$ shown in [1.120]

$$\Phi_F^i(t) = \sum_\mu \sum_\nu c_{\mu,i}(t) e^{in\omega t'} \chi_\mu \tag{1.120}$$

The time-dependent Fock-matrix in the presence of linearly-polarized laser along Z is constructed as given in Eq. [1.121],

$$\mathbf{F}(t') = \mathbf{H}_{core} + \mathbf{G} - \vec{E}(t') \cdot \vec{r} \tag{1.121}$$

In Eq. [1.121], $\mathbf{H}_{core}$ is related to the free-field one-electron matrix and G is the two-particle operator. The term $\vec{E}(t') \cdot \vec{r} = E_0\mathbf{Z}cos(\omega t')$ depicts the energy due to dipole interaction for a linearly polarized laser along Z-direction. The Fourier components of G in atomic basis is defined in Eq. [1.122].

$$\mathbf{G}_n = \sum_{kl} P_n^{kl}[(ij|kl) - \frac{1}{2}(il|kj)] \tag{1.122}$$

The *memory* effect or the history of time-dependent molecular orbitals are included through the splitting of density matrix ($\mathbf{P}$) into time-dependent and time-independent matrices: $\mathbf{P}(t') = \mathbf{P}(t_0) + \Delta\mathbf{P}(t')$. The expansion of $\Delta\mathbf{P}(t'$ in terms of Fourier basis is given in Eq. [1.123]

$$\Delta\mathbf{P}(t) = \mathbf{P}_0 + \sum_{n=1}^{\infty} \mathbf{P}_n cos(n\omega t) \tag{1.123}$$

The matrix form of Floquet-Fock operator is given by Eq. [1.124]

$$\langle \chi e^{in\omega t'} \mid \hat{F}_F(t') \mid \chi e^{in'\omega t'} \rangle\rangle = [F_0 + n\omega\mathbf{I}]\delta_{nn'} + G_n\delta_{nn\pm m} + \frac{E\mathbf{Z}}{2}\delta_{nn\pm 1} \tag{1.124}$$

In Eq. [1.124], **I** denotes identity matrix, **Z** denotes the dipole matrix along Z axis and $E = E_0 cos(\omega t')$. The solution of Eq. [1.124] involves evaluating the exponential of the Floquet-Fock matrix via a unitary block-diagonalization routine. This is followed by the calculation of coefficient matrix given by Eq. [1.125],

$$\mathbf{C}_F(t,t') = e^{-\frac{i}{\hbar}\mathbf{G}_{\mathbf{F}}^{n}\Delta t/2} \dots e^{-\frac{i}{\hbar}\mathbf{G}_{\mathbf{F}}^{1}\Delta t/2} e^{-\frac{i}{\hbar}\mathbf{F}_{\mathbf{T}}\Delta t} e^{-\frac{i}{\hbar}\mathbf{G}_{\mathbf{F}}^{1}\Delta t/2} \cdots e^{-\frac{i}{\hbar}\mathbf{G}_{\mathbf{F}}^{n}\Delta t/2}\mathbf{C}_{\mathbf{F}}(t', t - \Delta t) \tag{1.125}$$

In Eq. [1.125], Δt denotes the time-step for propagation.

1.5 Electron Densities

For a many particle normalized wavefunction $\Psi(\vec{r}_1, \vec{r}_2, \cdots \vec{r}_N)$, the quantum mechanical electron density at the position vector $\vec{r}$ is a physical quantity defined as,

$$\rho(\vec{r}) = N \sum_{\sigma} \int \Psi^*(\vec{x}, \vec{x}_2, \vec{x}_3, \cdots, \vec{x}_N)\Psi(\vec{x}, \vec{x}_2, \vec{x}_3, \cdots, \vec{r}_N) d^3r_2 d^3r_3 \cdots d^3r_N \tag{1.126}$$

The summation in Eq. [1.126] runs over all the spin coordinates σ, and integrates over all but one spatial coordinates. N represents the total number of electrons in the system. This implies the integration of $\rho(\vec{r})$ over the total space would be equal to the N, represented by the following Eq. [1.127],

$$\int \rho(\vec{r}) d^3r = N \tag{1.127}$$

It is observed from Eq. [1.126] that the electron densities are scalar field, non-negative quantities for all points in molecular space, $\rho(\vec{r}) \geq 0$. The electron densities $\rho(\vec{r})$ depicts the probability of finding an electron in a infinitesimally small volume element d^3r which is directly proportional to $\rho(\vec{r})d^3r$.

The practical and analytical forms for the evaluation of electron densities for molecular orbitals or molecular wavefunctions is given the following form,

$$\rho(\vec{r}) = \sum_{i}^{occ} n_i \Psi_i^*(\vec{r})\Psi_i(\vec{r}) \tag{1.128}$$

Here, the index i, represent the total number of occupied orbitals, n_i represents the occupancy of the i^{th} orbital. For example, for a system with N occupied orbitals with each having an occupancy of 2 will have the following form,

$$\rho(\vec{r}) = 2\sum_{i}^{N} \Psi_i^*(\vec{r})\Psi_i(\vec{r}) \tag{1.129}$$

The Eq. [1.128] represent the electron densities using the natural spin orbitals. The molecular wavefunctions ψ obtained from the solutions of Hartree-Fock method, can be expressed in the form of Slater determinants constructed from the molecular orbitals. These molecular orbitals can be expressed as linear combination of atomic orbitals $\{\phi_i\}$. The form of electron density using this can be represented as,

$$\rho(\vec{r}) = \sum_{\mu\nu} P_{\mu\nu}\phi_\mu(\vec{r})\phi_\nu(\vec{r}) \tag{1.130}$$

Where μ, ν are the summation indexes running over all the orbitals (occupied + virtual), and $P_{\mu\nu}$ is called the charge density bond order matrix and is given by,

$$P_{\mu\nu} = 2\sum_{a}^{N/2} C_{\mu a}^* C_{\nu a} \tag{1.131}$$

where $C_{\mu a}$ are the coefficients of the molecular orbitals.

The forms of Eq. [1.131] discussed above represent the electron densities in time-independent scenarios, since the wavefunctions are time-independent. However, for the time-dependent wavefunction, for a fixed nuclear geometry, the forms for the evaluation of electron densities would remain the same.

The electron densities are also physical observable through scattering experiments and hence used in structure determination via X-ray experiments. In the next section, we discuss the critical points, its topology and its chemical applications.

1.5.1 Critical Points of electron densities

The electron densities $\rho(\vec{r})$ for multi electron atoms and molecules are real, continuous 3D scalar functions whose first derivative exists at every point $\vec{r}$ in the molecular space. At the position vectors, $\vec{r}_c$, where the first derivative of MED vanishes, that is, $\nabla\rho(\vec{r}) = \vec{0}$, are termed as the *critical points* of MED. The $\nabla\rho(\vec{r})$ is denoted by Eq. [1.132],

$$\vec{\nabla}\rho = \hat{i}\frac{\partial\rho}{\partial x} + \hat{j}\frac{\partial\rho}{\partial y} + \hat{k}\frac{\partial\rho}{\partial z} \tag{1.132}$$

At $\vec{r}_c$, whether the MED function $\rho(\vec{r})$ is a maximum, minimum or a saddle, is determined by the sign of its second derivative or curvature. The second derivative matrix of a 3D function is called Hessian matrix. The nature of CPs is completely defined by the real, and symmetric Hessian matrix, which is defined as referred in Eq. [1.133],

$$H = \begin{bmatrix} \frac{\partial^2\rho}{\partial x^2} & \frac{\partial^2\rho}{\partial x\partial y} & \frac{\partial^2\rho}{\partial x\partial z} \\ \frac{\partial^2\rho}{\partial y\partial x} & \frac{\partial^2\rho}{\partial y^2} & \frac{\partial^2\rho}{\partial y\partial z} \\ \frac{\partial^2\rho}{\partial z\partial x} & \frac{\partial^2\rho}{\partial z\partial y} & \frac{\partial^2\rho}{\partial z^2} \end{bmatrix} \tag{1.133}$$

The characterization or classification to identify the type of CPs is done by diagonalization and thereafter obtaining the eigenvalues of the Hessian matrix. In general, diagonalization of the N-dimensional matrix gives N eigenvalues. In our case, for MEDs, we are concerned only with a three-dimensional Hessian matrix. The number of non-zero eigenvalues of the Hessian matrix is called its *Rank*, R. The Rank of a matrix is also equal to the number of linearly independent eigenvectors. Therefore, Rank is the largest square sub matrix whose determinant is non-zero. When all the Hessian eigenvalues are non-zero, those CPs are called non-degenerate CPs. These non-degenerate critical points are said to be stable, that is, Small displacements in the nuclei do not change the nature of critical points. If at least one of the eigenvalues of the Hessian becomes equal to zero, which implies there will be linearly dependent eigenvectors of all. In this case, the determinant of the Hessian is equal to zero, and the Rank of the Hessian matrix decreases from 3 to a lower dimension. The CPs found in such a case are said to be degenerate CPs. Degenerate CPs should not be confused with CPs located at different positions with the same function value. Graphically, A critical point in a 3D function is said to be a degenerate CPs if $\nabla\rho(\vec{r}) = 0$, $|H| = 0$, and there is at least one direction where it behaves as *a point of inflection*, i.e., it cannot be defined as a maximum or a minimum. The degenerate critical points are considered unstable, which means that even a tiny change in the electron density caused by the displacement of nuclei would either vanish or bifurcate two non-degenerate stable critical points. Therefore, the Rank of the Hessian matrix is an important parameter representing the dimensionality of the found critical points, irrespective of its function dimensionality.

The eigenvectors of the Hessian matrix represent the local and orthogonal vector directions along which the critical point is defined. Its eigenvalues are also invariant to any coordinate transformations. For a N-dimensional

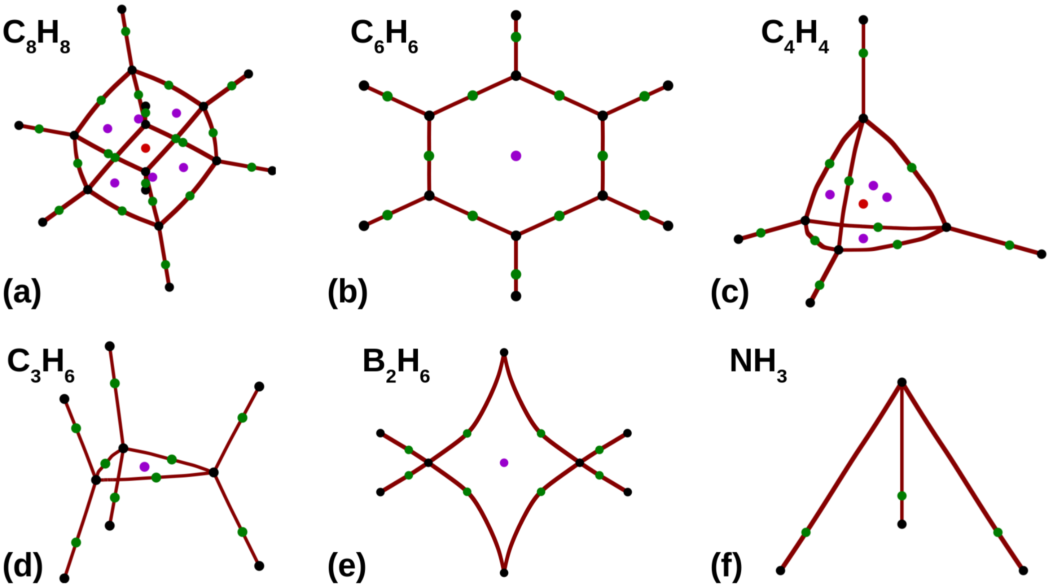

Figure 1.4: Molecular graphs for some prototypical molecules: (a) Cubane, (b) Benzene, (c) Tetrahedrane, (d) Cyclopropane, (e) Diborane, (f) Ammonia molecules are shown. Representation: (3,-3) - Black dots, (3,-1) - Green Dots, (3,+1) - Purple dots, (3,+3) - Red dots. The Maroon colored lines connecting the black dots via green dots depict the bond paths.

function, there can be N+1 types of non-degenerate critical points. Once a stationary point is identified ($\nabla\rho(\vec{r}) = 0$), to identify whether it is a maximum, minimum or a saddle, a term called signature, σ is calculated. The signature is defined as the sum of signs of the non-zero eigenvalues. So, the nomenclature used to classify the CPs are based on its values of rank and signature, depicted as (R, σ). For a 3D function, such as MED, there can be four types of non-degenerate CPs. Following are their types:

1. (3,-3): A critical point which is maximum in all directions.
2. (3,-1): The Hessian at this CPs has two negative and one positive eigenvalues. This represents a saddle CP, which is minimum in one direction while maximum in the other two directions.

3. (3,+1): A saddle critical point, which is maximum in one direction while minimum in the other two directions. There would be two positive and one negative eigenvalues of the Hessian at this CP.

4. (3,+3): Represents a critical point which is a local minimum in all directions.

These critical points of MED reflects its the molecular structure. The Fig. [1.4] present critical points of MED for some molecules. For all molecules, the two sets of (3,-3) CPs (black dots) next to each other are accompanied with (3,-1) CPs (green dots) lying in between. Also, the (3,+1) CPs are found in an enclosure of few (3,-3) CPs located in a circular fashion or ring. The (3,+3) CPs (red dots) are located only at the center of caged molecules (Cubane and Tetrahedrane). This relation of molecular structure through the critical points of MED is called *molecular graph*. For a fixed number of nuclei, the non-negative MED function follows a mathematical relationship called Poincaré-Hopf governs the number and type of critical points that can coexist in a system.

$$n_{-3} + n_{-1} + n_{+1} - n_{+3} = 1 \tag{1.134}$$

where n_{-3}, n_{-1}, n_{+1}, and n_{+3} is the number of $(3,-3)$, $(3,-1)$, $(3,+1)$ and $(3,+3)$ CPs. The collection of numbers (n_{-3}, n_{-1}, n_{+1}, and n_{+3}) is called the *characteristic set* of the molecule.

1.5.2 Topology of Electron Densities

Topology of atomic electron densities:

The distribution of atomic electron densities (AED) is quite simple. The distributions contain a maximum at the nuclear position, and the function monotonically decays off, going farther away from the atomic position's center. The 3D visual display would show the spherical symmetry ground state AED distributions. At the nuclear position, the spherical average of AED rigorously satisfies the Kato's cusp condition[89–92] as shown in Eq. [1.135]:

$$\frac{d\tilde{\rho}}{dr}|_{r=0} = -2Z\rho\tilde{(0)} \tag{1.135}$$

Where the spherically averaged charge density will be:

$$\tilde{\rho}(r) = \frac{1}{4\pi}\int_0^{\pi}\int_0^{2\pi}\rho(\vec{r})sin\theta d\theta d\phi \tag{1.136}$$

The asymtotic behaviour of charge density is described by the equation as follows,[93–96]

$$\frac{\partial ln[\tilde{\rho}(r)]}{dr}|_{r\longrightarrow\infty} = -2\sqrt{2\epsilon} \tag{1.137}$$

In the Eq. [1.135], Z represents the charge of the atomic nucleus, and ϵ in Eq. [1.137] represents the atomic ionization potential. At positions near the nucleus, the AED resembles e^{-2Zr}, and at far off nuclear regions AED follows $e^{-2r\sqrt{2\epsilon}}$. The logarithmic derivative of the density shows a series of shelves, one for each occupied orbital, between the cusp of electron density at the nucleus and the asymptotic decay. Some interesting postulates are proposed using the behaviour of $\tilde{\rho}(r)$ in the intermediate regions.[97, 98] The monotonic decay of ground state atomic density has been termed as monotonic density postulate.[99] For $0 < a < r$, the ground state atomic density can be expressed through the following relation,

$$\tilde{\rho}(r-a) > \tilde{\rho}(r) > \tilde{\rho}(r+a) \tag{1.138}$$

The relation in Eq. [1.138] can also be expressed as $d\rho/dr < 0$ for all r. Therefore, the charge densities always rise to maximum towards the nucleus, follow monotonic decay, and fall off exponentially. This is why AED does not contain any CPs other than nuclear maxima.

Topology of molecular electron densities:

The topographical picture of MEDs does not show monotonic decay in all directions, unlike AEDs. The sum of AEDs to form MEDs brings in drastic changes in the topological features of MEDs. The binding of AEDs leads to the redistribution of total electron densities in MEDs, as seen from its isocontour plots. In MEDs, the maxima at nuclear positions are their dominating topological features. The Kato's cusp condition at the nuclear position is still valid and similar to that of an isolated atom discussed earlier via Eq. [1.135]. However, MEDs do not follow for spherically averaged charge density relation as in Eq. [1.136]. For the molecular case, the Kato's cusp condition with nuclear position $\vec{R}_A$ as center follows Eq. [1.139]

$$\frac{d\tilde{\rho}}{dr}|_{r=0} = -2Z_A\tilde{\rho}(\vec{R}_A) \tag{1.139}$$

Similar to the AEDs, the asymptotic decay for MED is,

$$\tilde{\rho}(r)|r \longrightarrow \infty = r^{[(Z_{total}-N+1/\sqrt{\epsilon})-1]}e^{-2r\sqrt{2\epsilon}} \tag{1.140}$$

In Eq. [1.140], ϵ is the molecular ionization potential with effective screening for the charge. Now, with the asymptotic and the nature of MEDs at nuclear position understood, we analyze at the topology at the internuclear regions, giving rise to new topological features.

Fig. [1.4] presents the MED isosurface plots for some small molecules. The MED plots of these molecules depict the existence of maxima at the

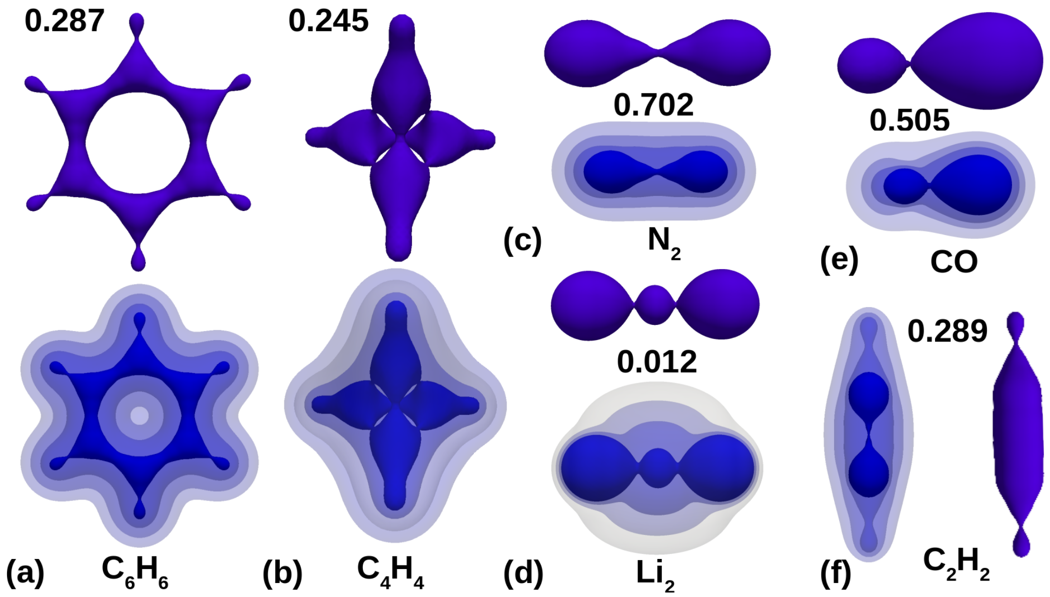

Figure 1.5: MED isosurface plots (Top: Blue colored plots) for some prototypical molecules: (a) Benzene, (b) Tetrahedrane, (c) Dinitrogen, (d) dilithium, (e) carbon monooxide, (f) ethylene molecules are shown. The top blue colored plot shows the density isosurface at one of their (3,-1) CPs (ρ_{-3}). The bottom blue colored plots depict density isosurfaces at decreasing MED values such that $\rho < \rho_{-3}$.

nuclear positions. However, from topography, it is seen that between two maximums, the MED function passes through at least a minimum. It is presented as a (3,-1) CP, a minimum along the direction connecting the two nuclei, and maxima along all other directions.[20, 100] Therefore, a directional minimum between two maximums is a topological necessity. The directional minimum would exist in several directions for a continuous 3D MED function and form a minimum density surface, also known as a *zero-flux surface*. For cyclic molecules, such as Benzene (See Fig. [1.4] (a)) or cyclopropane, there exists a (3,+1) CP, which is minimum in two directions (here, directions along the molecular plane), while maximum in one direction (perpendicular to the molecular plane). Since the (3,+1) CP generally exists only in molecules with nuclei arranged in an enclosed ring, they are called ring critical points. They are usually located at the geometrical center of the cyclic molecules. For caged molecules, for example, tetrahedrane (See Fig.

[1.4] (b)) or cubane, a (3,+3) CP is found. These CPs are found at the center of the caged molecule and depicts a local minimum of the electron density distribution.

There have been exceptions in finding maximums being found only at the nuclear positions of molecules. The MED of Molecules, such as Li_2, Na_2 have been found containing (3,-3) CPs, local maxima, at postions other than nuclei. These CPs are called non-nuclear maxima (NNMs) or non-nuclear attractors (NNAs).[101] The MED values of NNMs are usually very low when compared to MED values of nuclear maxima. The NNMs in MEDs are also termed as psuedoatoms. Fig. [1.4] (d), depicts the MED plot of Li_2 molecule, having a NNM at its center with $\rho = 0.012a.u.$ In diatomic molecules, its origin has been attributed to the evolution of chemical bonding as internuclear distances decrease.[102] NNMs have been experimentally detected in some metals such as Si clusters.[103]

1.5.3 Gradient Vector Fields, Bond Paths, and Zero-Flux Surfaces

Trajectories of the gradient vector field:

The gradient vector fields of electron densities are obtained by tracing out trajectories from the vector $\vec{\nabla}\rho(\vec{r})$. This trajectory of $\vec{\nabla}\rho(\vec{r})$ is called gradient paths of electron densities. The gradient paths could be traced out from a point, say $\vec{r}_0$, by displacing a distance $\Delta\vec{r}$ away from this point along the direction indicated by $\Delta\rho(\vec{r}_0)$. The displacement process from the previous points is repeated until the path generated terminates. This activity is similar to approximating a function f(x) numerically. The function f(x) can be written in terms of its tangent line at x_0, f($x_0 + \Delta x$) = f(x) + (df/dx)Δx. This definition of derivative becomes exact in the limit $\Delta x \longrightarrow 0$.

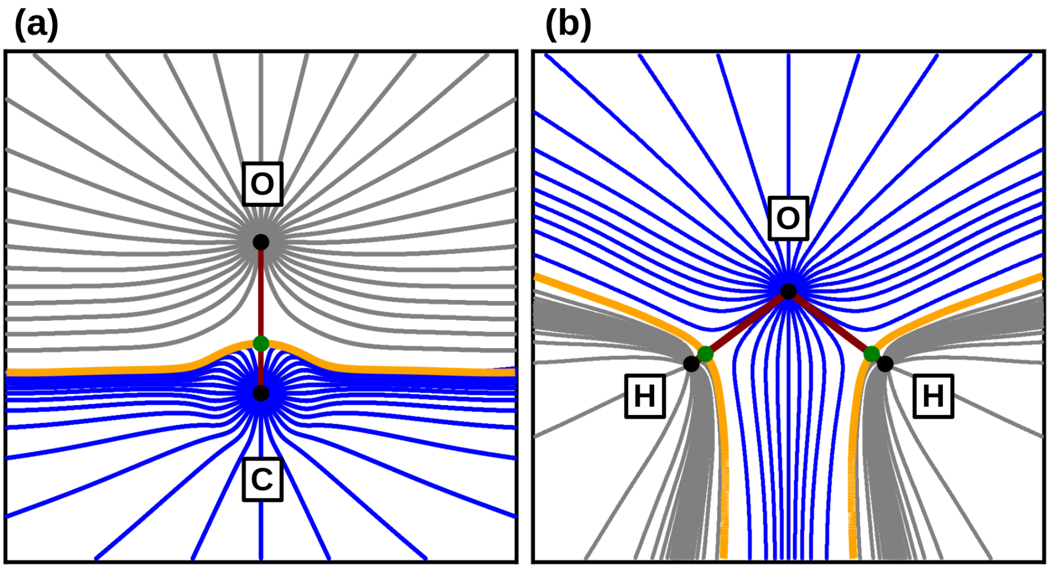

Figure 1.6: Plots depict the gradient vector field lines for two molecules, (a) Carbon Monoxide and (b) Water Molecules, on the molecular planes. The gradient field lines in the different basins on the molecular plane are plotted with different colors. The yellow colored line separates the two regions in the molecular plane. It is the only gradient field line which converges to a (3,-1) CP. The black dots and green dots represent (3,-3) and (3,-3) CPs. The maroon colored line depict the bond paths.

Fig. [1.5] represents the gradient vector field lines on the molecular plane for two molecules, CO, and H_2O. The trajectories of gradient field lines, also called gradient paths follows the following few properties,

1. At each $\vec{r}$, the $\nabla\rho(\vec{r})$ is a tangent to its trajectory.
2. The trajectories of $\nabla\rho(\vec{r})$ never cross each other.
3. Every trajectory originates or terminates at those points in space where $\nabla\rho(\vec{r}) = 0$, which implies critical points.
4. The gradient field lines at any point $\vec{r}$ always points towards the direction of greatest increase. Therefore, when followed always terminate to one of the local maxima.

The gradient paths depicted in Fig. [1.5], is an integral curve solving of the following differential Eq. [1.141],

$$\frac{dr(s)}{ds} = \nabla\rho(r(s)) \tag{1.141}$$

where the function r(s) implies that a point r on a given trajectory is dependent on the parameters s. The Eq. [1.141] is a 3D first order differential equation. Unique solutions are obtained for every initial values assigned to the three constants of integration. For example, initial value $s = s_0$, any trajectory passing through the point r(s_0) is obtained from the integrating Eq. [1.141], given by the following Eq. [1.142],

$$r(s) = r(s_0) + \int_{s_0}^{s} \nabla\rho(r(t))dt \tag{1.142}$$

Therefore, the trajectories of gradient paths of $\rho(\vec{r})$ are curves of parameterized integral solutions of the differential equation for $\nabla\rho(\vec{r})$. For a given point on a trajectory, the solutions of Eq. [1.142] can provide all the other points which fall on the same trajectory.

All except few of the trajectories presented in Fig. [1.5] originate at infinity and terminate at one of the (3,-3) CPs, the local maxima. Two trajectories and four trajectories of the gradient field lines plots in Fig. [1.5] (Yellow lines) terminate at the (3,-1) CP. All trajectories fall in one of the three types: (i) those originating from infinity and terminating at maximum, they called called attractors, (ii) those originating from a minimum and terminating at maximum, they are called repellers, and (iii) those originating from infinity and terminating at a saddles maximum direction.

Bond Paths:

Fig. [1.5] shows pairs of gradient lines (maroon colored) that originate at the (3,-1) CP and terminates at the neighboring (3,-1) CPs. The eigenvector corresponding to the unique positive eigenvalue of the (3,-1) CPs defines these trajectories. These gradient paths represent a line through the electron density distribution connecting the neighboring (3,-3) CPs. The $\rho(\vec{r})$ is the maximum w.r.t to any neighboring line for trajectories following along this line. Such lines are found between such pairs of nuclei whose atomic basins share a common interatomic surface. Generally, it is called *atomic interaction lines*.[20, 104, 105]

The presence of the atomic interaction lines indicate the electron density accumulation in between the pair of nuclei that are linked. The (3,-1) CP which lies inbetween the atomic interaction lines. It has two positive eigenvalues, which indicates the electron density being a maxima in the two directions perpendicular to the atomic interaction line. This line intersects the interatomic surface at the (3,-1) CP. From the theorectical observations, it could be concluded that accumulations of electronic density is necessary if two atoms are bonded to one another. Therefore, this interatomic line is also refered to as bond paths since it is line of maximum electron density connecting two bonded nuclei or (3,-3) CPs.[105]

For a given configuration **X** of nuclei, the union of closure of bond paths is called *molecular graph*. Fig. [1.4] shows a picture of the molecular graph presenting the network of bond paths linking pair of neighboring nuclei. It is to be noted that the bond path is not same as a representation of a bond. The existence of a bond path between a pair of nuclei indicates that the corresponding atoms are bonnded to one another. This interactions can be quantified in terms of the properties of electron density and its (3,-1) critical points.

Zero-Flux Surfaces:

Fig. [1.5] shows a gradient vector line (yellow colored) converging into the

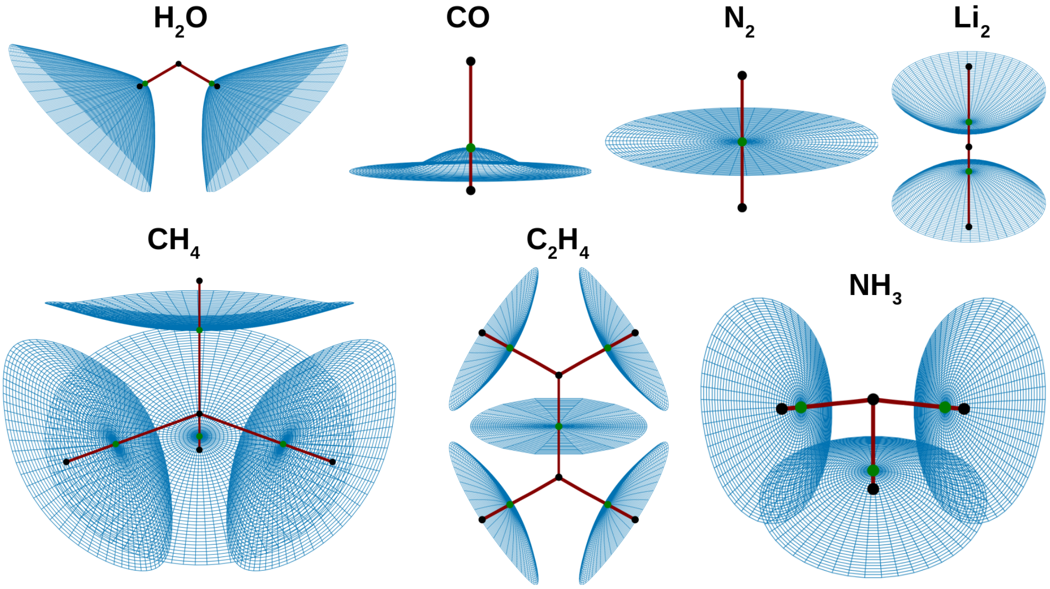

Figure 1.7: The plots shows zero-flux surface of the following molecules: H_2O, CO, N_2, Li_2, CH_4, C_2H_4, NH_3. The black and green dots represent the (3,-3) and (3,-1) CPs. The bond paths are depicted with the maroon colored lines.

(3,-1) CP. It acts as the *basin boundary* line on the plane, which divides the area on the molecular plane. A boundary on the whole molecular space is imposed using a plane called zero-flux surface which could be constructed using the two eigenvectors associated with negative eigenvalues of (3,-1) CPs. Since they exist between atomic basins, zero-flux surfaces are also referred to as interatomic surfaces. The zero-flux surface is defined as points $\vec{r}$ in the molecular space where the direction of the first derivative vector of $\vec{\nabla}\rho(\vec{r})$ is perpendicular to the unit normal surface. Mathematical, it satisfies the dot product between the two vectors to be zero, that is, $\vec{\nabla}\rho(\vec{r}) \cdot \hat{n} = 0$.

The response to perturbations in the electron densities could be pictured from the changes in its respective gradients and zero-flux surfaces. Eberhart and coworkers studied the influence of zero-flux surfaces on chemical reactions. They introduced the concept called *gradient bundle analysis*[106, 107] using the ideas from QTAIM and conceptual DFT. Using this concept they showed how motion of zero-flux surfaces between and within atomic basins plays a role in determining the energetic changes in undergoing chemical reactions.[29]

Fig. [1.7] The uniqueness regarding the zero-flux surfaces of MED is that they are curved and open surfaces. It is observed the nature of curvature is concave towards the less electronegative atom of the two bonded atoms. In addition to this, the zero-flux surfaces are close to the less electronegative atom. The presence of zero-flux surfaces in MED distributions has given the idea of partitioning the molecular space into disjoint non-overlapping regions. Hence, it led to the developing of a new theory called *quantum theory of atoms-in-molecules*. The QTAIM will be discussed in the next section.

1.5.4 Laplacian of Molecular Electron Densities

The Laplacian of MED $\nabla^2\rho(\vec{r})$ is a quantity derived from the double derivative Hessian matrix of MED function as the sum of its diagonal elements. The mathematical form of $\nabla^2\rho(\vec{r})$ is,

$$\nabla^2\rho(\vec{r}) = \frac{\partial^2\rho}{\partial x^2} + \frac{\partial^2\rho}{\partial y^2} + \frac{\partial^2\rho}{\partial z^2} \tag{1.143}$$

Laplacian of MED gives the local measurement of the charge concentration. If the value of MED $\rho(\vec{r})$ is greater than the average of its values over an infinitesimal sphere centered at $\vec{r}$, then $\nabla^2\rho(\vec{r}) < 0$. This example implies that a negatively valued Laplacian depicts a local charge concentration of MED. Similarly, when $\nabla^2\rho(\vec{r}) < 0$, the MED function value is less than the average of its values over an infinitesimal sphere centered at $\vec{r}$. The Laplacian at this $\vec{r}$ shows a local charge depletion.[20] The Laplacian can also be directly derived from the wave functions. The AED distribution is monotonically decreasing away from its center, however, there exist a wealth of topological features in the Laplacian of AED. The Laplacian of charge density is also related to the shell structure of atoms. The number of shells is found out by identifying the number of nodes in Laplacian, that is, at points $\vec{r}$ where $\nabla^2\rho(\vec{r}) = 0$. This kind of definition of shell structure for atoms was valid only for atoms with principle quantum number less than 20 (element - Calcium). The outer quantum shell of atom was divided into two regions, the first one is the inner region where $\nabla^2(\vec{r}) < 0$, and the second one as the outer region where $\nabla^2(\vec{r}) > 0$. The inner region is called valence shell charge concentration (VSCC) region.

The negative Laplacian in the regions of molecular space corresponds to covalently bonded regions. Therefore, this has been used as a sign of covalent bonding in the literature. Lone pair in molecules cannot be observed from the topological features of MED, but can be observed in terms its Laplacian's CPs. The works presented in the thesis only deals with the interpretation of Laplacian evaluated on regular grids. We do not compute its topographical features such as critical points.

1.5.5 Quantum Theory of *Atoms-In-Molecule*

Bader and coworkers proposed the quantum theory to define a bound atoms in a molecule. Since atoms or groups of atoms exhibit a characteristic set of properties, they postulated the existence of atoms in a molecule which led to the development of *quantum theory of atoms-in-molecule*.[20] Therefore, the theory of atoms in molecule is a result of observations made on the properties of MED.

First observations of *atoms-in-molecule* came from the investigation of the MED's isocontour plots of the Lithium-based diatomic molecules, LiX (X = H, F, O) by Bader and Beddall.[108] They introduced the consequences of a quantum mechanical description of an atom in a molecule. Bader defined bounded atoms in a molecule as the regions occupying non-overlapping, mutually exclusive subspaces of the total molecular space, each bounded by the zero-flux interatomic surfaces. These surfaces satisfy the zero-flux surfaces condition, that is given by the following Eq. [1.144],

$$\vec{\nabla}\rho(\vec{r}) \cdot d\vec{S} = 0 \tag{1.144}$$

These regions are called *Bader atoms*. Each region must contain only a single (3,-3) CP, *a local maximum* of MED. Therefore, the properties associated with regions is assumed to be average property of the subspace/region or Bader atoms.

The following conclusions were drawn by Bader and Beddall,[20, 108]

1. The total energy of the molecule can be expressed as the sum of all the atomic energies of the Bader atoms.
2. The average potential energy of an atom is defined as the average of the virial forces on it.
3. A relationship must exist between the distribution of charge and the virial of the total force exerted on each element of the charge density, the virial field.

The Laplacian of electron density integrated over these atomic regions Ω is zero (See Eq. [1.145]), which is proved using the zero-flux condition[20, 109] and the divergence theorem.[111]

$$L(\Omega) = \int_{\Omega} \nabla^2 \rho(\vec{r}) d^3 r = 0 \tag{1.145}$$

The Kinetic energy densities, $K(\Omega)$ and $G(\Omega)$ could be defined using the Eq. [1.145] as

$$K(\Omega) = -\frac{N}{4}\int_{\Omega}\int\cdots\int[\Psi^{*}(\vec{r},\vec{r_2},\cdots,\vec{r_N})\nabla_{\vec{r}}^{2}\Psi(\vec{r},\vec{r_2},\cdots,\vec{r_N}) \\ +\Psi(\vec{r},\vec{r_2},\cdots,\vec{r_N})\nabla_{\vec{r}}^{2}\Psi^{*}(\vec{r},\vec{r_2},\cdots,\vec{r_N})]d^3r_2\cdots d^3r_N d^3r \quad (1.146)$$

$$G(\Omega) = \frac{N}{2}\int_{\Omega}\int\cdots\int\nabla_{\vec{r}}\Psi^{*}(\vec{r},\vec{r_2},\cdots,\vec{r_N})\bullet\nabla_{\vec{r}}\Psi(\vec{r},\vec{r_2},\cdots,\vec{r_N}) \quad (1.147)$$

are equal quantities, Therefore,

$$L(\Omega) \equiv K(\Omega) = G(\Omega) = -\frac{1}{4}\nabla^2\rho(\vec{r})d^3r = 0 \quad (1.148)$$

Ψ depicts the total wave function of $\rho(\vec{r})$. The Eq. [1.148] represents the atomic virial theorem. In a numerical verification, small errors in the virial relationship may occur due to error in finding the right boundary surface or truncation errors in basis sets. For a perfect integration, the Laplacian integrated over atomic basin$L(\Omega)$ should be a number very small number close to zero in Eq. [1.148]. This is taken to be the fundamental *boundary condition* for an atom in molecule. The conditions validates the atomic virial theorem. Thus, the quantum mechanics of a Bader atom can be defined.[20] Using the Schwinger variation principles, several verifications of the QTAIM has also been provived.[112, 113]

Several atomic properties could be evaluated over the atomic regions Ω_A bounded by the zero-flux surfaces. Some of the commonly known properties such as norm, charges, electrostatic moments, electronic energy E_e, dipole moments of atomic regions Ω in the molecular space of MED can be defined as,

$$Norm \Rightarrow N(\Omega) = \int_{\Omega} \rho(\vec{r}) d^3 r \tag{1.149}$$

$$Charge \Rightarrow q(\Omega) = Z_A - \int_{\Omega} \rho(\vec{r}) d^3 r \tag{1.150}$$

$$ElectrostaticMoments \Rightarrow M_n(\Omega) = \int_{\Omega} r_{\Omega}^n d^3 r \tag{1.151}$$

$$DipoleMoment \Rightarrow \mu_x(\Omega) = \sum_{\Omega} Z_{\Omega} x_{\Omega} - \int_{\Omega} x \rho(\vec{r}) d^3 r \tag{1.152}$$

$$ElectronicEnergy \Rightarrow E_e(\Omega) = \frac{1}{2} \int_{\Omega} d^3 r \int \int \int \cdots \int \psi^* \nabla^2 \psi d\vec{r}_2 d\vec{r}_3 \cdots d\vec{r}_N \tag{1.153}$$

The shapes and sizes of Bader's atomic regions are not regular shapes and are bounded by open zero-flux surfaces. Locating these regions in molecular space is a challenging task. Therefore, In literature, the knowledge from the critical points and gradient paths of MED has been employed to find the zero-flux surfaces and identify the atomic regions in the molecular space. In the forthcoming thesis chapter, we will discuss the methods employed to find out Bader atomic regions and evaluate their average properties.

1.5.6 Chemical Applications of Electron Densities

Apart from being a descriptor for structure determination from the X-ray diffraction experiment observations or theoretical calculations, the eigenvalues of the Hessian matrix and electron density at the corresponding (3,-1) CP of MED have been used to identify bonding interactions such as bond ellipticity and bond orders in various molecular systems.[114–118]

Bader and co-workers have employed QTAIM which show that the charge density of topological atoms and the functional groups they comprise is transferrable.[119–121] That is, the charge densities of the same functional groups in different molecules are virtually identical. In the recent past, Eberbart and co-workers have developed QTAIM-based methods, called bond bundle and gradient bundle models. This have been used to investigate chemical reactivity, chemical bonds, and bond dissociation in molecules.[122–128]

The bond ellipticity ϵ is the estimation of amount of π *character* present in a bond. This is given in terms of the two negative curvatures (λ_1, λ_2, where $|\lambda_1| > |\lambda_2|$) via the relation as ϵ=(λ_1/λ_2 -1). The value of bond ellipticity $\epsilon > 0$ for a π bond, while for a triple bond it is close to zero. The empirical relation of bond order, $n = \exp[A\rho(r) - B]$ (where A and B are constants) evaluates the values as 1.0, 2.0 and 3.0 for ethane, ethylene and acetylene molecules respectively. Also, the position of the (3,-1) CP provides the measure of bond polarity.[2] The $\pi - \pi$ stacking interactions in benzene dimers and in stacked DNA bases and base-pairs have been found to be highly correlated to the (3,-1) CP and (3,+3) CP data between π-stacked monomers.[129–131] The potential energy density at the (3,-1) CP has been shown to be highly correlated with hydrogen bond energies.[132] The full interaction potentials in hydrogen bonds were recovered from the potential energy density at the (3,-1) CP. [133] The Bond CP properties has been used to study of drug design, a field pioneered by popelier and coworkers. These authors proposed the construction of a vector space from bond properties evaluated at the bond critical points, i.e. a point in this space is specified by a set of bond properties.[134–137]

1.6 Plan of the Thesis

In this thesis, we attempt to study the dynamics of molecular electron densities through its time-varying topographies, bond paths, zero-flux surfaces, and atoms-in-molecule properties in a laser. So, to begin with, in Chapter 1 of the thesis, we provide an introduction to the basic definitions, terminologies, and concepts essential to understanding subsequent Chapters. It introduces the electronic structure of atoms and molecules, the standard solutions of time-independent and time-dependent Schrödinger equations to obtain the wave functions essential to evaluate electron densities and properties. We describe the definition of LASERs and their various phenomena. We define gradients, critical points, and zero-flux surfaces in topology w.r.t 3D function. Bader's quantum theory of atoms-in-molecules is briefly explained. Additionally, the chemical applications of electron densities are mentioned. The final section of this chapter describes the plan for the thesis.

Chapter 2 describes the working of the code: **Ab-Initio Electronic Dynamics Properties**. The information on wave functions at each time step in the time-varying LASER field is used to evaluate the dynamics of electron densities and their properties. The code can compute time-dependent electronic properties - Molecular Electron Densities (MEDs) with their gradients, Hessians, Laplacians, vector-current densities, molecular orbitals, and electron localization function (ELF) for a multi-electron molecular system in position space over a three-dimensional cartesian grid. The code can compute the dynamics of topographies in time-dependent MEDs (TDMED). It can search for critical points, bond paths, and zero-flux surfaces in dynamical TDMED's molecular space. The ABELDYNPROP code can be employed to compute properties from **atoms-in-molecules** analysis in the presence of polarized LASERs. In principle, the code can work for specifically electronic wave functions obtained from any method solving the time-dependent Schrödinder equation. The work uses electronic wave functions from an in-house code-solving time-dependent Hartree-Fock (TDHF). The molecular orbital coefficients of the wave function are taken as input at each time step of the time-dependent electronic structure calculation. The analytic expressions of MED, their gradients, hessian, Laplacian, and ELF are evaluated primarily at all time steps using cartesian Gaussian basis sets over a grid. Apart from time-dependent properties, time-independent electronic properties in position space have also been integrated into this package. The program is written in FORTRAN 90 and is executed through a shell script. The code is also tuned for multi-processor machines with distributed memory through a message-passing interface (MPI). The package has been bench marked for various Gaussian basis sets for different molecules, showing a linear speedup on a parallel architecture.

In Chapter 3, using the ABELDYNPROP code on atoms in high intensity and high frequency linearly polarized laser field is investigated. We take Helium and Beryllium atoms in the presence of linearly polarized LASER fields as the test cases for studying. The energy difference between the atom's highest occupied and lowest unoccupied orbitals is the frequency of LASER used, while 0.10 a.u. is the LASER's electric field strength employed. In free-field cases, atomic electron density distribution shows a maximum at/near the nuclear position. At the same time, the distribution decays off in all the other directions of nuclear space. The isocontours of free-field atomic densities would depict concentric circles on a 2D plot throughout the position space. Since the free-field distribution remains the same along all the directions, i.e., X, Y, and Z. Any direction of laser polarization taken would show the same results. However, we have chosen Z as the direction of polarization. The investigation of dynamical atomic electron densities reveals the distributions get oriented along the path of LASER polarisation, that is, Z. The time-evolving atomic electron densities broaden in the ±Z directions. On the other hand, the electron densities shrink in the X and Y, the direction perpendicular to the laser polarization. The dynamical topographies show new critical points in the electron density distribution. In particular, it was observed that non-nuclear maxima (NNM) appear at peaks or valleys time steps of the LASER pulse. The NNMs are located on the ±Z axis. The NNMs are also accompanied by (3,-1) and (3,+3) critical points in some cases. The dynamics of gradient paths show the bends in the direction perpendicular to the direction of LASER polarization. The atoms-in-molecule analysis is done for dynamical atomic densities, which reveal the distribution of charges and norms. The nature of charge and norm follows in sync with the LASER pulse. New regions containing the NNM are also identified, and their respective charge and norms are evaluated.

Chapter 4 presents time-evolving molecular electron densities and their gradient lines, Laplacian, and difference electron densities in a linearly polarized laser field for the test case molecules, Hydrogen Fluoride, Water, Methane, and Ethylene molecules. The polarization direction of the laser field creates symmetric and cyclic deformations along the direction of polarization along the laser pulse. The gradient lines bend perpendicular to the direction of polarization, and the Laplacian shows plots depicting charge concentrations at either terminal of molecular space along the path of polarization. The contour plots' difference electron densities demonstrate increments or decrements in the molecular electron density in either direction of polarizations over the regions in the molecular space. For example, the positive-valued isocontours appear in one direction, while negative-valued isocontours would appear in the opposite direction. It was also noticed that the plot of the

MED-values of the bond critical points shows an oscillatory behavior along the laser pulse. In cases of Hydrogen Fluoride and a water molecule, the distance between the bond critical points and its nearest maximum critical points came very close. The closeness was such that the two critical points coalesced near that point. The novelty of the work lies in the newly found critical points of TDMED, especially non-nuclear maxima, through the topological analysis of all the test cases. The electronic population analysis done for the newly formed basins due to the creation of NNMs shows a significant number of electrons residing in these regions.

References Chapter 1

[1] J. Als-Nielsen, and D. Mcmorrow *Elements of Modern X-ray Physics*, John Wiley and Sons, ltd. 2011.

[2] R. G. Parr, and W. Yang *Density Functional Theory of Atoms and Molecules*, Clarendon Press, Oxford, 1989.

[3] C. Pellegrini, A. Marinelli, and S. Reiche, The physics of x-ray free-electron lasers, *Rev. Mod. Phys.* **88**, 015006 (2016)

[4] P. Emma, R. Akre, J. Arthur et al., First lasing and operation of an Angstrom-wavelength free-electron laser, *Nat. Photon.* **4**, 641 (2012)

[5] T. Ishikawa, H. Aoyagi, T. Asaka et al., A compact X-ray free-electron laser emitting in the sub-angstrom region, *Nat. Photon.* **6**, 540 (2010)

[6] N. Hartmann, G. Hartmann, R. Heider et al., Attosecond time–energy structure of X-ray free-electron laser pulses, *Nat. Photon.* **12**, 215 (2008)

[7] J. Duris, S. Li, T. Driver et al., Tunable isolated attosecond X-ray pulses with gigawatt peak power from a free-electron laser, *Nat. Photon.* **14**, (2020)

[8] E. Lindroth, F. Calegari, L. Young et al., Challenges and opportunities in attosecond and XFEL science, *Nat. Rev. Phys.* **1**, 107 (2017)

[9] M. Peplow, The next big hit in molecule Hollywood, *Nature* **544**, 408 (2017)

[10] G. Dixit, and R. Santra, Imaging electronic quantum motion with light, *Proc. Natl. Acad. Sci. USA* **109**, 11636 (2012)

[11] K. Barrett, A. Metrano, and P. Rablen, Spontaneous transfer of chirality in an atropisomerically enriched two-axis system, *Nature* **509**, 71 (2014)

[12] A. H. Zewail, Femtochemistry: Atomic-Scale Dynamics of Chemical Bond, *J. Phys. Chem. A* **104**, 24 (2000)

[13] A. Douhal, S. K. Kim, and A. H. Zewail, Femtosecond molecular dynamics of tautomerization in model base pairs, *Nature* **378**, 260 (1995)

[14] F. Krausz, and M. Ivanov, Attosecond Physics, *Rev. Mod. Phys.* **81**, 163 (2009)

[15] F. Lepine, M. Y. Ivanov, and M. J. J. Vrakking, Attosecond molecular dynamics, *Nature Photonics* **8**, 195 (2014)

[16] N. V. Golubev, and A. I. Kuleff, Control of charge migration in molecules by ultrashort laser pulses, *Phys. Rev. A* **91**, 051401 (2015)

[17] R. E. Carley, E. Hessel, and H. H. Fielding, Femtosecond lasers in gas phase chemistry, *Chem. Soc. Rev.* **34**, 949 (2005)

[18] N. E. Henriksen, Laser control of chemical reactions, *Chem. Soc. Rev.* **31**, 37 (2002)

[19] A. W. Kleyn, Molecular beams and chemical dynamics at surfaces, *Chem. Soc. Rev.* **32**, 87 (2003)

[20] R. F. W Bader, *Atoms in Molecules: A Quantum Theory*, Clarendon Press, Oxford, 1994.

[21] K. Kraka, and D. Cremer, *Theoretical Models of Chemical Bonding Part 2, The Concept of the Chemical Bond*, Ed. Z. B. Maksic, Springer, New York (1990)

[22] R. F. W. Bader, T. T. Nguyen-Dang, and Y. Tal, Quantum topology of molecular charge distributions. II. Molecular structure and its change, *J. Chem. Phys.* **70**, 4316 (1979)

[23] P. L. A. Popelier, Quantum Molecular Similarity. 1. BCP Space, *J. Phys. Chem. A* **103**, 2883 (1999)

[24] S. E. O'Brien, and P. L. A. Popelier, Quantum molecular similarity. Part 2: The relation between properties in BCP space and bond length, *Can. J. Chem.* **77**, 28 (1999)

[25] S. E. O'Brien, and P. L. A. Popelier, Quantum Molecular Similarity. 3. QTMS Descriptors, *J. Amer. Chem. Soc.* **115**, 7434 (1994)

[26] P. L. A. Popelier, A method to integrate an atom in a molecule without explicit representation of the interatomic surface, *Comput. Phys. Comm.* **108**, 180 (1998)

[27] E. Sanville, S. D. Kenny, R. Smith, and G. Henkelman, A fast and robust algorithm for Bader decomposition of charge density, *J. Comp. Chem.* **28**, 899 (2007)

[28] J. I. Rodriguez, A. M. Koster, P. W. Ayers, A. Santos-Valle, A. Vela, and G. Merino, An efficient grid-based scheme to compute QTAIM atomic properties without explicit calculation of zero-flux surfaces, *J. Comput. Chem.* **30**, 1082 (2008)

[29] A. Morgenstern, C. Morgenstern, J. Miorelli, T. Wilson and M. E. Eberhart, The influence of zero-flux surface motion on chemical reactivity *Phys. Chem. Chem. Phys.* **18**, 5683 (2016).

[30] K. B. Wigberg, R. F. W. Bader, and C. H. Lau, Theoretical Analysis of Hydrocarbon Properties. 2. Additivity of Group Properties and the Origin of Strain Energy, *J. Amer. Chem. Soc.* **109**, 985 (1987)

[31] S. J. Grabowski, What Is the Covalency of Hydrogen Bonding?, *Chem. Rev.* **111**, 2597 (2011)

[32] S. J. Grabowski, QTAIM Characteristics of Halogen Bond and Related Interactions, *Chem. Rev.* **111**, 2597 (2011)

[33] R. Parthasarathi, V. Subramanian, and N. Sathyamurthy, Hydrogen Bonding in Phenol, Water, and Phenol-Water Clusters, *J. Phys. Chem. A* **109**, 843 (2004)

[34] Y. Hirano, K, Takeda, and K. Miki, Charge-density analysis of an iron-sulfur protein at an ultra-high resolution, *Nautre* **534**, 284 (2016)

[35] C. F. Matta, N. Castillo, and R. J. Boyd, Extended Weak Bonding Interactions in DNA: π-Stacking (Base-Base), Base-Backbone, and Backbone-Backbone Interactions *J. Phys. Chem. B.* **110**, 563 (2006).

[36] G. A. Arteca, and P. G. Mezey, Deformation of electron densities in static external fields: shape group analysis for small molecules, *Chem. Phys.* **161**, 1 (1992)

[37] R. Meir, H. Chen, W. Lai, and S. Shaik, Oriented Electric Fields Accelerate Diels–Alder Reactionsand Control theendo/exoSelectivity, *ChemPhysChem* **11**, 301 (2010).

[38] S. Shaik, S. P. De Visse, and D. Kumar, External Electric Field Will Control the Selectivity of Enzymatic-Like Bond Activations, *J. Am. Chem. Soc.* **126**, 11746 (2004).

[39] M. Paul, R. K. Pathak, and P. Balanarayan, Rotatory Response of Molecular Electron Momentum Densities in Linear, Homogeneous

Weak Electric Fields: A Topographical Analysis, *J. Phys. Chem. A* **124**, 943 (2020).

[40] J. Stark, Observation of the Separation of Spectral Lines by an Electric Field, *Nature* **92**, 401 (1913).

[41] S. D. Fried, and S. G. Boxer, Electric Fields and Enzyme Catalysis, *Annu. Rev. Biochem.* **86**, 387 (2017).

[42] S. J. Formosinho, and L. G. Arnaut, Excited-State Proton Transfer reaction II. Intramolecular reactions, *J. Photochem. Photobiol. Chem.* **75**, 21 (1993).

[43] S. Sowlati-Hashjin, and C. F. Matta, The chemical bond in external electric fields: Energies, geometries, and vibrational Stark shifts of diatomic molecules, *J. Phys. Chem.* **139**, 14410 (2013).

[44] P. Papanikolaou, and P. Karafiloglou, Investigating sigma bonds in an electric field from the Pauling's perspective: The behavior of Cl–X and H–X (X = C, Si) bonds, *Theor. Chem. Acc.* **123**, 213 (2010).

[45] M. Protopapas, C. H. Keitel, and P. L. Knight, Reports on Progress in Physics Atomic physics with super-high intensity lasers, *Rep. Prog. Phys.* **60**, 389 (1997).

[46] M. Pont, N. R. Walet, M. Gavrilla, and C. W. McCurdy, Dichotomy of the Hydrogen Atom in Superintense, High-Frequency Laser Fields, *Phys. Rev. Lett.* **61**, 939 (1988).

[47] M. Gavrilla, Atomic stabilization in superintense laser fields, *J. Phys. B: At., Mol. Opt. Phys.* **35**, 147 (2002).

[48] J. H. Eberly, and K. C. Kulander, Atomic stabilization by super-intense lasers, *Science* **5137**, 1129 (1993).

[49] Q. Wei, S. Kais, and N. Moiseyev, New stable multiply charged negative atomic ions in linearly polarized superintense laser fields, *J. Chem. Phys.* **124**, 201108 (2006).

[50] H. A. Kramers, Collected Scientific Papers, North-Holland: Amsterdam , p262 (1956).

[51] W. C. Hennenberger, Perturbation Method for Atoms in Intense Light Beams, *Phys. Rev. Lett.* **21**, 838 (1968).

[52] U. Eichmann, A. Saenz, S. Eilzer, T. Nubbemeyer, and W. Sandner, Observing Rydberg Atoms to Survive Intense Laser Fields, *Phys. Rev. Lett.* **110**, 203002 (2013).

[53] M. P. de Boer, J. H. Hoogenraad, R. B. Vrijen, L. D. Noordam, and H. G. Muller, Indications of high-intensity adiabatic stabilization in neon, *Phys. Rev. Lett.* **71**, 3263 (1993).

[54] U. Eichmann, T. Nubbemeyer, H. Rottke et al., Acceleration of neutral atoms in strong short-pulse laser fields, *Nature* **461**, 1261 (2009).

[55] M. Matthews, F. Morales, A. Patas et al., Amplification of intense light fields by nearly free electrons, *Nat. Phys.* **14**, 695 (2018).

[56] R. Chavez-Calvillo, and J. Hernadez-Trujillo, Quantum Molecular Dynamics of the Topological Properties of the Electron Density: Charge Transfer in H_3^+ and LiF, *J. Phys. Chem. A* **115**, 45 (2010).

[57] S. Shin, and H. Meitu, Nonadiabatic effects on the charge transfer rate constant: A numerical study of a simple model system, *J. Chem. Phys.* **102**, 9285 (1995).

[58] M. Erdmann, P. Marquetand, and V. Engel, Combined electronic and nuclear dynamics in a simple model system, *J. Chem. Phys.* **119**, 672 (2003).

[59] M. Erdmann, and V. Engel, Combined electronic and nuclear dynamics in a simple model system. II. Spectroscopic transitions, *J. Chem. Phys.* **120**, 158 (2004).

[60] C. Jhala, and M. Lein, Multiconfiguration time-dependent Hartree approach for electron-nuclear correlation in strong laser fields, *Phys. Rev. A* **81**, 063421 (2010).

[61] H. Chevreau, Time dependent topological analysis of the electron density in the allyl radical, *Chem. Phys. Lett.* **1**, 59 (2004).

[62] H. Chevreau, Exploratory study of the electron-density relocalization process in benzene through a time-dependent topological analysis, *J. Chem. Phys.* **122**, 244316 (2005).

[63] P. Soler, J. Berges, F. Fuster, and H. Chevreau, Dynamical hydrogen-induced electronic relocalization in S_2H_2 and $S_2H_2^-$, *Chem. Phys. Lett.* **1**, 117 (2005).

[64] T. Maiman, Stimulated Optical Radiation in Ruby, *Nature* **187**, 493 (1960).

[65] A. Javan, W. R. Bennett, and D. R. Herriott, Population inversion and continous optical Maser oscillation in a gas discharge containing a He-Ne mixture, *Phys. Rev. Lett.* **6**, 106 (1961).

[66] L. V. Keldysh, Diagram Technique for non equilibrium process, *Zh. Eksp. Teor. Fiz.* **47**, 1515 (1964).

[67] D. M. Wolkow, Über eine Klasse von Lösungen der Diracschen Gleichung, *Z. Phys.* **94**, 250 (1935).

[68] K. Yang, Gauge transformations and quantum mechanics II. Physical interpretation of classical gauge transformations, *Ann. Phys.* **101**, 97 (1976).

[69] B. Berche, D. Malterre, and E. Medina, Gauge transformations and conserved quantitites in classical and quantum mechanics, *Am. J. Phys.* **84**, 616 (2016).

[70] R. M. O. Galvao, and L. C. M. Miranda, Quantum theory of an electron in external fields using unitary transformations, *Am. J. Phys.* **51**, 729 (1983).

[71] M. Belloni, and W. Chritian, Time development in quantum mechanics using a reduced Hilbert space approach, *Am. J. Phys.* **76**, 385 (2008).

[72] W. Li, D. H. Zhang, and Z. Sun, Efficient Fourth-Order Split Operator for Solving the Triatomic Reactive $Schrödinder$ Equation in the Time-Dependent Wavepacket Approach, *J. Phys. Chem. A* **118**, 9801 (2014).

[73] N. Balakrishnan, C. Kalyanaraman and N. Sathyamurthy, Time-dependent quantum mechanical approach to reactive scattering and related processes, *Phys. Rep.* **280**, 79 (1997).

[74] N. Sathyamurthy, and S. Mahapatra, Time-dependent quantum mechanical wavepacket dynamics, *Phys. Chem. Chem. Phys.* **23**, 7586 (2021).

[75] U. Peskin, and N. Moiseyev, The solution of the time dependent $Schrödinder$ equation by the (t,t^{prime}) method: Theory, Computational Algorithm and Applications, *J. Chem. Phys.* **99**, 4590 (1993).

[76] U. Peskin, R. Kosloff, and N. Moiseyev, The solution of the time dependent $Schrödinder$ equation by the (t,t^{prime}) method: The use of global polynomial propagators for time dependent Hamiltonians, *J. Chem. Phys.* **100**, 8849 (1994).

[77] U. Peskin, O. E. Alon, and N.Moiseyev, Thw solution of the time-dependent Schrodinger equation by the (t,t'),method: Multiphoton

ionization/dissociation probabilities in different gauges of the electromagnetic potentials, *J. Chem. Phys.* **100**, 7310 (1994).

[78] P. Raj, A. Gugalia, and P. Balanarayan, Quantum Dynamics with Explicitly Time Dependent Hamiltonians in Multiple Time Scales: A New Algorithm for (t,t') and (t,t',t'') Methods in Laser Matter Interactions, *J. Chem. Theory Comput.* **16**, 35 (2020).

[79] P. Krause, J. A. Sonk, and H. B. Schlegel, Strong Field ionization rates simulated with time-dependent configuration interaction and an absorbing potential, *J. Chem. Phys.* **140**, 174113 (2014).

[80] P. Krause, and H. B. Schlegel, Angle-Dependent ionization of Hydrides AH_n calculated by the time-dependent configuration interaction with an absorbing potential, *J. Chem. Phys.* **119**, 10212 (2015).

[81] J. J. Sakurai, *Modern Quantum Mechanics, Chapter II*, 2nd ed., Addison-Wesley: Reading, MA, (1992).

[82] D. J. Tannor, *Introduction to Quantum Mechanics: A time-dependent prespective*, Vol. I, University Science Books (2007).

[83] C. Cohen-Tannoudji, B. Diu, and F. Laloe, *Quantum Mechanics*, Vol. I, Wiley-Interscience: Paris (1997).

[84] P. Raj, and P. Balanarayan, ABELDYN: An Ab-initio Electron-Dynamics package *Manuscript to be submitted*

[85] P. Raj, Electronic Quantum Dynamics of Molecules in Strong LASER fields: Novel Algorithms and Effects, *Dotoral Dissertation* (2022)

[86] R. G. Parr, D. P. Craig and I. G. Ross, Molecular Orbital Calculations of the Lower Excited Electronic Levels of Benzene, Configuration Interaction Included *J. Chem. Phys.* **18**, 1561 (1950).

[87] M. Born, and R. Oppenheimer, Zur Quantentheorie der Molekeln, *Annalen der Physik* **389**, 457 (1927).

[88] A. Szabo, and N. S. Ostlund, *Modern Quantum Chemistry: Introduction to Advanced Electronic Structure Theory* DOVER PUBLICATIONS, INC. Mineola, New York (1996)

[89] T. Kato, On the eigenfunctions of many-particle systems in quantum mechanics, *Commun. Pure App. Math.* **10**, 157 (1957).

[90] E. Steiner, Charge Densities in Atoms, *J. Chem. Phys.* **39**, 2365 (1963).

[91] C. P. Hue, and D. P. Chong, On the use of integral electron cusp conditions as constraints, *Theoret. Chim. Acta* **12**, 431 (1968).

[92] J. A. Chapman, and D. P. Chong, Cusp constraints for atomic wavefunctions, *Can. J. Chem.* **48**, 2722 (1970).

[93] M. M. Morrell, R. G. Parr, and M. Levy, Calculation of ionization potentials from density matrices and natural functions, and the long-range behavior of natural orbitals and electron density, *J. Chem. Phys.* **62**, 549 (1975).

[94] M. Hoffman-Ostenhof, and T. Hoffman-Ostenhof, "Schrödinger inequalities" and asymptotic behavior of the electron density of atoms and molecules, *Phys. Rev. A* **16**, 1782 (1977).

[95] R. Ahlriches, M. Hoffmann-Ostenhof, T. Hoffman-Ostenhof, and J. D. Morgan, III, Bounds on the decay of electron densities with screening, *Phys. Rev. A* **23**, 2106 (1981).

[96] H. J. Silverstone, Long-range behavior of electronic wave functions. Generalized Carlson-Keller expansion, *Phys. Rev. A* **23**, 1030 (1981).

[97] H. Weinstein, P. Politzer, and S. Srebrenik, A misconception concerning the electronic density distribution of an atom, *Theoret. Chem. Acta.* **38**, 159 (1975).

[98] A. M. Simas, R. P. Sagar, A. C. T. Ku, and V. H. Smith jr., The radial charge distribution and the shell structure of atoms and ions, *Can. J. Chem.* **66**, 1923 (1988).

[99] P. W. Ayers, and R. G. Parr, Sufficient condition for monotonic electron density decay in many-electron systems, *Int. J. Quantum Chem.* **95**, 877 (2003).

[100] K. Collard, and G. G. Hall, Orthogonal trajectories of the electron density, *Int. J. Quantum Chem.* **12**, 623 (1977).

[101] W. L. Cao, C. Gatti, P. J. MacDougall, and R. F. W. Bader, On the presence of non-nuclear attractors in the charge distributions of Li and Na clusters, *Chem. Phys. Lett.* **141**, 380 (1987).

[102] A. M. Pendas, M. A. Blanco, A. Costlaes, P. M. Sanchez, and V. Luana, Non-nuclear Maxima of the Electron Density, *Phys. Rev. Lett.* **83**, 1930 (1999).

[103] M. Sakata, and M. Sato, Accurate structure analysis by the maximum-entropy method, *Acta. Cryst.* **46**, 263 (1990).

[104] G. R. Runtz, R. F. W. Bader, and R. Messer, Definition of bond paths and bond directions in terms of the molecular charge distribution, *Can. J. Chem.* **55**, 3040 (1977).

[105] R. F. W. Bader, and H. Essen, The characterization of atomic interactions, *J. Chem. Phys.* **80**, 1943 (1984).

[106] A. Morgenstern, and M. Ebarhart, Bond dissociation energies from the topology of the charge density using gradient bundle analysis, *Phys. Scr.* **91**, 023012 (2016).

[107] T. R. Wilson, A. Morgenstern, A. N. Alexandraova, and M. E. Eberhart, Bond Bundle Analysis of Ketosteroid Isomerase, *J. Phys. Chem. B* **126**, 9443 (2022).

[108] R. F. W. Bader, and P. M. Beddall, Virial Field Relationship for Molecular Charge Distributions and the Spatial Partitioning of Molecular Properties, *J. Chem. Phys.*, **56**, 3320 (1972)

[109] P. L. A. Popelier, Atoms in Molecules - An Introduction, *Prentice Hall: Harlow-England*, (2000)

[110] P. L. A. Popelier, fast algorithm to compute atomic charges based on the topology of the electron density, *Theor. Chem. Acc.*, **105**, 393 (2001)

[111] P. L. A. Popelier, fast algorithm to compute atomic charges based on the topology of the electron density, *Theor. Chem. Acc.*, **105**, 393 (2001)

[112] S. Srebrenik, and R. F. W. Bader, Towards the development of the quantum mechanics of a subspace, *J. Chem. Phys.*, **63**, 3495 (1975)

[113] S. Srebrenik, and R. F. W. Bader, Sufficient conditions for fragment and regional virial theorems, *J. Chem. Phys.*, **61**, 2536 (1974)

[114] R. F. W. Bader, T. S. Slee, D. Cremer, and E. Kraka, Description of conjugation and hyperconjugation in terms of electron distributions, *J. Am. Chem. Soc.*, **105**, 5061 (1983)

[115] D. Cremer, and E. Kraka, A Description of the Chemical Bond in Terms of Local Properties of Electron Density and Energy, *Croatia Chem. Acta*, **57**, 1259 (1984)

[116] T. -H. Tang, E. Deretey, S. J. K. Jensen, and I. G. Csizmadia, Hydrogen bonds: relation between lengths and electron densities at bond critical points, *Eur. Phys. J. D*, **37**, 212 (2006)

[117] R. J. Boyd, and S. C. Choi, Hydrogen bonding between nitriles and hydrogen halides and the topological properties of molecular charge distributions, *Chem. Phys. Lett.*, **129**, 62 (1986)

[118] M. V. Vener, A. V. Shiskina, A. A. Rykownov, and V. G. Tsirelson, Cl···Cl Interactions in Molecular Crystals: Insights from the Theoretical Charge Density Analysis, *J. Phys. Chem. A*, **117**, 8459 (2013)

[119] R. F. W. Bader, Transferability of atomic properties and the theorem of Hohenberg and Kohn *Chem. Phys. Lett.* **148**, 452 (1988).

[120] R. F. W. Bader, A. Larouche, C. Gatti, M. T. Caroll, P. J. MacDougall, and K. B. Wiberg, Properties of atoms in molecules: Dipole moments and transferability of properties *J. Chem. Phys.* **87**, 1142 (1987).

[121] R. F. W. Bader, P. L. A. Popelier, T. A. Keith, Theoretical Definition of a Functional Group and the Molecular Orbital Paradigm *Angew. Chem., Int. Ed.* **33**, 620 (1994).

[122] A. Morgenstern, C. Morgenstern, J. Miorelli, T. Wilson and M. E. Eberhart, The influence of zero-flux surface motion on chemical reactivity *Phys. Chem. Chem. Phys.* **18**, 5683 (2016).

[123] A. Morgenstern, and M. E. Eberhart, Bond dissociation energies from the topology of charge density using gradient bundle analysis. *Phys. Scr.* **91**, 023012 (2016).

[124] J. Miorell, T. Wilson, A. Morgenstern, T. Jones and M. E. Eberhart, A Full Topological Analysis of Unstable and Metastable Bond Critical Points *ChemPhysChem* **16**, 152 (2014).

[125] A. Morgenstern, T. Wilson, J. Miorelli, T. Jones, and M. E. Eberhart, In search of intrinsic chemical bond *Comput. Theor. Chem.* **1053**, 31 (2015).

[126] T. E. Jones, M. E. Eberhart, S. Emlay, and C. Mackey Bond Bundles and the Origins of Functionality *J. Phys. Chem. A* **115**, 12582 (2011).

[127] A. Morgenstern, T. R. Wilson, and M. E. Eberhart, Predicting Chemical Reactivity from the Charge Density through Gradient Bundle Analysis: Moving beyond Fukui Functions *J. Chem. Phys. A* **121**, 4341 (2017).

[128] M. E. Eberhart, The metallic bond: Elastic Properties *Acta Matter.* **44**, 2495 (1996).

[129] O. A. Zhikol, O. Shishkin, and K. A. Lyssenko, Electron density distribution in stacked benzene dimers: A new approach towards the estimation of stacking interaction energies, *J. Chem. Phys.* **122**, 144104 (2005).

[130] M. P. Waller, A. Robertazzi, J. A. Platts, D. E. Hibbs, and P. A. Williams, Hybrid density functional theory for π-stacking interactions: Application to benzenes, pyridines, and DNA bases, *J. Comput. Chem.* **27**, 491 (2006).

[131] C. F. Matta, N. Castillo, and R. J. Boyd, Extended Weak Bonding Interactions in DNA: π-Stacking (Base-Base), Base-Backbone, and Backbone-Backbone Interactions *J. Phys. Chem. B.* **110**, 563 (2006).

[132] E. Espinosa, E. Molins, and C. Lecomte, Hydrogen bond strengths revealed by topological analyses of experimentally observed electron densities *Chem. Phys. Lett.* **285**, 170 (1998).

[133] E. Espinosa, and E. Molins, Retrieving interaction potentials from the topology of the electron density distribution: The case of hydrogen bonds *J. Chem. Phys.* **113**, 5686 (2000).

[134] S. E. $O'Brien$, and P. L. A. Popelier, Quantum molecular similarity. Part 2: The relation between properties in BCP space and bond length *Can. J. Chem.* **77**, 28 (1999).

[135] P. L. A. Popelier, Quantum Molecular Similarity. 1. BCP Space, *J. Phys. Chem. A* **103**, 2883 (1999).

[136] S. E. $O'Brien$, and P. L. A. Popelier, Quantum Molecular Similarity. 3. QTMS Descriptors *J. Chem. Inf. Comput. Sci.* **41**, 764 (2001).

[137] U. A. Chaudry, and P. L. A. Popelier, Estimation of pKa Using Quantum Topological Molecular Similarity Descriptors: Application to Carboxylic Acids, Anilines and Phenols *J. Org. Chem.* **69**, 233 (2004).

Chapter 2 | ABELDYNPROP: A parallel program for the evaluation of time-dependent electronic properties in position space

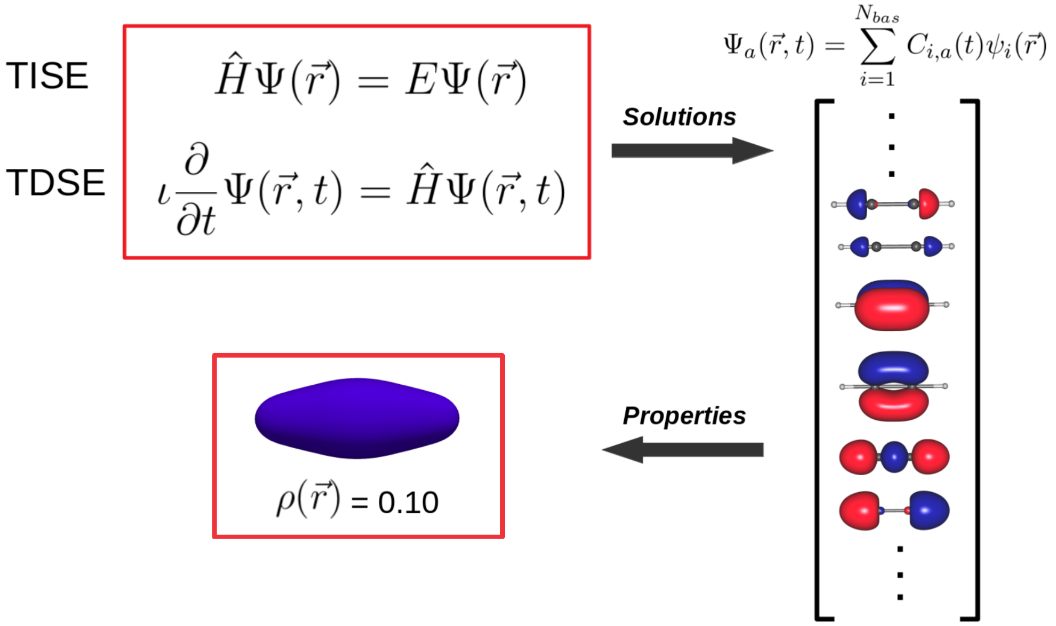

---

[1] The graphical abstract depict molecular orbitals as solutions obtained from TISE and TDSE. These solutions are further used to evaluate properties. These properties are evaluated using the ABELDYNPROP codes.

Abstract

The present work describes a code to evaluate time-dependent electronic properties - Molecular Electron Density (MED) with its gradients, Hessian, Laplacian for a multi-electron molecular system in position space over a three-dimensional Cartesian grid. The integrated code also searches for critical points and zero-flux surfaces of electron densities. The code is also built to compute gradient paths, bond paths and basin boundaries. A feature to evaluate these quantities on a planar grid is also enabled in the code. In principle, the code works specifically for electronic wave functions obtained from the methods solving the time-dependent Schrödinder equation. The work uses electronic wave functions from an in-house code-solving time-dependent Hartree-Fock (TDHF). The code takes molecular orbital coefficients of the wavefunction as input at each time step of the time-dependent electronic structure calculation. The analytical expressions of MED, their gradients, Hessian, Laplacian are calculated at all time steps using Cartesian Gaussian basis sets over a grid. Apart from time-dependent properties, this package has also integrated time-independent electronic properties in position space. The program is written in FORTRAN 90 and executed through a shell script. The code is also tuned for multi-processor machines with distributed memory through a message-passing interface (MPI). The package has been bench marked for various Gaussian basis sets for different molecules showing a linear speedup on a parallel architecture.

2.1 Introduction

According to the fundamental postulate of quantum theory, wavefunctions contain all the information about the quantum system. Investigating the time evolution in chemical/physical processes in a quantum system requires the knowledge of time-dependent wavefunctions. With the advent of the current century, research in light-matter interaction led to the development of laser pulses in sub-femtosecond and attosecond timescales.[1] Such timescales, comparable to the motion of electrons, allow one to gauge electronic dynamics in atoms and molecules. Subsequently, the development of theoretical methods provided the electronic wavefunctions obtained from the solutions of the time-dependent Schrödinder equation (TDSE) in laser fields. In similar works, Raj *et al.*[2–4] developed a fast and efficient algorithm to solve TDSE for molecules interacting with short laser pulses. With the time-dependent electronic wavefunction in a fixed nuclear geometry, a natural extension would be calculating electronic properties. In literature, no such program exists to compute time-evolving scalar field molecular electronic properties, specifically time-dependent electron densities.

However, there have been reports where Rodgido and coworkers[5] analyzed the time evolution of the topology of the electron density to study charge transfer in ${H_3}^+$ and LIF as models, using quantum theory of atoms in molecules (QTAIM). Close to this approach, another work, Gronager *et al.*[6], studied the photodissociation of NaI molecule, which showed electron transfer taking place by electron density contributions from two valence orbitals. There are also reports on the coupled electronic-nuclear dynamics, including the time dependence of electron density, which has been carried out for simple model systems.[7] Gross and coworkers[8] have carried out a study on time-dependent electron localization function, allowing the time-resolved observation of the formation and breaking of the chemical bond using two examples: (i) the excitation of acetylene by a strong laser pulse, and (ii) the scattering of a high-energy proton from ethene molecule.

Analytical forms have been derived using wavefunction to evaluate scalar field electronic properties of atoms and molecules. The scalar field electronic properties, such as molecular electron density (MED),[9–14] electronic momentum density (EMD),[15] electron localization function (ELF),[16] and molecular electrostatic potentials (MESP),[17] are experimentally realized via scattering experiments. These properties contain a wealth of information and play a major role in understanding the electronic structure and chemical reactivity. In this respect, the theoretical evaluation of these properties from wavefunction provides us with tools to quantify and understand chemical notions such as charge transfer and chemical bonding.[18–24]

Several software packages for the field-free case have been published that can calculate electron density, gradient paths, Laplacian, critical points, and *Quantum theory of atoms-in-molecules*(QTAIM) analysis in position space. However, no such package exists that computes time-evolving electron density, its respective topological properties, and QTAIM analysis. The packages that calculate Bader's QTAIM are AIMALL by Keith,[25] AIM2000 by Biegler-Konig,[26] BADER by Henkelman group,[27] MORPHY by popelier,[28, 29] CRITIC,[30, 31] DGRID,[32] MULTIWFN.[33] Vega *et. al*[34] has developed a C library for the topological study of electronic charge density on a grid. Later, the same group developed an application, AIM-UC,[35] for drawing gradient paths, Laplacian, and density isolines, which uses cube data files as input. The package Octopus,[36–39] developed by Rubio and coworkers, has made several efficient versions of code to perform excited state dynamics using time-dependent density functional theory of atoms and molecules in the presence of ultrashort laser pulses. The codes mentioned perform QTAIM analysis for the field-free case.

Hence, there is a need for a package that can calculate time-evolving electron densities, its topology, and QTAIM analysis from the time-dependent wavefunctions obtained from the solutions of TDSE. In this work, we used the coefficients of the position space wavefunction (complex-valued) as an input received from the in-house code.[3, 4] However, these time-dependent wavefunctions from any code-solving TDSE can also be used as input. The program can evaluate molecular electron density, its gradient in X, Y, and Z, and Laplacian for a 3D grid at all timesteps in the time-dependent field. We use the analytical forms for Gaussian-type orbitals, their first and second derivatives, to calculate them. The computation can be performed in a parallel fashion over a distributed memory. Parallelization is achieved, at all time steps, by dividing the total number of grid points by the total number of nodes specified by the user through input file. The program can also calculate the critical points (CPs) of the TDMED, gradient vector lines, bond paths, basin boundaries, and zero-flux surfaces to perform topological studies. Using the information of CPs and gradients, we also identify the regions of *atoms-in-molecules* in the time-dependent fields and their respective properties (Populations, Bader Charge, Kinetic energies, electrostatic moments, and dipole moments).

The rest of this manuscript is organized as follows: Section: Theoretical background briefs regarding the properties, their relevant equations, analytical forms, and steps carried out via the codes, Section: Methodology, to outline the construct, working, implementation of the several modules/subroutines of the program, results through plots on some test molecules and then finally summarizing the work with a conclusion section.

2.2 Theoretical Description

2.2.1 Molecular Electron Densities

Electron density (ED), $\rho(\vec{r})$, is an observable quantity routinely obtained from calculations and experiments for the structure determination of molecules.[9–14] ED is a one-particle charge density of an N-electron system, extracted from many-particle 4N dimensional wavefunction $\Psi(\vec{x_1}, \vec{x_2}, \vec{x_3} \cdots, \vec{x_N})$ as

$$\rho(\vec{r}) = N \sum_{\sigma} \int |\Psi(\vec{x}, \vec{x_1}, \vec{x_2}, \vec{x_3}, \cdots, \vec{x_N})|^2 d^3r_2 d^3r_3 \cdots d^3r_N \tag{2.1}$$

Here, the wavefunctions Ψ are the antisymmetric solutions obtained from solving the time-independent Schrödinder equation (TISE), retrievable from standard electronic structure packages.[40] The coordinates $\vec{x}$ represent the position $\vec{r}$ and spin σ of the electron. The summation in Eq. [2.1] runs over all the spin coordinates and integrates all but one spatial coordinate $\vec{r}$. N is the total number of electrons in the system. Apart from few exceptions, the topology of molecular electron density (MED) reveals the presence of local maxima only at atomic positions. Therefore, this information helps in elucidating the structure of molecules.

At a given time instant, we use all the occupied time-dependent MOs to calculate the time-evolving molecular electron density $\rho(\vec{r}, t)$. The time-dependent molecular orbitals or molecular wavefunctions ($\Psi_a(\vec{r}, t)$) are mathematical constructs to describe electrons in atoms and molecules. The probability of finding an electron at $\vec{r}$ at a time t, in a^{th} MO $\Psi_a(\vec{r}$,t) is $\Psi_a(\vec{r}, t)\Psi_a^*(\vec{r}, t)$ d^3r. In the case closed shell molecule containing total N_e electron, where the time-dependent MOs contain two electrons each, then the total charge density or molecular electron density of the molecule will be,

$$\rho(\vec{r},t) = 2\sum_{i=1}^{N_e/2} \Psi_i(\vec{r},t)\Psi_i^*(\vec{r},t) \tag{2.2}$$

The summation index *i* runs over all the doubly occupied ($N_{occ} = N_e/2$) time-dependent molecular orbitals. Time-dependent calculations from the ABELDYN code[3, 4] also provides the information of norm i.e. the total sum of electrons. If the norm is conserved in that calculation, then at that time t, the integral of molecular electron density should be equal to number of electrons, *that is* $\int \rho(\vec{r},t)dr^3 = N$. Alternative form of $\rho(\vec{r},t)$ is obtained using MO in atomic basis expanded form as

$$\Psi_a(\vec{r},t) = \sum_{i=1}^{N_{bas}} C_{i,a}(t)\psi_i(\vec{r}) \tag{2.3}$$

Using the form of Eq. [2.3] in Eq. [2.2] will lead to another form of $\rho(\vec{r},t)$ shown in follwing Eq.

$$\begin{aligned}
\rho(\vec{r},t) &= 2\sum_{i=1}^{N_e/2}\left[\sum_{\nu=1}^{N_{bas}} C_{\nu i}^*(t)\psi_\nu^*(\vec{r})\sum_{\mu=1}^{N_{bas}} C_{\mu i}(t)\psi_\mu(\vec{r})\right] \\
&= \sum_{\mu,\nu=1}^{N_{bas}}\left[2\sum_{i}^{N_e/2} C_{\mu i}(t)C_{\nu i}^*(t)\right]\psi_\mu(\vec{r})\psi_\nu^*(\vec{r}) \\
&= \sum_{\mu,\nu=1}^{N_{bas}} P_{\mu\nu}(t)\psi_\mu(\vec{r})\psi_\nu^*(\vec{r}) \qquad (2.4)
\end{aligned}$$

The term, $P_{\mu\nu}$ is called the time-dependent *density matrix* or *charge-density bond-order matrix*.[41] Thus, the time-dependent in molecular electron density is induced by the time-dependent coefficients of the MOs.

For an open shell system, containing N_e electrons, calculation of molecular electron density would require the summation over all the occupied (N_{occ})

orbitals $\psi_i(\vec{r},t)$, the molecular electron density $\rho(\vec{r},t)$ would be calculated as,

$$\rho(\vec{r},t) = \sum_{i=1}^{N_{occ}} (n_i)(\Psi_i(\vec{r},t)\Psi_i^*(\vec{r},t)) \tag{2.5}$$

where, n_i is the fractional occupancy of the i^{th} natural spin orbital in Eq. [2.5].

To moniter the changes in time-dependent electron density, ABELDYN-PROP code enables the calculation of difference electron density. The difference electron density is calculated w.r.t to free-field molecular electron density $\rho_0(\vec{r})$ (at t=0),

$$\Delta\rho(\vec{r},t) = \rho(\vec{r},t) - \rho_0(\vec{r}) \tag{2.6}$$

The total number of operation counts for the calculation of molecular electronic density using the Eq. [2.1] and [2.3] are $\left(N_e/2\right)$ and $(N_{bas} \times N_{bas})$ respectively. The $\left(N_e/2\right)$ is the number of doubly occupied MOs, and the relation $N_{occ} \leq (N_{bas} \times N_{bas})$ holds true in all cases, therefore, calculation of $\rho(\vec{r},t)$ is faster with Eq. [2.2] than Eq. [2.4].

2.2.2 Gradients of Molecular Electron Density

The gradients of a 3D scalar function is a 3D vector $\vec{\nabla} f = (\partial f/\partial x)\hat{x} + (\partial f/\partial y)\hat{y} + (\partial f/\partial z)\hat{z}$, at a position vector $\vec{r}$, informs about the nature of function around $\vec{r}$, that is increasing, decreasing or flat. Starting from a point $\vec{r}$ in 3D, following the maximum function value, gradient vector traces out paths called *gradient paths*, which could lead to maximum. Similarly, other critical points of the 3D function could also be attained. For the dynamical systems, such as in the time-dependent molecular electron density, the motion of *gradient paths* in the time evolving gradients, will talk about the nature the molecular electron density in all directions, *x, y, and z*, as a function of time. The time-dependent gradients of molecular electron density has the following Eq. [2.7] by using Eq. [2.2],

$$\vec{\nabla}\rho(\vec{r},t) = 2\sum_{i=1}^{N_e/2}\Bigg[\left(\Psi_i^*(\vec{r},t)\frac{\partial\Psi_i(\vec{r},t)}{\partial x} + \Psi_i(\vec{r},t)\frac{\partial\Psi_i^*(\vec{r},t)}{\partial x}\right)\hat{x} + \left(\Psi_i^*(\vec{r},t)\frac{\partial\Psi_i(\vec{r},t)}{\partial y} + \Psi_i(\vec{r},t)\frac{\partial\Psi_i^*(\vec{r},t)}{\partial y}\right)\hat{y} + \left(\Psi_i^*(\vec{r},t)\frac{\partial\Psi_i(\vec{r},t)}{\partial z} + \Psi_i(\vec{r},t)\frac{\partial\Psi_i^*(\vec{r},t)}{\partial z}\right)\hat{z}\Bigg] \tag{2.7}$$

In the Eq. [2.7], using the Ψ_i in the terms of atomic orbitals and solving for i^{th} MO $\Psi_i(\vec{r},t)$ w.r.t x in Eq. [2.8]. The gradient w.r.t y, and z will have similar forms.

$$\frac{\partial\Psi_i(\vec{r},t)}{\partial x} = \sum_{\mu=1}^{N_{bas}} C_{\mu i}(t)\left(\frac{\partial\psi_i(\vec{r})}{\partial x}\right) \tag{2.8}$$

$$\frac{\partial\Psi_i(\vec{r},t)}{\partial x} = \sum_{\mu=1}^{N_{bas}} C_{\mu i}(t)\left(\sum_{j=1}^{N_{pg}} c_j\frac{\partial\chi(\vec{r};\{\alpha_j,\vec{R_A}\})}{\partial x}\right) \tag{2.9}$$

The expression in Eq. [2.9] gives the derivative of the MO w.r.t x in terms of contracted Gaussian functions. Therefore, the gradients of time-dependent molecular electron density w.r.t *x, y and z* depends solely the first order derivatives of cartesian Gaussian functions.

The total number of operation counts for the calculation of time-dependent gradients of molecular electron density required is 6 N_{occ} with reference to Eq. [2.7].

2.2.3 Hessian of Molecular Electron Density

The Hessian, represents 2^{nd}-order partial derivative of time-dependent molecular electron density w.r.t to coordinates which is symmetric matrix form as shown in 2.10.

$$H(\rho(\vec{r},t)) = \begin{bmatrix} \frac{\partial^2 \rho(\vec{r},t)}{\partial x^2} & \frac{\partial^2 \rho(\vec{r},t)}{\partial x \partial y} & \frac{\partial^2 \rho(\vec{r},t)}{\partial x \partial z} \\ \frac{\partial^2 \rho(\vec{r},t)}{\partial y \partial x} & \frac{\partial^2 \rho(\vec{r},t)}{\partial y^2} & \frac{\partial^2 \rho(\vec{r},t)}{\partial y \partial z} \\ \frac{\partial^2 \rho(\vec{r},t)}{\partial z \partial x} & \frac{\partial^2 \rho(\vec{r},t)}{\partial z^2} & \frac{\partial^2 \rho(\vec{r},t)}{\partial z \partial x} \end{bmatrix} \tag{2.10}$$

The evaluation of Hessian is an essential quantity required to characterize the probable critical points. The eigenvalues and eigenvectors of the Hessian matrix, provide the information in deciding the rank (R) and signature (S) of the critical point. Since, the calculation of Hessian is computationally expensive step, it should only be used for characterizing the probable critical points which may be identified in the form of gradient vectors with its norm nearing zero ($\sim 10^{-10}$ or less).

The evaluation time-dependent Hessian of molecular electron density w.r.t to x and y will have the following form, given by Eq. [2.11]

$$\frac{\partial^2 \rho(\vec{r},t)}{\partial x \partial y} = 2 \sum_{i=1}^{N_e/2} \left[\frac{\partial \Psi_i(\vec{r},t)}{\partial y} \frac{\partial \Psi_i^*(\vec{r},t)}{\partial x} + \Psi_i^*(\vec{r},t) \frac{\partial^2 \Psi_i(\vec{r},t)}{\partial x \partial y} + \right. \\ \left. \frac{\partial \Psi_i(\vec{r},t)}{\partial x} \frac{\partial \Psi_i^*(\vec{r},t)}{\partial y} + \Psi_i(\vec{r},t) \frac{\partial^2 \Psi_i^*(\vec{r},t)}{\partial x \partial y} \right] \tag{2.11}$$

In the Eq. [2.11], the first partial derivatives will have the same form in terms of primitive Gaussian functions as described in the previous subsection.

The operation count for the calculation of one double derivative element of Hessian, would require $4N_{occ}$ multiplications. The total number of operations would lead to $24N_{occ}$ operations for the calcution of six lower diagonal elements of symmetric Hessian matrix.

2.2.4 Laplacian of Molecular Electron Density

The Laplacian of time-dependent electron density, $\nabla^2\rho(\vec{r},t) = (\partial^2/\partial x^2 + \partial^2/\partial y^2 + \partial^2/\partial z^2)\ \rho(\vec{r},t)$, is, the sum of diagonal elements of Hessian. The free-field Laplacian gives a measure of the locally charge concentrated or depleted regions. The MED in the presence of time-dependent fields show the electron density accumulating in the direction of field. Therefore, the $\nabla^2\rho(\vec{r},t)$ is a quantity which can be used to gauge the time-evolving charge concentrated or depleted regions of the molecule.

In the Eq. [2.11], the 2^{nd}-order derivative w.r.t to x, would become the form as shown in Eq. [2.12],

$$\begin{aligned}\frac{\partial^2\rho(\vec{r},t)}{\partial^2 x} = 2\sum_{i=1}^{N_e/2}\Bigg[\frac{\partial\Psi_i(\vec{r},t)}{\partial x}\frac{\partial\Psi_i^*(\vec{r},t)}{\partial x} + 2\Psi_i^*(\vec{r},t)\frac{\partial^2\Psi_i(\vec{r},t)}{\partial x\partial x} \\ +\Psi_i(\vec{r},t)\frac{\partial^2\Psi_i^*(\vec{r},t)}{\partial x\partial x}\Bigg]\end{aligned} \tag{2.12}$$

The total number of operations required to evaluate Laplacian of MED would be $9N_{occ}$ multiplications.

2.2.5 Quantum Mechanical Vector Current Density

The QM vector current density $\vec{J}(\vec{r},t)$, is the particle density flux and analytically computed over all the occupied molecular orbitals as

$$\vec{J}(\vec{r},t) = i\frac{\hbar}{2m}\sum_{i=1}^{N_e/2}[\Psi_i^*(\vec{r},t)\vec{\nabla}\Psi_i(\vec{r},t) - \Psi_i(\vec{r},t)\vec{\nabla}\Psi_i^*(\vec{r},t)] \tag{2.13}$$

Analogous to charge conservation in electrodynamics, this quantity is involved in the conservation of probability as shown in the following Eq.

$$\frac{\partial \rho(\vec{r},t)}{\partial t} + \vec{\nabla} \cdot \vec{J}(\vec{r},t) = 0 \tag{2.14}$$

The computation of time-varying $\vec{J}(\vec{r},t)$ w.r.t to x will have the following form,

$$\vec{J}_x(\vec{r},t) = i\frac{\hbar}{2m}\sum_{i=1}^{N_e/2}\left[\Psi^*(\vec{r},t)\frac{\partial \Psi_i(\vec{r},t)}{\partial x} + \Psi_i(\vec{r},t)\frac{\partial \Psi_i^*(\vec{r},t)}{\partial x}\right] \tag{2.15}$$

$\vec{J}_y(\vec{r},t)$ and $\vec{J}_z(\vec{r},t)$ will have the similar analytical forms. In the ABELDYNPROP package they are evaluated over regular equally spaced grids by using the keyword VDEN.

2.2.6 Critical points of Molecular Electron Density

A point r_c is a critical point for a 3D MED scalar function, the following criteria should be satisfied,

1. The gradient vector of time independent or time-dependent MED is zero,
   $\nabla(\vec{r},t) = 0.$
2. The norm of gradient should be zero, that is,
   $|\nabla\rho(r,\vec{t})| = \sqrt{(\partial\rho/\partial x)^2 + (\partial\rho/\partial y)^2 + (\partial\rho/\partial z)^2}$

Eigenvalues and Eigenvectors of the Hessian at points of non-zero MED value are evaluated to characterize them as one of the four known types of CPs. The eigenvectors of Hessian at CPs are the principal directions, and eigenvalues are the principal curvatures. The number of linearly independent eigenvectors defines the rank (R), and the algebraic sum of the signs of eigenvalues is called the signatures (S) of the CP. **Fours types of CPs of MED are: (3,-3) [Maxima], (3,-3) [Minima], (3,-1) [1^{st}-order Saddle], and (3,+1) [2^{nd}-order Saddle]**. Apart from a few exceptions (Li_2, Na_2), the MED in most of the systems, the (3,-1) saddle CPs appear in-between two (3,-3) maxima CPs. The (3,+1) CPs are in the middle of several bonds forming closed ring like molecules such as $Benzene, Napthalene$. Those points where the MED is a local minimum in all directions depict (3,+3) CPs, usually found in enclosed caged molecules like $Tetrahedrane, Cubane$.

The chemical parameters such as bond polarity, bond ellipticity, and bond order have been quantified and formulated in terms of eigenvalues of Hessian matrix and MED-value at the corresponding (3,-1) CP.[18, 43, 44] Collard and coworkers showed that a change in structure brings the variation in the number and nature of CPs in MEDs.[45] Bader *et al.* investigated the nature of catastrophes during the C_{2V} dissociation of the H_2O molecule.[46] In summary, reactivity patterns and structural changes can be studied from the topography of MED.

Several algorithms to find the CPs of MED is available in the literature. The Program SADDLE,[47] part of the AIMPAC package, is one such code based on Newton-Raphson (NR) algorithm. The MORPHY[28, 29] program developed by Popelier provides an eigenvector following method-based modified NR-technique based on involving scalar values called *shift parameters*. However, another improved and faster algorithm[48] to find CPs of MED was based on the topological connectivity of CPs through selected gradient paths. Balanarayan *et. al.*[49] presented an efficient and fast algorithm to search for CP for, in general, any 3D-scalar field functions. The algorithm is based on providing a guess from surface extrema (Maxima, minima, or saddles) of appropriately defined atom-centered spheres. After that, a ray search is performed using the Bisection method to locate local minima and maxima. Finally, the NR technique using these ray minima/maxima is used as a guess to search CPs. Another recent work by Alberto[50] finds CPs on the 3D grid employing poly harmonic spline interpolation combined with smoothening function based on molecular density.

We present the algorithm used in the ABELDYNPROP code to calculate all the critical points of MED.

Guess Points: We provide points on the *spherical grid* centered around the atomic positions as guess points. In addition, the atomic centers and their midpoints are also taken as guess points. The spherical polar coordinates (r, θ, ϕ) are used to generate points on the guess sphere. The inputs of number of points required for the grid of these coordinates, r_{max}, nr, nθ, nϕ, are user-defined parameters.

To find critical points $\vec{r}_{critic}$ of electron density, one needs to solve for the solutions of the equation $\nabla\rho(\vec{r}_{critic}) = \vec{0}$. A way to solve this equation is to use the Newton-Raphson[51] (NR) method. In this method, starting with a guess point vector $\vec{r}_i$, a new vector $\vec{r}_{i+1}$ is evaluated using the shift vector which is evaluated as $\vec{h} = -\mathbf{H}_i\nabla\rho(\vec{r}_i)$. Thus, the calculation of new vector follows $\vec{r}_{i+1} = \vec{r}_i + t\vec{h}$, where t is a small scalar value, less than 1. The calculations using the equations mentioned are iterated until $\vec{\nabla}\rho(\vec{r})$ is equal to the vector $\vec{0}$ or has a small norm. There could be high oscillations near to the critical points, when the gradient has a high norm value in critical point neighbourhood, which is avoided by taking t $<$ 1. The maximum number of iterations and path length are defined by the user in the input file.

The Algorithm:

1. We have an iteration that runs over all guess points. At each step, a new guess point is assigned as a (3 $\times$ 1) column vector, say V_0, where

$V_{11} = r_x$, $V_{21} = r_y$, and $V_{31} = r_z$. The guess vector is the first input to the NR routine in the next step.

2. The gradient vector $G_{3\times1}$ and Hessian $H_{3\times3}$ of MED are evaluated at the first guess vector V_0. A new vector V_1 is generated using the gradient vector and inverse Hessian of the previous vector V_0 using NR relation. The new vector serves as an input to the next NR step. In general, to generate $[V_{n+1}]_{3\times1}$ vector from $[V_n]_{3\times1}$ vector, the following NR relation is used,

$$[V_{n+1}]_{3\times1} = [V_n]_{3\times1} - [H_n]^{-1}_{3\times3}[G_n]_{3\times1} \tag{2.16}$$

   Generating new vectors at each step continues until one of the two conditions is satisfied. The first condition is the number of iterations. If the number of iterations steps exceeds more than 100, the iterations stop and proceed to the next step. The second condition is on norm of difference vector $\vec{\nabla}V = [V_n]_{3\times1} - [V_{n+1}]_{3\times1}$, given by Eq. [2.17], becomes less than 10^{-10}.

$$|\vec{\nabla}V| = \sqrt{\nabla V_{11}{}^2 + \nabla V_{21}{}^2 + \nabla V_{31}{}^2} \tag{2.17}$$

   This condition confirms the convergence in the last vector found. When the iterations stop, the previous V_{n+1} vector, along with its gradient and MED value, proceeds to the next step for further checks and assignment of critical point type.

3. In this step, we identify the type of critical point found. Eigenvalues and Eigenvectors of the invertible Hessian $(det(H_{n+1}) \neq 0)$ is calculated to assign rank and signature at converged vector V_{n+1}. To avoid any false or spurious converged points (for e.g. points far from atoms where $\rho(\vec{r}) < 10^{-8}$), we perform certain checks before diagonalizing H_{n+1} to

obtain eigenvalues and eigenvectors. A conditional check is performed on the norm value ($|\nabla\vec{V}| < 10^{-10}$) and non-zero MED value ($\rho > 10^{-4}$) at position depicted by V_{n+1}. This condition only allows converged V_{n+1} having non-zero MED values. To ensure, the first order derivative is numerically close to zero at V_{n+1}, the gradient norm $|\nabla G_{n+1}|$, it is ensured its value should be less that 10^{-5}.

After performing all the checks and removing all the recurring or repeating CPs, the unique ones are sorted based on their type and written in different files. The coordinates of $(3, -1)$, $(3, -3)$, $(3, +1)$, and $(3, +3)$ CPs are written out in *cpm1.dat, cpm3.dat, cpp1.dat, and cpp3.dat* files respectively. **The data concerning each CP:** x, y, z coordinates, MED value, gradient vector, Eigenvalues, and Eigen-vector of Hessian, for all $(3, -1)$, $(3, -3)$, $(3, +1)$, and $(3, +3)$ CPs are printed in respective *criticm1.dat, criticm3.dat, criticp1.dat* and *criticp3.dat* files.

2.2.7 Gradient paths, Bond paths, and Zero-flux surfaces of MED

The trajectories traced out by the gradient vector fields of MED are called *gradient paths*, which are obtained from the solutions of the following differential Eq. [2.18], for some initial value r(0)=r_0.

$$\frac{d(\mathbf{r}(s))}{ds} = \nabla\rho(\vec{r}(s)) \tag{2.18}$$

Therefore, the points r(s) of the gradient path through r_0 are given by,

$$r(s) = r_0 + \int_0^s \nabla\rho(r(s))ds \tag{2.19}$$

The Eq. [2.19] can also be expressed in terms of arc length along the gradient vector (the path length l), through the following expression,

$$\frac{d\mathbf{r}}{dl} = \frac{\nabla\rho(\vec{r})}{|\nabla\rho(\vec{r})|} \tag{2.20}$$

Starting at some arbitrary point $\mathbf{r}_0$, the trajectory of $\nabla\rho(\vec{r})$ is obtained by calculating $\nabla\rho(\vec{r_0})$, moving a distance Δr away from $\mathbf{r}_0$, in the direction indicated by gradient vector $\nabla\rho(\vec{r_0})$ and repeating the procedure until the path, so generated terminates.

The role of critical points is essential in defining the topological properties of MED. All the gradient field vectors either originate or terminate at these critical points. The (3,-3) critical points behave as an attractor of the gradient vector field. An attractor of $\nabla\rho$, A $\subset R^3$, should satisfy these conditions, (i) being invariant to the flow of $\nabla\rho$, (ii) trajectories originating in A are contained in A, and (iii) an open invariant neighborhood B of A exists such that any trajectories originating in B terminates at A. The basin of A is defined w.r.t the largest neighborhood B_{max}, which satisfies this condition.

The subspaces in th molecular electron density are determined by the presence of only a single local maximum in charge density located at nuclei (and at non-nuclear positions in some cases), which acts as the attractor of the gradient vector field. Using these observations on gradient field vectors, Bader and coworkers concluded that the molecular space of electron density can be partitioned into non-overlapping disjoint regions, also referred to as the basins, each containing only one point attractor. Hence, they defined *atoms in a molecule as a union of attractor and its associated basin*. Over the years, it has been investigated that Bader's atoms can contain the attractors at nuclear and non-nuclear positions, also called as pseudo atoms.

According to Bader's theory, the atoms in a molecule can be defined in terms of their boundaries present in the molecular space. The basin of an atom in a molecule contains a single nuclear attractor in the whole molecular space R^3. The molecule's atoms form basins, an open subset of R^3. These atomic basins are separated from other atoms by interatomic surfaces. These interatomic surfaces pass through the (3,-1) critical points, and the gradient paths on these surfaces terminate at the same (3,-1) CPs. The two eigenvectors v_1 and v_2 associated with the two negative eigenvalues of the Hessian matrix of such a critical point are used to generate this interatomic surface. The interatomic surfaces S_{AB} satisfies the following condition, given by the following Eq. [2.21],

$$\nabla\rho(\vec{r}) \cdot \hat{n}(\vec{r}) = 0 \quad \forall \quad \vec{r} \in S_{AB} \tag{2.21}$$

where $\hat{n}(\vec{r})$ is the unit vector normal to the surface at $\vec{r}$. A surface which satisfies Eq. [2.21] is called the *zero-flux surface*. Therefore, an atom in real space occupies a region which a a contains a single nuclear attractor bounded by interatomic surface or the zero-flux surface.

The interatomic surface coincides with its tangent plane in a very small neighbourhood of the (3,-1) critical point. The entire interatomic surface is spanned using vectors v_1 and v_2 with the gradients paths in very small steps. A representation of the same is given in Fig. [2.1]. The following steps describe the construction of zero-flux surface in the ABELDYNPROP code.

1. User-specified points on a small circle of radius 0.0001 a.u. are generated on the plane using the eigenvectors $\vec{v}_1$ and $\vec{v}_2$ of the corresponding to the two negative eigenvalues of the hessian matrix at (3,-1) CP, $\vec{r}_0$. The new points generated are calculated as in Eq. [2.22], where s is

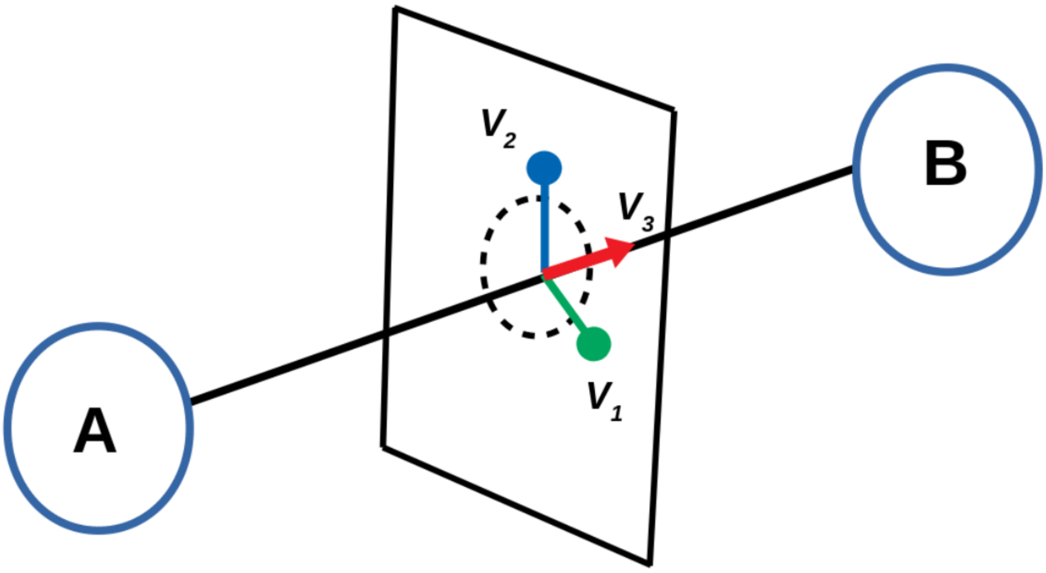

Figure 2.1: A representation of an eigenplane constructed by two eigenvectors corresponding to two negative eigenvalues of a (3,-1) CP of MED between two atoms A and B.

a small scalar parameter chosen to be 0.0001 a.u. The parameter s is also user defined.

$$\vec{r_1} = \vec{r_0} + (s)(v_1 \cos\theta + v_2 \sin\theta) \tag{2.22}$$

2. Starting with a point on the small radius circle, $\vec{r}_0$, the analytical gradients at $\vec{r}_0$ are calculated to generate trajectory of $\vec{\nabla}\rho(\vec{r}_0)$. It is moved a distance Δr away from $\vec{r}_0$ in the direction of $\vec{\nabla}\rho(\vec{r}_0)$ using the user-defined step-size to generate a new point, $\vec{r}_{i+1} = \vec{r}_i + t\vec{\nabla}\rho(\vec{r}_i)$ in the trajectory, where t is the user defined step-size parameter of vector $\vec{\nabla}\rho(\vec{r}_i)$. The procedure is repeated and followed up to generate the next point in the trajectory. The total number of points in the trajectory are decided by the user-input.
3. The non-uniform grid points generated for each trajectory are is stored and passed on to a triangulating subroutine to generate the zero-flux

surface in *visual toolkit* (vtk) format file for the purpose of surface visualization.

The role of gradient paths in defining the bonds paths is discussed in the following paragraphs.

Bond Paths: These are trajectories generated from the eigenvectors $\vec{v}_3$ associated with the only positive eigenvalue of the (3,-1) critical points. The two gradient paths can be carved out, each from ± directions of eigenvector $\vec{v}_3$. These two gradient paths trace out a line through the charge distribution along which $\rho(\vec{r})$ is a maximum concerning any lateral displacement. These two lines originated from the (3,-1) CP moving towards and terminating each at one (3,-3) CP. Since these connect the two neighboring nuclear maxima, such lines are often called *bond paths*. The union of bond paths is defined as molecular graphs for a given nuclear geometrical configuration. Pictorially, the molecular graph is the network of bond paths linking pairs of neighboring nuclear attractors.

The (3,+1) and (3,+3) critical points in the molecular graph appear as the consequence of a particular geometrical arrangement of bond paths and define the remaining elements of molecular structure - *rings and cages*. The eigenvectors associated with the two positive values of the Hessian of a (3,+1) critical point span a ring surface in a molecular region and hence called ring critical point. The other eigenvector corresponding to the negative eigenvalue generates a pair of gradient paths that define an axis perpendicular to the ring surface at the critical point. The properties at ring critical points have been used to characterize H-bond strength in aromatic and weakly hydrogen-bonded systems.[52–54] The eigenvectors associated with the (3,+3) critical points denote a local minimum in $\rho(\vec{r})$, which is the origin for the generation of infinite gradient paths in the molecular space.[55]

2.2.8 Atomic Properties

The quantum theory of atoms in molecules proposes that the molecular region of electron density partitions into non-overlapping regions, each basin containing a local maximum. Consequently, any atomic property P_A is the average over the atomic basin of an effective single-particle density p($\vec{r}$). Thus the value of property P_A for the basin Ω is given by Eq. [2.23],

$$P_A(\Omega) = \int_\Omega p(\vec{r}) d^3r \tag{2.23}$$

The follow-up definition of the average P value for the total molecular system is the sum of all the basins containing the local maximum. The total property P_T for the molecular system is given in Eq. [2.24],

$$P_T = \sum_\Omega P_A(\Omega) \tag{2.24}$$

To evaluate the properties of $P_A(\Omega)$, the surface bounding the basin region Ω must be determined. These surface regions do not have trivial solutions since the bounded regions may have irregular shapes and sizes, which makes the basin integration in Eq. [2.23] difficult. Using zero-flux condition[18, 19] and the divergence theorem[56], it is derived that the Laplacian of electron density over atomic basin is zero,

$$\int_\Omega \nabla^2 \rho(\vec{r}) d^3r = 0 \tag{2.25}$$

Using in Eq. [2.25], the kinetic energy quantities, $K(\Omega)$ and $L(\Omega)$, is defined as,

$$\begin{aligned} K(\Omega) = -\frac{N}{4} \int_\Omega \int \cdots \int [&\Psi^*(\vec{r}, \vec{r_2}, \cdots, \vec{r_N}) \nabla_{\vec{r}}^2 \Psi(\vec{r}, \vec{r_2}, \cdots, \vec{r_N}) \\ &+ \Psi(\vec{r}, \vec{r_2}, \cdots, \vec{r_N}) \nabla_{\vec{r}}^2 \Psi^*(\vec{r}, \vec{r_2}, \cdots, \vec{r_N})] d^3r_2 \cdots d^3r_N d^3r \end{aligned} \tag{2.26}$$

$$L(\Omega) = \frac{N}{2}\int_{\Omega}\int\cdots\int \nabla_{\vec{r}}\Psi^{*}(\vec{r},\vec{r_2},\cdots,\vec{r_N}) \bullet \nabla_{\vec{r}}\Psi(\vec{r},\vec{r_2},\cdots,\vec{r_N}) \\ d^3r_2\cdots d^3r_N d^3r \qquad (2.27)$$

and are equal because,

$$L(\Omega) \equiv K(\Omega) - G(\Omega) = -\frac{1}{4}\int \nabla^2\rho(\vec{r})d^3r = 0 \qquad (2.28)$$

Here, Ψ represents the total electronic wavefunction related to $\rho(\vec{r})$. The Eq. [2.28] represents the atomic virial theorem, which is satisfied when $K(\Omega)$ and $G(\Omega)$ are equal to minus one times the energy of Bader atom Ω.[18] The quality of integration is measure traditionally in terms of L(Ω). For a perfect integration, this quantity vanishes. The properties calculated using QTAIM can be used for wave-function-based methods and density-functional theory. However, the validity of Eq. [2.27] and [2.28] could be checked only for electronic wavefunctions, Ψ, that calculate electron density $\rho(\vec{r})$. In this code, we compute atomic properties and check the quality of integration using verification from Eq. [2.27] and [2.28]. We also verify if the sum of the atomic property recovers the corresponding molecular property.

QTAIM employs the topology of electron density to perform analysis. Critical points play a vital role in the QTAIM analysis. The critical points corresponding to the electron density maxima, called attractors, are categorized as nuclear/atomic or non-nuclear attractors. Each point in every basin draws a gradient ascent path that terminates at its corresponding maximum or attractor. Partitioning algorithms to integrate properties for these basins developed by Popelier and Geerlings was complex and computationally expensive.[57, 58] The commonly used algorithms[18, 28, 59] involves (i) finding the critical points of MED where $\nabla\rho(\vec{r}) = 0$, followed by (ii) the construction of interatomic surfaces which intersect these points then (iii) integration of the electronic density within each region. Determining interatomic surfaces was the most time-consuming step in these algorithms. They made several improvements after the initial methods of finding Bader regions. Popelier used the bisection method[61] to find the boundary surfaces and employed Chebyshev polynomials[62] to improve the basin integration method. Popelier has suggested the calculation of enclosed charge[57] using the divergence theorem by integrating the electric field on the dividing surface around the atom. In the early 2000s, Macmolm and Popelier[63, 64] used dynamic grid techniques, firstly implemented by Silvi and coworkers[65, 66] to effectively treat complicated molecule bonding regions. Henkkelman and group[27, 67–69] developed a fast and robust algorithm and further improved it to calculate Bader charges using the pre-calculated density grid files. They implemented a powerful algorithm since it finds no critical points or zero-flux surfaces. The algorithm uses the steepest accent gradient path following approach, w.r.t its neighboring points, which converge to one of the local maxima. Rodgriguez and coworkers[70, 71] developed a grid-based scheme to compute QTAIM properties without explicitly calculating zero-flux surfaces. In this scheme, the integration grid in real space is partitioned in subsets, Ω_i. The subset, Ω_i, makes up all the grid points in the atomic basin, Ω_i. Therefore, the integrations over Ω_i are reduced to quadrature over the points in Ω_i.

In this work, we present a scheme that uses the spherical polar grid to assign atomic basins following the basic philosophy of steepest ascent path of gradient paths in the works of Henkelman et al.[67] Unlike the work by Henkelman and group, we calculate the number of local maxima in the electron density distribution. We employ a user-defined spherical grid (r, θ, Φ) centered on the local maxima. It is followed by identifying the sets (r, θ, Φ) belonging to the corresponding atomic basin. The integration over the identified set of r, θ, Φ to calculate the properties such as Bader charges, Laplacian, Kinetic energies, electrostatic moments, and dipole moment.

Algorithm: A vector $\vec{r}_o$ of user-defined length is drawn from the (3,-3) CPs as the center for all θ and Φ of the spherical grid. For a given θ and Φ, we will determine the cutoff length r_{cut} of vector $\vec{r}_o$ which belongs to the basin by tracing the steepest-density-ascent gradient path to an attractor. We use analytical forms to calculate gradient paths of density. A small step size should be chosen to control the accuracy of gradient paths. However, at the same time, the smaller step sizes would increase the computational time. The steepest ascent path is terminated once it enters *atomic trust sphere*, which could help reduce time to make it faster. For a given (3,-3) CP, for all θ and ϕ, the largest value of r, r_{max}, belonging to this basin is determined. Once this information is obtained, we integrate all the basin regions to compute average properties, such as charges, norm, kinetic energies, dipole, and electrostatic moments.

Atomic Trust Sphere: It was observed that the algorithm would be faster if the atomic trust sphere (ATS) had a larger radius. It is calculated once for all the (3,-3) CPs and then used in the main basin finding subroutine. It is defined as the sphere's radius for every θ and ϕ, where each point inside it would terminate at the (3,-3) CP. The biggest radius r_s satisfying this condition would be chosen as the radius of ATS.

Screening the NNMs: The electron density and its gradients are numerically very small at distances far away from any nucleus. In our quest for the topological behavior of TDMED, we have also located new low-valued NNMs at distances away from the bonds of molecules, especially along the direction of laser polarization. To identify non-nuclear attractors in the electron density, we find all the points in space that satisfy:

1. $\rho(\vec{r}_0) > \epsilon$. The values of ϵ is user defined. $\epsilon \in [10^{-4} - 10^{-7}]$.

2. The norm of converged gradient vector $\nabla\rho(\vec{r}_0)$ is almost zero.

3. The Hessian at $\vec{r}_0$ should have three negative eigenvalues.

Steps of the overall algorithm:

1. All local maxima are located for the time-varying electron density distribution at a time-step. This is evaluated using the same subroutine of code discussed earlier in the manuscript. Since, the total number of atomic basins (nuclear and non-nuclear, if any) equals the total number of (3,-3) CPs, therefore the total local maxima are identified. Thereafter, the MPI-paralleled version of the code is invoked. This invokes nodes equivalent to the number of local maxima, and then it calculates the properties of each basin on a separate distributed memory node.

2. A user-defined spherical polar grid (r, θ, Φ) is constructed with (3,-3) CPs as the center. The number of points are the grid n_r, n_θ, n_ϕ are inputs to the code via input file. Here, the value of r is a user-defined parameter and $\theta \in$ [0,π] and $\phi \in$ [0,2π]. Additionally, the choice for grids to be either equally spaced or be a *gauss-legendre* type is provide with the user.

3. We determine the **atomic trust sphere** of each of the local maximum. The maximum grid step in r, r_{i+1}, where every θ and ϕ, where all points inside would converge to the local (3,-3) CP. If r $< r_{ATS}$, it helps in reducing the number of iterative steps.

4. In this step, we identify the value of r_{max} for each set of θ and ϕ. The r_{max} is identified using the gradients following the steepest ascent path. We follow these sub-steps to find r_{max}.

    a. A search through r grid (equally spaced/gauss-legendre) in user-defined increments, r_{ns}, to find the i^{th} step in r which terminates to the local (3,-3) CP. In the process, we perform termination/elimination of gradient path steps if (i) it diverges to other neighbouring maxima (case: $\rho_r > \rho_{-3}$) (ii) it enter the ATS radius (case: $r < r_{ATS}$).

b. Since, the ZFS are open surfaces, two kind of scenarios are encountered in finding the r_{max}. For the regions not bounded by ZFS, the r_{max} would be equal to the radius defined by the user in the input file. On other hand, regions separated by ZFS, a *bisection* is performed taking r in i^{th} (found in step a) and $i + 1^{th}$ step as guess points to find r_{max} with better precision. Kindly note, the increasing precision increases the computational cost. The precision control parameter is user-defined.

5 The information of r_{max} at each set of θ and ϕ is used for perform numerical integration over the basin to evaluate the properties. The integration type is regular spherical polar integration or gauss-legendre type integration. The average properties of atomic basins and total properties are evaluated for the following listed analytical forms

$$N(\Omega) = \int_{\Omega} \rho(\vec{r}) d\tau \tag{2.29}$$

$$q(\Omega) = Z_A - \int_{\Omega} \rho(\vec{r}) d\tau \tag{2.30}$$

$$M_1(\Omega) = -\int_{\Omega} r_{\Omega} \rho(\vec{r}) d\tau \tag{2.31}$$

$$M_2(\Omega) = -\int_{\Omega} r_{\Omega}^2 \rho(\vec{r}) d\tau \tag{2.32}$$

$$Q_{XX}(\Omega) = -\int_{\Omega} (3x_{\Omega}^2 - r_{\Omega}^2) d\tau \tag{2.33}$$

$$Q_{YY}(\Omega) = -\int_{\Omega} (3y_{\Omega}^2 - r_{\Omega}^2) d\tau \tag{2.34}$$

$$Q_{ZZ}(\Omega) = -\int_{\Omega} (3z_{\Omega}^2 - r_{\Omega}^2) d\tau \tag{2.35}$$

$$Q_{10}(\Omega) = -\int_{\Omega} z \rho(\vec{r}) d\tau \tag{2.36}$$

$$Q_{11c}(\Omega) = -\int_{\Omega} x\rho(\vec{r})d\tau \tag{2.37}$$

$$Q_{11s}(\Omega) = -\int_{\Omega} y\rho(\vec{r})d\tau \tag{2.38}$$

$$Q_{20}(\Omega) = -\int_{\Omega} \frac{1}{2}(3z^2 - r^2)\rho(\vec{r})d\tau \tag{2.39}$$

$$Q_{21c}(\Omega) = -\int_{\Omega} \sqrt{3}xz\rho(\vec{r})d\tau \tag{2.40}$$

$$Q_{21s}(\Omega) = -\int_{\Omega} \sqrt{3}yz\rho(\vec{r})d\tau \tag{2.41}$$

$$Q_{22e}(\Omega) = -\int_{\Omega} \frac{1}{2}\sqrt{3}(x^2 - y^2)\rho(\vec{r})d\tau \tag{2.42}$$

$$Q_{22s}(\Omega) = -\int_{\Omega} \sqrt{3}xy\rho(\vec{r})d\tau \tag{2.43}$$

$$\mu_x = \sum_{\Omega} Z_{\Omega}x_{\Omega} - \int_{\Omega} x\rho(\vec{r})d\tau \tag{2.44}$$

where $d\tau$ is the volume element. The above mentioned analytical forms represent Norm (N(Ω)), Bader's charge (q(Ω)), first and second-order moments ($M_1(\Omega)$, $M_2(\Omega)$), Quadrapole moment in X, Y, Z (Q$_{XX}(\Omega)$, Q$_{YY}(\Omega)$, Q$_{ZZ}(\Omega)$), electrostatic moments (Q$_{10}(\Omega)$, Q$_{11c}(\Omega)$, Q$_{11s}(\Omega)$, Q$_{20}(\Omega)$, Q$_{21c}(\Omega)$, Q$_{21s}(\Omega)$, Q$_{22e}(\Omega)$, Q$_{22s}(\Omega)$)), and dipole moments (μ_x, μ_y, μ_z).

2.3 Methodology

The **ABELDYNPROP** package calculates electronic properties using wavefunctions or molecular orbitals coefficients as input. The time-dependent coefficients obtained from the solutions of the TDSE are used to evaluate time-dependent properties. The ABELDYNPROP code, in general, can use inputs from any code-solving TDSE. However, we performed all the tests and checks using molecular orbitals coefficients from the in-house ABELDYN code.[3]

The program uses exponents and contraction coefficients of Gaussian basis function as input to form the time-independent or time-dependent wavefunctions. A general Gaussian-type functions is given by[72]

$$\begin{aligned} \eta(\vec{r}) = N_c(x - x_A)^{l_x}(y - y_A)^{l_y}(z - z_A)^{l_z} \\ \exp[-\alpha|(x - x_A)^2 + (y - y_A)^2 + (z - z_A)^2|] \end{aligned} \tag{2.45}$$

where α is the exponent of the Gaussian. The notations l_x, l_y, and l_z represent the indexes of the angular momentum labels along x, y, z directions. The position vector $\vec{A}$ is the center of the Gaussian-orbitals which denotes the position of the atom placed at x_A, y_A, z_A in three-dimensional space. The factor N_c represents the normalization constant and is calculated as follows,

$$N_c = (2\pi\alpha)^{3/4}\left[\frac{(4\alpha)^{l_x+l_y+l_y}}{(2l_x - 1)!!(2l_y - 1)!!(2l_z - 1)!!}\right]^{\frac{1}{2}} \tag{2.46}$$

The evaluation of any properties in real space requires the evaluation of three-dimensional wavefunction or molecular orbitals. The molecular orbitals are computed using coefficients C_{ai} obtained from the solutions of TISE/TDSE. The a^{th} orbital are calculated as,

$$\Psi_a(\vec{r}) = \sum_{i=1}^{N_{bas}} C_{ai}M_i\Phi_i(\vec{r}) \tag{2.47}$$

where M_i represent the normalized contraction coefficients, and the summation goes over the total number of basis functions N_{bas}, which are basically all the contracted Gaussian functions in the system. $\Phi_i(\vec{r})$'s are basis functions constructed using the linear combination of primitive Gaussian functions. The following forms describes the construction of contracted Gaussian $\Phi_i(\vec{r})$,

$$\Phi_i(\vec{r}) = \sum_{j=1}^{J} a_{ij}f_j(\vec{r}) \tag{2.48}$$

In Eq. [2.48], the i^{th} contraction includes J primitive Gaussian functions and a_{ij} is the pre-fixed coefficient to the primitive Gaussian. Given the set of all molecular orbitals $\Psi_a(\vec{r})$, the electronic properties in position space are calculated.

The codes in the ABELDYNPROP package are written in Fortran 90. The main driver routine of code reads the specifications provided through the input file, *input.dat*. Each property is assigned a specific keyword in the code, which calls that required specific subroutine to calculate and present the output to the user. The ABELDYNPROP is executed through bash shell scripting to perform computation for a batch of input time steps files.

Pre-requisites: For the execution of the code would require fortran complier (*gfortran*), and numerical linear algebra libraries (essentially LAPACK, BLAS) to be pre-installed on the machine. The code is tuned in for multi-processing machine with distributed memory system, therefore, installation of *message passing interface* (MPI) is necessary.

2.3.1 Description of an input file, and bash shell script to execute the program

The ABELDYNPROP code specially designed to evaluate dynamic properties in time-dependent fields is executed through a bash shell script, runtd.sh. However, before the execution of the bash shell script, we require a set to input files/folders to be provided beforehand. To compute properties for a set of time-dependent wavefunctions $\Psi(\vec{r}, t_i)$, the working directory should contain two folders, *inpdir*, *timefiles* and the executable *run.exe*.

- **inpdir:** This folder should include two files. The first one, (a) *input.dat* - Provides information on the type of job and user-defined parameters regarding the molecular propertry in position space to be calculated. A detailed description of *input.dat* is to be provided in the subsequent sections of the manuscript. The second file is (b) the molecular information file obtained from the GAMESS[40] output, a *.dat* formatted file. This file contains information about the atom, its atomic number, cartesian coordinates in Angstrom, exponents, and pre-fixed coefficients of primitive Gaussian functions. This file also includes free-field molecular orbital coefficients for the same basis functions. The file name of this *.dat* is provided in the *input.dat* file.

- **timefiles:** This folder contains the files that provide the coefficients of the complex wavefunction at each time step of the time-dependent fields such as lasers. The complex-valued wavefunction for all timesteps is obtained by executing the in-house built ABELDYN code in the form of two files, one containing the real part (say, tmcofr.dat) and the other the imaginary part (say, tmcofi.dat). Each row of both of these files, represent the all the coefficients of the wavefunction of the size $(N_{bas} * N_{bas})$. Using a simple fortran code, *makemo.f90*, each row in these files (tmcofi.dat, tmcofr.dat) are converted into a single column and each one is stored in a seperate files pertaining to the timestep file. The *makemo.f90* code takes total basis function N_{bas}, total timesteps N_t and files names of the complex wavefunction files. This is done for both the real and imaginary parts of complex-valued wavefunction.

- **run.exe:** This is the executable created by compiling the code using Fortran 90. All the main programs, subroutines, and functions of the ABELDYNPROP code are provided in the **prog** folder. We provide a bash shell script, *comp.sh*, which, when executed, creates the executable *run.exe* when the user installs the ABELDYNPROP code. The bash shell script runtd.sh uses this executable script to evaluate the properties.

The ABELDYNPROP's code executable, *run.exe*, reads the information regarding the atom coordinates, basis functions, property to calculate keywords, user-defined parameters required for the job-type, and timestep indexes via input.dat file kept in the *inpdir* folder. For a time-dependent property job, A sample *input.dat* file is described here,

```
# SECTION-PROPERTY
PROPERTY_TO_CALCULATE     :: EDEN
ATOM_BASIS_FILE           :: h2o.dat
MO_REAL_OR_COMPLEX        :: COMPLEX
N_PROCS                   :: 4

# SECTION-PARAMETER
CART_GRID_XMIN_XMAX_NX    :: -8.000000000, 8.000000000, 11
CART_GRID_YMIN_YMAX_NY    :: -8.000000000, 8.000000000, 11
CART_GRID_ZMIN_ZMAX_NZ    :: -8.000000000, 8.000000000, 11
DATA_FILE_TYPE_CUBE/VTK   :: cube

# SECTION-TIMEFILE
TIMEFILE_PREFIX           :: tmcoef
TIMEFILE_START_INDEX      :: 1
TIMEFILE_END_INDEX        :: 2
TIMEFILE_STEP_SIZE        :: 1
```

This input file is divided into three section. The first section in the input file is, SECTION-PROPERTY. This sections describes about the type of property to be calculated, name of atom-basis file and type of wavefunction used in the calculation. We shall describe the lines in this section,

```
1. PROPERTY_TO_CALCULATE    ::
```

The list of keywords implimented in the code and with their properties are mentioned here,

1.1 EDEN: Evaluates the Molecular Electron Density (MED) on a three-dimensional cartesian grid. The grid specifications are provided in the Section-parameter. Analytical form used for calculation is shown in Eq. [2.2]. We generate eden.cube/eden.vtk files as output.

1.2 EGRD: The analytical gradients of MED in x, y, and z are calculated on a 3D grid. Analytical form used for calculation is shown in Eq. [2.7]. We get egrd.cube/egrd.vtk as output.

1.3 EHES: The Hessian of MED are calculated on a 3D grid. Analytical form used for calculation is shown in Eq. [2.11]. Since, Hessian matrix is symmetric, we only calculate lower diagonal elements of the Hessian matrix (See Eq. [2.10]). The output we get are ehes.cube/ehes.vtk files.

1.4 ELAP: The Laplacian of MED are calculated on a 3D grid. Only the sum of diagonal elements of Hessian matrix (three terms) are evaluated using the form described in Eq. [2.12]. The output we get are ehes.cube/ehes.vtk files.

1.5 VDEN: Calculates the X, Y, and Z components of the vector current density on the grid. The output file is names vden.cube/vden.vtk.

1.6 ELF: Computes the electron localization function on the 3D provided. The data is stored in output files named elf.cube/elf.vtk.

1.7 MORB: The user-defined molecular orbitals are calculated on a 3D cartesian grid. They are evaluated Eq. [2.3]. For the time-dependent calculation, separate data files for real and imaginary parts are created for the a_k^{th} orbital (morbra_k.cube/morbra_k.vtk and morbia_k.cube/morbia_k.vtk).

1.8 ALLCRITIC: Locates all the 4 types of three dimensional non-degenerate critical points (if it exists) of the molecular electron density distribution. The procedure to find critical finds are mentioned in the sections above using NR method and using Eq. [2.16] and [2.17]. The user-defined parameters to locate critical points are mentioned later in the parameters section. The coordinates of the critical points are stored in *cpm1.dat*, *cpm3.dat*, *cpp1.dat*, and *cpp3.dat*. The details of electron density, their gradient norm, eigenvectors and eigenvalues regarding the critical points are provided in *criticm1.dat*, *criticm3.dat*, $textitcriticp1.dat$, and *criticp3.dat* data files.

1.8 ZEROFS: For all the (3,-1) CPs found, interatomic surface or zeroflux surface is computed using this keyword. The surface is created using Eq. [2.22]. The output is stored in cpa_i.vtk (the index depict the a_i^{th} (3,-1) CP) files which can be used for visualization. In addition to this, we also evaluate bond paths, gradient paths, basin boundaries and molecular graphs in the MED distribution. The output of bondpaths, gradient paths and basin boundaries are stored in *bondpath.dat*, *cp3grad.dat*, and *cp1grad.dat* data files respectively.

1.9 BDPARTSP: All the (3,-3) CPs are located, their Bader regions are identified and average properties in these regions are calculated. We calculate the norm, bader charge, kinetic energies, bader volume, electrostatic moments, dipole moment and stored in a file named *bader.dat*.

1.10 PLDEN: Through this keyword, MED, its gradient, Laplacian, and vector current densities could be calculated on the plane. The data is stored in out files named *denplane.dat, lapplane.dat, gradplane.dat*, and *vdenplane.dat*.

1.11 DIPMOM: Dipole moment components in X, Y and Z are evaluated using the points provided by the user. The values of dipole moment in x,y, and z are provided in atomic units and Debyes respectively in the output file *output.log*.

1.11 ELEMOM: The electrostatic moments, also called dipole integral matrix elements are computed using this keyword. The integral matrix elements are printed in the *output.log* file. This keyword is only applicable for REAL type wavefunctions in the code.

```
2. ATOM_BASIS_FILE          :: h2o.dat
```

A file containing the information regarding the cartesian coordinates of atom, exponents and coefficients of primitive Gaussian functions centered on atoms. Additionally, they also contained coefficients of the free-field wavefunctions. This is *.dat* formatted file and could be obtained by using GAMESS for the desired system and job type.

```
3. MO_REAL_OR_COMPLEX       :: COMPLEX
```

The information, if the wavefunction/MO is REAL or COMPLEX is provided here. In the cases the input wavefunction REAL, it is read directly from the GAMESS .dat Atom-basis file. When the wavefunction is COMPLEX, all the time-step files should be provided in the *timefiles* folder.

The second section of the input file, SECTION-PARAMETER. Specific user-defined inputs are required for the calculation of properties, which are provided in this section. For the grid-based properties, with keyword, EDEN, EGRD, EHES, ELAP, require the input of x, y, z, range and number of points to be calculated. The input keywords in the parameter section are,

```
4.1 CART_GRID_XMIN_XMAX_NX    :: -8.000000000, 8.000000000, 11
    CART_GRID_YMIN_YMAX_NY    :: -8.000000000, 8.000000000, 11
    CART_GRID_ZMIN_ZMAX_NZ    :: -8.000000000, 8.000000000, 11
    DATA_FILE_TYPE_CUBE/VTK   :: cube
```

Cartesian grid values of X_{min}, X_{max}, Y_{min}, Y_{max}, Z_{min}, Z_{max} are provided. Also, the number of points along each grid N_x, N_y, and N_z should be included. The data storing format type, either .cube or .vtk is specified in this section. Since the calculation of molecular orbitals using MORB keyword requires the value of N^{th} orbital, this information is provided using the parameters with a extra line above the grid specifications, as shown in next lines

```
MOL_ORB_N                 :: 5
CART_GRID_XMIN_XMAX_NX    :: -8.000000000, 8.000000000, 51
CART_GRID_YMIN_YMAX_NY    :: -8.000000000, 8.000000000, 51
CART_GRID_ZMIN_ZMAX_NZ    :: -8.000000000, 8.000000000, 51
DATA_FILE_TYPE_CUBE/VTK   :: cube
```

If the property keyword is ALLCRITIC, the following parameter file is used,

```
4.2 R_NR_NTHETA_NPHI          :: 8.000000, 11, 21, 21
    MAX_NEWTON-RAPHSON_ITER   :: 50
    CONVERGENCE               :: 1.0E-8
    MINIMUM_DENSITY           :: 1.0E-8
```

The first line takes the inputs of a radius of the guess sphere, the total number of points for N_r, N_θ, N_Φ. The second lines provides the input of the maximum number of iterations to be used in the Newton-Raphson routine NR_{max} to find CPs. The convergence criteria ϵ_c for the new critical point found is set using this third line in parameter section. The last line provides the cutoff density r_c, only critical points are found if $\rho > 1.0^{-8}$ a.u. in this example. The

$\epsilon_c = |\vec{r}_i - \vec{r}_{i+1}|$, refers to the norm of the difference vector between the new and old vector found between the i^{th} and $(i+1)^{th}$ iteration. A critical point could be found if ϵ_c user-defined value.

When the property keyword used is ZEROFS, the parameters are detailed as follows,

```
4.3 R_NR_NTHETA_NPHI          :: 8.000000, 11, 11, 11
    MAX_NEWTON-RAPHSON_ITER   :: 50
    CONVERGENCE               :: 1.0E-7
    MINIMUM_DENSITY           :: 1.0E-6
    ZFS_TOTAL_CIRCLE_POINTS   :: 50
    ZFS_GRADIENT_STEP_SIZE    :: 0.05
    ZFS_POINTS_ALONG_VECTOR   :: 100
    BP_GVEC_STEP_SIZE         :: 0.00010
    BP_MAX_POINTS             :: 100000
    GP_PLANE_VECTOR_1         :: 0.00, 1.00, 0.00
    GP_PLANE_VECTOR_2         :: 0.00, 0.00, 1.00
    GP_PLANE_CIRCLE_POINTS    :: 32
    GP_VECTOR_STEP            :: 0.001
    GP_TOTAL_STEPS            :: 6000
```

The first four lines are similar parameters that were used for finding CPs. The following three lines provide the parameters required for the construction of ZFS. The fifth line in this parameter section provides the total number of points to be taken on the small circle (of radius 0.0001 a.u.), as mentioned in steps of the ZFS construction algorithm, using Eq. 2.22. The step size of the analytical gradients and the total number of steps to be followed along the gradient line is mentioned in the subsequent 6^{th} and 7^{th} line. The parameters for the calculation of bond-paths and gradient paths are provided in the next set of 7 lines.

On the other hand, when the property keyword used is BDPARTSP, the parameters are detailed as follows. For this keyword, the program utilizes the first four lines in the parameter file to locate all the (3,-3) CPs. The same number of nodes are invoked as the number of (3,-3) CPs found in the code.

```
4.3 R_NR_NTHETA_NPHI             :: 8.000000, 11, 21, 21
    MINIMUM_DENSITY              :: 0.0001
    MAX_NEWTON-RAPHSON_ITER      :: 50
    CONVERGENCE                  :: 1.0E-10
    PART-RMAX_NR_NTHETA_NPHI     :: 9.000000, 101, 20, 40
    STEPS_MOVE_NR                :: 20
    SCALAR_GRADIENT_STEP         :: 0.05
    MAX_STEP_ITER                :: 200
    BISECTON_ERROR               :: 1.0E-07
    INTEGRATION_METHOD           :: 1
    TOTAL_INTEG_POINTS           :: 301
```

After the fourth line, We mention the parameters required to implement Bader's partitioning. In the 5^{th} line, the maximum value of r, r_{max}, and the number of points N_r, N_θ, N_Φ in spherical polar grid (r, θ, Φ) are mentioned. The algorithm does not run for all steps in the r grid but at specified intervals; therefore, the step size in r is provided in the 6^{th} line. The next two lines provide the scale value describing the step-size and maximum number of iterations to be followed of the analytical gradients used in the routine. The error ϵ_{bs} between the two points near the two points in the bisection method, which finds the R_{cut}, is described in the next line. For example, in the case mentioned above, the bisection method would terminate when $\epsilon_{bs} < 1.0E-07$ or less.

For the property keyword PLDEN, the parameters of the plane grid should be provided as mentioned in the following syntax,

```
4.4 PLANE_ORIGIN            :: 0.00,-12.00,-12.00
    PLANE_VECTOR_1          :: 0.00,1.00,0.00
    PLANE_VECTOR_2          :: 0.00,0.00,1.00
    VECTOR_STEP_SIZE        :: 0.2
    TOTAL_STEPS_N1_N2       :: 101, 101
```

Here, the first line describes the origin point of the grid, while the next two lines defines the X, Y and Z components of the two vectors to be be utilized to construct the points of the plane's grid. The fourth lines provides the input for the step-size of the vector to be used, while the last line provides the number of steps to be followed along the vectors v_1 and v_2.

The next property keyword is DIPMOM, which evaluates the dipole moment vector components μ_x, μ_y and μ_z.

```
4.5 CENTER_POINT            :: 0.00,0.00,0.00
```

We provide the only a point using which dipole is evaluated as parameters for the calculation in the following way described in the above line.

```
5.1 TIMEFILE_PREFIX         :: tmcoef
    TIMEFILE_START_INDEX    :: 1
    TIMEFILE_END_INDEX      :: 100
    TIMEFILE_STEP_SIZE      :: 5
```

The third and last section of the input file is SECTION-TIMEFILE. It defines the prefix name of the timefile in the first line, the start index, the end index in the next two lines (2^{nd} and 3^{rd}) and the step size of time file execution in the fourth line. For the example shown here, represents that in the *timefiles* folder the timefile are named as (tmcoefr1.txt, tmcoefr2.txt,$\cdots$, tmcoefi1.txt,tmcoefi2.txt,$\cdots$). The jobs will be processed, starting from the first timefiles and continuing till the last 100^{th} files in steps of 5, executed through the bash shell script run.sh.

We have discussed about the ABELDYN code in the chapter 1, which is important for obtaining the time-evolving wave functions. In the next subsection, we briefly describe the various input parameters required to run the ABELDYN ocde.

2.3.2 Description of the Sample input file for ABELDYN code

The sample input file format required to execute the ABELDYN code is shown here. The example input file presented specifies the input files and parameters required to set up the calculation for acetylene molecule in the presence of linearly polarized laser along z-direction with laser frequency and electric field strength of 0.114 a.u. and 0.054 a.u. respectively. The successful run provides a set of output files concerning the data related to: properties of system, error check, population, charge, occupancy, density matrix, orbital coefficients (Real and Imaginary parts), and fourier components, at time instances with step size of 0.10 a.u. along the full laser pulse.

```
#-------------------------------------------------------------------------------
# Parameters for the time-dependent calculations
#-------------------------------------------------------------------------------
" onelectron integral file 1-D array lower diag :: "./matrx/onelec.txt
" unique twolectron integral file 1-D array     :: "./matrx/twelc.txt
" dipole AO integral file 1-D array lower diag  :: "./matrx/dplao.txt
" CAP AO integral file 1-D array lower diag     :: "./matrx/capao.txt
```

```
" coefficient matrix file in AO 2-D array       :: "./matrx/coef.txt
" molecule type/coordinate/basis input file     :: "./matrx/molcord.xyz
" laser electric field strength                 :: "  0.0540000D+00
" laser frequency                               :: "  0.1140000D+00
" initial pahse of the laser                    :: "  0.0000000D+00
" direction of the laser(1. x, 2. y, 3. z )     :: " 3
" strength of complex absorbing potential       :: "  1.0000000D+00
" number of Floquet channel for (t,t')-method   :: " 25
" number of Fourier components of density matrix:: " 5
" number of optical cycles for starting pulse   :: " 2
" number of optical cycles for cw-region pulse  :: " 2
" number of optical cycles for ending pulse     :: " 2
" total number of optical cycles                :: " 8
" delta t eg. (1,10; dt=0.1), (2,10; dt=10)     :: " 1, 10
" number of orbital energies to be written      :: " 10
" number of steps in which density is written   :: " 1
" file out for the properties                   :: "tmprp.txt
" file out for the error check                  :: "tmerr.txt
" file out for the population and TD charges    :: "tmpop.txt
" file out for the time-dependent charges       :: "tmchrg.txt
" file out for the time-dependent occupancy     :: "tmocc.txt
" file out for time-dependent density matrix    :: "tmden.txt
" file time-dependent imag coefficient matrix   :: "tmcoefi.txt
" file time-dependent real coefficient matrix   :: "tmcoefr.txt
" Time-dependent Fourier components             :: "tmfrr.txt
```

The first six lines of the input file require data files containing information related to one-electron integrals (*oneelec.txt*), two-electron integrals (*twelec.txt*), dipole integrals along X, Y, and Z directions (*dplao.txt*), complex absorbing potential (*capao.txt*), field-free molecular orbital coefficients (*coef.txt*), number of atoms, atomic charge, multiplicity, number of basis function on each atom and coordinates of atoms in molecule (*molcord.xyz*). These data files are prepared in column (oneelec.txt, twoelec.txt, dplao.txt, capao.txt) and 2D matrix (coef.txt) formats. These data files should be available before performing calculations using ABELDYN code. The one-electron integrals, two-electron integrals, dipole integrals, field-free molecular orbital coefficients are obtained from the Hartree-Fock theory calculations performed using the modified source code of the electronic structure package GAMESS.[40] The molecular information, that is, the number of atoms, charges, multiplicity, number basis function on each atom and coordinates of atoms in the molecule are read from a *.xyz* file. An in-house code is executed to obtain complex absorbing potential (CAP), for a box-type grid as input. The CAP is imaginary potentials, $i\eta W$ (η = CAP strength, W = real and positive potential), added to the Hamiltonians to change the boundary condition of problem such that the wavefunction becomes from scattering to square-integrable. **The use of CAP is essential w.r.t evolution of wavefunction; hence we describe this briefly here:**

In the evolution of wave packets, often, the solutions are carried out using a discrete representation of Hamiltonian and wavefunction on a finite grid. However, in scattering processes, the wavefunction could move towards some outgoing asymptotic state where the effect of interaction or even some in parts could vanish since one or more coordinates reach infinity at the boundary. This spatial finite grid box does not represent this indefinite process because it will get reflected when the wavefunction arrives at the box edge. The reflected wave could interfere with the part of the wave remaining in the box and spoil the physical validity of the calculation. Increasing the boundaries may solve the problem but at an expensive calculation cost. An alternate and effective way is the addition of *complex absorbing potential* at the boundaries.[73] The complex absorbing potential absorbs the wavefunction without making any changes in the physical wavefunction in the inner part of the grid. This makes the method numerically robust.

The next set of 14 lines (from 7th to 20th line) ask for inputs related to laser parameters, the number of Floquet channels (N_F), number of Fourier components to be considered in the Fourier expansion series of the density matrix, time-step size (Δt), and number of molecular orbitals, (N_{orb}) energies and coefficients to be printed. All the parameters are to be specified in atomic units. In the sample input file, the laser frequency (ω), and electric field strength (ϵ) are 0.054 a.u. $(\sim 4.48 \times 10^{-16} s)$ and 0.114 a.u. $(\sim 0.40 \times 10^{16} W/cm^2)$ respectively with laser polarization along Z direction with zero initial phase. The strength of CAP, η, is taken as 1.0. To calculate the time-dependent part of density matrix, it is expanded into Fourier series. The number of Fourier components of the density matrix is taken as 5 in the sample input file. To construct the full Floquet Fock matrix, the number of Floquet channels used is 25. The next set of parameters specifies the number of optical cycles for the starting pulse region, continuous-wave pulse region, and ending pulse region of the laser. The inputs to these three regions' optical cycles is used to be 2,2 and 2, respectively. The total number of optical cycles (N_{cycle}) of the laser pulse is specified to be 8. The following function gives the form of the laser pulse,

$$f(t) = \begin{cases} \epsilon_0 \sin^2 \left[\frac{\pi}{2} \frac{t}{t_{on}} \right], 0 \leq t \leq t_{on} \\ \epsilon_0, t_{on} \leq t \leq t_{off} \\ \epsilon_0 \cos^2 \left[\frac{\pi}{2} \frac{(t - t_{off})}{(t_{max} - t_{off})} \right], t_{off} > t \end{cases} \tag{2.49}$$

For a frequency of 0.114 a.u., the total laser time period, $T_{tot} = N_{cycle} \times \tau$ where $\tau = (\frac{2\pi}{\omega})$, calculated to 440.92 a.u. The time-step size parameter takes two values as input. The first input specifies the type of step-size preferred (choose either 1 or 2) and the second input specifies the step-size value to be taken to calculate the time-step size. For *e.g.*, if one specifies (1, 10), the Δt will $\frac{1}{10}$ *i.e.* 0.10 whereas if input is (2, 10), the Δt will 10.00. The total number of time-steps to be calculated N_t will be $(\frac{T_{tot}}{\Delta t})$, which is approximately 4409 time steps for the case of sample input file. The next input is the number of orbital values N_{orb} (orbital energy and orbital coefficient), to be written out in the properties and population output files respectively. The density matrix values are written out in the *tmden.txt* files in steps of 1 which is specified in the sample input file.

As shown in the sample input file, in the *tmprp.txt* file, the columns contain laser time ($\frac{T_t}{\tau}$), the value of *f(t)* at time t, induced dipole moment at time t, the sum of the real part of electronic energy and nuclear energy, the imaginary part of electronic energy and the list of orbital energies (N_{orb}) as specified by the user, at time t. A list of checks is performed on the time-evolving molecular orbitals, atomic orbitals, electronic energies, and norms are reported in the *tmerr.txt*. The population file *tmpop.txt*, contains, time-dependent coefficients of N_{orb} molecular orbitals. The time-dependent Mülliken charges on all atoms in molecules are written out in *tmchrg.txt*. The orbital occupancy of all molecular orbitals is written out at all time steps in *tmocc.txt* file. The time-evolving real and imaginary part of all molecular orbitals at all time steps is written out in *tmcoefr.txt* and *tmcoefi.txt* respectively. Also, the time-dependent density matrices are printed in *tmden.txt*. The final output *tmfrr.txt* provides the time-dependent Fourier components.

The output files, *tmcoefr.txt* and *tmcoefi.txt*, provide the time-dependent real and imaginary coefficients of molecular orbitals data in a matrix form. Each row of these files represents all the values $(= N_{bas} \times N_{bas})$ of molecular orbitals at each time step. Furthermore, to be used in ABELDYNPROP code, each row of *tmcoefr.txt* and *tmcoefi.txt* are written out as columns in separate files using a simple *gfortran* code.

2.3.3 Execution of the ABELDYNPROP program

The algorithm for ABELDYNPROP code is presented in Fig. [2.2]. The runtd.sh script reads the timefile prefix, the start-index, end-index and time-step size for the job to run. For each iteration the run.exe is executed. The program reads the input keyword, atom-basis file name and COMPLEX/REAL type molecular orbtial from the file from the input file. Since, all properties are evaluated on a grid. If the keyword are any of EDEN, EGRD, EHES, ELAP, MORB, parameters of uniform grid are read from the parameter section to evaluate the properties to be stored in .cube/.vtk data files. On the other hand, if the keyword is ALLCRITIC, ZEROFS,

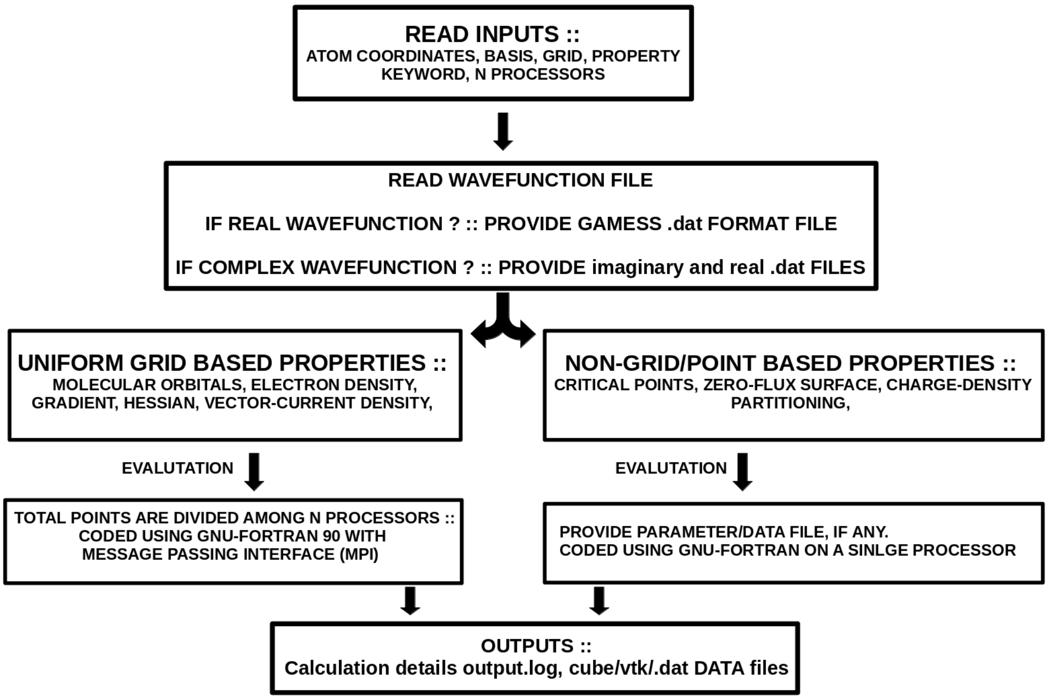

Figure 2.2: A flow chart depicting the steps involved in the ABELDYNPROP code to calculate the time-dependent properties.

or BDPARTSP, properties are evaluate based on the user-defined parameters from the input.dat. For each index of the timefile, the output is stored in a folder named *property*step*index*.

2.4 Results and Discussion

The ABELDYNPROP code is tested and implemented for a closed shell atom Beryllium, diatomic homonuclear molecule Dinitrogen N_2, diatomic heteronuclear molecule Carbon monoxide CO, ring molecular systems, Cyclopropane C_3H_6), Benzene C_6H_6, and one cage molecule Tetrahedrane (C_4H_4). The optimization of test molecules is performed at HF/*aug-cc-pvdz* level of theory. The optimization is chosen such that diatomic systems are oriented along the Z-axis, the Cyclopropane, Benzene molecules on the XY-plane, and Tetrahedrane is oriented such that one of the CH bonds falls on the Z-axis. The time-evolving wavefunctions are obtained using frequency parameters described in table 2.1 as an input in the ABELDYN in-house

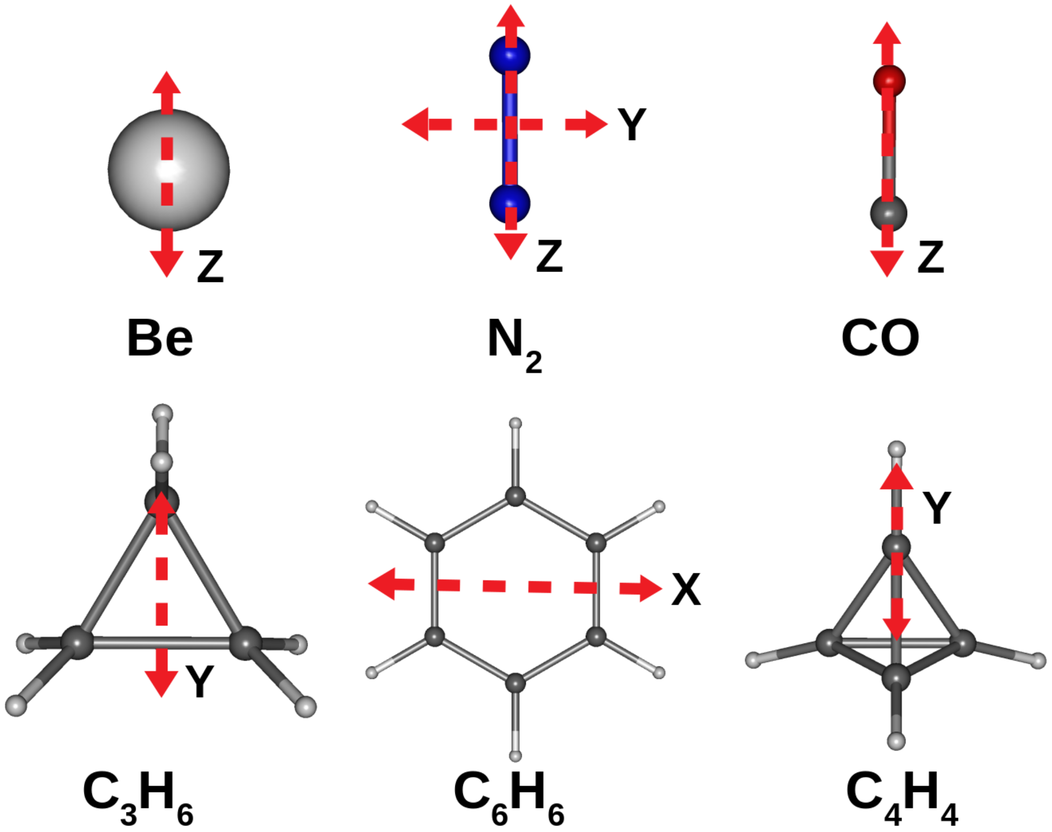

Figure 2.3: Test systems used to implement the ABELDYNPROP code: Beryllium atom, Dinitrogen, Carbon monooxide, Cyclopropane, Benzene and Tetrahedrane in linearly polarized laser field. The direction of laser polarization is depicted by the red colored double-ended arrow. The molecules in the set of test systems are optimized using HF/aug-cc-pvdz level of theory and the wavefunction obtained from ABELDYN in-house code. The electric field strength of laser used in calculations is 5.14 $\times$ 10^8 V/cm, while the frequency used is mentioned in table 2.1. The inputs: atom coordinates is considered in bohr, LASER parameters in atomic units and the calculation of output: MED and properties derived from MED are performed in atomic units.

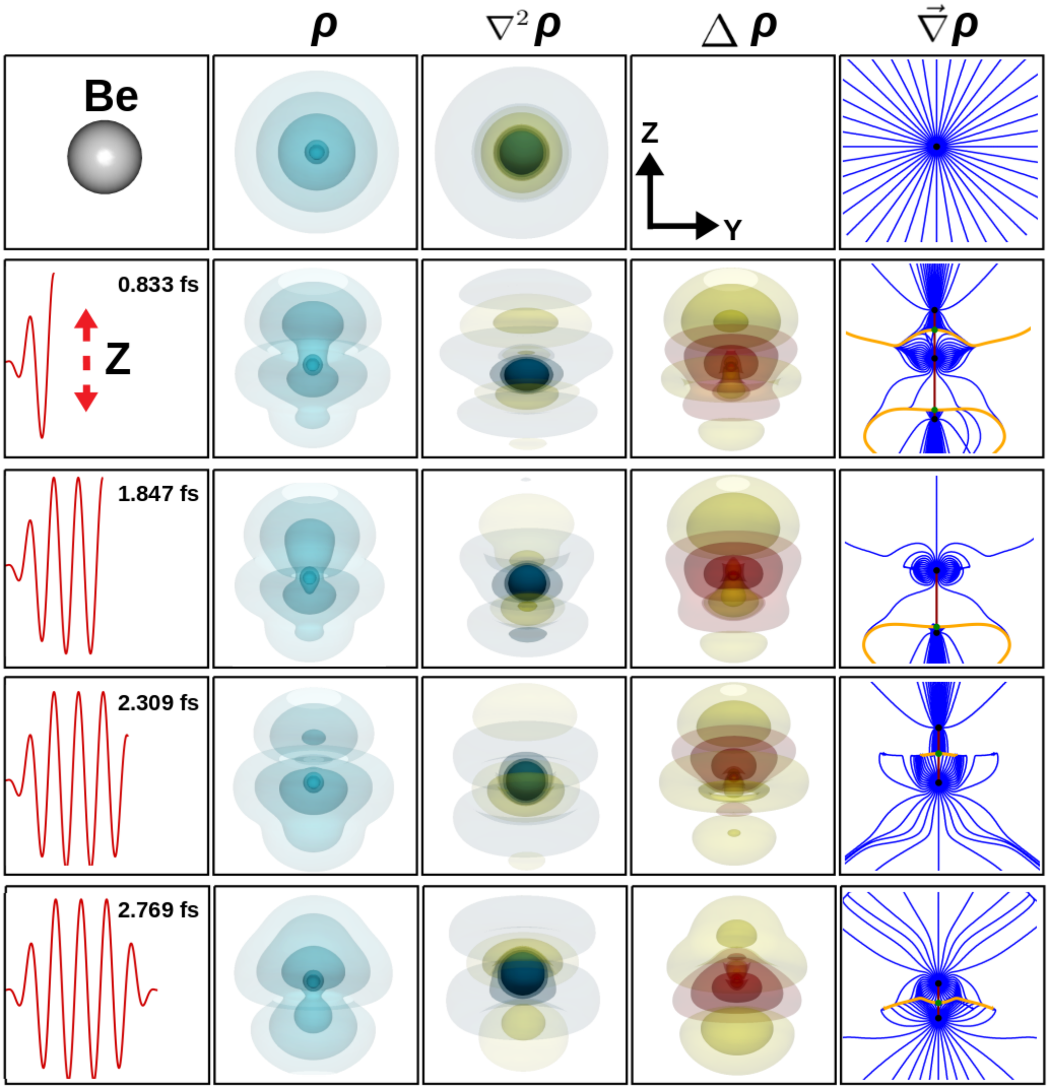

Figure 2.4: Beryllium Atom properties in linearly polarized laser along Z at five different time-steps. The columns represent time-dependent atomic electron density (second), its Laplacian (third), difference density (fourth) and gradient lines (fifth).The iso-contour are ρ: (0.37,0.1,0.01,0.001,0.0001), $\nabla^2\rho$: ($\pm$ 0.35,$\pm$ 0.1,$\pm$ 0.01, $\pm$ 0.001) and $\Delta\rho$: ($\pm$ 0.1,$\pm$ 0.01,$\pm$ 0.001, $\pm$ 0.0001). The blues lines and yellow in presents the gradient lines and basin boundaries. Black Dots: (3,-3) CPs, Green Dots: (3,-1) CPs, Purple Dots: (3,+1) CPs and Red Dots: (3,+3) CPs. The laser parameters are mentioned in table [2.1]. The inputs: atom coordinates is considered in bohr, LASER parameters in atomic units and the calculation of output: MED and properties derived from MED are performed in atomic units.

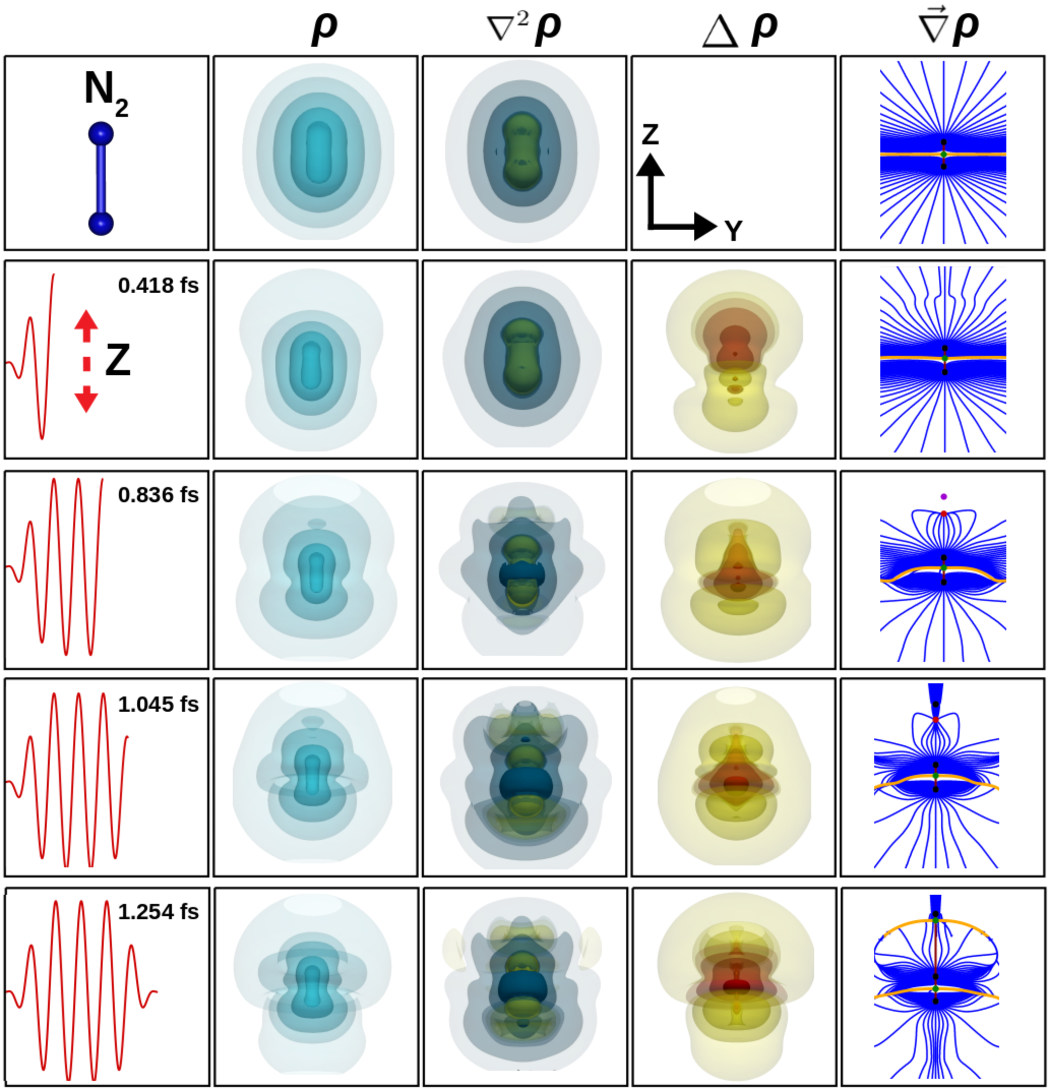

Figure 2.5: Dinitrogen properties in linearly polarized laser along Z at five different time-steps. The columns represent time-dependent molecular electron density (second), its Laplacian (third), difference density (fourth) and gradient lines (fifth).The iso-contour are ρ: (0.37,0.1,0.01,0.001,0.0001), $\nabla^2\rho$: ($\pm$ 0.35,$\pm$ 0.1,$\pm$ 0.01, $\pm$ 0.001) and $\Delta\rho$: ($\pm$ 0.1,$\pm$ 0.01,$\pm$ 0.001, $\pm$ 0.0001). The blues lines and yellow in presents the gradient lines and basin boundaries. Black Dots: (3,-3) CPw, Green Dots: (3,-1) CPs, Purple Dots: (3,+1) CPs and Red Dots: (3,+3) CPs. The laser parameters are mentioned in table [2.1]. The inputs: atom coordinates is considered in bohr, LASER parameters in atomic units and the calculation of output: MED and properties derived from MED are performed in atomic units.

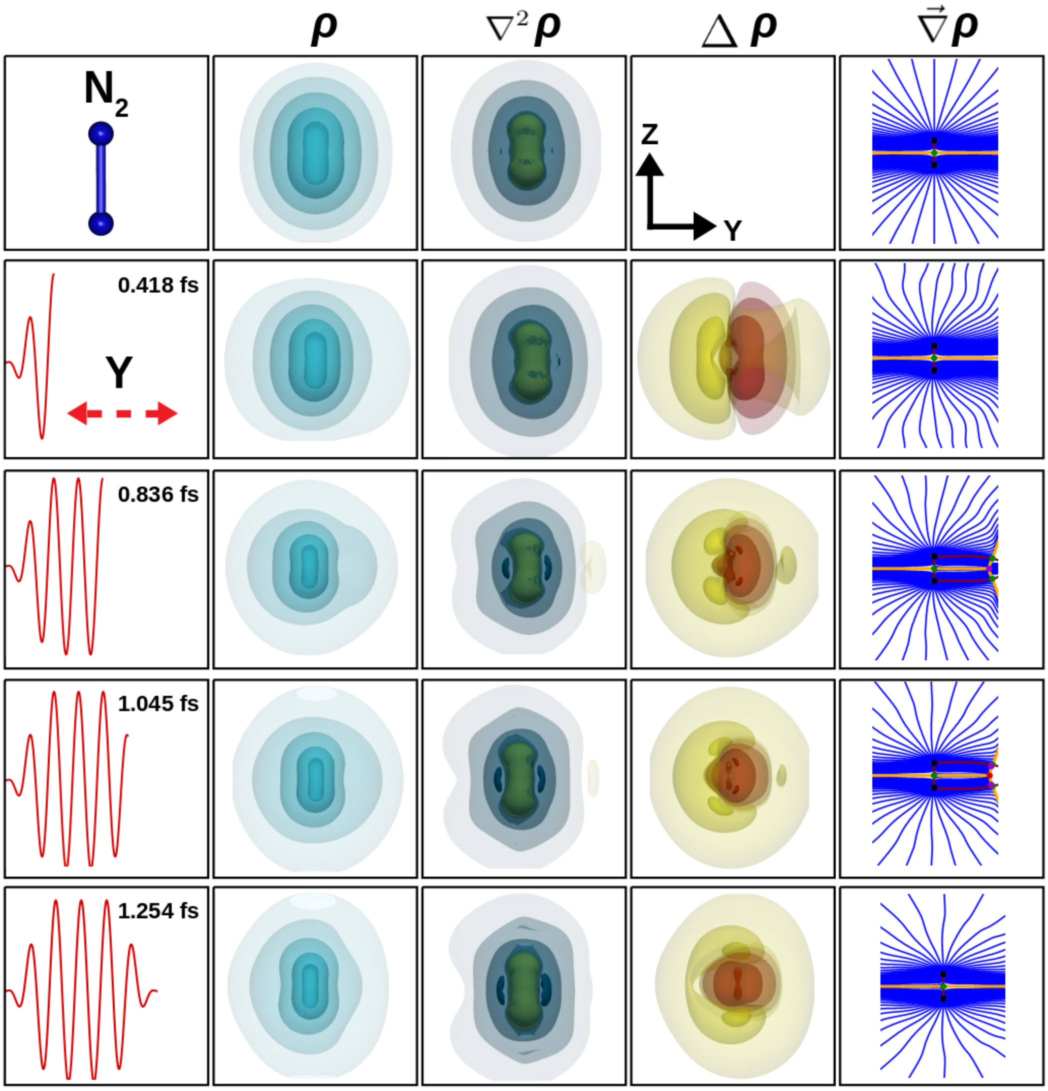

Figure 2.6: Dinitrogen properties in linearly polarized laser along Y at five different time-steps. The columns represent time-dependent molecular electron density (second), its Laplacian (third), difference density (fourth) and gradient lines (fifth).The iso-contour are ρ: (0.37,0.1,0.01,0.001,0.0001), $\nabla^2\rho$: (± 0.35,± 0.1,± 0.01, ± 0.001) and $\Delta\rho$: (± 0.1,± 0.01,± 0.001, ± 0.0001). The blues lines and yellow in presents the gradient lines and basin boundaries. Black Dots: (3,-3) CPw, Green Dots: (3,-1) CPs, Purple Dots: (3,+1) CPs and Red Dots: (3,+3) CPs. The laser parameters are mentioned in table [2.1]. The inputs: atom coordinates is considered in bohr, LASER parameters in atomic units and the calculation of output: MED and properties derived from MED are performed in atomic units.

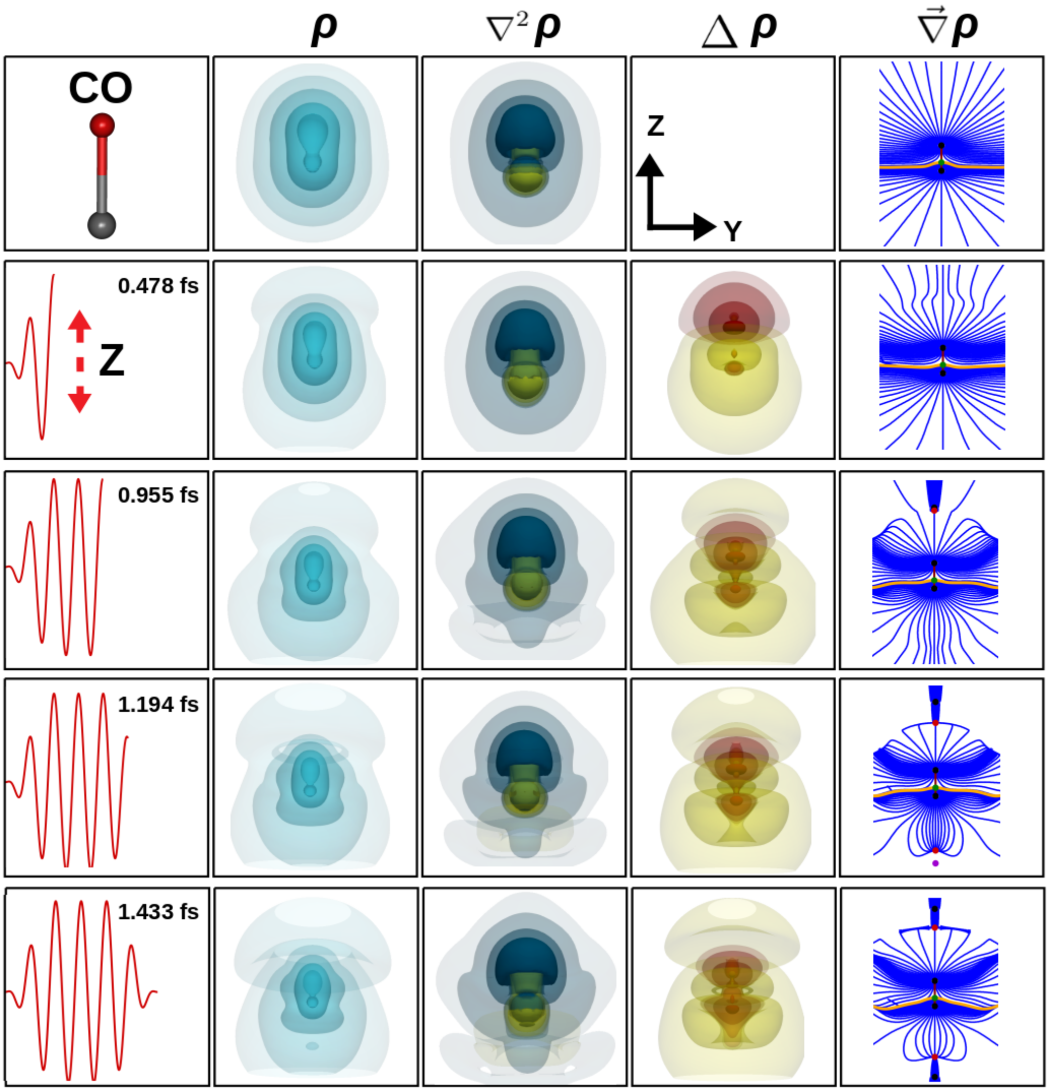

Figure 2.7: Carbon Monooxide properties in linearly polarized laser along Z at five different time-steps. The columns represent time-dependent molecular electron density (second), its Laplacian (third), difference density (fourth) and gradient lines (fifth).The iso-contour are ρ: (0.37,0.1,0.01,0.001,0.0001), $\nabla^2\rho$: ($\pm$ 0.35,$\pm$ 0.1,$\pm$ 0.01, $\pm$ 0.001) and $\Delta\rho$: ($\pm$ 0.1,$\pm$ 0.01,$\pm$ 0.001, $\pm$ 0.0001). The blues lines and yellow in presents the gradient lines and basin boundaries. Black Dots: (3,-3) CPw, Green Dots: (3,-1) CPs, Purple Dots: (3,+1) CPs and Red Dots: (3,+3) CPs. The laser parameters are mentioned in table [2.1]. The inputs: atom coordinates is considered in bohr, LASER parameters in atomic units and the calculation of output: MED and properties derived from MED are performed in atomic units.

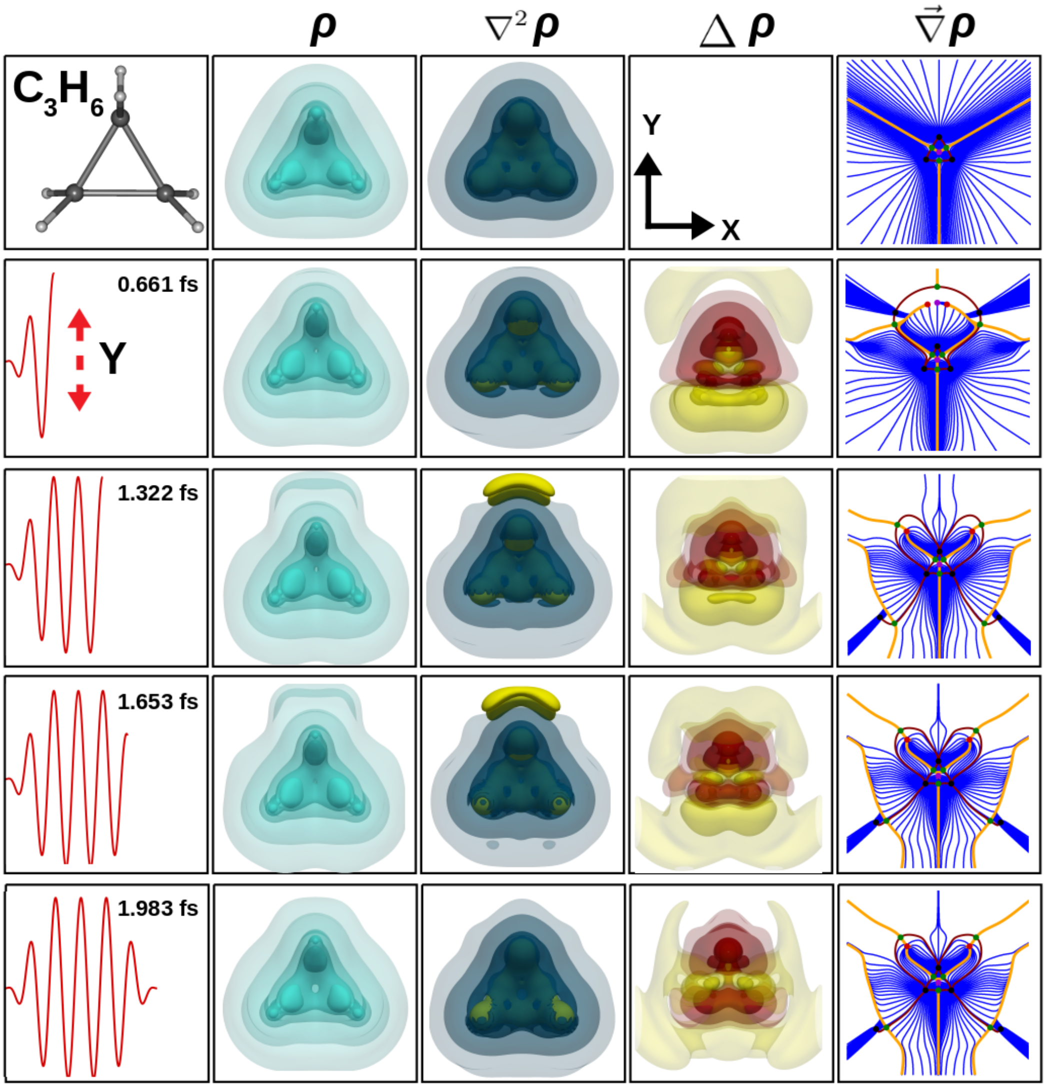

Figure 2.8: Cyclopropane properties in linearly polarized laser along Y at five different time-steps. The columns represent time-dependent molecular electron density (second), its Laplacian (third), difference density (fourth) and gradient lines (fifth).The iso-contour are ρ: (0.28,0.1,0.01,0.001,0.0001), $\nabla^2\rho$: ($\pm$ 0.35,$\pm$ 0.1,$\pm$ 0.01, $\pm$ 0.001) and $\Delta\rho$: ($\pm$ 0.1,$\pm$ 0.01,$\pm$ 0.001, $\pm$ 0.0001). The blues lines and yellow in presents the gradient lines and basin boundaries. Black Dots: (3,-3) CPw, Green Dots: (3,-1) CPs, Purple Dots: (3,+1) CPs and Red Dots: (3,+3) CPs. The laser parameters are mentioned in table [2.1]. The inputs: atom coordinates is considered in bohr, LASER parameters in atomic units and the calculation of output: MED and properties derived from MED are performed in atomic units.

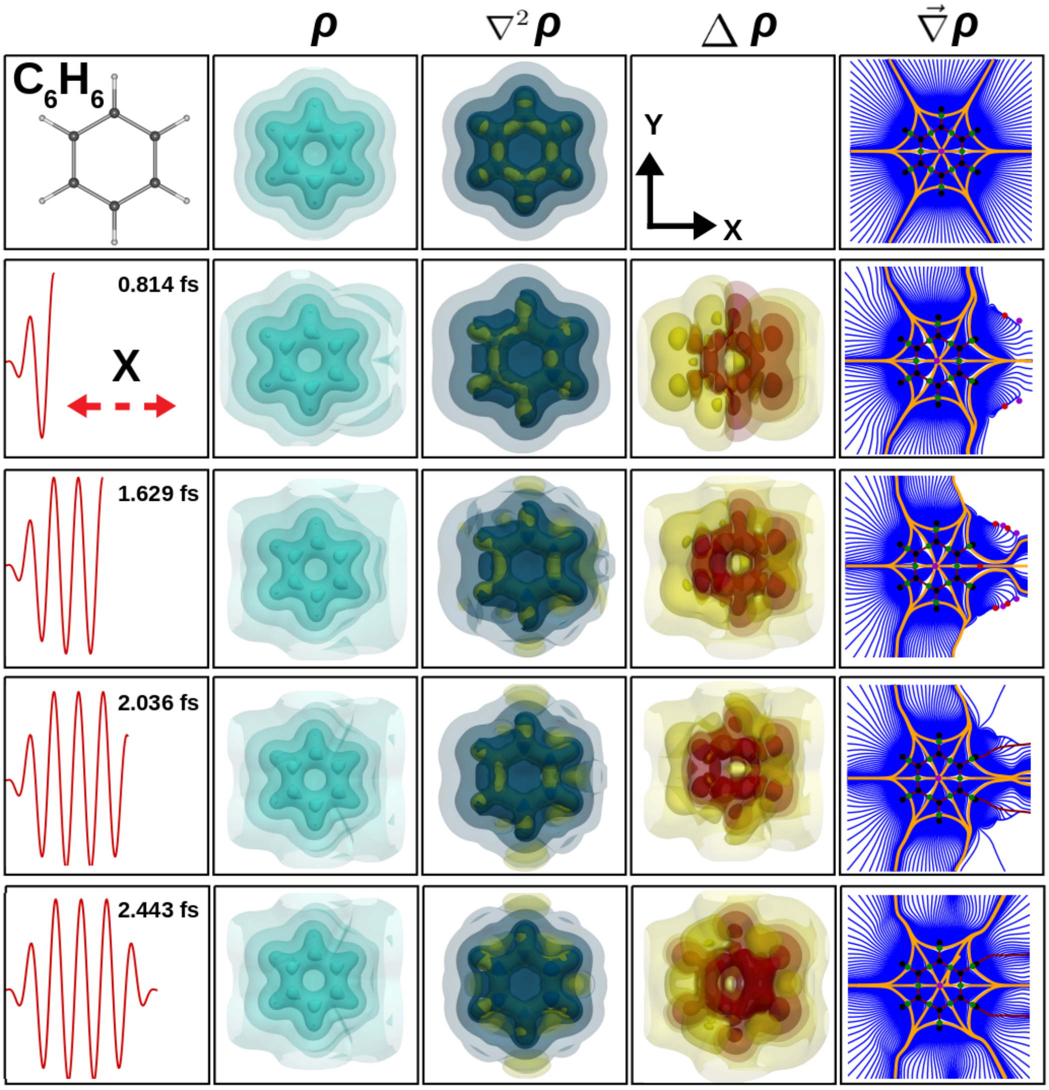

Figure 2.9: Benzene properties in linearly polarized laser along X at five different time-steps. The columns represent time-dependent molecular electron density (second), its Laplacian (third), difference density (fourth) and gradient lines (fifth).The iso-contour are ρ: (0.33,0.1,0.01,0.001,0.0001), $\nabla^2\rho$: ($\pm$ 0.35,$\pm$ 0.1,$\pm$ 0.01, $\pm$ 0.001) and $\Delta\rho$: ($\pm$ 0.1,$\pm$ 0.01,$\pm$ 0.001, $\pm$ 0.0001). The blues lines and yellow in presents the gradient lines and basin boundaries. Black Dots: (3,-3) CPw, Green Dots: (3,-1) CPs, Purple Dots: (3,+1) CPs and Red Dots: (3,+3) CPs. The laser parameters are mentioned in table [2.1]. The inputs: atom coordinates is considered in bohr, LASER parameters in atomic units and the calculation of output: MED and properties derived from MED are performed in atomic units.

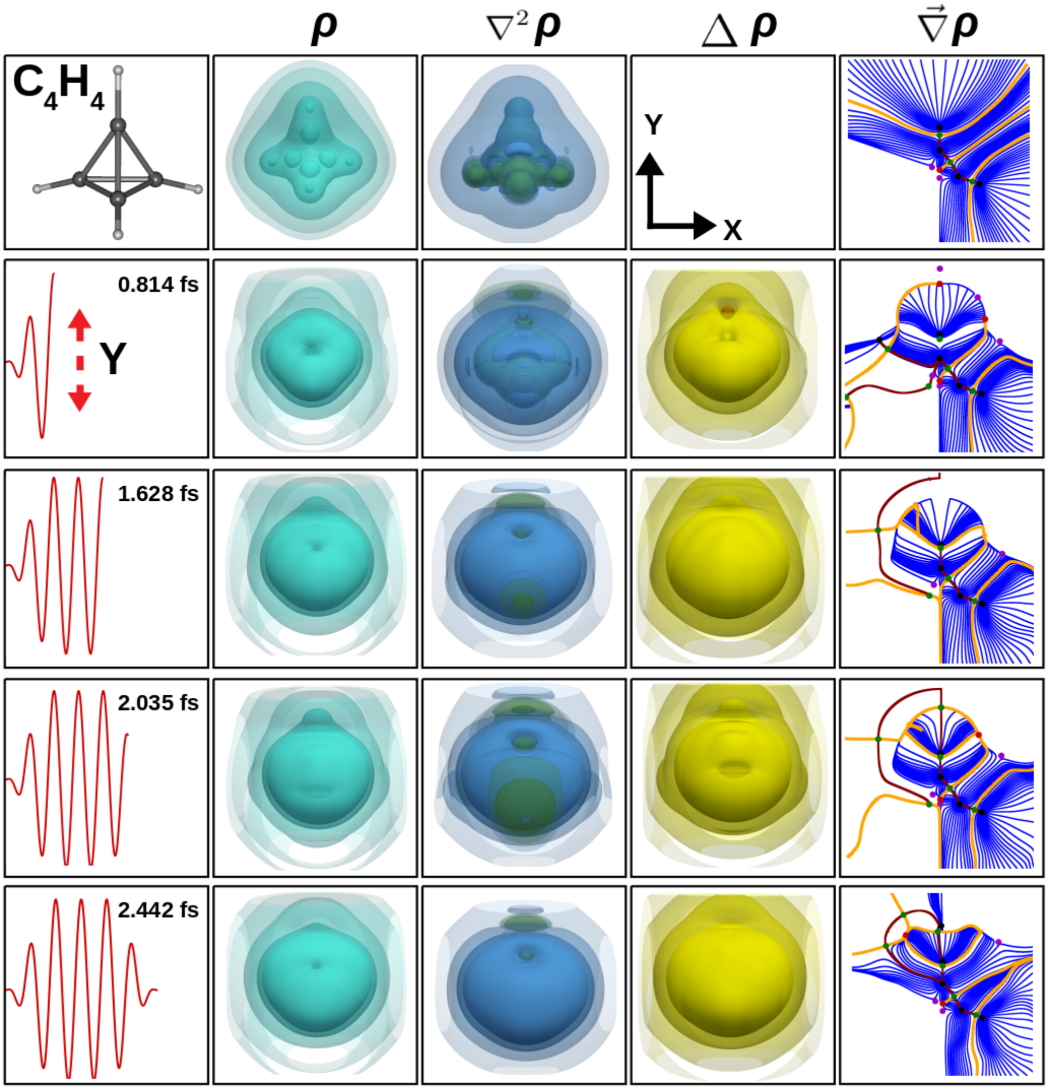

Figure 2.10: Tetrahedrane properties in linearly polarized laser along Y at five different time-steps. The columns represent time-dependent molecular electron density (second), its Laplacian (third), difference density (fourth) and gradient lines (fifth).The iso-contour are ρ: (0.30,0.1,0.01,0.001,0.0001), $\nabla^2\rho$: ($\pm$ 0.35,$\pm$ 0.1,$\pm$ 0.01, $\pm$ 0.001) and $\Delta\rho$: ($\pm$ 0.1,$\pm$ 0.01,$\pm$ 0.001, $\pm$ 0.0001). The blues lines and yellow in presents the gradient lines and basin boundaries. Black Dots: (3,-3) CPw, Green Dots: (3,-1) CPs, Purple Dots: (3,+1) CPs and Red Dots: (3,+3) CPs. The laser parameters are mentioned in table [2.1]. The inputs: atom coordinates is considered in bohr, LASER parameters in atomic units and the calculation of output: MED and properties derived from MED are performed in atomic units.

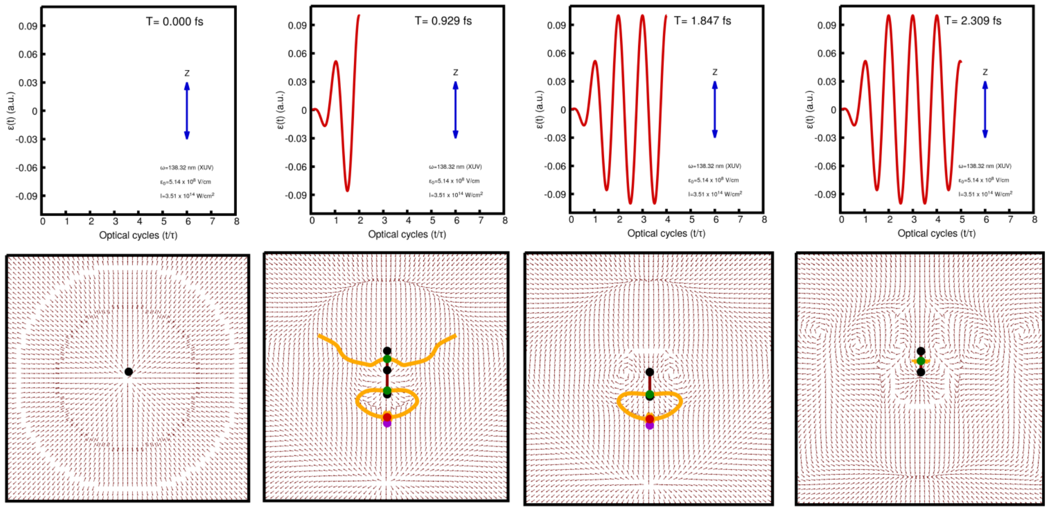

Figure 2.11: QM vector current density plots on the YZ-plane for the Be atom in the presence of linearly polarized laser at different time-steps is shown. The time-evolving movies are provided in supplementary files. The inputs: atom coordinates is considered in bohr, LASER parameters in atomic units and the calculation of output: MED and properties derived from MED are performed in atomic units.

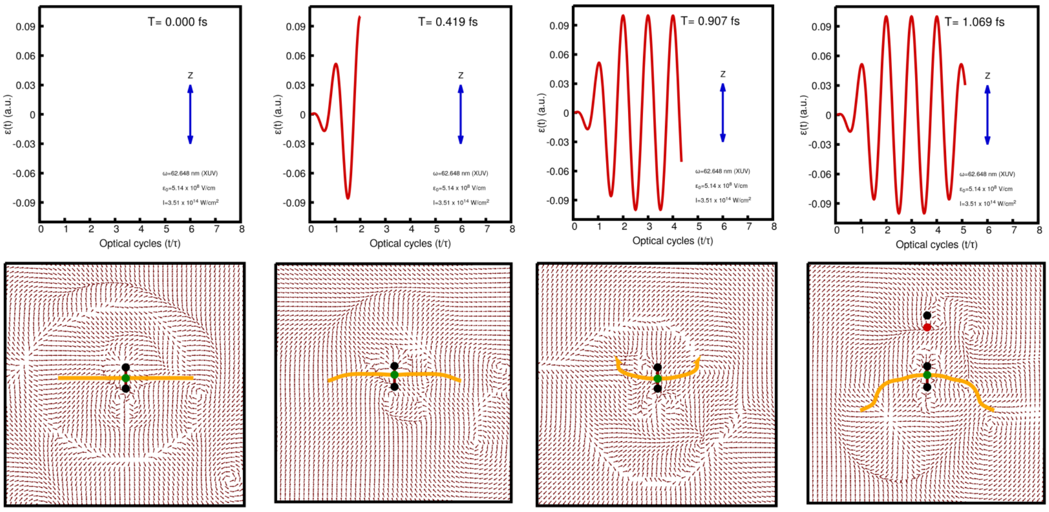

Figure 2.12: QM vector current density plots on the YZ-plane for the N_2 molecule in the presence of linearly polarized laser at different time-steps. The time-evolving movies are provided in supplementary files. The inputs: atom coordinates is considered in bohr, LASER parameters in atomic units and the calculation of output: MED and properties derived from MED are performed in atomic units.

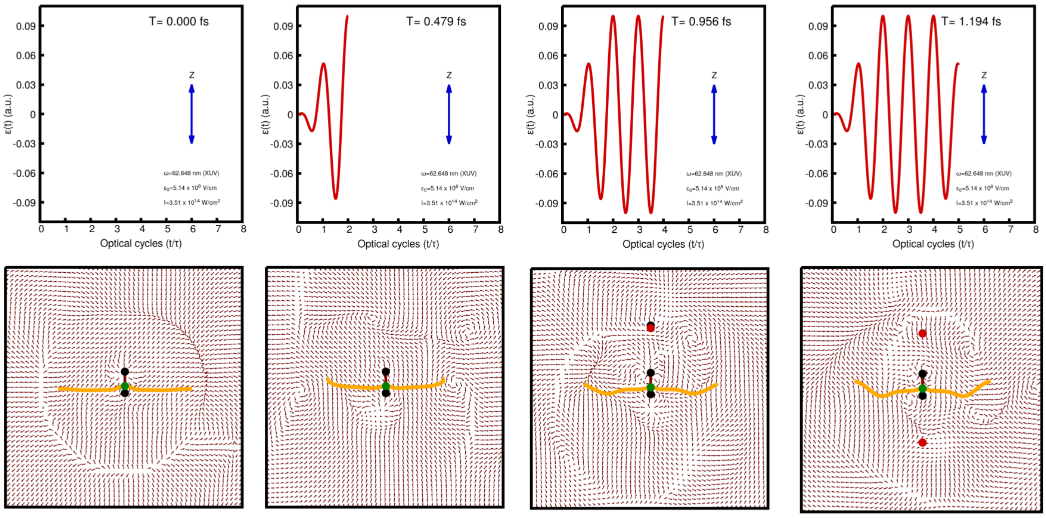

Figure 2.13: QM vector current density plots on the YZ-plane for the CO molecule in the presence of linearly polarized laser at different time-steps. The time-evolving movies are provided in supplementary files. The inputs: atom coordinates is considered in bohr, LASER parameters in atomic units and the calculation of output: MED and properties derived from MED are performed in atomic units.

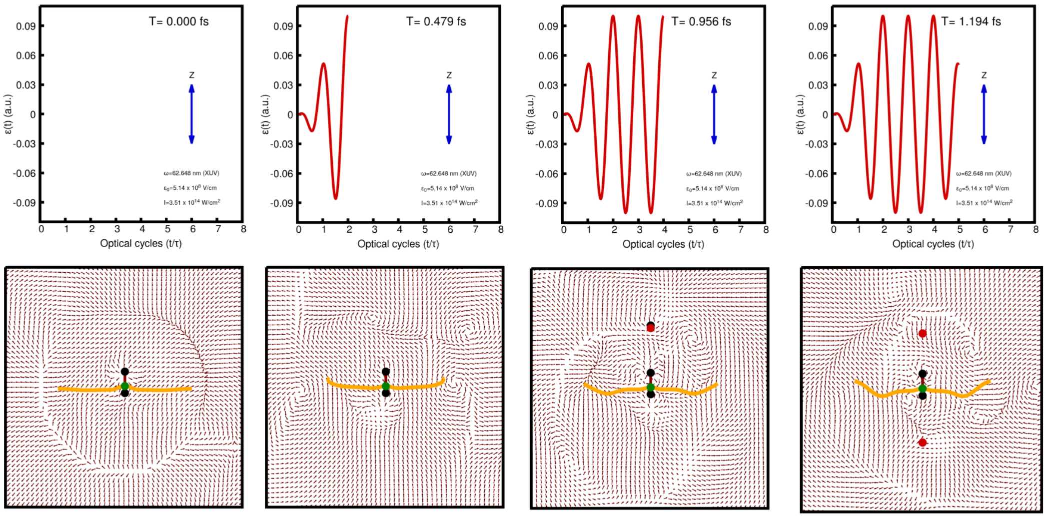

Figure 2.14: QM vector current density plots on the YZ-plane for the C_6H_6 molecule in the presence of linearly polarized laser at different time-steps. The time-evolving movies are provided in supplementary files. The inputs: atom coordinates is considered in bohr, LASER parameters in atomic units and the calculation of output: MED and properties derived from MED are performed in atomic units.

Table 2.1: Laser parameters used for the calculating properties of the test systems shown in Fig. [2.3]. The level of theory HF/aug-cc-pvdz was used to optimize molecules. The table mentions the total basis functions N_{bas}, frequency ω, classical quiver distance α, total time of the eight optical cycle pulse, polarization direction of the linear laser and its orientation w.r.t molecule.

System	N_{bas}	ω(a.u.)	α_0(a.u.)	T_{tot}(fs)	L_{dir}	System axis
Be	35	0.3294	0.9216	3.69	Z	-
N_2	50	0.7273	0.1890	1.66	Z	Parallel to N-N
					Y	Perpendicular to N-N
CO	50	0.6362	0.2470	1.91	Z	Parallel to C-O
C_3H_6	129	0.4598	0.4730	2.64	Y	C_2-axis of Molecule
C_6H_6	204	0.3732	0.7180	3.25	X	C_2(X)-axis of Molecule
C_4H_4	136	0.3735	0.7168	3.25	Z	C_3(X)-axis of molecule

code. The electric field strength of the laser used in the calculations was 0.10 a.u. In addition, table 2.1 also mentions the total number of basis functions N_{bas}, the classical quiver distance, the molecule's total time in the laser field, and finally, the direction of laser polarization and orientation of the molecule w.r.t laser, which were used in the calculations. The red arrows in Fig. [2.3] visually depict the laser polarization direction w.r.t laser orientation. The direction of laser polarization is chosen along the Z-axis for the Be atom, along the X and Z-axis, which is parallel and perpendicular to the N-N bond in N_2 molecule, Z-axis parallel to the C-O bond in the CO molecule, Y-axis parallel to C_2 axis of XY-oriented Cyclopropane, X-axis parallel to the C_2 axis of XY-oriented of Benzene, Y-axis parallel to the C_3 axis of passing through the C-H bond of Tetrahedrane molecule.

Fig. [2.4], [2.5], [2.6], [2.7], [2.8], [2.9], and [2.10] depicts the time-evolution of electron density ρ, its Laplacian $\nabla^2\rho$, difference density $\Delta\rho$, and gradient field lines $\vec{\nabla}\rho$ at five time snapshots of the linear laser pulse. The electron density, Laplacian, gradient lines, and critical points are calculated for the first time step of the laser, showing faithful replications w.r.t to the free-field properties calculated with other packages.[35], for all test cases, we observe deformations in the distribution of electron density and related properties depicted in the timesteps along the laser. As depicted in the blue-colored isosurface plot in Fig. [2.4] of the Be atom, the electron density distribution shrinks in the Y direction while widening in the Z direction. When the laser's polarization direction was parallel to the bond N-N (in N_2) and C-O, the electron density distribution showed elongation in the Z-axis while narrowed in the region near the mid of the bond. In the case of the Planar ring molecule, the electron density distribution blows up in the +ve direction of polarization while shrinking in the -ve direction. A similar trend is observed for tetrahedrane molecules in the polarized laser parallel along one of its C-H bonds. Therefore, the electron density generally tends to align along the direction of the field's polarization. The third column in the plots depicts the Laplacian of electron density in the time-evolving field. The plots depicted by the blue and green regions show $\nabla^2\rho > 0$ and $\nabla^2\rho < 0$. The regions where $\nabla^2\rho > 0$ depict the charge depleted regions and $\nabla^2\rho < 0$ show the charge accumulated regions. The movement of charge density shifting, depleting, and concentrating at various timesteps are represented in the red and yellow colored isocontour plots of difference density in the fourth column. From these plots, it was observed that the value of electron density gets lowered and higher w.r.t the free-field case in the region towards the +ve direction and -ve directions of the field of polarization. This trend reverses and repeats at the peaks and valleys of the laser pulse. The topological changes brought in by deformations in the electron density distribution are depicted in the fifth column in the plots. We show the gradient field lines (royal blue), basin boundaries (yellow), bond paths (maroon red), and critical points in the plot. Since the electron density gets deformed, the topological changes are reflected through the bends in gradient field lines, basin boundaries, and shifts in the positions and values of critical points.

2.5 Conclusions

The chapter describes the capabilities, methodologies, and working implementations of the ABELDYNPROP code. It can compute time-dependent electron densities of atoms and molecules in position space over three-dimensional regular grids. The analytical forms of the first and second derivatives of electron density are programmed to evaluate gradient, hessian, and Laplacian. The code is capable of computing these properties over 3D as well as 2D-defined planes. This section of code is parallelized for distributed memory systems using MPI to evaluate electron densities, its gradient, hessian, and Laplacian over 3D regular grids. One can explore the topological features of the time-evolving, such as critical points, gradient paths, bond paths, and interatomic surfaces/zero-flux surfaces, using the ABELDYNPROP code. The ABELDYNPROP code also includes subroutines to evaluate several average properties of all the basins in the time-dependent electron densities. These subroutines present the *atoms-in-molecule* analysis of the code. The ABELDYNPROP code uses the coefficients of the time-evolving wave functions obtained from the in-house code ABELDYN code. The ABELDYNPROP code uses analytical forms of Gaussian-type orbitals specifically for S, P, D, and F functions, whose mathematical expressions are described in the appendix section. Bash shell scripting enables the package to execute the code at each time step, making the file and job handling easy and non-tedious.

References Chapter 2

[1] P. M. Paul, E. S. Toma, P. Breger, G. Mullot, F. A. P. Balcou, H. G. Mullet, and P. Agostini, Observation of a Train of Attosecond Pulses from High Harmonic Generation, *J. Chem. Phys.* **122**, 117 (2005).

[2] P. Raj, A. Gugalia, P. Balanarayan, Quantum Dynamics with Explicitly Time-Dependent Hamiltonians in Multiple Time Scales: A New Algorithm for (t, t') and (t, t', t') Methods in Laser–Matter Interactions, *J. Chem. Theory Comput.*, **16**, 35, (2020).

[3] P. Raj, A. Gugalia, and P. Balanarayan, ABELDYN: Ab-initio Electron Dynamic package, *Manuscript to be submitted*.

[4] P. Raj, Electronic Quantum Dynamics of Molecules in Strong LASER fields: Novel Algorithms and Effects, Dotoral Dissertation (2022).

[5] R. Chávez-Calvillo, and J. Hernández-Trujillo, Quantum Molecular Dynamics of the Topological Properties of the Electron Density: Charge Transfer in H_3^+ and LiF, *J. Phys. Chem. A*, **115**, 13036, (2011).

[6] M. Gronager, and N. E. Henriksen, Real-time control of electronic motion: Application to NaI, *J. Chem. Phys.*, **109**, 4335, (1998).

[7] M. Erdmann, P. Marquetand and P. Engel, Combined electronic and nuclear dynamics in a simple model system, *J. Chem. Phys.*, **119**, 672, (2003).

[8] T. Burnus, M. A. L. Marques and E. K. U. Gross, Time-dependent electron localization function, *Phys. Rev. A*, **71**, 01050, (2005).

[9] F. K. Larsen, Diffraction studies of crystals at low temperatures - crystallography below 77 K, *Acta Cryst.*, **51**, 468, (1995).

[10] P. A. Midgley, and P. Saunders, Quantitative electron diffraction: From atoms to bonds, *Contemp. Phys.*, **37**, 441, (1996).

[11] P. Coppens, Experimental charge densities in chemistry: what is next?, *J. Phys. Chem.*, **93**, 7979, (1989).

[12] Z. Su, and P. Coppens, Relativistic X-ray Elastic Scattering Factors for Neutral Atoms $Z = 1 - 54$ from Multiconfiguration Dirac-Fock Wavefunctions in the 0-12Å^{-1} sin[θ] /[λ] Range, and Six-Gaussian Analytical Expressions in the 0-6Å-1 Range, *Acta Cryst.*, **A53**, 749, (1997).

[13] P. Coppens, Charge-Density Analysis at the Turn of the Century, *Acta Cryst.*, **54**, 779, (1998).

[14] T. S. Koritsanszky, and P. Coppens, Chemical Applications of X-ray Charge-Density Analysis, *Chem. Rev.*, **101**, 1583, (2001).

[15] D. L. Ansatassopoulos, G. D. Priftis, N. I. Papanicolaon, N. C. Bacalis, and D. A. Papaconstantpoulos, Calculation of the electron momentum density and Compton scattering measurements for nickel *J. Phys. Condens. Matter*, **3**, 1099, (1991).

[16] V. Tsirelson, and A. Stash, Determination of the electron localization function from electron density, *Chem. Phys. Lett.*, **351**, 142, (2002).

[17] R. F. Stewart, On the mapping of electrostatic properties from bragg diffraction data, *Chem. Phys. Lett.*, **65**, 335, (1979).

[18] R. F. W Bader, *Atoms in Molecules: A Quantum Theory*, Clarendon Press, Oxford, (1994).

[19] P. L. A. Popelier, *Atoms in Molecules - An Introduction*, Prentice Hall: Harlow-England, (2000).

[20] R. J. Gillespie, and P. L. A. Popelier, *Chemical Bonding and Molecular Geometry: From Lewis to Elctron Densities*, Oxford University Press: New York, Oxford, (2001).

[21] C. F. Matta, and R. J. Boyd,*The Quantum Theory of Atoms in Molecules*, WILEY-VCH Verlag GmbH and Co. KGaA, Weinhein, (2007).

[22] S. R. Gadre, and R. N. Shirsat, *Electrostatics of Atoms and Molecules*, Univerities Press (India) Limited, (2000).

[23] R. Chauvin, C. Lepetit, B. Silvi, and E. Aikhani, *Applications of Topological Methods in Molecular Chemistry, Springer International Publishing*, (2016).

[24] M. J. Brunger, D. A. Winkler, M. T. Michalewicz, and E. Weigold, Momentum distributions and molecular property information for trans 1,3 butadiene: An electron momentum spectroscopy and density functional theory investigation *J. Chem. Phys.*, **108**, 1859, (1998).

[25] AIMAll (Version 19.10.12), Todd A. Keith, TK Gristmill Software, Overland Park KS, USA, 2019 (aim.tkgristmill.com)

[26] F. Biegler-König, and J. Schönbóhm, Update of the AIM2000-Program for atoms in molecules, *J. Comput. Chem.*, **5**, 549, (2001).

[27] W. Tang, and E. Sanville, and G. Henkelman, A grid-based Bader analysis algorithm without lattice bias, *J. Phys. Condens. Matter*, **21**, 084204, (2009).

[28] P. L. A. Popelier, MORPHY, a program for an automated “atoms in molecules” analysis, *Comp. Phys. Comm.*, **93**, 212, (1996).

[29] P. L. A. Popelier, A method to integrate an atom in a molecule without explicit representation of the interatomic surface, *Comp. Phys. Comm.*, **108**, 180, (1998).

[30] A. Otero-de-la-Roza, M. A. Blanco, A. M. Pendás, V. Luaña, Critic: a new program for the topological analysis of solid-state electron densities, *Comp. Phys. Comm.*, **180**, 157, (2009).

[31] A. Otero-de-la-Roza, E. R. Johnson and V. Luaña, Critic2: A program for real-space analysis of quantum chemical interactions in solids, *Comp. Phys. Comm.*, **185**, 1007, (2014).

[32] M. Kohout, DGrid 4.6, User's Guide, Max Planck Institute for Chemical Physics of Solids, Dresden, Germany, (2011).

[33] T. Lu, and F. Chen, Multiwfn: A multifunctional wavefunction analyzer, *J. Comput. Chem.*, 33, 580, (2012).

[34] D. Vega, Y. Aray, and J. Rodriguez, C library for topological study of the electronic charge density, *J. Comput. Chem.*, 33, 2536, (2012).

[35] D. Vega, and D. J. Almeida ,AIM-UC: An application for QTAIM analysis, *J. Comput. Methods Sci. Eng.*, 14, 131, (2014).

[36] M. A. L. Marques, A. Castro, G. F. Bertsch, A. Rubio, octopus: a first-principles tool for excited electron–ion dynamics, *Comput. Phys. Commun.*, 151, 60, (2003).

[37] A. Castro, H. Appel, M. Oliveira, C. A. Rozzi, X. Andrade, F. Lorenzen, F. Marques, E. K. U. Gross, A. Rubio, octopus: a tool for the application of time-dependent density functional theory, *Comput. Phys. Commum.*, 11, 2465, (2006).

[38] X. Andrade, D. Strubbe, U. D. Giovannini, A. H. Larsen, M. J. T. Oliveria, J. Alberdi-Rodriguez, A. Varas, I. Theophilou, N. Helbig, M. J. Verstraete, L. Stella, F. Nogueira, A. Aspuru-Guzik, A. Castro, M. A. L. Marques, A. Rubio, Real-space grids and the Octopus code as tools for the development of new simulation approaches for electronic systems, *Phys. Chem. Chem. Phys.*, 17, 31371, (2015).

[39] N. Toacogne-Dejean, M. J. T. Oliveira, X. Andrade, H. Appel, C. H. Borca, C. H. Breton, F. Buchholz, A. Castro, S. Corni, A. A. Correa, U. D. Giovannini, A. Delgado, F. G. Eich, J. Flick, G. Gli, A. Gomez, N. Helbig, H. Hubener, R. Jestadt, J. Jornet-Somoza, A. H. Larsem, I. V. Lebedeva, M. Lunders, M. A. L. Marques, S. T. Ohimann, S. Pipolo, M. Rampp, C. A. Rozzi, D. A. Strubbe, S. A. Sato, C. Schafer, I. Theophilou, A. Welden, A. Rubio, Octopus, a computational

framework for exploring light-driven phenomena and quantum dynamics in extended and finite systems, *J. Chem. Phys.*, 152, 124119, (2020).

[40] M. W. Schmidt, K. K. Baldridge, J. A. Boatz, S. T. Elbert, M. S. Gordon, J. H. Jensen, S. Koseki, N. Matsunaga, K. A. Nguyen, S. Su, T. L. Windus, M. Dupuis, J. A. Montgomery-Jr, General atomic and molecular electronic structure system, *J. Comput. Chem.*, 14, 1347, (1993).

[41] A. Szabo, and N. S. Ostlund, *Modern quantum chemistry: Introduction to advanced electronic structure theory*, DOVER PUBLICATIONS, INC, Mineola, New York, (1996).

[42] R. F. W. Bader, D. Cremer and E. Kraka, Description of conjugation and hyperconjugation in terms of electron distributions, *J. Am. Chem. Soc.*, 105, 5062, (1983).

[43] K. Kraka, D. Cremer, *Theoretical Models of Chemical Bonding Part 2, The Concept of the Chemical Bond*, Ed. Z. B. Maksic, Springer, New York, (1990).

[44] R. G. Parr, W. Yang, *Density Functional Theory of Atoms and Molecules*, Oxford, New York, (1989).

[45] K. Collard, and G. G. Hall, Orthogonal trajectories of the electron density, *Intern. J. Quantum Chem.*, 12, 623, (1977).

[46] R. F. W. Bader, T. T. Nguyen-Dang, and Y. Tal, Quantum topology of molecular charge distributions. II. Molecular structure and its change, *J. Chem. Phys.*, 70, 4316, (1979)

[47] AIMPAC suite of programs, Bader group at McMaster Univ., Canada. Available via "bader@mcmail.cis.memaster.ca".

[48] P. L. A. Popelier, A robust algorithm to locate automatically all types of critical points in the charge density and its Laplacian, *Chem. Phys. Lett.*, 160, 228, (1994).

[49] P. Balanarayan, and S. R. Gadre, Topography of molecular scalar fields. I. Algorithm and Poincaré–Hopf relation, *Chem. Phys. Lett.*, 119, 5037, (2003).

[50] A. Otero-de-la-Roza, Finding critical points and reconstruction of electron densities on grids, *J. Chem. Phys.*, 156, 224116, (2022).

[51] W. Press, S. Teukolsky, W. Vetterling, B. Flannery, *Numerical Recipes in C*, Cambridge Univerity Press, New York, (1992).

[52] M. Palusiak, and T. M. Krygowski, Application of AIM Parameters at Ring Critical Points for Estimation of π-Electron Delocalization in Six-Membered Aromatic and Quasi-Aromatic Rings, *Chem. Eur. J.*, 13, 7996, (2007).

[53] A. Mohajeri, and A. Ashrafi, Aromaticity in terms of ring critical point properties, *Chem. Phys. Lett.*, 458, 378, (2008).

[54] A. A. Ebrahimi, R. Ghiasi, C. Foroutan-Nejad, Topological characteristics of the Ring Critical Points and the aromaticity of groups IIIA to VIA hetero-benzenes, *J. Mol. Structure: THEOCHEM*, 941, 47, (2010).

[55] N. Castillo, C. F. Matta, and R. J. Boyd, The first example of a cage critical point in a single ring: A novel twisted α-helical ring topology, *Chem. Phys. Lett.*, 409, 265, (2005).

[56] S. Lang, *Calculus of Several Variable*, Springer-Verlag: New York, (1987).

[57] P. L. A. Popelier, A fast algorithm to compute atomic charges based on the topology of the electron density, *Theor. Chem. Acc.*, 105, 393, (2001).

[58] F. D. Proft, C. V. Alsenoy, A. Peeters, W. Langenaeker, and P. Geerlings, Atomic charges, dipole moments, and Fukui functions using the Hirshfeld partitioning of the electron density, *J. Comput. Chem.*, 23, 1198, (2002).

[59] B. B. Stefanov, and J. Closlowski, *J. Comput. Chem.*, 16, 1394, (1995).

[60] P. L. A. Popelier, A method to integrate an atom in a molecule without explicit representation of the interatomic surface, *Comp. Phys. Commun.*, 108, 180, (1998).

[61] P. L. A. Popelier, A method to integrate an atom in a molecule without explicit representation of the interatomic surface, *Comp. Phys. Commun.*, 108, 180, (1998).

[62] P. L. A. Popelier, An analytical expression for interatomic surfaces in the theory of atoms in molecules, *Theor. Chem. Acta*, 86, 465, (1994).

[63] N. O. J. Malcolm, and P. L. A. Popelier, An improved algorithm to locate critical points in a 3D scalar field as implemented in the program MORPHY, *J. Comput. Chem.*, 23, 437, (2003).

[64] N. O. J. Malcolm, and P. L. A. Popelier, An algorithm to delineate and integrate topological basins in a three-dimensional quantum mechanical density function, *J. Comput. Chem.*, 24, 1276, (2003).

[65] S. Noury, X. Krokidis, F, Fuster, and B. Silvi, Computational tools for the electron localization function topological analysis, *Comp. Chem.*, 23, 597, (1999).

[66] B. Silvi, and C. Gatti, Direct Space Representation of the Metallic Bond, *J. Phys. Chem. A*, 104, 947, (2000).

[67] G. Henkelman, A. Arnaldsson, and H. Jonsson, A fast and robust algorithm for Bader decomposition of charge density, *Comput. Mater. Sci.*, 36, 354, (2006).

[68] E. Sanville, S. D. Kenny, R. Smith, and G. Henkelman, Improved grid-based algorithm for Bader charge allocation, *J. Comput. Chem.*, 28, 899, (2007).

[69] M. Yu, and D. R. Trinkle, Accurate and efficient algorithm for Bader charge integration, *J. Chem. Phys.*, 134, 064111, (2011).

[70] J. I. Rodriguez, A. M. Koster, P. W. Ayers, A. Santos-Valle, A. Vela, and G. Merino, *J. Comput. Chem.*, 30, 1082, (2009).

[71] J. I. Rodriguez, R. F. W. Bader, P. W. Ayers, C. Michel, A. W. Gotz, and C. Bo, A high performance grid-based algorithm for computing QTAIM properties, *Chem. Phys. Lett.*, 472, 149, (2009).

[72] E. Clementi, *Modern Techniques in Computational Chemistry*, International Business Machines Corporation Kingston, New York 12401, U.S.A (1989).

[73] J. G. Muga, J. P. Palao, B. Navarro, and I. L. Egusquiza, Complex absorbing potentials *Phys. Reports* **395**, 357 (2004).

Chapter 3 Atomic electron densities in Linearly polarized laser

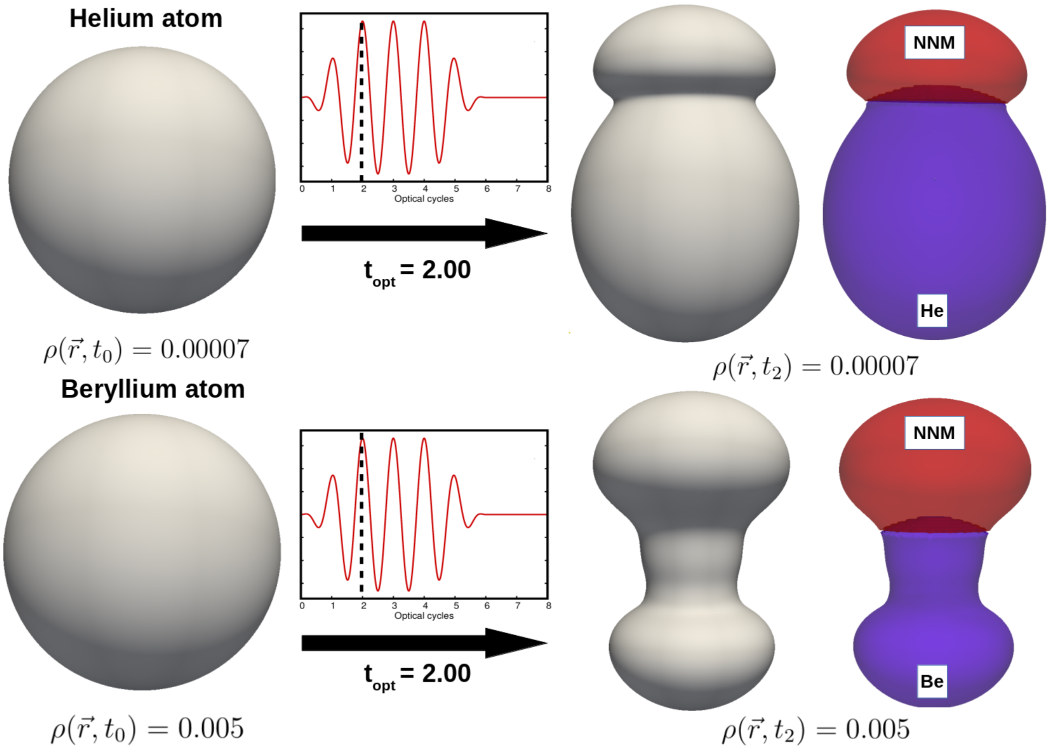

---

[1] Graphical abstract presents the changes in the distribution of the spherically symmetric electron densities of at a time-step in the Z-polarized linear laser field.

Abstract

The chapter presents the application of the ABELDYNPROP code on the two test systems, Helium and Beryllium atoms, in the presence of a Z-polarized linear laser field. The time-evolving atomic electron densities, gradient paths, Laplacian, difference densities, topology, and the time-varying norm are evaluated and discussed. Time-dependent plots of electron density distributions show symmetric deformations. This distribution spreads along the laser polarization directions while shrinking in perpendicular directions. These changes are elucidated through the time evolutions of gradient paths, Laplacian, and difference densities plots. New topological features are found regarding critical points, especially non-nuclear maxima accompanied with (3,-1) CPs. All basin's norms are evaluated, which justifies redistributing electronic charges from the atomic basin region to another non-nuclear basin's regions. These deformations and redistributions are observed repeatedly over the half and full cycles of the laser pulses.

3.1 Introduction

Many electron atoms time-independent quantum mechanical electron densities show a spherically symmetric distribution in all directions centered around their atomic position. In most cases, the atomic electron densities possess a single nuclear maximum, a (3,-3) CP at the origin in the ground state. From theory, this fact can be proved using Kato's *cusp condition*. The electron density value at a nuclear position, ρ_0 of a free atom in the Hartree-Fock approximation is roughly proportional to the cube of the atom's nuclear charge, which has the mathematical form $\rho_0 = 0.4798Z^{3.1027}$ a.u., for $1 < Z < 55$.[1] The atomic electron density distribution shows exponential and monotonic decay along the radial distance,[1–3] starting from the nuclear position along all directions. In the free-field scenario, the gradient vectors in all the atomic space would always converge to the nuclear position. Additionally, there does not exist any zero-flux surface in the case of free-field atomic densities. Due to the absence of any other atom in its vicinity, the atomic electron densities lack any other bond, ring, or cage CPs except the maximum CP in the free-field cases.

The three-dimensional topology of the electron density of atoms may appear to be a spherical isosurface. On the other hand, the topology of Laplacian $\nabla^2\rho(\vec{r})$ of electron density exhibits a very different topology. The determination of a radius at which $\nabla^2\rho(\vec{r})$ is a minimum determines the radius of the sphere at which charge density is maximally concentrated and vice versa.[1] The electron densities exhibit a maximum at nuclear positions, but this does not mean that the electron density would be concentrated at all distances when moving toward the nucleus. Additionally, the integral of $\nabla^2\rho(\vec{r})$ over the whole space of the atom is zero because of the zero-flux condition. Because of this condition, there will be regions where the electron density would be locally concentrated ($\nabla^2\rho(\vec{r}) < 0$) and locally depleted ($\nabla^2\rho(\vec{r}) > 0$) regions towards the nucleus along a radial line. Since $\nabla^2\rho(\vec{r})$ is a continuous and a differentiable function in the molecular space, there must exist regions where $\nabla^2\rho(\vec{r}) = 0$. Therefore, it is elucidated that these regions show spherical nodes in the Laplacian $\nabla^2\rho(\vec{r})$ of atomic electron densities. The number of nodes in the Laplacian distribution is found to have a relation with its shell structure. Bader and coworkers[4, 5] found out that for each principle quantum shell, there exists a pair of regions, each consisting of one positive and one negative region. Sagar,[6] Boyd and coworkers[7] have defined the number of shells like this by the Laplacian of charge density. It was defined for atoms whose atomic number Z < 40, that the number of shells has a direct relation with the number of maxima in the radial distribution.

All the topological features exhibited by the free-field atomic electron densities result from the attractive force exerted by bound potential created by the nuclei on the electronic charge distribution. However, in the presence of an external field, apart from the two potential (nuclear-electron and electron-electron) terms in Hamiltonian, an additional term is introduced for an atom in a LASER. This additional term for a linearly polarized laser pulse is $\vec{E}(t) \cdot \vec{r}$, where $\vec{E}(t) = E_0 cos(\omega t)$ for laser with frequency ω. Therefore, the updated electronic Hamiltonian for N-electron atom would be,[8]

$$\hat{H}_{ele} = -\sum_{i=1}^{N} \frac{1}{2}\nabla_i^2 - \sum_{i=1}^{N} \frac{Z_A}{r_{iA}} + \sum_{i=1}^{N}\sum_{j>i}^{N} \frac{1}{r_{ij}} + \vec{E}(t) \cdot \vec{r} \tag{3.1}$$

Several phenomena, such as quasi-bound states, metastable states, and slow ionizations, have been predicted theoretically and experimentally verified at high-intensity and high-frequency regimes of LASER fields.[9] Moiseyev and coworkers predicted that atoms and anions could achieve stable states by overcoming the binding potential and following to and fro motions about the classical turning points of the high-frequency LASER fields.[10–13] The results showed time-averaged dichotomic states of atoms in high-intensity and high-frequency fields. This meant that the electron density of a single atom would resemble a homonuclear diatomic molecule. Kramer and Henneberger were the first to pioneer these concepts, which were later realized for noble gases like helium and neon.[14–16]

This chapter presents the time evolution of atomic electron densities, their Laplacian, and difference electron densities of Helium and Beryllium atoms in the presence of a linearly polarized laser. The topological tools will analyze the critical points, isocontours, and gradient paths. The results and discussions section will discuss the time-evolving norm of the atomic basin and other non-nuclear basins.

3.2 Computational details

Two atoms, Helium and Beryllilum are taken to be the test system in this study. The basis set used are *d-aug-cc-pvdz* (35 functions) and aug-cc-pvdz (25 functions) for Helium and Beryllium atoms respectively. The coordinates of Helium and Beryllium were used as an input to obtain free-field molecular orbitals, one-electron, two-electron, and dipole integrals (in X, Y, and Z directions) from the modified GAMESS-US code. We use these in ABELDYN code to obtain molecular orbitals coefficients for the test systems at each timestep in a continuous wave Linearly polarized laser (CW-LPL) field. The chosen polarization direction of the laser was to be along the Z-direction. We choose the laser pulse frequency as the free field energy difference between highest occupied and lowest unoccupied orbitals in the ground state for both atoms. The frequency used for Helium, and Beryllium are $\omega_{He} = 0.9371$, and $\omega_{Be} = 0.3294$ a.u. respectively. These frequency ranges fall within the extreme UV range of light. The electric field strength of the laser used was $\epsilon = 0.100 a.u.$ We use a total of 8 optical cycles. The two cycles times the laser pulse rising ($t_{on} = 0 - 2$), two optical cycles in the CW region ($t_{cw} = 2 - 4$), and two cycles times the laser pulse switches off ($t_{on} = 4 - 6$), and and the remaining two free cycles makes up the total laser pulse duration. A box-type complex absorbing potential with the box length of (10.00,10.00,10.00) a.u. was used for both Helium and Beryllium atoms. The strength of complex absorbing potential used was 1.00. The total norm is preserved in the case of Helium atom while the norm decays to 3.65 a.u. for the Beryllium atom's calculation. The input details are provided in the supplementary information file provide all the parameters of the calculations. The orbital coefficients obtained from the ABELDYN code[17, 18] are used as input to calculate the electron density, and its critical points, the gradient path, Laplacian, norm, critical points and *atoms-in-molecule* analysis, using the in-house properties code ABELDYNPROP.

3.3 Results and Discussion

Atomic electron densities of Helium: The Helium atom's field-free electron density (ED) exhibits a spherically symmetric density distribution in all directions centered around its nuclear position. This ED distribution contains a single maximum at the Helium atom with an ED value of 3.341 a.u. and decays monotonically in an exponential fashion away from the nuclear position. All the gradient vector lines converge at the nuclear attractor, corresponding to the maximum.

This electron density of He atom is one of the simplest models to study the time-varying topography of electron density in linearly polarized laser fields. Fig. [3.1] shows the Helium atom's time-dependent electron density (TDED) distribution, gradient lines of electron density, its Laplacian, and density difference at different time steps in the Z-polarized linear laser field. The TDED distribution of the Helium atom loses the spherically symmetric shape and causes deformations majorly along the polarization direction Z in the linear laser field. The laser field's electron density tends to align along the direction of field polarization (Refer to TDED movie of Helium in Appendix).

The contour plots of TDED $\rho(\vec{r},t)$ reveal the distribution becoming wider in $\pm$Z while narrowed in the Y-direction. The red-color contour plots show the negative values of the time-dependent Laplacian, which indicates the charge accumulated regions containing the non-nuclear maxima in the electron density distribution. The redistribution of electron density is elucidated from the time-varying difference density contour plots, where the density value gets curtailed down mostly near the regions close to the atom (red-colored). It gets amplified in the atomic spaces away from the nucleus (grey-colored). The deformations in TDED and related properties

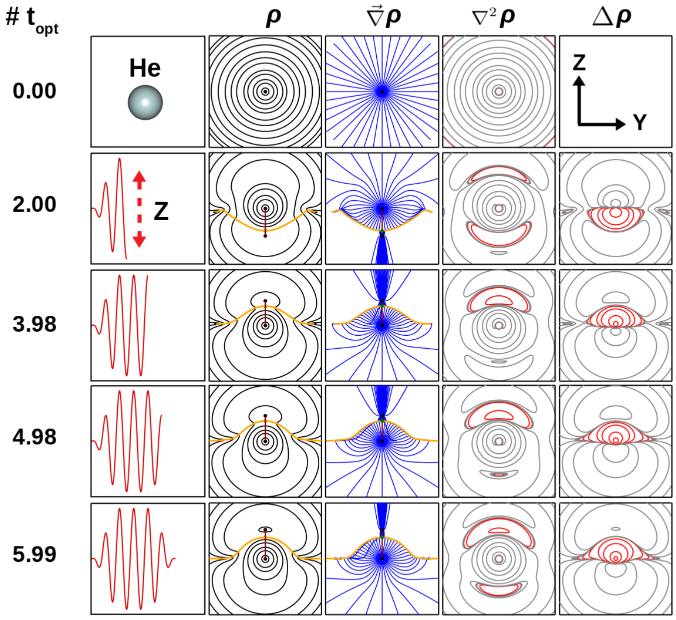

Figure 3.1: Time dependent electronic properties of Helium (placed at origin) in the presence of linearly polarized laser field (Parameters - $\epsilon_0 = 0.100$, and $\omega = 0.937$ a.u.) along Z-direction: laser time step t_{opt} - first column, molecular electron density $\rho(\vec{r})$ - second column, gradients lines of electron density $\nabla\rho(\vec{r})$ - third column, Laplacian of electron density $\nabla^2\rho(\vec{r})$ - fourth column, difference density $\Delta\rho(\vec{r})$ - fifth column, calculated on the YZ-plane, x=0. Negative values are represented by red-colored contours, and positive values by black/grey-colored contours. The critical points representation: Black dots - (3,-3) CPs, Green dots - (3,-1) CPs, Red dots - (3,+3) CPs, Purple dots - (3,+1) CPs. The yellow and maroon colored lines depict basin boundaries and bond paths, respectively. Level of theory: *TDHF/d-aug-cc-pVDZ*. The intermediate steps are shown in Appendix section, Fig. [4.1]. All the properties are mentioned in atomic units.

along the laser pulse follow a cyclic pattern, i.e., similar deformation in shapes of distributions are repeated at full and half cycles of the laser pulse.

We observe a to and fro motion of Helium's nuclear maximum, the (3,-3) CPs on the Z-axis, i.e. (0.0,0.0,±z) where z∼(-0.0003 to 0.0006), and its respective TDED values show small increments/decrements. The topological investigation of the deformed TDED distribution shows the appearance of new features characterized by the formation of low ED-valued (3,-3), (3, -1), and (3,+3) CPs. These CPs are located at distances ranging ∼4-7 a.u. from the Helium's nuclear maximum on the

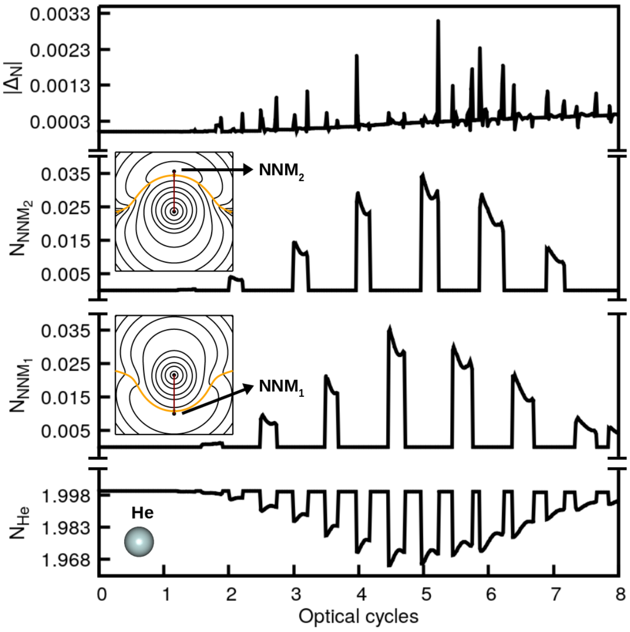

Figure 3.2: Average number of electrons N(Ω) in non-overlapping regions of time-depended electron density distribution of Helium atom (placed at origin) in the presence of linearly polarized laser field (Parameters - $\epsilon_0 = 0.100$, and $\omega = 0.937$ a.u.) along Z-direction. Lowest panel - norm of helium nuclear maxima's basin N_{He}, the middle two panel - norm of non-nuclear maxima's basin N_{NNM_1}, and N_{NNM_2}, and topmost panel - error in total norm $|\Delta N|$. Level of theory: *TDHF/d-aug-cc-pVDZ*. All the properties are mentioned in atomic units.

Z-axis. The (3,-3) CPs are non-nuclear positions (NNMs) are accompanied by (3,-1) BCPs, appear at time steps near the peaks (complete cycles, t_{opt}=3.00, 4.00, 5.00, 6.00) and valleys (half cycles, t_{opt}=2.50, 3.50, 4.50, 5.50) of the laser pulse.

At time steps near peaks and valleys of the laser pulse, NNMs appear at +Z and -Z directions, respectively, along the laser polarization. The redistribution of the TDED in the Helium's atomic space is also reflected through the deviation in the paths of gradient lines. The gradient lines bend in the direction perpendicular to the polarization field, which are the X and Y-directions in this case. The extent of bending is maximum near peaks and valleys when NNMs appear. Here, the atomic space of TDED is divided into two regions separated via zero-flux surface (depicted as the yellow-colored boundary basin, Refer Fig. [3.1]). Fig. [3.2] plots the average number of electrons, *norm* in each region containing the nuclear maximum and

NNMs. The region's norm contained Helium's nuclear maxima, N$_{He}$ ranges from 1.968 to 1.999 a.u. Whereas the norm in the areas having each of the two NNMs, N$_{NNM_1}$, N$_{NNM_2}$ ranges from 0.005 to 0.035 a.u.

Atomic electron densities of Beryllium: Fig. [3.3] depicts the five-time steps in the time-evolving atomic electron densities, its gradient, Laplacian, and difference densities of Beryllium atom in the presence of linearly polarized laser along Z-direction. The appendix section of the thesis provides the picture of intermediate steps and the weblink to the time-evolving movie (`https://youtu.be/6KtGtCQ2HNk`) of these properties .

The first panel presents the properties in the first time-step of LASER. At this step, the concentric isocontours represent the spherically symmetric electron density distribution in all directions centered around the nuclear position. A maximum exists at the Beryllium's position with the electron density value of 33.952 a.u. and decays monotonically along all directions going away from the nucleus. The first panel of Fig. [3.3] shows all the gradient vectors converging to the nuclear maximum, and two negative valued contours of the Laplacian plot represent the two shells of the Be atom.

The following four panels of Fig. [3.3] represent the Beryllium atom's time-evolving electron densities, its respective gradient paths, Laplacian, and difference electron densities at four time-steps, that is, 2^{nd}, 4^{th}, 5^{th} and 6^{th} optical cycles of the LASER pulse. The time-evolving picture shows that the electron densities are no longer spherically symmetric in shape. Just like that of Helium atom's densities, Fig. [3.3] shows the deformation in the electron density distribution occurs such that it experiences elongation in the direction of laser polarization, that is, along ±Z-direction, and the distribution shrinks along the perpendicular direction to the laser polarization, X and Y-directions. It is also observed new critical points, specially $(3, -3)$ and $(3, -1)$, appear on the (0,0,±Z) line. The motion of gradient paths (blue-colored lines) shows a bend in the direction X and Y, perpendicular to the polarization direction. The gradient path lines tend to bundle up/close up along

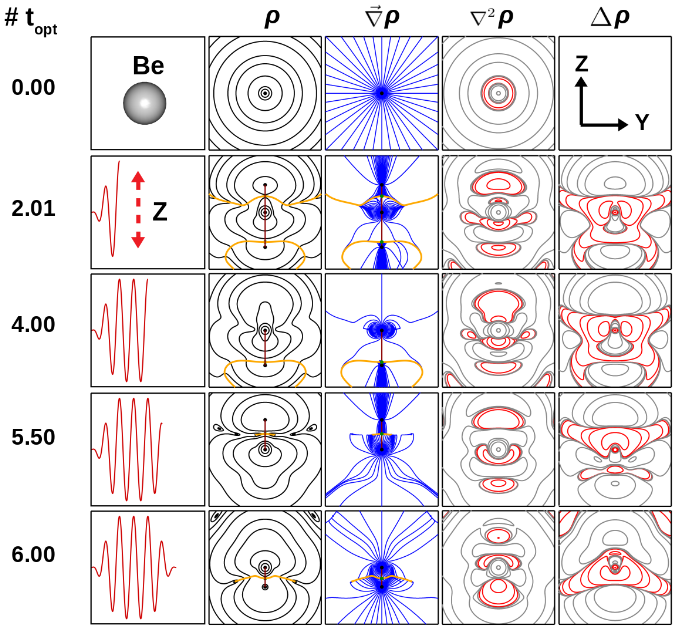

Figure 3.3: Time dependent electronic properties of Beryllium (placed at origin) in the presence of linearly polarized laser field (Parameters - $\epsilon_0 = 0.100$, and $\omega = 0.329$ a.u.) along Z-direction: laser time step t_{opt} - first column, molecular electron density $\rho(\vec{r})$ - second column, gradients lines of electron density $\nabla\rho(\vec{r})$ - third column, Laplacian of electron density $\nabla^2\rho(\vec{r})$ - fourth column, difference density $\Delta\rho(\vec{r})$ - fifth column, calculated on the YZ-plane, x=0. Negative values are represented by red-colored contours, and positive values by black/grey-colored contours. The critical points representation: Black dots - (3,-3) CPs, Green dots - (3,-1) CPs, Red dots - (3,+3) CPs, Purple dots - (3,+1) CPs. The yellow and maroon colored lines depict basin boundaries and bond paths, respectively. Level of theory: *TDHF/aug-cc-pVDZ*. The intermediate steps are shown in Appendix section, Fig. [4.2]. All the properties are mentioned in atomic units.

the Z-direction. At the same time, few lines appear in the Y-direction since they move away/disappear owing to a decrease in the electron density value along the Y-axis. The red-colored isocontour plots depicted the negatively valued Laplacian and difference densities. The negatively valued isocontours appear in the regions of ±Z-axis, which indicates local charge accumulation at these regions. These are the same regions where the non-nuclear maxima, the (3,-3) CPs appear. Similarly, the difference density isocontour plots depict electron density getting depleted in the region closer to the atom while increasing in the regions away from the atomic center. A cyclic pattern in the deformations of time-evolving density and its related properties appear over the half and full cycles of the laser pulse.

The electron density values at the nuclear maximum in the presence of laser show marginal increments and decrements, $\Delta\rho \sim (-1.11$ to $0.00)$ a.u. Even the position of nuclear maximum remains almost the same with marginal displacements $\Delta r \sim (0.0, 0.0, \pm 0.00002)$ a.u. The investigation of the time-evolving topology reveals the presence of new features found in the form of (3,-3), (3,-1), and (3,+1) critical points at various time steps along the laser. Since the choice of laser is linear along Z, the CPs are always positioned on the (0,0,±Z). The local non-nuclear maxima, (3,-3) CPs appears at the distances $(0.00, 0.00,\pm R_{nnm})$, where R_{nnm} ranges from 3.2 to 6.1 a.u. The value of electron densities at these NNMs ranges from 0.002 to 0.018 a.u. These NNMs are also accompanied by (3,-1) CPs. Just like Helium, here as well, appear at time steps near the peaks (complete cycles, t_{opt} = 3.00, 4.00, 5.00, 6.00) and valleys (half cycles, t_{opt} = 2.50, 3.50, 4.50, 5.50) of the laser pulse. At time steps near Peaks and valleys, NNMs appear at +Z and -Z directions, respectively. However, there also exist certain time steps around the peaks and valleys of the laser when NNMs appear at ±Z simultaneously. The redistribution of time-dependent electron density is reflected through gradient paths, Laplacian, and difference density plots. The gradient paths show maximum bends in the Y-direction (perpendicular to the laser). The appearance of NNMs in electron density dictates that the whole atomic space could be partitioned into sub-regions, each containing a local maximum and separated by zero-flux surfaces. It is to be noted that no zero-flux surfaces exist for free-field atomic electron densities, which is not the case for time-evolving atomic electron densities of Beryllium and Helium atoms.

We have performed atoms-in-molecules analysis of time-dependent electron densities to evaluate properties such as charge, Norm, moments, and kinetic energies. The calculations here show the time-varying decay in the norm. Fig. [3.4] shows the variation of Norm in the Beryllium's atomic basin N_{Be} and two non-nuclear maximum's basins N_{NNM_1}, N_{NNM_2}. There is a loss in the Norm along time-steps of the laser pulse. We observe that whenever there is a decrease in the Norm of

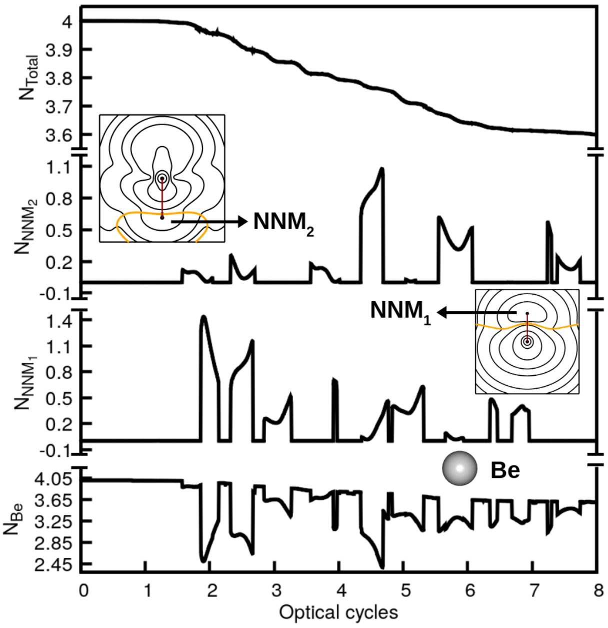

Figure 3.4: Average number of electrons $N(\Omega)$ in non-overlapping regions of time-dependent electron density distribution of Beryllium atom (placed at origin) in the presence of linearly polarized laser field (Parameters - $\epsilon_0 = 0.100$, and $\omega = 0.329$ a.u.) along Z-direction. Lowest panel - norm of Be nuclear maxima's basin N_{Be}, the middle two panel - norm of non-lium nuclear maxima's basin $N_{NNM_1}, and N_{NNM_2}$, and topmost panel shown total norm N_{Total}. Level of theory: *TDHF/aug-cc-pVDZ*. All the properties are mentioned in atomic units.

Beryllium's atomic basin, there is an increase in one of the non-nuclear maximum's basin. This redistribution of total electrons in the whole system at the time steps is done through the decrease of norm property in one basin (atomic basin) and simultaneous increase in the other (NNM's basin). The region's Norm contained Beryllium's nuclear maximum, N$_{Be}$ ranges from 2.45 to 3.99 a.u., Whereas the Norm in the areas having each of the two NNMs, N$_{NNM_1}$, N$_{NNM_2}$ ranges from 0.005 to 1.4 a.u. Since we observe a decrease in Norm in this case, the increase in both the NNMs is not symmetric like what was observed in Helium's case.

3.4 Conclusion

The time-dependent atomic electron densities and their properties are computed for the test case, Helium and Beryllium atoms in the presence of Z-polarized linearly laser fields. Because of the spherical symmetry of free-field atomic electron density, different polarization directions will have the same effect as that of the Z-direction. The nuclear electron densities are observed to lose their spherical symmetry and get a new deformed yet symmetric shape in the presence of a laser pulse. The electron density distribution shows alignment such that it elongates along the polarization direction while shrinking in the perpendicular direction. Assertion of this fact is demonstrated through the isocontour plots. It is also reflected in time-varying gradient paths, which bends maximum at half and full cycles of laser pulses. The gradients tend to bundle up in the direction of laser polarization. The time-varying Laplacian depicts charge concentration at the regions of $\pm$Z, and the field-free shell structure is distorted. There seems to exist more number of nodes, that is, regions where $\nabla^2\rho(\vec{r}) = 0$ along the time-varying fields. The difference in densities depicts electron density values becoming negative in regions nearer to the atom's center and positive in regions far from it. The total norm in the Helium's calculation is conserved to 2.00, while it is not conserved in the Beryllium's calculation. The redistribution of time-dependent electron density is confirmed by calculating the time-varying norm of the atomic basins and their counterpart non-nuclear basins. The increase in the electron count in the non-nuclear basins compensates for the number of electrons decreasing in the atomic basin. This trend is observed at each half and full cycle of the linearly polarized laser pulses.

References Chapter 3

[1] R. F. W Bader, *Atoms in Molecules: A Quantum Theory*, Clarendon Press, Oxford, 1994.

[2] C. F. Matta, and R. J. Boyd,*The Quantum Theory of Atoms in Molecules*, WILEY-VCH Verlag GmbH and Co. KGaA, Weinhein, (2007).

[3] P. L. A. Popelier, *Atoms in Molecules - An Introduction*, Prentice Hall: Harlow-England, (2000).

[4] R. F. W. Bader, and P. M. Beddall, Virial Field Relationship for Molecular Charge Distributions and the Spatial Partitioning of Molecular Properties, *J. Chem. Phys.* **56**, 3320 (1972).

[5] R. F. W. Bader, and H. Essen, The characterization of atomic interactions, *J. Chem. Phys.* **80**, 1943 (1984).

[6] R. P. Sagar, A. C. T. Ku, V. H. Smith Jr., and A. M. Simas, The Laplacian of the charge density and its relationship to the shell structure of atoms and ions, *J. Chem. Phys.* **88**, 4367 (1988).

[7] Z. Shi, and R. J. Boyd, The shell structure of atoms and the Laplacian of the charge density, *J. Chem. Phys.* **88**, 4375 (1988).

[8] A. Szabo, and N. S. Ostlund, *Modern Quantum Chemistry: Introduction to Advanced Electronic Structure Theory* DOVER PUBLICATIONS, INC. Mineola, New York (1996)

[9] H. A. Kramers, Collected Scientific Papers, North-Holland: Amsterdam , p262 (1956).

[10] M. Pont, N. R. Walet, M. Gavrilla, and C. W. McCurdy, Dichotomy of the Hydrogen Atom in Superintense, High-Frequency Laser Fields, *Phys. Rev. Lett.* **61**, 939 (1988).

[11] M. Gavrilla, Atomic stabilization in superintense laser fields, *J. Phys. B: At., Mol. Opt. Phys.* **35**, 147 (2002).

[12] J. H. Eberly, and K. C. Kulander, Atomic stabilization by super-intense lasers, *Science* **5137**, 1129 (1993).

[13] Q. Wei, S. Kais, and N. Moiseyev, New stable multiply charged negative atomic ions in linearly polarized superintense laser fields, *J. Chem. Phys.* **124**, 201108 (2006).

[14] M. P. de Boer, J. H. Hoogenraad, R. B. Vrijen, L. D. Noordam, and H. G. Muller, Indications of high-intensity adiabatic stabilization in neon, *Phys. Rev. Lett.* **71**, 3263 (1993).

[15] U. Eichmann, T. Nubbemeyer, H. Rottke et al., Acceleration of neutral atoms in strong short-pulse laser fields, *Nature* **461**, 1261 (2009).

[16] M. Matthews, F. Morales, A. Patas et al., Amplification of intense light fields by nearly free electrons, *Nat. Phys.* **14**, 695 (2018).

[17] P. Raj, A. Gugalia, and P. Balanarayan, ABELDYN: Ab-initio Electron Dynamic package, *Manuscript to be submitted*.

[18] P. Raj, Electronic Quantum Dynamics of Molecules in Strong LASER fields: Novel Algorithms and Effects, Dotoral Dissertation (2022).

Chapter 4 Molecular electron densities in a Linearly polarized laser: A topological study and Non-nuclear maxima

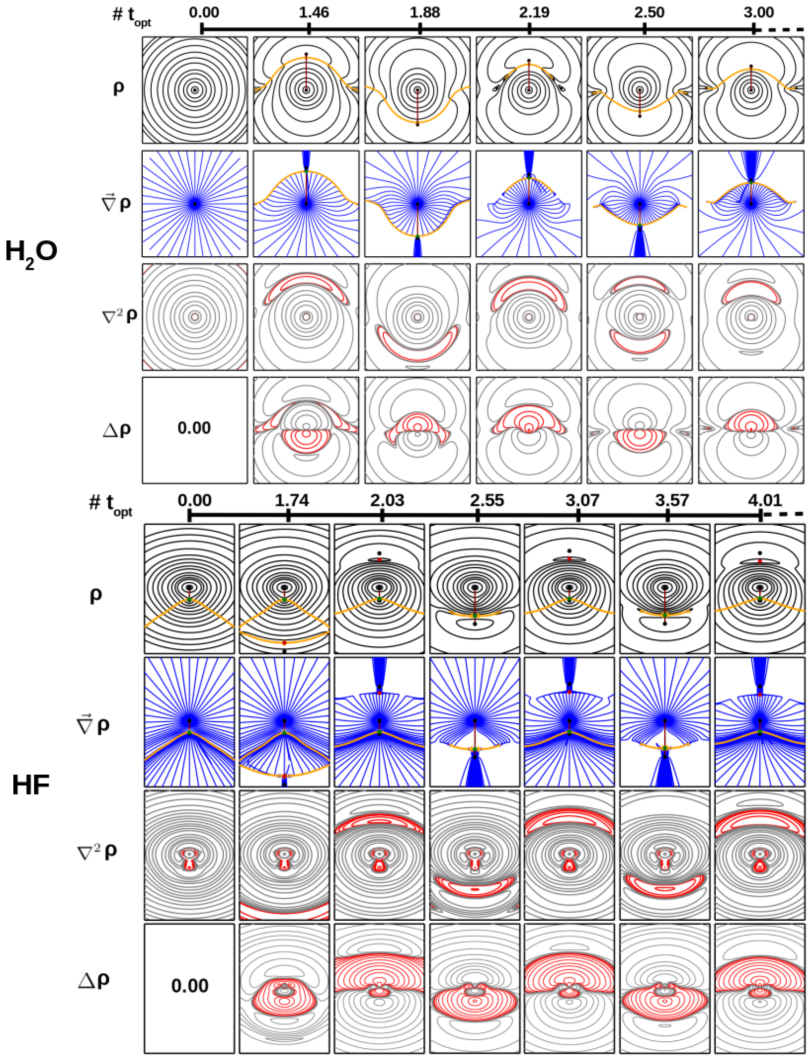

---

[1] The graphical abstracts shows the time evolving properties of water and HF molecules in Z-polarized linear laser field.

Abstract

This work presents time-evolving molecular electron densities and their gradient lines, Laplacian, and difference electron densities in a Z-polarized linear laser field for the test cases: Hydrogen Fluoride, Water, Methane, and Ethylene molecules. The polarization direction of the laser field creates symmetric and cyclic deformations along the path of polarization along the laser pulse. The gradient lines bend in the directions perpendicular to the direction of polarization, and the Laplacian show plots depicting charge concentrations at the terminal of molecular space. The contour plots of electron density difference demonstrates increase or decrease in the molecular electron density over certain regions in the molecular space. This work's novelty lies in the critical points of TDMED, especially non-nuclear maxima, through the topological analysis of all the test cases. The electronic population analysis done for the newly formed basins due to the creation of NNMs shows a significant number of electrons residing in these regions.

4.1 Introduction

Recent advancements in the twenty-first century led to the development of coherent light sources, creating ultra-short laser pulses of few attosecond $(1as = 10^{-18}s)$ timescales. Such timescales provide a way to directly control the rapid motion of electrons in a molecule. Since the time evolution in time-dependent electron density is responsible for bond-breaking and bond-forming in chemical reactions, this has opened up another way of doing chemistry called attochemistry.[1–3] Attosecond technology has investigated ultrafast electronic dynamics in atoms and molecules.[4, 5] Light-induced ultrafast electronic dynamics play an essential role in the early stages of photosynthesis processes, radiation damages of biologically relevant molecules, and chemical and biological processes where electron transfer occurs.[6] In this respect, the quantum electron dynamical models have been developed, solving the time-dependent Schrödinger equation (TDSE) with explicit time-dependent Hamiltonian to simulate interactions of atoms and molecules in the presence of ultrashort laser pulses. When the Hamiltonian is time-dependent, the solution to TDSE has the following form,

$$\psi(\vec{r},t) = \hat{\tau} e^{\frac{-\iota}{\hbar}\int_{t_0}^{t}\hat{H}(\vec{r},t')dt'}\psi(\vec{r_0},t) \tag{4.1}$$

where $\hat{\tau}$ is the time-ordering operator. The formalism of time-ordering operator arises because the time-dependent Hamiltonian is non-commutative at two different time instances, that is $[\hat{H}(\vec{r},t), \hat{H}(\vec{r},t')] \neq 0$. The Chebychev Propagator method[7] and (t,t') method[8–10] are two such numerical receipes incorportating time evolution operator which have been developed to solve the TDSE with explicit time-dependent Hamiltonians. Recently, Raj *et al.* have proposed a efficient and fast algorithm to solve TDSE using (t,t') and (t,t',t'') method for molecules interacting with short laser pulses.[11] The solutions obtained from solving TDSE by these methods, provide the time evolving molecular electronic wavefunctions $\psi(\vec{r},t)$ or molecular orbitals for atoms and molecules, in the presence of time-dependent oscillating electric fields such as lasers. As a consequence, this interplay between theory and experiments allows for the microscopic characterization of chemical processes.

According to the basic postulate of quantum mechanics, the wavefunction can be used to determine all the physically observable informations about a quantum system. Molecular electron density (MED) is one such important observable which is a non-negative real-valued scalar-field property analytically obtained from the wavefunctions or molecular orbitals (MOs). MED are quantities routinely evaluated for molecules using X-ray scattering experiments.[12, 13] Therefore, MEDs find its role important in understanding the molecular structure parameters and chemical reactivity. The MED is evaluated from the 4N-dimensional time-independent wavefunction $\psi(\mathbf{x}_1,\mathbf{x}_2,\cdots,\mathbf{x}_N)$ as

$$\rho(\vec{r}) = N \sum_{\sigma} \int |\psi(\mathbf{x}, \mathbf{x}_2, \cdots, \mathbf{x}_N)|^2 d^3r_2 \cdots d^3r_N \tag{4.2}$$

Here, the $\mathbf{x}_1, \mathbf{x}_2, \cdots, \mathbf{x}_N$ represents the set of spin-coordinates (spin and position). The summation runs over all the spin-coordinate, the integration over all but one spatial coordinate, and N is the total number of electrons. MED, $\rho(\vec{r})$, is defined as the probability of finding an electron at $\vec{r}$ around the volume element d^3r. In this work, we present the study of electronic dynamics for time-dependent molecular electron density (TDMED) using analysis from topological tools, in the presence of linearly-polarized lasers for various chemically different test molecules. The time-evolution in TDMED $\rho(\vec{r}, t)$ is incorporated via the time-dependent molecular electronic wavefunctions $\psi(\vec{r}, t)$ obtained from the solutions of TDSE. At the time instant t, for the time-dependent wavefunction, $\psi(\vec{r}, t) = \psi(\mathbf{x}_1, \mathbf{x}_2 \cdots, \mathbf{x}_N, t)$, the TDMED is evaluated as

$$\rho(\vec{r}, t) = \sum_{i}^{occ} \psi_i(\vec{r}, t)\psi_i^*(\vec{r}, t) \tag{4.3}$$

where the summation index *i* goes over all the set of occupied molecular orbitals $\psi(\vec{r}, t)$. Exploring the electronic dynamics of TDMED requires the study of the response of electron density to the time-dependent linearly polarized laser. For the free-field MEDs, Bader and coworkers showed the response of chemical reactions resulted in the movement of critical points producing topological catastrophes.[14, 15] Ayers *et. al.* added to this notion through the electron preceding picture. In this model, the electron-density response around the critical point correlates with the magnitude of eigenvectors of the Hessian of $\rho(\vec{r})$.[16–18] In addition to this, Eberhart and coworkers have recently developed a scheme called gradient bundle analysis, which uses changes in the gradients and topology of MED to study the response of electron density to external perturbations to gain insights into chemical reactivity.[19, 20]

The information concerning the electronic dynamics of TDMED is not abundant in the literature. However, few reports related to quantum molecular dynamics of MED are present. The charge transfer in H_3^+ and LiF is studied using quantum molecular dynamics of MED's topological properties.[21]. The report on the study of the coupled electronic-nuclear dynamics, including the time dependence of electron density, has been carried out for model systems.[22, 23] Another report presented the photodissociation of NaI molecules with electron transfer, followed graphically by the electron density contribution of the two valence orbitals.[24]

Bader and coworkers explored the in-depth topology of MED and developed the *quantum theory of atom-in-molecules* (QTAIM).[14] The gradients of MED terminate at one of the atomic nuclei. Bader utilized[25] this gradient feature to develop the concept of partitioning the molecular space into atomic basins. The partitioning of molecular space happens into exhaustive and nonoverlapping regions enclosing a nuclei and separated by boundaries called *interatomic surfaces* or *zero-flux surfaces* (ZFS). The ZFS of MED is an open surface, i.e.; it does not surround atomic nuclei in the molecule from all directions. The MED-based atomic basins obeys the local virial theorem. Therefore it is utilized to integrate the electron density and calculate the average properties of these subsystems (atomic basins), such as charges, electrostatic moments, polarizability, and kinetic energies. The MED-based QTAIM has been utilized to study chemically relevant quantities such as electronegativity, lewis acidity and basicity.[26, 27]

The gradient vector field of MED, $\nabla\rho(\vec{r}) = \frac{\partial\rho}{\partial x}\hat{x} + \frac{\partial\rho}{\partial y}\hat{y} + \frac{\partial\rho}{\partial z}\hat{z}$, informs about the nature of the function at $\vec{r}$, i.e. if increasing, decreasing or flat. The solutions to the differential equation $d\vec{r}(s)/ds = \nabla\rho(\vec{r}(s))$ provides a set of points drawing a path called *gradient paths*, $\vec{r}(s)$. All the non-zero density points where gradient vanishes, $\nabla\rho(\vec{r}) = 0$, represent the critical point (CP) of MED. The eigenvalues and eigenvectors of the Hessian $H_{ij}(\vec{r}) = \partial^2\rho(\vec{r})/\partial r_i\partial r_j$ at those points are used to find its rank and signature (λ, σ) and thereafter characterize the kind of CP. The Laplacian of MED, L($\vec{r}$) = -$\nabla^2\rho(\vec{r}, t) = (\partial^2/\partial x^2 + \partial^2/\partial y^2 + \partial^2/\partial z^2)\rho(\vec{r}, t)$, that is, the sum of diangonal elements of Hessian. The regions where $\nabla^2\rho(\vec{r})$<0 shows charge concentration and regions show charge depletion when $\nabla^2\rho(\vec{r})$>0. The Laplacian has been utilized to locate electrophilic site.[14, 28]

The dominant form of MED presents local maxima, (3,-3) critical points mostly near the atomic nuclei in the molecule, with few exceptions. For each pair of local maxima of MED in molecules, there exists a (3,-1) CP, referred to as bond cp (BCP). This BCP represents being maximum in two directions while minimum along the path joining the pair of local maxima. The MED of every molecule features the presence of (3,-3) and (3,-1) CPs. Also, the two other kinds, (3,+1) and (3,+3) CPs, may be present in molecules. The (3,+1) CPs manifest the arrangement of the (3,-1) BCPs in a ring fashion, called ring cp (RCP). The (3,+3) CPs represent the local minima of MED in molecules. It results from the enclosed arrangement of BCP and RCPs, called cage cp (CCP). Cyclopropane and tetrahedrane molecular examples show RCP and CCP, respectively. Since there always exists a (3,-1) BCP in between a pair of (3,-3) CPs, the gradient path line forming between those (3,-3) CPs through (3,-1) BCP they are referred to as *bond paths*. The eigenvalues of the Hessian and electron density at BCP have been used to determine parameters such as bond ellipticity (a measurement of π *character*) and bond order.[29–33]

The molecular electron density distributions, $\rho(\vec{r})$, shows maxima at the nuclear positions and then decays off exponentially. However, this being the most dominating feature of ρ, there have been exceptions when maxima appear at non-nuclear positions, which are called non-nuclear maxima (NNMs) or non-nuclear attractors

(NNAs). NNMs was first theoretically predicted in alkali metal clusters [34–36], and later experimentally observed in metallic beryllium and magnesium.[37] Dilithium, Li_2 molecule, has been studied with advanced theoretical methods to confirm that the occurrence of NNM is not an artifact due to the level of theory employed.[38–42] Glaser *et al.*[38] discussed that the third valence molecular orbital of Li_2 causes a negative curvature in the central bonding region, which is the reason for the occurrence of NNM in Li_2. Most of the advanced calculations support the existence of NNM in the middle of the Li-Li bond, but for other systems, the same cannot be said conclusively. In 1999, Pendas and co-workers[43] attempted to resolve this uncertainty for homonuclear systems. They introduced the promolecular model, in which the electron density of a molecule is made by the superposition of free atomic densities. Observations from the internuclear variations predicted that NNMs occurred in specific ranges, including the equilibrium bond length.[44] According to them, the atomic shell structures could be a responsible factor for the formation of NNMs when two atoms bind.

In this work, we present the study of time-dependent topology of TDMED in the presence of linearly-polarized laser-driven fields for Hydrogen Fluoride, Water, Methane and Ethylene molecules as test cases. We employ *atoms-in-molecule* analysis to compute the properties of atomic basins. All the topological properties of TDMED are evaluated using the time-evolving wavefunctions along the laser pulse. These time-dependent electronic wavefunctions are the output obtained from the in-house package called *Ab-initio Electron Dynamics* (ABELDYN), which incorporates a numerical solution to the TDSE using a (t, t') real-time Hartree Fock method.[11] A general trend of the with-field response of electron density, $\rho(\vec{r}, t)$, in TDMED in the presence of a linearly polarized laser shows an oscillatory motion about the free-field MED. This picture elucidates the expansion and contraction of electron density isocontours with time compared to the field-free MED. This fact is further confirmed via density depletion and accumulation picture from the difference molecular electron density, $\Delta\rho(\vec{r}, t) = \rho_t(\vec{r}, t) - \rho_0(\vec{r}, t)$ plots. These oscillatory motions of electron density create deformations. As a consequence, they get reflected in their topological features. The gradients of TDMED, $\nabla\rho(\vec{r}, t)$, provide information to perform time-dependent topological analysis concerning the time evolution in critical points, gradient-path, bond paths, and zero-flux surfaces. The MED in the laser-driven field gets deformed. We observe new critical points appearing at $\epsilon = 0.100 a.u.$, especially NNMs, at the laser pulse's peaks and valleys of optical cycles. The NNMs appear in LPLs along Z for electric field strengths $\epsilon \geq 0.100 a.u.$ In this manuscript, we measure the electron density response in linear-polarized laser through the time evolution in topology.

4.2 Computational details

The test systems, Hydrogen Fluoride, Water, Methane and Ethylene molecules were optimized at HF/aug-cc-pvdz using the electronic structure package Gaussian 09. The optimization of Water, Ethylene molecule is done such that it lies on the YZ plane, and the HF on the Z-axis. Two coordinates are chosen for Methane molecule in such a way that the Z-axis coincides with its C_2 axis in one and C_3 axis in the other. The coordinates of the optimized geometry were used as an input to obtain free-field molecular orbitals, one-electron, two-electron, and dipole integrals (in X, Y, and Z directions) from the modified GAMESS-US code. We take the free-field parameters as input to the in-house RTHF code. We used the code to obtain molecular orbitals coefficients for the test systems at each timestep in a continuous wave Linearly polarized laser (CW-LPL) field. The chosen polarization direction of the laser was to be along the Z-direction. We choose the laser pulse frequency as the free field energy difference between HOMO and LUMO, $\omega_{HF} = 0.688$, $\omega_{water} = 0.547 a.u$, $\omega_{methane} = 0.579$ and $\omega_{ethylene} = 0.419$ a.u. These frequency ranges fall within the extreme UV range of light. The electric field strength of the laser used was $\epsilon = 0.100 a.u.$. We use a total of 8 optical cycles. The two cycles times the laser pulse rising ($t_{on} = 0 - 2$), two optical cycles in the CW region ($t_{cw} = 2 - 4$), two cycles times the laser pulse switch off ($t_{off} = 4 - 6$) and the remaining two free cycles make up the total laser pulse duration. A box-type complex absorbing potential with the box length of (20.00,20.00,20.00) a.u. was used for all the molecules. The strength of complex absorbing potential used was 1.00. The input details are provided in the supplementary information file provide all the parameters of the calculations. The norm (N_{tot}) throughout the pulse duration is conserved in our calculation. The molecular orbital coefficients obtained from the RTHF code are used as input to calculate the electron density and related properties, the gradients, hessian, Laplacian, norm, critical points and *atoms-in-molecules* analysis, using the in-house properties code, Ab-initio electron dynamics (ABELDYNPROP).

In the present work, we use the time evolving electronic wavefunctions from an in-house code Ab-Initio Electron Dynamics (ABELDYN), solving Real Time Hartree-Fock (RTHF) using (t, t') method.[11, 45, 46] The molecular orbital coefficients of this electronic wavefunction are used as an input at each time step for the calculation of electronic properties. In the next subsections, we provide the description and working of in-house ABELDYN code, which we have used to obtain time-dependent molecular orbital coefficients.

Time-dependent molecular orbital coefficients obtained from the solutions from RTHF using (t, t') method: The ABELDYN-PROP the code requires inputs in the form of pre-calculated molecular orbital coefficients for the user-specified molecular system, at those time-step for which the time-dependent properties are to be evaluated. The time-dependent molecular orbital coefficients are retrieved from the output of in-house code ABELDYN, that solves time-dependent Schrödinder equation numerically from the mean-field approach of RTHF using (t, t') formalism for a fixed nuclear geometry.[45, 46] The codes incorporates the effects from an oscillating electric field such as lasers, through suitable changes made in the electronic hamiltonian. One of the main benefits from solutions of RTHF calculations is that, it provides direct visualization of orbitals mixing and time-evolving densities and observe what happens to electrons in molecules in the presence of ultrashort laser fields.

The next sections provides a discussion to the set of results obtained for the properties calculated using ABELDYNPROP code using wave function information from ABELDYN code.

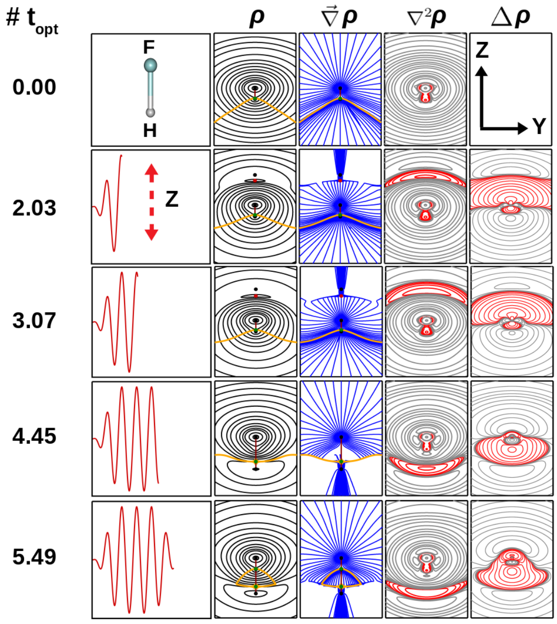

Figure 4.1: Time dependent electronic properties of Hydrogen fluoride molecule (placed at Z-axis) in the presence of linearly polarized laser field (Parameters - $\epsilon_0 = 0.100$, and $\omega = 0.688$ a.u.) along Z-direction: laser time step t_{opt} - first column, molecular electron density $\rho(\vec{r}, t_{opt})$ - second column, gradients lines of electron density $\nabla\rho(\vec{r}, t_{opt})$ - third column, Laplacian of electron density $\nabla^2\rho(\vec{r}, t_{opt})$ - fourth column, difference density $\Delta\rho(\vec{r}, t_{opt})$ - fifth column, calculated on the YZ-plane, x=0. Negative values are represented by red-colored contours, and positive values by black/grey-colored contours. The critical points representation: Black dots - (3,-3) CPs, Green dots - (3,-1) CPs, Red dots - (3,+3) CPs, Purple dots - (3,+1) CPs. The yellow and maroon colored lines depict basin boundaries and bond paths, respectively. Level of theory: *TDHF/aug-cc-pVDZ*. The intermediate steps are shown in Appendix Section, Fig. [4.3]. All the properties are mentioned in atomic units.

4.3 Results and Discussion

Hydrogen Fluoride: The molecular electron density (MED), gradient vector lines, and Laplacian of Hydrogen fluoride in the field-free case has been demonstrated in the first row of Fig. [4.1]. We considered the HF molecule to be oriented along the Z-axis. The field-free MED distribution centered around the Fluorine atom is the widest in Z, followed by the Y direction. At the same time, it shrinks in Y when going down from Fluorine to the Hydrogen atom in the HF molecule. It contains two (3,-3)

CPs corresponding to local nuclear maxima at Fluorine and Hydrogen atoms in HF with MED values of 429.28 and 0.394 a.u. respectively. A (3,-1) Bond CP, whose MED value is 0.390 a.u., lies between the two maxima closer to the Hydrogen atom. All the gradient lines converge to one of the local maxima, dividing the molecular space into two non-overlapping regions separated by basin boundary. The field-free norms of Fluorine and Hydrogen basins are 9.760 and 0.240 a.u. respectively. The computed dipole for the HF molecule is 0.747 a.u. The two atoms, Hydrogen and Fluorine, in HF, are very different chemically. Therefore, the effect of the laser field on their respective basins would be very different.

Fig. [4.1] presents the MED, its gradients, Laplacian, and difference density plots in the presence of the Z-polarized laser field. The TDMED distribution of the HF molecule widens in the Y direction. The gradient vector lines bend in the Y direction. The red and grey-colored contour plots in Fig. [4.1] represent negative valued Laplacian and difference density. The negatively valued Laplacian shows the charge-accumulated regions positioned over and below the Fluorine and Hydrogen atoms. The difference density plots reveal that the electron density values go down in either $\pm$Z directions at half cycle and full cycle of the laser. In Fig. [4.2], the bottom two panels plot the time-dependent norm of Fluorine and Hydrogen basins. The norm of atomic basins, N$_F$ and N$_H$, shows a complementary relationship. At full cycle timesteps of the laser, the Hydrogen's basin N$_H$ population increases, while in Fluorine's basin, N$_H$ population decreases. The vice-versa is followed at half-cycle steps. The time-dependent norm of atomic basins ranges from $\sim$9.3 to 10.0 a.u. for N$_F$, whereas it ranges from $\sim$0.00 to 0.60 a.u. for N$_H$. The field-free (3,-1) BCP and (3,-3) CP (of Hydrogen) are very close, and their MED values differ marginally by 0.004 a.u. When subjected to a Z-polarized laser field, at half-cycle timesteps along the laser, these two CPs merge, forming a degenerate CP. At the same timestep, at the extended Z-axis $(0.0, 0.0, -Z)$, an NNM forms. The basin population of this NNM, N$_{NNM_1}$, near the 2.5 optical cycles is 0.02 a.u., which increases to 0.035 a.u. at the 4.50 cycle and decreases after that in the succeeding half cycles of the laser. Moreover, the formation of another NNM, NNM$_2$, occurs near full cycles of the laser. These NNMs are located near Fluorine on the Z-axis $(0.0, 0.0, +Z)$. The maximum

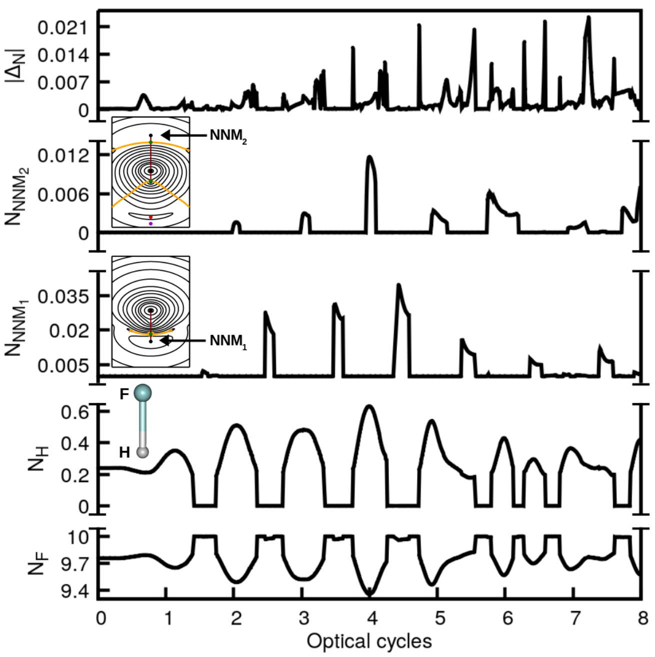

Figure 4.2: Average number of electrons $N(\Omega)$ in non-overlapping regions of time-dependent electron density distribution of Hydrogen fluoride molecule (placed at Z-axis) in the presence of linearly polarized laser field (Parameters - $\epsilon_0 = 0.100$, and $\omega = 0.688$ a.u.) along Z-direction. Lowest panel - norm of Fluorine nuclear maxima's basin N_F, second panel - norm of Hydrogen nuclear maxima's basin N_H, third and fourth panel - norm of non-nuclear maxima's basin $N_{NNM_1}, andN_{NNM_2}$, and topmost panel - error in total norm $|\Delta N|$. Level of theory: *TDHF/aug-cc-pVDZ*. All the properties are mentioned in atomic units.

norm of basins containing these NNMs, N$_{NNM_2}$ is 0.012, which is almost $(1/3)^{rd}$ of N$_{NNM_1}$.

Water: In the YZ-oriented water molecule, Z being the principle axis, the field-free MED distribution is spread widest along Z, followed by Y and X. It contains three (3,-3) CPs, the local maxima at positions near Oxygen and Hydrogen atoms with MED values 297.40 and 0.404 a.u. According to QTAIM, the field-free molecular space of the MED function may be divided into three disjoint subspaces, one region corresponding to the Oxygen basin and two other of Hydrogen basins. The average number of electrons in the Oxygen and Hydrogen atomic basins are 9.259 and 0.370 a.u. respectively. Each Hydrogen basin is separated from the Oxygen basin by cone-shaped *zero-flux surface*. The yellow colored line in Fig. 4.3 row 1 is its 2D

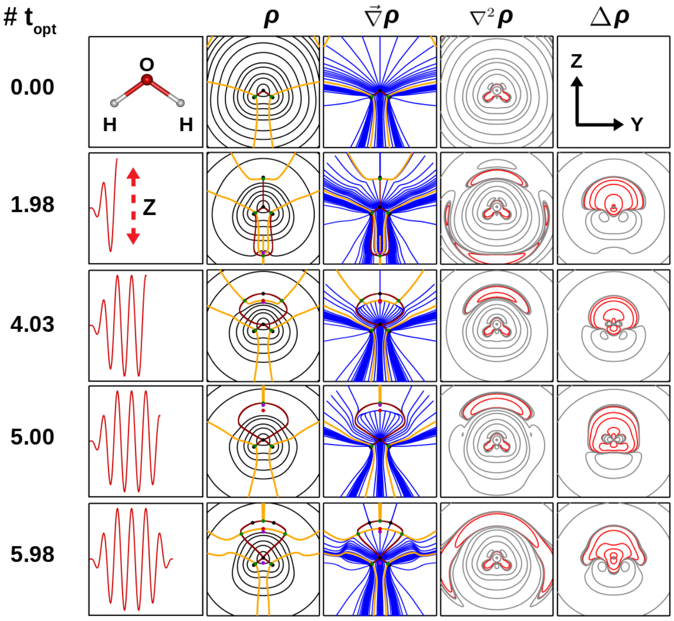

Figure 4.3: Time dependent electronic properties of water molecule (oriented at YZ-plane) in the presence of linearly polarized laser field (Parameters - $\epsilon_0 = 0.100$, and $\omega = 0.546$ a.u.) along Z-direction: laser time step t_{opt} - first column, molecular electron density $\rho(\vec{r}, t_{opt})$ - second column, gradients lines of electron density $\nabla\rho(\vec{r}, t_{opt})$ - third column, Laplacian of electron density $\nabla^2\rho(\vec{r}, t_{opt})$ - fourth column, difference density $\Delta\rho(\vec{r}, t_{opt})$ - fifth column, calculated on the YZ-plane, x=0. Negative values are represented by red-colored contours, and positive values by black/grey-colored contours. The critical points representation: Black dots - (3,-3) CPs, Green dots - (3,-1) CPs, Red dots - (3,+3) CPs, Purple dots - (3,+1) CPs. The yellow and maroon colored lines depict basin boundaries and bond paths, respectively. Level of theory: *TDHF/aug-cc-pVDZ*. The intermediate steps are shown in Appendix Section, Fig. [4.4]. All the properties are mentioned in atomic units.

depiction on the YZ plane, called the basin boundaries. The basin boundaries are parallel in the negative Z-axis and arranged almost linearly in the Y.

TDMED, its gradient vector lines, Laplacian, and difference density plots on the YZ-plane for water in the Z-polarized linear laser fields are portrayed in Fig. 4.3. The deformations of MED in the Z-polarized field follow C_{2V} symmetry throughout the laser pulse. At time steps of full cycles (2.0, 3.0. 4.0. 5.0, and 6.0), the time-dependent MED distribution shrinks in the region near and above the oxygen atom (wider in Z and narrower in Y) and expands in the region near and below

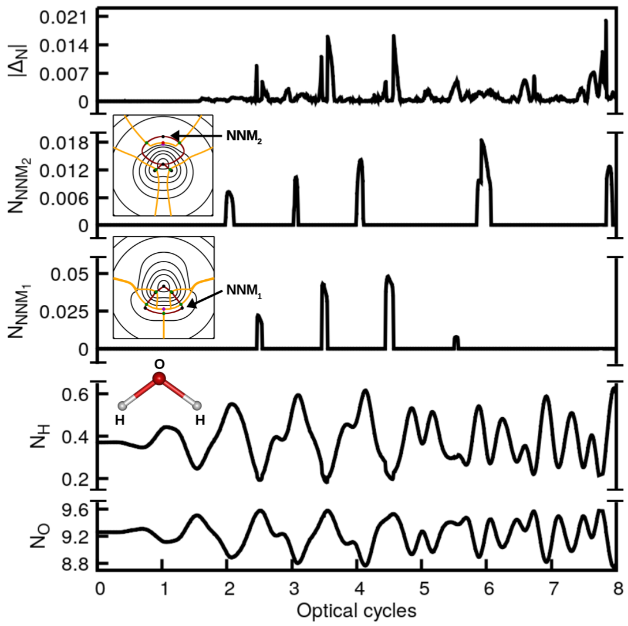

Figure 4.4: Average number of electrons $N(\Omega)$ in non-overlapping regions of time-dependent electron density distribution of water molecule (oriented on YZ-plane) in the presence of linearly polarized laser field (Parameters - $\epsilon_0 = 0.100$, and $\omega = 0.688$ a.u.) along Z-direction. Lowest panel - norm of oxygen nuclear maxima's basin N_O, second panel - norm of Hydrogen nuclear maxima's basin N_H, third and fourth panel - norm of non-nuclear maxima's basin $N_{NNM_1}, andN_{NNM_2}$, and topmost panel - error in total norm $|\Delta N|$. Level of theory: *TDHF/aug-cc-pVDZ*. All the properties are mentioned in atomic units.

hydrogen atoms (narrower in Z and wider in Y). The trend is reversed at half-cycle (2.50, 3.50, 4.50, 5.50) time steps. At the full cycles, the Laplacian depicts a red region above the Oxygen atom, signaling charge concentration and vice-versa at half cycles. Similar patterns of MED value depletion and increments are shown in difference density plots. Fig. 4.4, panel 1 and 2 (from the bottom) shows Hydrogen and Oxygen basin populations. The norm of Oxygen and both Hydrogen ranges (8.8-9.6) and (0.20-0.60) a.u. respectively. The time-varying norms of Oxygen and Hydrogen show an inverse relation w.r.t to each other; that is, as the norm of the Oxygen basin increases, there is a decrease in Hydrogen's norm. The reason is evident because in the laser-driven field when the molecular region of the atomic basin of Oxygen atoms swells up, the regions of the atomic basin of Hydrogen atoms shrink simultaneously.

The gradient lines bend in the direction perpendicular to the polarization field direction, i.e., X and Y directions. The topological analysis of TDMED at full cycles reveals an NNM accompanied by a (3,-1) CP located on the positive Z-axis above the Oxygen atom. However, it could be accompanied by more number of (3,-1) CPs or (3,+1) RCPs, (3,+3) CCPs. The time-dependent 2D movie shows the gradient vector lines emptying this region by bending away or closing/converging towards a (3,-1) BCP or (3,+3) CCP. A well-shaped boundary separates the region containing this NNM. In addition to this, At half cycles, the formation of two NNMs on the YZ plane in the extended OH-bond direction takes place. At the same YZ-plane and same time steps, in addition to these NNMs, the formation of three (3,-1) BCPs, one (3,+1) RCP, and one (3,+3) CCP, or more may take place along the laser. A separate basin containing these NNMs is formed at these, whose boundaries are very close to Hydrogen's atomic basin. In addition, a basin boundary is formed on the XY-plane, which borders the two NNMs basins. We call this NNM as NNM type 1, NNM$_1$, and the other kind as NNM as NNM$_2$. The MED values of NNM$_1$ are of the order $10^{-2} - 10^{-4}$ a.u., while that of NNM$_2$, appearing near Oxygen atom are of the order $10^{-3} - 10^{-6}$ a.u. The norm population of NNM$_1$, N$_{NNM_1}$ is around 0.025 at 2.50 opt cycles, increasing to about 0.05 at 3.50 and 4.50 optical cycles. The population of electrons in the NNM$_2$ basin, N$_{NNM_2}$ is 0.006 a.u. at the 2.00 cycle and increases to 0.012 and 0.0.16 a.u., at 3.00 and 4.00 optical cycles. It is to be noticed that the norm of NNM$_1$ is always higher than the norm of NNM$_2$. Therefore, electron density redistribution is more facile towards the Hydrogen's side than the Oxygen's region.

Time-dependent electron density properties for the Y-polarized laser field case have been depicted in Fig. [4.5]. Unlike the Z-polarized laser, the TDMED follows C_S symmetry in the Y-polarized laser field. The TDMED expands in the positive Y-direction and shrinks in the negative Y at half-cycle time steps and vice-versa at full cycles. The time-dependent difference density contour plots show red regions representing the decreased value of MED at those molecular spaces. These regions appear symmetrically in positive and negative Y directions along the laser. Also, the Laplacian along the laser pulse shows red-colored contour plots depicting its

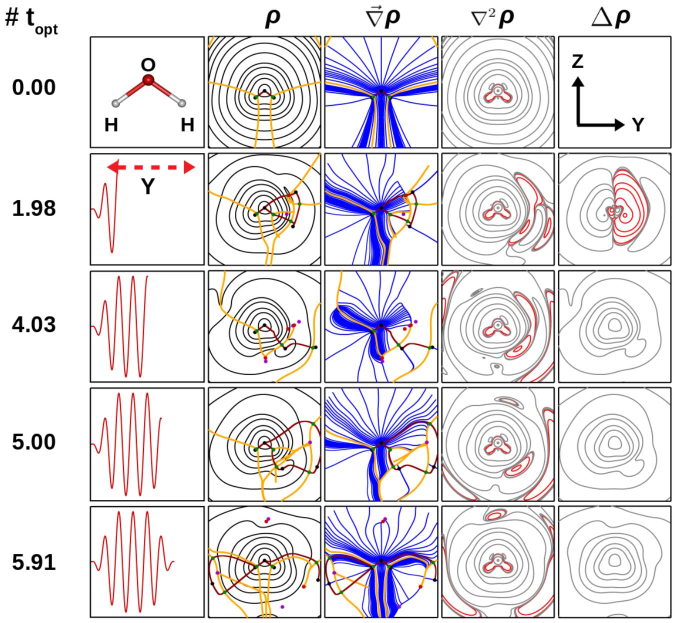

Figure 4.5: Time dependent electronic properties of water molecule (oriented at YZ-plane) in the presence of linearly polarized laser field (Parameters - $\epsilon_0 = 0.100$, and $\omega = 0.546$ a.u.) along Y-direction: laser time step t_{opt} - first column, molecular electron density $\rho(\vec{r}, t_{opt})$ - second column, gradients lines of electron density $\nabla\rho(\vec{r}, t_{opt})$ - third column, Laplacian of electron density $\nabla^2\rho(\vec{r}, t_{opt})$ - fourth column, difference density $\Delta\rho(\vec{r}, t_{opt})$ - fifth column, calculated on the YZ-plane, x=0. Negative values are represented by red-colored contours, and positive values by black/grey-colored contours. The critical points representation: Black dots - (3,-3) CPs, Green dots - (3,-1) CPs, Red dots - (3,+3) CPs, Purple dots - (3,+1) CPs. The yellow and maroon colored lines depict basin boundaries and bond paths, respectively. Level of theory: *TDHF/aug-cc-pVDZ*. The intermediate steps are shown in Appendix section, Fig. [4.5]. All the properties are mentioned in atomic units.

negative value. The 2D plots are shown in Fig. [4.5] row 2 points their locations at the top and bottom right of the YZ-plane. Similar plots are shown in row 3 but at the top and bottom left of the YZ plane. These regions depict charge-concentrated regions. The time-dependent gradient vector lines tend to move in the ±Z directions. The norm of Oxygen (N_O) and Hydrogen (N_{H_r}, N_{H_l}) atoms is very different from what was noticed in the TDMED along Z-polarized laser (refer Fig. [4.6]). Here the electron population changes have an inverse relation among the hydrogen atoms. The population in the left Hydrogen basin decreases while it increases in the right Hydrogen basin. This population N_{H_r}, N_{H_l}, ranges from 0.00 to 0.70 au. The

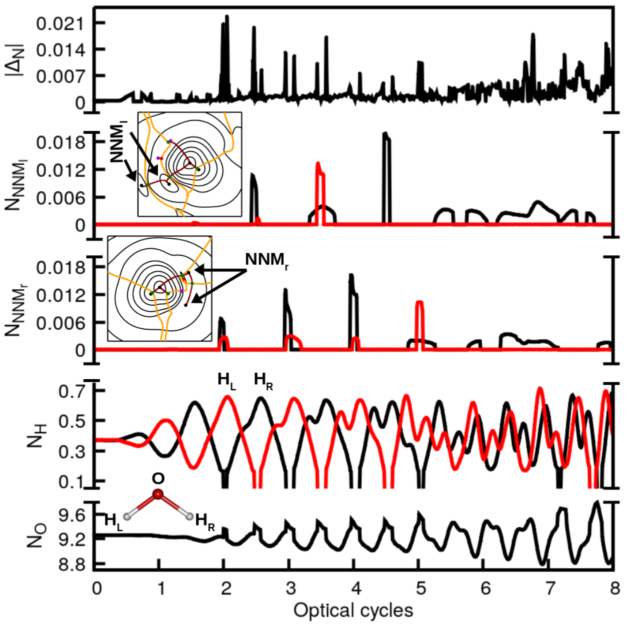

Figure 4.6: Average number of electrons $N(\Omega)$ in non-overlapping regions of time-dependent electron density distribution of water molecule (oriented on YZ-plane) in the presence of linearly polarized laser field (Parameters - $\epsilon_0 = 0.100$, and $\omega = 0.688$ a.u.) along Y-direction. Lowest panel - norm of oxygen nuclear maxima's basin N_O, second panel - norm of Hydrogen nuclear maxima's basin N_H, third and fourth panel - norm of non-nuclear maxima's basin $N_{NNM_1}, andN_{NNM_2}$, and topmost panel - error in total norm $|\Delta N|$. Level of theory: *TDHF/aug-cc-pVDZ*. All the properties are mentioned in atomic units.

population of the Oxygen basin changes cyclically but remains like this till the 7th optical cycle and increases marginally from there on. The population of the Oxygen basin, N_O, ranges (from 8.8 to 9.6). We observe that near the half and full-cycle timesteps, one of the Hydrogen's (3,-3) CP coalesces with its respective (3,-1) CP. The topological analysis of this TDMED shows that after the coalesce formation of NNM CPs (one or two) takes place and (3,-1) BCPs, (3,+1) RCPs, and (3,+3) CCPs may appear. The critical points appear symmetrically on the YZ plane's left and right sides. The population of the NNMs formed on the right side, N_{NNM_r}, ranges from 0.006 to 0.018. A similar population range is observed on the left side as well.

Methane: Fig. [4.7] and [4.9] demonstrate the TDMED distribution of methane molecule and its gradient, Laplacian, and difference density plots. The linear laser field's polarization direction is the Z direction, but the molecule is oriented such that the polarization would become parallel to its C_2 and C_3 axis. Fig. [4.7] and [4.9] shows the plots on the YZ plane containing the H-C-H bond of methane molecule for when the polarization is parallel to C_2 and C_3 respectively. Since the molecule is symmetrical, plotting TDMED and its properties in one of the H-C-H would suffice to understand similar or complementary changes in other H-C-H planes or Hydrogens and the molecule overall. The field-free MED distribution is depicted on the YZ-plane in the first rows of Fig. [4.7] and [4.9]. The distribution shows similarities to Water's MED distribution. The difference is that the heavy atom, the Carbon, in this case, occupies less molecular space when compared to hydrogen. Also, the basin boundaries are V-shaped, unlike Water's free-field MED distribution. The free-field MED of Methane contains 5 (3,-3) CPs, one of Carbon and the other four of hydrogen, with MED values of 120.57 and 0.388 a.u. respectively. In Bader's analysis, we would find five Bader volumes according to QTAIM theory, each containing one atomic nuclear maximum. The average number of electrons in the Carbon basin is 5.695 a.u. While in Hydrogen basins is 1.076 a.u.

The nature of TDMED and its properties of methane in a Z-polarized laser field (|| to C_2) show similarities with the TDMED of Water. The TDMED distribution becomes wider in Y and Z. The gradient vector lines on the YZ plane move away from the Z directions and bend towards the ±Y directions to the linear field. The topological investigation of TDMED of methane reveals the presence of NNM accompanied with (3,-1) BCPs on the YZ-plane near the half cycles timesteps (2.50, 3.50, 4.50, 5.50) of the laser pulse (refer Fig. [4.7], row 3). NNMs would be observed on the other H-C-H plane perpendicular to the former near the laser's full cycle timesteps (2.00, 3.00, 4.00, 5.00, 6.00). These NNMs and their respective (3,-1) BCPs are found to be located on the YZ-plane along the extended C-H bond sites. One of the features observed in TDMED distributions contains gradient vector lines converging to (3,+1) RCPs and (3,+3) CCPs on the YZ plane. These RCPs and CCPs are found to be located on the Z-axis above the Carbon atoms or middle left/right position in the frame of the YZ-plane shown in Fig. [4.7] The red-colored contour plots in the time-dependent Laplacian representing charge-concentrated regions in the molecular space are arranged in an enclosing fashion around the H-C-H of methane.

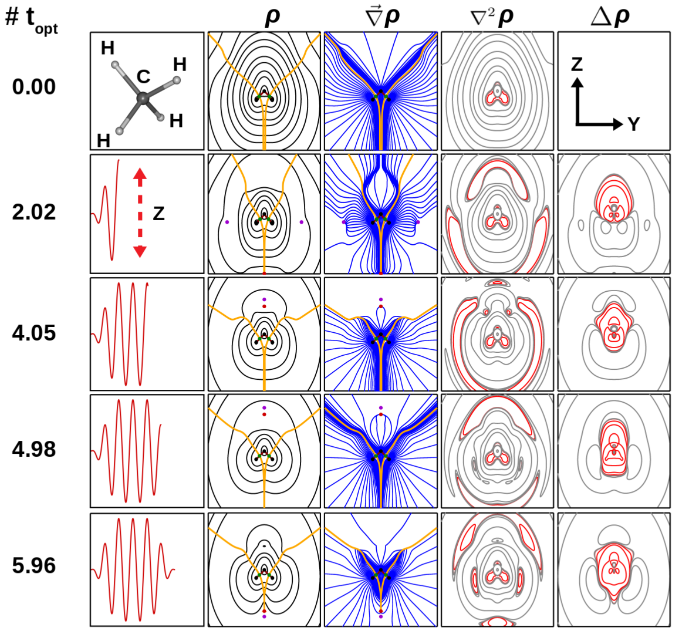

Figure 4.7: Time dependent electronic properties of methane molecule in the presence of linearly polarized laser field (Parameters - $\epsilon_0 = 0.100$, and $\omega = 0.5799$ a.u.) along Z-direction parallel to its C_2-axis: laser time step t_{opt} - first column, molecular electron density $\rho(\vec{r}, t_{opt})$ - second column, gradients lines of electron density $\nabla\rho(\vec{r}, t_{opt})$ - third column, Laplacian of electron density $\nabla^2\rho(\vec{r}, t_{opt})$ - fourth column, difference density $\Delta\rho(\vec{r}, t_{opt})$ - fifth column, calculated on the YZ-plane, x=0. Negative values are represented by red-colored contours, and positive values by black/grey-colored contours. The critical points representation: Black dots - (3,-3) CPs, Green dots - (3,-1) CPs, Red dots - (3,+3) CPs, Purple dots - (3,+1) CPs. The yellow and maroon colored lines depict basin boundaries and bond paths, respectively. Level of theory: *TDHF/aug-cc-pVDZ*. The intermediate steps are shown in Appendix Section, Fig. [4.6]. All the properties are mentioned in atomic units.

The 2D time-dependent movies depict the enclosed plot moving around the H-C-H in two major semi-circle island-like features. The time-dependent norm of Carbon and Hydrogen atoms are shown in the Fig. [4.8]. The behaviour of norm in the pairs (H_1, H_2) and (H_3, H_4) (See Methane molecule depicted inside the plot in Fig. [4.8]) follows a inverse relation shown in black and red colors.

The TDMED of methane in the Z-polarized laser field parallel to the C_3-axis is very different to that discussed above. Here, the Z-polarization is parallel to one of the C-H bonds in methane. Plots for these are shown in Fig. [4.9]. The time-dependent

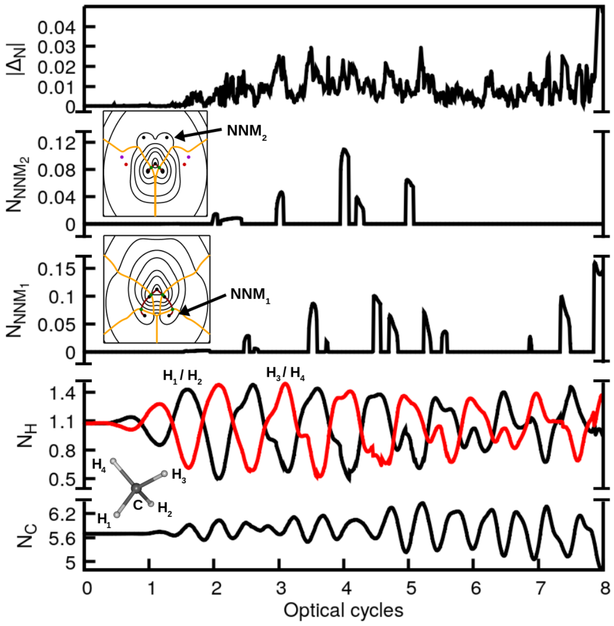

Figure 4.8: Average number of electrons $N(\Omega)$ in non-overlapping regions of time-dependent electron density distribution of methane molecule in the presence of linearly polarized laser field (Parameters - $\epsilon_0 = 0.100$, and $\omega = 0.579$ a.u.) along Z-direction, parallel to its C_2 axis. Lowest panel - norm of carbon nuclear maxima's basin N_O, second panel - norm of Hydrogen nuclear maxima's basin N_H, third and fourth panel - norm of non-nuclear maxima's basin $N_{NNM_1}, and N_{NNM_2}$, and topmost panel - error in total norm $|\Delta N|$. Level of theory: *TDHF/aug-cc-pVDZ*. All the properties are mentioned in atomic units.

topology of TDMED of methane in this case show two kinds of NNMs on the ±Z-axis. The first kind of NNM, NNM_1, is located on the +Z axis above the Hydrogen atom of the C-H bond, while the other one NNM_2 is found on the -Z axis, right at the center of the three Hydrogen atoms. These NNMs are accompanied with other (3,-1) BCPs, (3,+1) RCPs, and (3,+3) CCPs on the YZ-plane shown in the plots. The time-dependent norms shown Fig. [4.10]. In TD norm plot of the Hydrogens (second panel from bottom), N_H, shows black colored plots for Hydrogen basins, H_1, H_2, and H_3 (See the location of H_2, H_3 and H_4 in the inset figure of Methane) which ranges from 0.30 to 1.50 a.u. In the same panel, the red-colored plot shows the H_1 atom basin's norm, which lies on the C-H bond parallel to the polarization axis. When the norm in H_1 increases, the norm in H_2, H_3, and H_4 basins decrease. No specific pattern is drawn in the norm of Carbon atom's basin. However, this norm

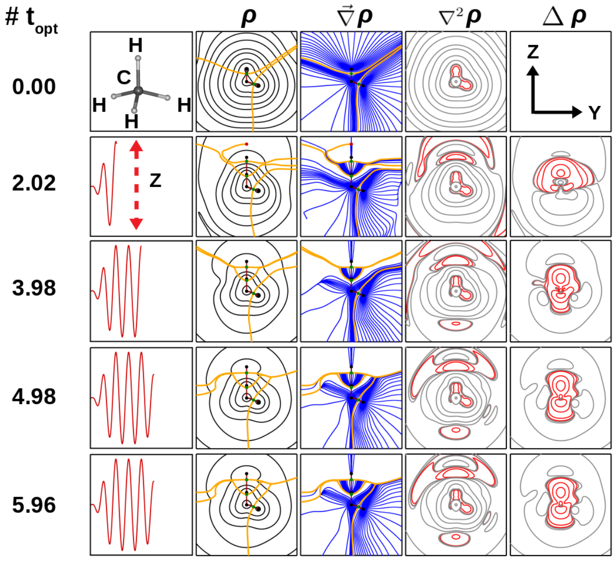

Figure 4.9: Time dependent electronic properties of methane molecule in the presence of linearly polarized laser field (Parameters - $\epsilon_0 = 0.100$, and $\omega = 0.579$ a.u.) along Z-direction which is parallel to its C_3-axis: laser time step t_{opt} - first column, molecular electron density $\rho(\vec{r}, t_{opt})$ - second column, gradients lines of electron density $\nabla\rho(\vec{r}, t_{opt})$ - third column, Laplacian of electron density $\nabla^2\rho(\vec{r}, t_{opt})$ - fourth column, difference density $\Delta\rho(\vec{r}, t_{opt})$ - fifth column, calculated on the YZ-plane, x=0. Negative values are represented by red-colored contours, and positive values by black/grey-colored contours. The critical points representation: Black dots - (3,-3) CPs, Green dots - (3,-1) CPs, Red dots - (3,+3) CPs, Purple dots - (3,+1) CPs. The yellow and maroon colored lines depict basin boundaries and bond paths, respectively. Level of theory: *TDHF/aug-cc-pVDZ*. The intermediate steps are shown in Appendix section, Fig. [4.7]. All the properties are mentioned in atomic units.

oscillates between 4.9 to 6.4 a.u. The norms of NNM, NNM_1, N_{NNM_1} maximizes to 0.29 a.u., which is quite significant. While its lowest value of norm is 0.05 a.u. The norm range for NNM_2 from 0.04 to 0.12 a.u.

Ethylene: The field-free MED of ethylene molecules, placed on the YZ-plane, is distributed widest along the Z direction while narrower in the Y direction, as shown in Fig. [4.11], row 1. This MED contains six (3,-3) CPs, two nuclear maximums corresponding to Carbon ($\rho_{-3} = 120.79$), and four nuclear maximum ($\rho_{-3} = 0.394$) corresponding to Hydrogen atoms. Also, the distribution includes five (3,-1) BCPs ($\rho_{-1} = 0.350$ between C-C bond, $\rho_{-1} = 0.287$) between C-H bond). The Elliptical

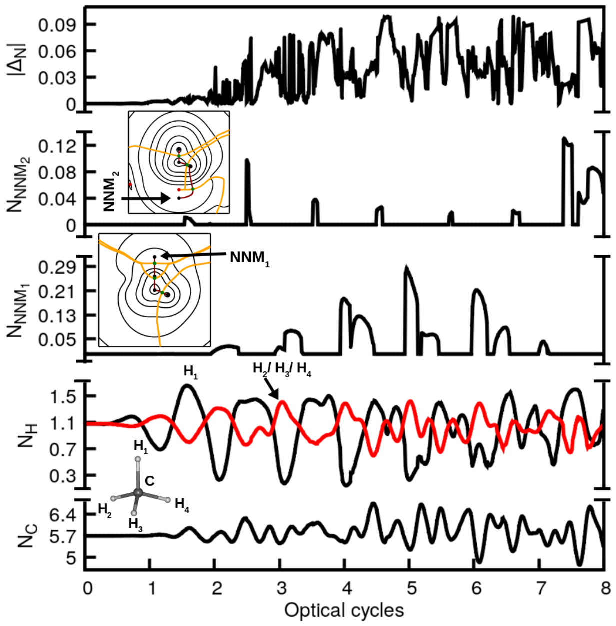

Figure 4.10: Average number of electrons $N(\Omega)$ in non-overlapping regions of time-dependent electron density distribution of methane molecule in the presence of linearly polarized laser field (Parameters - $\epsilon_0 = 0.100$, and $\omega = 0.579$ a.u.) along Z-direction, parallel to its C_3 axis. Lowest panel - norm of carbon nuclear maxima's basin N_O, second panel - norm of Hydrogen nuclear maxima's basin N_H, third and fourth panel - norm of non-nuclear maxima's basin $N_{NNM_1}, andN_{NNM_2}$, and topmost panel - error in total norm $|\Delta N|$. Level of theory: *TDHF/aug-cc-pVDZ*. All the properties are mentioned in atomic units.

plane separates the C-C atomic basins, while the C-H atomic basins are divided by a curved ZFS. For this molecule, we used two axes of polarization: the Z and Y directions. The polarization direction Z is parallel to the C-C bond of the ethylene molecule, while the Y direction is perpendicular to it.

Fig. [4.11] depicts the time-dependent MED, gradient lines, Laplacian, and difference density plots for Methane in Z-polarized laser fields. For the Z-polarized laser, the TDMED contour plots show the distribution becoming elongated along the Z axis while getting narrower in Y. For this case, the gradient vector field lines tend to move away and bend toward the Y direction. These gradient vector lines converge into minima (3,+3) CPs. These minimum CPs are located either on the ±Z axis or at the end winds of the basin boundaries for the C-C bonds. The topological analysis shows the presence of NNMs in the TDMED distribution. The NNMs are present

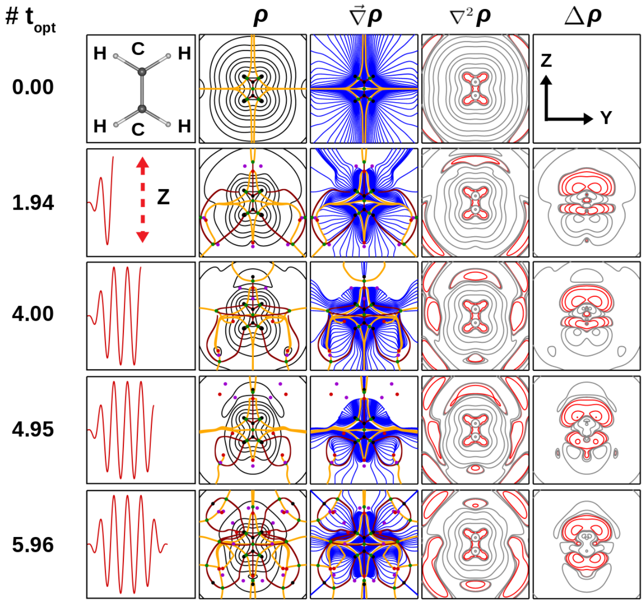

Figure 4.11: Time dependent electronic properties of Ethylene molecule in the presence of linearly polarized laser field (Parameters - $\epsilon_0 = 0.100$, and $\omega = 0.419$ a.u.) along Z-direction which is parallel to the C-C bond of C_2H_4 molecule: laser time step t_{opt} - first column, molecular electron density $\rho(\vec{r}, t_{opt})$ - second column, gradients lines of electron density $\nabla\rho(\vec{r}, t_{opt})$ - third column, Laplacian of electron density $\nabla^2\rho(\vec{r}, t_{opt})$ - fourth column, difference density $\Delta\rho(\vec{r}, t_{opt})$ - fifth column, calculated on the YZ-plane, x=0. Negative values are represented by red-colored contours, and positive values by black/grey-colored contours. The critical points representation: Black dots - (3,-3) CPs, Green dots - (3,-1) CPs, Red dots - (3,+3) CPs, Purple dots - (3,+1) CPs. The yellow and maroon colored lines depict basin boundaries and bond paths, respectively. Level of theory: *TDHF/aug-cc-pVDZ*. The intermediate steps are shown in Appendix Section, Fig. [4.8]. All the properties are mentioned in atomic units.

at two sites. They could be situated along the ±Z-axis or on the right/left top or bottoms on the YZ-plane shown in the plots. It is also noticed that the ZFS plane between the C-C bond also shows significant bends in either direction of polarized field Z.

Similar properties plots with different Y-polarized linearly laser fields are depicted in Fig. [4.12]. This polarization direction is perpendicular to the C-C bond of the ethylene molecule. The TDMED contour plots show that the distribution blows up in the +Y direction at full cycle timesteps while the vice-versa is observed in the -Y

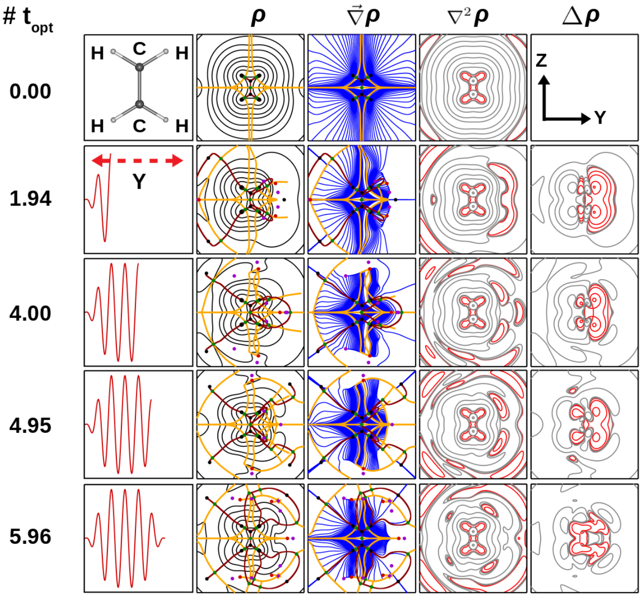

Figure 4.12: Time dependent electronic properties of Ethylene molecule in the presence of linearly polarized laser field (Parameters - $\epsilon_0 = 0.100$, and $\omega = 0.419$ a.u.) along Y-direction which is perpendicular to the C-C bond of C_2H_4 molecule: laser time step t_{opt} - first column, molecular electron density $\rho(\vec{r}, t_{opt})$ - second column, gradients lines of electron density $\nabla\rho(\vec{r}, t_{opt})$ - third column, Laplacian of electron density $\nabla^2\rho(\vec{r}, t_{opt})$ - fourth column, difference density $\Delta\rho(\vec{r}, t_{opt})$ - fifth column, calculated on the YZ-plane, x=0. Negative values are represented by red-colored contours, and positive values by black/grey-colored contours. The critical points representation: Black dots - (3,-3) CPs, Green dots - (3,-1) CPs, Red dots - (3,+3) CPs, Purple dots - (3,+1) CPs. The yellow and maroon colored lines depict basin boundaries and bond paths, respectively. Level of theory: *TDHF/aug-cc-pVDZ*. The intermediate steps are shown in Appendix section, Fig. [4.9]. All the properties are mentioned in atomic units.

direction. The gradient field lines show them moving away and bending towards the ±Z directions. These gradient field lines converge to minima (3,+3) CPs. These CPs are located near the ±Y-axis on the YZ plane. The NNMs in the TDMED are located either on the ±Y or top and bottom around the Y axis. In addition, bow-shaped basin boundaries get formed in either direction of the oscillation field Y.

4.4 Conclusion

The TDMED and its properties are evaluated for test cases, Hydrogen Fluoride, Water, Methane, and Ethylene molecules in the presence of Z and Y-polarized linear laser fields. It is evident through the contour plots of TDMED distribution that it shows deformations, as it tends to align in the direction of field polarization. The behavior of deformations is symmetric and cyclic w.r.t polarization direction over the laser pulse timesteps. The Hydrogen's nuclear maxima (3,-3) CPs and its respective (3,-1) CPs coalesced for the cases of HF in Z-polarized laser and water in Y-polarization. In this work, for every test case, we have found new critical points, mainly NNMs, along the Z-axis or the extended bonding regions of the molecule. The average number of electrons, the norm of each nuclear and non-nuclear atomic basin, is calculated. The time-dependent norms among nuclear basins (such as the Oxygen-Hydrogen pair and carbon-hydrogen pair) have been found to follow an inverse relationship. The population of electrons in basins containing NNMs has been small in magnitude but yet significant when compared to atomic basins.

References Chapter 4

[1] F. Krausz, and M. Ivanov, Attosecond physics, *Rev. Mod. Phys.* **81**, 163 (2009).

[2] F. Lepine, M. Ivanov, and M. Vrakking, Attosecond molecular dynamics: fact or fiction?, *Nature Photon* **8**, 194 (2014).

[3] N. V. Golubev, and A. I. Kuleff, Control of charge migration in molecules by ultrashort laser pulses, *Phys. Rev. A* **91**, 051401 (2014).

[4] E. Goulielmakis, Z. Loh, A. Wirth, V. S. Yakovlev, S. Zherebtsov, A. M. Azzeer, M. F. Kling, S. R. Leone, and F. Ktausz, Real time observation of valence electron motion *Nautre* **466**, 739 (2010).

[5] M. Drescher, M. Hentschel, R. Kienberger, M. Uiberacker, V. Yakovlev, A. Scrinzi, T. Westerwalbesloh, U. Lleineberg, U. Heinzman, and F. Krausz, Time-resolved atomic inner-shell spectroscopy *Nature* **419**, 803 (2002).

[6] F. Calegari, D. Ayuso, A. Trabattoni, L. Belshaw, S. D. Camillis, S. Anumula, F. Frassetto, L. Poletto, A. Palacios, P. Decleva, J. B. Greenwood, F. Martin and N. Nisoli, Ultrafast electron dynamics in phenylalanine initiated by attosecond pulses *Science* **346**, 6207 (2014).

[7] M. Ndong, H. Tal-Ezer, R. Kosloff, and C. P. Koch, Chebychev propagator with iterative time ordering for explicitly time-dependent Hamiltonians *J. Chem. Phys.* **132**, 064105 (2010).

[8] U. Peskin, and N. Moiseyev, The Solution of the time-dependent Schrödinger equation by the (t, t') method: Theory, Computational algorithm and applications *J. Chem. Phys.* **99**, 4950 (1993).

[9] U. Peskin, O. E. Alon and N. Moiseyev, The solution of the time-dependent Schrödinger equation by the (t, t') method: Multiphoton ionization/dissociation probabilities in different gauges of the eletromagnetic potential *J. Chem. Phys.* **100**, 7310 (1994).

[10] U. Peskin, R. Kosloff, and N. Moiseyev, The solution of the time-dependent Schrödinger equation by the (t, t') method: The use of global polynomial propagators for time dependent Hamiltonians *J. Chem. Phys.* **100**, 8849 (1994).

[11] P. Raj, A. Gugalia, and P. Balanarayan, Quantum Dynamics with Explicitly Time-Dependent Hamiltonians: A New Algorithm for (t, t') and (t, t', t'') Methods in Laser-Matter Intractions *J. Chem. Theory Comput.* **16**, 35 (2019).

[12] N. K. Hansen, and P. Coppens, Testing aspherical atom refinements on small-molecule data sets *Acta. Cryst.* **34**, 909 (1978).

[13] T. S. Koritsanszky, and P. Coppens, Chemical Applications of X-Ray Charge-Density Analysis *Chem. Rev.* **101**, 1583 (2001).

[14] R. F. W Bader, *Atoms in Molecules: A Quantum Theory*, Clarendon Press, Oxford, 1994.

[15] R. F. W Bader, T. T. Nguyen-Dang, and Y. Tal Quantum topology of molecular charge distributions. II. Molecular structure and its change *J. Chem. Phys.* **70**, 4316 (1979).

[16] P. W. Ayers, and S. Jenkins An electron-preceding perspective on the deformation of materials *J. Chem. Phys.* **130**, 154104 (2009).

[17] A. Guevara-Garcia, E. Echegarray, A. Toro-Labbe, S. Jenkins, S. R. Kirk, and P. W. Ayers Pointing the way to the products? Comparison of the stress tensor and the second-derivative tensor of the electron density *J. Chem. Phys.* **134**, 234106 (2011).

[18] A. Guevara-Garcia, P. W. Ayers, S. R. Kirk, E. Echegargay and A. Toro-Labbe Electronic Effects in Organic Chemistry, part of *Topics in Current Chem* **351**, 103 (2014).

[19] T. E. Jones, and M. E. Eberhart The bond bundle in open systems *Int. J. Quantum Chem.* **110**, 1500 (2010).

[20] A. Morgenstern, C. Morgensternand, J. Mioreli, T. Wilson, and M. E. Eberhart The influence of zero-flux surface motion on chemical reactivity *Phys. Chem. Chem. Phys.* **18**, 5638 (2016).

[21] R. Chavez-Calvillo, and J. Hernandez-Trujillo, Quantum Molecular Dynamics of the topological Properties of the electron density: Charge transfer in H_3^+ and LiF *J. Phys. Chem.* **115**, 13036 (2011).

[22] M. Erdmann, P. Marquetand, and V. J. Engel Combined electronic and nuclear dynamics in a simple model system *J. Chem. Phys.* **119**, 672 (2003).

[23] M. Erdmann,and V. J. Engel Combined electronic and nuclear dynamics in a simple model system. II. Spectroscopic transitions *J. Chem. Phys.* **120**, 158 (2004).

[24] M. Gronager, and N. E. Henriksen, Real-time control of electronic motion: Application to NaI *J. Chem. Phys.* **109**, 4335 (1998).

[25] R. F. W Bader, T. A. Keith, K. M. Gough and K. E. Laidig Properties of atoms in molecules: additivity and transferability of group polarizabilities *Mol. Phys.* **75**, 1167 (1991).

[26] R. J. Boyd, and K. E. Edgecombe Atomic and group electronegativities from the electron-density distributions of molecules *J. Am. Chem. Soc.* **110**, 4182 (1988).

[27] P. L. A. Popelier On the full topology of the Laplacian of the electron density *Coord. Chem. Rev.* **197**, 169 (2000).

[28] K. Karka, and D. Cramer, Theorectical Models of Chemical Bonding Part 2, The Concept of the Chemical Bond *Ed. Z. B. Maksic, Springer*, New York (1990).

[29] R. F. W. Bader, T. S. Slee, D. Cremer,and E. Kraka Description of conjugation and hyperconjugation in terms of electron distributions *J. Am. Chem. Soc.* **105**, 5016 (1983).

[30] D. Cremer, and E. Kraka A Description of the Chemical Bond in Terms of Local Properties of Electron Density and Energy *Croatica Chem. Acta* **57**, 1259 (1984).

[31] R. G. Parr, and W. Yang *Density Functional Theory of Atoms and Molecules*, Clarendon Press, Oxford, (1989).

[32] K. Collard, and G. G. Hall Orthogonal trajectories of electron density *Int. J. Quantum Chem.* **12**, 623 (1977).

[33] R. F. W. Bader, T. T. Nguyen-Dang, and Y. Tal Quantum topology of molecular charge distributions. II. Molecular structure and its change *J. Chem. Phys.* **70**, 4316 (1979).

[34] C. Gatti, P. Fantucci, and G. Pacchioni, Charge Density Topological Study of Bonding in Lithium Clusters, *Theor. Chim. Acta* **72**, 433 (1987).

[35] W. L. Cao, C. Gatti, P. J. MacDougall, and R. F. W. Bader, On the Presence of Non-Nuclear Attractors in the Charge Distributions of Li and Na Clusters, *Chem. Phys. Lett* **141**, 380 (1987).

[36] C. J. Mei, and K. E. Edgecombe, Topological Analysis of the Charge Density of Solids: BCC Sodium and Lithium, *Int. J. Quantum Chem.* **48**, 287 (1993).

[37] B. B. Iversen, F. K. Larsen, M. Souhasau, and M. Takata, Experimental evidence for the existence of non-nuclear maxima in the electron-density distribution of metallic beryllium. A comparative study of the maximum entropy

method and the multipole refinement method, *Acta. Crystallogr. Sect B* **51**, 580 (1995).

[38] R. Glaser, R. F. Waldron and K. B. Wiberg, Origin and Consequences of the Nonnuclear Attractor in the ab Initio Electron Density Functions of Dilithium, *J. Phys. Chem.* **94**, 7357 (1990).

[39] J. C, ioslowski, Non-nuclear attracter in the Li_2 Molecule, *J. Phys. Chem.* **94**, 5496 (1990).

[40] G. I. Bersuker, C. Peng and J. E. Boggs, The Nature of the Covalent Bond: The Existence and Origin of Nonnuclear Attractors, *J. Phys. Chem.* **97**, 9323 (1993).

[41] K. E. Edgecombe, R. O. Esquivel, and V. H. Smith, Pseudoatoms of the Electron Density, *J. Chem. Phys.* **97**, 2593 (1992).

[42] F. E. Penotti, On the Electronic Structure of Li_2 (X ^{1} Σ_g^+) and Its Changes with Internuclear Distance, *Int. J. Quantum Chem.* **78**, 378 (1999).

[43] A. M. Pendas, M. A. Blanco, A. Costales, P. M. Sanchez, and V. Luana, Non-nuclear Maxima of the Electron Density*Phys. Rev. Lett.* **83**, 1930 (1999).

[44] A. Costales, M. A. Blanco, A. M. Pendas, P. Mori-Sanchez, and V. Luana, Universal Features of the Topological Bond Properties of the Electron Density *J. Phys. Chem. A* **108**, 2794 (2004).

[45] P. Raj, and P. Balanarayan, ABELDYN: An Ab-initio Electron-Dynamics package *Manuscript to be submitted*

[46] P. Raj, Electronic Quantum Dynamics of Molecules in Strong LASER fields: Novel Algorithms and Effects, *Dotoral Dissertation* (2022)

[47] M. W. Schmidt, K. K. Baldridge, J. A. Boatz, S. T. Elbert, M. S. Gordon, J. H. Jensen, S. Koseki, N. Matsunaga, K. A. Nguyen, S. Su, T. L. Windus, M. Dupuis, and J. A. Montgomery Jr, General atomic and molecular electronic structure system *J. Comput. Chem.* **14**, 1347 (1993).

[48] J. G. Muga, J. P. Palao, B. Navarro, and I. L. Egusquiza, Complex absorbing potentials *Phys. Reports* **395**, 357 (2004).

Appendix

A1. Physical quantites in atomic units and conversion factors

The physical quantities such as distance, time, frequency often are mentioned in atomic units in the present thesis. We here provide a brief description of atomic units for these quantites.

Distance, r: The unit of distance in atomic units is provided by the defination of Bohr radius, a_0. Formally, $1 a.u. \sim 0.529 \times 10^{-11} m$. This conversion is calculated using the following form,

$$r = \frac{(4\pi\epsilon_0\hbar)}{4\pi^2 m_e e^2} \tag{4.1}$$

Here, in Eq. [4.1], m_e, and e represents the mass$(9.11 \times 10^{31} kg)$ and charge$(1.9 \times 10^{19} C)$ of electron respectively. $\hbar(6.626 \times 10^{-34} m^2 kg s^{-1})$ is the plank's constant.

Time, t: The time taken for an electron to travel a distance equivalent of 1 Bohr radius or 1 a.u. The value of atomic unit in time is equal to $2.42 \times 10^{-17} s$. It is calculated using the following form, $\frac{h^3}{8\pi^3 m_e e^4}$.

Energy, ϵ: Two times the binding energy of a Hydrogen atom is considered as one unit of energy in atomic units. One unit energy in atomic units 27.211 eV and evaluate using the form, $\frac{4\pi^2 m_e e^4}{(4\pi\epsilon_0 h)^2} = 4.36 \times 10^{-18} J$.

Frequency, ν: The frequency in atomic units is given as, $\nu = \frac{\epsilon}{h} = \frac{4\pi^2 m_e e^4}{(4\pi\epsilon_0)^2 h^3} = 4.134 \times 10^{16} Hz$.

Angular Frequency, ω**:** The angular frequency is defined as, $\omega = 2\pi\omega = \frac{8\pi^3 m_e e^4}{(4\pi\epsilon_0)^2 h^3} = 2.597 \times 10^{17} rad/s$.

Electric Field Strength, E_0**:** In atomic units, the Electric Field Strength is equivalent to $5.14 \times 10^{11} V/m$. It is evaluated using the following form, $E_0 = \frac{\epsilon}{ea_0} = \frac{4\pi^3 m_e e^3}{h^2}$.

Intensity, I: Intensity in atomic units is related to the square of electric field in vaccum. It is given by, $I = \frac{1}{2}\epsilon c E_0 = 3.51 \times 10^{16} W/cm^2$.

Quiver distance in a plane wave field, α_0**:** When an electron is subjected to one atomic unit of field intensity of any plane wave. It is given by, $\alpha_0 = \frac{E_0}{\omega^2}$.

A2. Appendix: Chapter 2

The ABELDYNPROP code is written specifically for cartesian gaussian functions. The general form of a cartesian gaussian function for a exponent α, centered around an atom $\vec{A}$ with angular indices l ($\equiv$ *l,m,n*) is given by Eq. [4.2]

$$\eta(\alpha, \vec{A}, \vec{l}) = (x - x_A)^l (y - y - A)^m (z - z_A)^n \exp[-\alpha \mid \vec{r} - \vec{A} \mid^2] \qquad (4.2)$$

The exponent α is a real and positive scalar quantity, and the vector $\vec{A}$ represent the 3D cartesian of atom A, that is, (x_A, y_A, z_A). The qunatity $|\vec{r} - \vec{A}|$ represents the distance between the two vectors and calculate as given in Eq.

$$\mid \vec{r} - \vec{A} \mid = [(x - x_A)^2 + (y - y_A)^2 + (z - z_A)^2]^{\frac{1}{2}} \qquad (4.3)$$

A2.1. Analytical expression for cartesian gaussian-type functions in position space

The following list of equations represents the **S, P, D and F-type cartesian gaussian functions**.

S-type function:

$$\Phi_S(\vec{r}) = \exp[-\alpha \mid \vec{r} - \vec{A} \mid^2] \qquad (4.4)$$

P-type function:

$$\Phi_{P_X}(\vec{r}) = (x - x_A)\exp[-\alpha \mid \vec{r} - \vec{A} \mid^2] \tag{4.5}$$

$$\Phi_{P_Y}(\vec{r}) = (y - y_A)\exp[-\alpha \mid \vec{r} - \vec{A} \mid^2] \tag{4.6}$$

$$\Phi_{P_Z}(\vec{r}) = (z - z_A)\exp[-\alpha \mid \vec{r} - \vec{A} \mid^2] \tag{4.7}$$

D-type function:

$$\Phi_{D_{XX}}(\vec{r}) = (x - x_A)^2\exp[-\alpha \mid \vec{r} - \vec{A} \mid^2] \tag{4.8}$$

$$\Phi_{D_{YY}}(\vec{r}) = (y - y_A)^2\exp[-\alpha \mid \vec{r} - \vec{A} \mid^2] \tag{4.9}$$

$$\Phi_{D_{ZZ}}(\vec{r}) = (z - z_A)^2\exp[-\alpha \mid \vec{r} - \vec{A} \mid^2] \tag{4.10}$$

$$\Phi_{D_{XY}}(\vec{r}) = (x - x_A)(y - y_A)\exp[-\alpha \mid \vec{r} - \vec{A} \mid^2] \tag{4.11}$$

$$\Phi_{D_{XZ}}(\vec{r}) = (x - x_A)(z - z_A)\exp[-\alpha \mid \vec{r} - \vec{A} \mid^2] \tag{4.12}$$

$$\Phi_{D_{YZ}}(\vec{r}) = (y - y_A)(z - z_A)\exp[-\alpha \mid \vec{r} - \vec{A} \mid^2] \tag{4.13}$$

F-type function:

$$\Phi_{F_{XXX}}(\vec{r}) = (x - x_A)^3\exp[-\alpha \mid \vec{r} - \vec{A} \mid^2] \tag{4.14}$$

$$\Phi_{F_{YYY}}(\vec{r}) = (y - y_A)^3\exp[-\alpha \mid \vec{r} - \vec{A} \mid^2] \tag{4.15}$$

$$\Phi_{F_{ZZZ}}(\vec{r}) = (z - z_A)^3\exp[-\alpha \mid \vec{r} - \vec{A} \mid^2] \tag{4.16}$$

$$\Phi_{F_{XXY}}(\vec{r}) = (x - x_A)^2(y - y_A)\exp[-\alpha \mid \vec{r} - \vec{A} \mid^2] \tag{4.17}$$

$$\Phi_{F_{XXZ}}(\vec{r}) = (x - x_A)^2(z - z_A)\exp[-\alpha \mid \vec{r} - \vec{A} \mid^2] \tag{4.18}$$

$$\Phi_{F_{YYZ}}(\vec{r}) = (y - y_A)^2(z - z_A)\exp[-\alpha \mid \vec{r} - \vec{A} \mid^2] \tag{4.19}$$

$$\Phi_{F_{XYY}}(\vec{r}) = (x - x_A)(y - y_A)^2\exp[-\alpha \mid \vec{r} - \vec{A} \mid^2] \tag{4.20}$$

$$\Phi_{F_{XZZ}}(\vec{r}) = (x - x_A)(z - z_A)^2\exp[-\alpha \mid \vec{r} - \vec{A} \mid^2] \tag{4.21}$$

$$\Phi_{F_{YZZ}}(\vec{r}) = (y - y_A)(z - z_A)^2\exp[-\alpha \mid \vec{r} - \vec{A} \mid^2] \tag{4.22}$$

$$\Phi_{F_{XYZ}}(\vec{r}) = (x - x_A)(y - y_A)(z - z_A)\exp[-\alpha \mid \vec{r} - \vec{A} \mid^2] \tag{4.23}$$

A2.2. Analytical expression for the first order cartesian gaussian-type functions

First order derivatives of the above mentioned functions are given below. **First order derivative of S-type function:**

$$\frac{\partial}{\partial x}\Phi_S(\vec{r}) = -2\alpha(x - x_A)\exp[-\alpha \mid \vec{r} - \vec{A} \mid^2] \tag{4.24}$$

$$\frac{\partial}{\partial y}\Phi_S(\vec{r}) = -2\alpha(y - y_A)\exp[-\alpha \mid \vec{r} - \vec{A} \mid^2] \tag{4.25}$$

$$\frac{\partial}{\partial z}\Phi_S(\vec{r}) = -2\alpha(z - z_A)\exp[-\alpha \mid \vec{r} - \vec{A} \mid^2] \tag{4.26}$$

First order derivative of P_X function:

$$\frac{\partial}{\partial x}\Phi_{P_X}(\vec{r}) = [1-2\alpha(x-x_A)^2]\exp[-\alpha \mid \vec{r}-\vec{A}\mid^2] \tag{4.27}$$

$$\frac{\partial}{\partial y}\Phi_{P_X}(\vec{r}) = -2\alpha(y-y_A)(x-x_A)\exp[-\alpha \mid \vec{r}-\vec{A}\mid^2] \tag{4.28}$$

$$\frac{\partial}{\partial z}\Phi_{P_X}(\vec{r}) = -2\alpha(z-z_A)(x-x_A)\exp[-\alpha \mid \vec{r}-\vec{A}\mid^2] \tag{4.29}$$

First order derivative of P_Y function:

$$\frac{\partial}{\partial x}\Phi_{P_Y}(\vec{r}) = -2\alpha(x-x_A)(y-y_A)\exp[-\alpha \mid \vec{r}-\vec{A}\mid^2] \tag{4.30}$$

$$\frac{\partial}{\partial y}\Phi_{P_Y}(\vec{r}) = [1-2\alpha(y-y_A)^2]\exp[-\alpha \mid \vec{r}-\vec{A}\mid^2] \tag{4.31}$$

$$\frac{\partial}{\partial z}\Phi_{P_Y}(\vec{r}) = -2\alpha(z-z_A)(y-y_A)\exp[-\alpha \mid \vec{r}-\vec{A}\mid^2] \tag{4.32}$$

First order derivative of P_Z function:

$$\frac{\partial}{\partial x}\Phi_{P_Z}(\vec{r}) = -2\alpha(x-x_A)(z-z_A)\exp[-\alpha \mid \vec{r}-\vec{A}\mid^2] \tag{4.33}$$

$$\frac{\partial}{\partial y}\Phi_{P_Z}(\vec{r}) = -2\alpha(y-y_A)(z-z_A)\exp[-\alpha \mid \vec{r}-\vec{A}\mid^2] \tag{4.34}$$

$$\frac{\partial}{\partial z}\Phi_{P_Z}(\vec{r}) = [1-2\alpha(z-z_A)^2]\exp[-\alpha \mid \vec{r}-\vec{A}\mid^2] \tag{4.35}$$

First order derivative of D_{XX} function:

$$\frac{\partial}{\partial x}\Phi_{D_{XX}}(\vec{r}) = [2-2\alpha(x-x_A)^2](x-x_A)exp[-\alpha \mid \vec{r}-\vec{A}\mid^2] \tag{4.36}$$

$$\frac{\partial}{\partial y}\Phi_{D_{XX}}(\vec{r}) = -2\alpha(y-y_A)(x-x_A)^2 exp[-\alpha \mid \vec{r}-\vec{A}\mid^2] \tag{4.37}$$

$$\frac{\partial}{\partial z}\Phi_{D_{XX}}(\vec{r}) = -2\alpha(z-z_A)(x-x_A)^2 exp[-\alpha \mid \vec{r}-\vec{A} \mid^2] \tag{4.38}$$

First order derivative of D_{YY} function:

$$\frac{\partial}{\partial x}\Phi_{D_{YY}}(\vec{r}) = -2\alpha(x-x_A)(y-y_A)^2 exp[-\alpha \mid \vec{r}-\vec{A} \mid^2] \tag{4.39}$$

$$\frac{\partial}{\partial y}\Phi_{D_{YY}}(\vec{r}) = [2-2\alpha(y-y_A)^2](y-y_A) exp[-\alpha \mid \vec{r}-\vec{A} \mid^2] \tag{4.40}$$

$$\frac{\partial}{\partial z}\Phi_{D_{YY}}(\vec{r}) = -2\alpha(z-z_A)(y-y_A)^2 exp[-\alpha \mid \vec{r}-\vec{A} \mid^2] \tag{4.41}$$

First order derivative of D_{ZZ} function:

$$\frac{\partial}{\partial x}\Phi_{D_{ZZ}}(\vec{r}) = -2\alpha(x-x_A)(z-z_A)^2 exp[-\alpha \mid \vec{r}-\vec{A} \mid^2] \tag{4.42}$$

$$\frac{\partial}{\partial y}\Phi_{D_{ZZ}}(\vec{r}) = -2\alpha(y-y_A)(z-z_A)^2 exp[-\alpha \mid \vec{r}-\vec{A} \mid^2] \tag{4.43}$$

$$\frac{\partial}{\partial z}\Phi_{D_{ZZ}}(\vec{r}) = [2-2\alpha(z-z_A)^2](z-z_A) exp[-\alpha \mid \vec{r}-\vec{A} \mid^2] \tag{4.44}$$

First order derivative of D_{XY} function:

$$\frac{\partial}{\partial x}\Phi_{D_{XY}}(\vec{r}) = [1-2\alpha(x-x_A)^2](y-y_A) \exp[-\alpha \mid \vec{r}-\vec{A} \mid^2] \tag{4.45}$$

$$\frac{\partial}{\partial y}\Phi_{D_{XY}}(\vec{r}) = [1-2\alpha(y-y_A)^2](x-x_A) \exp[-\alpha \mid \vec{r}-\vec{A} \mid^2] \tag{4.46}$$

$$\frac{\partial}{\partial z}\Phi_{D_{XY}}(\vec{r}) = -2\alpha(z-z_A)(x-x_A)(y-y_A) \exp[-\alpha \mid \vec{r}-\vec{A} \mid^2] \tag{4.47}$$

First order derivative of D_{XZ} function:

$$\frac{\partial}{\partial x}\Phi_{D_{XZ}}(\vec{r}) = [1-2\alpha(x-x_A)^2](z-z_A) \exp[-\alpha \mid \vec{r}-\vec{A} \mid^2] \tag{4.48}$$

$$\frac{\partial}{\partial y}\Phi_{D_{XZ}}(\vec{r}) = -2\alpha(y-y_A)(x-x_A)(z-z_A)\exp[-\alpha \mid \vec{r}-\vec{A}\mid^2] \tag{4.49}$$

$$\frac{\partial}{\partial z}\Phi_{D_{XZ}}(\vec{r}) = [1-2\alpha(z-z_A)^2](x-x_A)\exp[-\alpha \mid \vec{r}-\vec{A}\mid^2] \tag{4.50}$$

First order derivative of D_{YZ} function:

$$\frac{\partial}{\partial x}\Phi_{D_{YZ}}(\vec{r}) = -2\alpha(x-x_A)(y-y_A)(z-z_A)\exp[-\alpha \mid \vec{r}-\vec{A}\mid^2] \tag{4.51}$$

$$\frac{\partial}{\partial y}\Phi_{D_{YZ}}(\vec{r}) = [1-2\alpha(y-y_A)^2](z-z_A)\exp[-\alpha \mid \vec{r}-\vec{A}\mid^2] \tag{4.52}$$

$$\frac{\partial}{\partial z}\Phi_{D_{YZ}}(\vec{r}) = [1-2\alpha(z-z_A)^2](y-y_A)\exp[-\alpha \mid \vec{r}-\vec{A}\mid^2] \tag{4.53}$$

First order derivative of F_{XXX} function:

$$\frac{\partial}{\partial x}\Phi_{F_{XXX}}(\vec{r}) = [3-2\alpha(x-x_A)^2](x-x_A)^2\exp[-\alpha \mid \vec{r}-\vec{A}\mid^2] \tag{4.54}$$

$$\frac{\partial}{\partial y}\Phi_{F_{XXX}}(\vec{r}) = -2\alpha(y-y_A)(x-x_A)^3\exp[-\alpha \mid \vec{r}-\vec{A}\mid^2] \tag{4.55}$$

$$\frac{\partial}{\partial z}\Phi_{F_{XXX}}(\vec{r}) = -2\alpha(z-z_A)(x-x_A)^3\exp[-\alpha \mid \vec{r}-\vec{A}\mid^2] \tag{4.56}$$

First order derivative of F_{YYY} function:

$$\frac{\partial}{\partial x}\Phi_{F_{YYY}}(\vec{r}) = -2\alpha(x-x_A)(y-y_A)^3\exp[-\alpha \mid \vec{r}-\vec{A}\mid^2] \tag{4.57}$$

$$\frac{\partial}{\partial y}\Phi_{F_{YYY}}(\vec{r}) = [3-2\alpha(y-y_A)^2](y-y_A)^2\exp[-\alpha \mid \vec{r}-\vec{A}\mid^2] \tag{4.58}$$

$$\frac{\partial}{\partial z}\Phi_{F_{YYY}}(\vec{r}) = -2\alpha(z-z_A)(y-y_A)^3\exp[-\alpha \mid \vec{r}-\vec{A}\mid^2] \tag{4.59}$$

First order derivative of F_{ZZZ} function:

$$\frac{\partial}{\partial x}\Phi_{F_{ZZZ}}(\vec{r}) = -2\alpha(x-x_A)(z-z_A)^3 \exp[-\alpha \mid \vec{r}-\vec{A}\mid^2] \tag{4.60}$$

$$\frac{\partial}{\partial y}\Phi_{F_{ZZZ}}(\vec{r}) = -2\alpha(y-y_A)(z-z_A)^3 \exp[-\alpha \mid \vec{r}-\vec{A}\mid^2] \tag{4.61}$$

$$\frac{\partial}{\partial z}\Phi_{F_{ZZZ}}(\vec{r}) = [3-2\alpha(z-z_A)^2](z-z_A)^2 \exp[-\alpha \mid \vec{r}-\vec{A}\mid^2] \tag{4.62}$$

First order derivative of F_{XXY} function:

$$\frac{\partial}{\partial x}\Phi_{F_{XXY}}(\vec{r}) = [2-2\alpha(x-x_A)^2](x-x_A)(y-y_A) \exp[-\alpha \mid \vec{r}-\vec{A}\mid^2] \tag{4.63}$$

$$\frac{\partial}{\partial y}\Phi_{F_{XXY}}(\vec{r}) = [1-2\alpha(y-y_A)^2](x-x_A)^2 \exp[-\alpha \mid \vec{r}-\vec{A}\mid^2] \tag{4.64}$$

$$\frac{\partial}{\partial z}\Phi_{F_{XXY}}(\vec{r}) = -2\alpha(z-z_A)(x-x_A)^2(y-y_A) \exp[-\alpha \mid \vec{r}-\vec{A}\mid^2] \tag{4.65}$$

First order derivative of F_{XXZ} function:

$$\frac{\partial}{\partial x}\Phi_{F_{XXZ}}(\vec{r}) = [2-2\alpha(x-x_A)^2](x-x_A)(z-z_A) \exp[-\alpha \mid \vec{r}-\vec{A}\mid^2] \tag{4.66}$$

$$\frac{\partial}{\partial y}\Phi_{F_{XXZ}}(\vec{r}) = -2\alpha(y-y_A)(x-x_A)^2(z-z_A) \exp[-\alpha \mid \vec{r}-\vec{A}\mid^2] \tag{4.67}$$

$$\frac{\partial}{\partial z}\Phi_{F_{XXZ}}(\vec{r}) = [1-2\alpha(z-z_A)^2](x-x_A)^2 \exp[-\alpha \mid \vec{r}-\vec{A}\mid^2] \tag{4.68}$$

First order derivative of F_{YYZ} function:

$$\frac{\partial}{\partial x}\Phi_{F_{YYZ}}(\vec{r}) = -2\alpha(x-x_A)(y-y_A)^2(z-z_A) \exp[-\alpha \mid \vec{r}-\vec{A}\mid^2] \tag{4.69}$$

$$\frac{\partial}{\partial y}\Phi_{F_{YYZ}}(\vec{r}) = [2 - 2\alpha(y - y_A)^2](y - y_A)(z - z_A)\exp[-\alpha \mid \vec{r} - \vec{A} \mid^2] \tag{4.70}$$

$$\frac{\partial}{\partial z}\Phi_{F_{YYZ}}(\vec{r}) = [1 - 2\alpha(z - z_A)^2](y - y_A)^2\exp[-\alpha \mid \vec{r} - \vec{A} \mid^2] \tag{4.71}$$

First order derivative of F_{XYY} function:

$$\frac{\partial}{\partial x}\Phi_{F_{XYY}}(\vec{r}) = [1 - 2\alpha(x - x_A)^2](y - y_A)^2\exp[-\alpha \mid \vec{r} - \vec{A} \mid^2] \tag{4.72}$$

$$\frac{\partial}{\partial y}\Phi_{F_{XYY}}(\vec{r}) = [2 - 2\alpha(y - y_A)^2](y - y_A)(x - x_A)\exp[-\alpha \mid \vec{r} - \vec{A} \mid^2] \tag{4.73}$$

$$\frac{\partial}{\partial z}\Phi_{F_{XYY}}(\vec{r}) = -2\alpha(z - z_A)(y - y_A)^2(x - x_A)\exp[-\alpha \mid \vec{r} - \vec{A} \mid^2] \tag{4.74}$$

First order derivative of F_{XZZ} function:

$$\frac{\partial}{\partial x}\Phi_{F_{XZZ}}(\vec{r}) = [1 - 2\alpha(x - x_a)^2](z - z_A)^2\exp[-\alpha \mid \vec{r} - \vec{A} \mid^2] \tag{4.75}$$

$$\frac{\partial}{\partial y}\Phi_{F_{XZZ}}(\vec{r}) = -2\alpha(y - y_A)(z - z_A)^2(x - x_A)\exp[-\alpha \mid \vec{r} - \vec{A} \mid^2] \tag{4.76}$$

$$\frac{\partial}{\partial z}\Phi_{F_{XZZ}}(\vec{r}) = [2 - 2\alpha(z - z_A)^2](z - z_A)(x - x_A)\exp[-\alpha \mid \vec{r} - \vec{A} \mid^2] \tag{4.77}$$

First order derivative of F_{YZZ} function:

$$\frac{\partial}{\partial x}\Phi_{F_{YZZ}}(\vec{r}) = -2\alpha(x - x_A)(z - z_A)^2(y - y_A)\exp[-\alpha \mid \vec{r} - \vec{A} \mid^2] \tag{4.78}$$

$$\frac{\partial}{\partial y}\Phi_{F_{YZZ}}(\vec{r}) = [1 - 2\alpha(y - y_A)^2](z - z_A)^2\exp[-\alpha \mid \vec{r} - \vec{A} \mid^2] \tag{4.79}$$

$$\frac{\partial}{\partial z}\Phi_{F_{YZZ}}(\vec{r}) = [2 - 2\alpha(z - z_A)^2](z - z_A)(y - y_A)\exp[-\alpha \mid \vec{r} - \vec{A} \mid^2] \tag{4.80}$$

First order derivative of F_{XYZ} function:

$$\frac{\partial}{\partial x}\Phi_{F_{XYZ}}(\vec{r}) = [1 - 2\alpha(x - x_A)^2](y - y_A)(z - z_A)\exp[-\alpha \mid \vec{r} - \vec{A} \mid^2] \tag{4.81}$$

$$\frac{\partial}{\partial y}\Phi_{F_{XYZ}}(\vec{r}) = [1 - 2\alpha(y - y_A)^2](x - x_A)(z - z_A)\exp[-\alpha \mid \vec{r} - \vec{A} \mid^2] \tag{4.82}$$

$$\frac{\partial}{\partial z}\Phi_{F_{XYZ}}(\vec{r}) = [1 - 2\alpha(z - z_A)^2](x - x_A)(y - y_A)\exp[-\alpha \mid \vec{r} - \vec{A} \mid^2] \tag{4.83}$$

A2.3. Analytical expression for the second order cartesian gaussian-type functions

Second order derivatives of functions mentioned in subsection 4.4 are given below.

Second order derivative of S-type function:

$$\frac{\partial^2}{\partial x^2}\Phi_S(\vec{r}) = [1 - 2\alpha(x - x_A)^2](-2\alpha)\exp[-\alpha \mid \vec{r} - \vec{A} \mid^2] \tag{4.84}$$

$$\frac{\partial^2}{\partial y^2}\Phi_S(\vec{r}) = [1 - 2\alpha(y - y_A)^2](-2\alpha)\exp[-\alpha \mid \vec{r} - \vec{A} \mid^2] \tag{4.85}$$

$$\frac{\partial^2}{\partial z^2}\Phi_S(\vec{r}) = [1 - 2\alpha(z - z_A)^2](-2\alpha)\exp[-\alpha \mid \vec{r} - \vec{A} \mid^2] \tag{4.86}$$

$$\frac{\partial^2}{\partial x \partial y}\Phi_S(\vec{r}) = 4\alpha^2(x - x_A)(y - y_A)\exp[-\alpha \mid \vec{r} - \vec{A} \mid^2] \tag{4.87}$$

$$\frac{\partial^2}{\partial x \partial z}\Phi_S(\vec{r}) = 4\alpha^2(x - x_A)(z - z_A)\exp[-\alpha \mid \vec{r} - \vec{A} \mid^2] \tag{4.88}$$

$$\frac{\partial^2}{\partial y \partial z}\Phi_S(\vec{r}) = 4\alpha^2(y - y_A)(z - z_A)\exp[-\alpha \mid \vec{r} - \vec{A} \mid^2] \tag{4.89}$$

Second order derivative of P_X function:

$$\frac{\partial^2}{\partial x^2}\Phi_{P_X}(\vec{r}) = [3 - 2\alpha(x - x_A)^2](-2\alpha)(x - x_a)\exp[-\alpha \mid \vec{r} - \vec{A} \mid^2] \tag{4.90}$$

$$\frac{\partial^2}{\partial y^2}\Phi_{P_X}(\vec{r}) = [1 - 2\alpha(y - y_A)^2](-2\alpha)(x - x_A)\exp[-\alpha \mid \vec{r} - \vec{A} \mid^2] \tag{4.91}$$

$$\frac{\partial^2}{\partial z^2}\Phi_{P_X}(\vec{r}) = [1 - 2\alpha(z - z_A)^2](-2\alpha)(x - x_A)\exp[-\alpha \mid \vec{r} - \vec{A} \mid^2] \tag{4.92}$$

$$\frac{\partial^2}{\partial x \partial y}\Phi_{P_X}(\vec{r}) = [-2\alpha(y - y_A)][1 - 2\alpha(x - x_A)^2]\exp[-\alpha \mid \vec{r} - \vec{A} \mid^2] \tag{4.93}$$

$$\frac{\partial^2}{\partial x \partial z}\Phi_{P_X}(\vec{r}) = [-2\alpha(z - z_A)][1 - 2\alpha(x - x_A)^2]\exp[-\alpha \mid \vec{r} - \vec{A} \mid^2] \tag{4.94}$$

$$\frac{\partial^2}{\partial y \partial z}\Phi_{P_X}(\vec{r}) = 4\alpha^2(z - z_A)(y - y_A)(x - x_A)\exp[-\alpha \mid \vec{r} - \vec{A} \mid^2] \tag{4.95}$$

Second order derivative of P_Y function:

$$\frac{\partial^2}{\partial x^2}\Phi_{P_Y}(\vec{r}) = [1 - 2\alpha(x - x_A)^2](-2\alpha)(y - y_A)\exp[-\alpha \mid \vec{r} - \vec{A} \mid^2] \tag{4.96}$$

$$\frac{\partial^2}{\partial y^2}\Phi_{P_Y}(\vec{r}) = [3 - 2\alpha(y - y_A)^2](-2\alpha)(y - y_A)\exp[-\alpha \mid \vec{r} - \vec{A} \mid^2] \tag{4.97}$$

$$\frac{\partial^2}{\partial z^2}\Phi_{P_Y}(\vec{r}) = [1 - 2\alpha(z - z_A)^2](-2\alpha)(y - y_A)\exp[-\alpha \mid \vec{r} - \vec{A} \mid^2] \tag{4.98}$$

$$\frac{\partial^2}{\partial x \partial y}\Phi_{P_Y}(\vec{r}) = [-2\alpha(x-x_A)][1-2\alpha(y-y_A)^2]\exp[-\alpha \mid \vec{r}-\vec{A} \mid^2] \tag{4.99}$$

$$\frac{\partial^2}{\partial x \partial z}\Phi_{P_Y}(\vec{r}) = 4\alpha^2(z-z_A)(y-y_A)(x-x_A)\exp[-\alpha \mid \vec{r}-\vec{A} \mid^2] \tag{4.100}$$

$$\frac{\partial^2}{\partial y \partial z}\Phi_{P_Y}(\vec{r}) = [-2\alpha(z-z_A)][1-2\alpha(y-y_A)^2]\exp[-\alpha \mid \vec{r}-\vec{A} \mid^2] \tag{4.101}$$

Second order derivative of P_Z function:

$$\frac{\partial^2}{\partial x^2}\Phi_{P_Z}(\vec{r}) = [1-2\alpha(x-x_A)^2](-2\alpha)(z-z_A)\exp[-\alpha \mid \vec{r}-\vec{A} \mid^2] \tag{4.102}$$

$$\frac{\partial^2}{\partial y^2}\Phi_{P_Z}(\vec{r}) = [1-2\alpha(y-y_A)^2](-2\alpha)(z-z_A)\exp[-\alpha \mid \vec{r}-\vec{A} \mid^2] \tag{4.103}$$

$$\frac{\partial^2}{\partial z^2}\Phi_{P_Z}(\vec{r}) = [3-2\alpha(z-z_A)^2](-2\alpha)[z-z_A]\exp[-\alpha \mid \vec{r}-\vec{A} \mid^2] \tag{4.104}$$

$$\frac{\partial^2}{\partial x \partial y}\Phi_{P_Z}(\vec{r}) = 4\alpha^2(y-y_A)(x-x_A)(z-z_A) \mid \exp[-\alpha \mid \vec{r}-\vec{A} \mid^2] \tag{4.105}$$

$$\frac{\partial^2}{\partial x \partial z}\Phi_{P_Z}(\vec{r}) = [-2\alpha(x-x_A)][1-2\alpha(z-z_A)^2]\exp[-\alpha \mid \vec{r}-\vec{A} \mid^2] \tag{4.106}$$

$$\frac{\partial^2}{\partial y \partial z}\Phi_{P_Z}(\vec{r}) = [-2\alpha(y-y_A)][1-2\alpha(z-z_A)^2]\exp[-\alpha \mid \vec{r}-\vec{A} \mid^2] \tag{4.107}$$

Second order derivative of D_{XX} function:

$$\frac{\partial^2}{\partial x^2}\Phi_{D_{XX}}(\vec{r}) = [4\alpha^2(x-x_A)^4-10\alpha(x-x_A)^2+2]\exp[-\alpha \mid \vec{r}-\vec{A} \mid^2] \tag{4.108}$$

$$\frac{\partial^2}{\partial y^2}\Phi_{D_{XX}}(\vec{r}) = [1-2\alpha(y-y_A)^2](-2\alpha)(x-x_A)^2\exp[-\alpha \mid \vec{r}-\vec{A} \mid^2] \tag{4.109}$$

$$\frac{\partial^2}{\partial z^2}\Phi_{D_{XX}}(\vec{r}) = [1 - 2\alpha(z - z_A)^2](-2\alpha)(x - x_A)^2 \exp[-\alpha \mid \vec{r} - \vec{A} \mid^2] \quad (4.110)$$

$$\frac{\partial^2}{\partial x \partial y}\Phi_{D_{XX}}(\vec{r}) = [-2\alpha(y - y_A)][2 - 2\alpha(x - x_A)^2](x - x_A) \exp[-\alpha \mid \vec{r} - \vec{A} \mid^2] \quad (4.111)$$

$$\frac{\partial^2}{\partial x \partial z}\Phi_{D_{XX}}(\vec{r}) = [-2\alpha(z - z_A)][2 - 2\alpha(x - x_A)^2](x - x_A) \exp[-\alpha \mid \vec{r} - \vec{A} \mid^2] \quad (4.112)$$

$$\frac{\partial^2}{\partial y \partial z}\Phi_{D_{XX}}(\vec{r}) = 4\alpha^2(z - z_A)(y - y_A)(x - x_A)^2 \exp[-\alpha \mid \vec{r} - \vec{A} \mid^2] \quad (4.113)$$

Second order derivative of D_{YY} function:

$$\frac{\partial^2}{\partial x^2}\Phi_{D_{YY}}(\vec{r}) = [1 - 2\alpha(x - x_A)^2](-2\alpha)(y - y_A)^2 \exp[-\alpha \mid \vec{r} - \vec{A} \mid^2] \quad (4.114)$$

$$\frac{\partial^2}{\partial y^2}\Phi_{D_{YY}}(\vec{r}) = [4\alpha^2(y - y_A)^4 - 10\alpha(y - y_a)^2 + 2] \exp[-\alpha \mid \vec{r} - \vec{A} \mid^2] \quad (4.115)$$

$$\frac{\partial^2}{\partial z^2}\Phi_{D_{YY}}(\vec{r}) = [1 - 2\alpha(z - z_A)^2](-2\alpha)(y - y_A)^2 \exp[-\alpha \mid \vec{r} - \vec{A} \mid^2] \quad (4.116)$$

$$\frac{\partial^2}{\partial x \partial y}\Phi_{D_{YY}}(\vec{r}) = [-2\alpha(x - x_A)][2 - 2\alpha(y - y_A)^2](y - y_A) \exp[-\alpha \mid \vec{r} - \vec{A} \mid^2] \quad (4.117)$$

$$\frac{\partial^2}{\partial x \partial z}\Phi_{D_{YY}}(\vec{r}) = 4\alpha^2(z - z_A)(x - x_A)(y - y_A)^2 \exp[-\alpha \mid \vec{r} - \vec{A} \mid^2] \quad (4.118)$$

$$\frac{\partial^2}{\partial y \partial z}\Phi_{D_{YY}}(\vec{r}) = [-2\alpha(z-z_A)][2-2\alpha(y-y_A)^2](y-y_A)\exp[-\alpha \mid \vec{r}-\vec{A}\mid^2] \quad (4.119)$$

Second order derivative of D_{ZZ} function:

$$\frac{\partial^2}{\partial x^2}\Phi_{D_{ZZ}}(\vec{r}) = [1-2\alpha(x-x_A)^2](-2\alpha)(z-z_A)^2\exp[-\alpha \mid \vec{r}-\vec{A}\mid^2] \quad (4.120)$$

$$\frac{\partial^2}{\partial y^2}\Phi_{D_{ZZ}}(\vec{r}) = [1-2\alpha(y-y_A)^2](-2\alpha)(z-z_A)^2\exp[-\alpha \mid \vec{r}-\vec{A}\mid^2] \quad (4.121)$$

$$\frac{\partial^2}{\partial z^2}\Phi_{D_{ZZ}}(\vec{r}) = [4\alpha^2(z-z_A)^4-10\alpha(z-z_A)^2+2]\exp[-\alpha \mid \vec{r}-\vec{A}\mid^2] \quad (4.122)$$

$$\frac{\partial^2}{\partial x \partial y}\Phi_{D_{ZZ}}(\vec{r}) = 4\alpha^2(y-y_A)(x-x_A)(z-z_A)^2\exp[-\alpha \mid \vec{r}-\vec{A}\mid^2] \quad (4.123)$$

$$\frac{\partial^2}{\partial x \partial z}\Phi_{D_{ZZ}}(\vec{r}) = [-2\alpha(x-x_A)][2-2\alpha(z-z_A)^2](z-z_A)\exp[-\alpha \mid \vec{r}-\vec{A}\mid^2] \quad (4.124)$$

$$\frac{\partial^2}{\partial y \partial z}\Phi_{D_{ZZ}}(\vec{r}) = [-2\alpha(y-y_A)][2-2\alpha(z-z_A)^2](z-z_A)\exp[-\alpha \mid \vec{r}-\vec{A}\mid^2] \quad (4.125)$$

Second order derivative of D_{XY} function:

$$\frac{\partial^2}{\partial x^2}\Phi_{D_{XY}}(\vec{r}) = [3-2\alpha(x-x_A)^2](-2\alpha)(x-x_A)(y-y_A)\exp[-\alpha \mid \vec{r}-\vec{A}\mid^2] \quad (4.126)$$

$$\frac{\partial^2}{\partial y^2}\Phi_{D_{XY}}(\vec{r}) = [3-2\alpha(y-y_A)^2](-2\alpha)(x-x_A)(y-y_A)\exp[-\alpha \mid \vec{r}-\vec{A}\mid^2] \quad (4.127)$$

$$\frac{\partial^2}{\partial z^2}\Phi_{D_{XY}}(\vec{r}) = [1-2\alpha(z-z_A)^2](-2\alpha)(x-x_A)(y-y_A)\exp[-\alpha \mid \vec{r}-\vec{A} \mid^2] \quad (4.128)$$

$$\frac{\partial^2}{\partial x\partial y}\Phi_{D_{XY}}(\vec{r}) = [1-2\alpha(x-x_A)^2][1-2\alpha(y-y_A)^2]\exp[-\alpha \mid \vec{r}-\vec{A} \mid^2] \quad (4.129)$$

$$\frac{\partial^2}{\partial x\partial z}\Phi_{D_{XY}}(\vec{r}) = [-2\alpha(z-z_A)][1-2\alpha(x-x_A)^2](y-y_A)\exp[-\alpha \mid \vec{r}-\vec{A} \mid^2] \quad (4.130)$$

$$\frac{\partial^2}{\partial y\partial z}\Phi_{D_{XY}}(\vec{r}) = [-2\alpha(z-z_A)][1-2\alpha(y-y_A)^2](x-x_A)\exp[-\alpha \mid \vec{r}-\vec{A} \mid^2] \quad (4.131)$$

Second order derivative of D_{XZ} function:

$$\frac{\partial^2}{\partial x^2}\Phi_{D_{XZ}}(\vec{r}) = [3-2\alpha(x-x_A)^2](-2\alpha)(x-x_A)(z-z_A)\exp[-\alpha \mid \vec{r}-\vec{A} \mid^2] \quad (4.132)$$

$$\frac{\partial^2}{\partial y^2}\Phi_{D_{XZ}}(\vec{r}) = [1-2\alpha(y-y_A)^2](-2\alpha)(x-x_A)(z-z_A)\exp[-\alpha \mid \vec{r}-\vec{A} \mid^2] \quad (4.133)$$

$$\frac{\partial^2}{\partial z^2}\Phi_{D_{XZ}}(\vec{r}) = [3-2\alpha(z-z_A)^2](-2\alpha)(x-x_A)(z-z_A)\exp[-\alpha \mid \vec{r}-\vec{A} \mid^2] \quad (4.134)$$

$$\frac{\partial^2}{\partial x\partial y}\Phi_{D_{XZ}}(\vec{r}) = [-2\alpha(y-y_A)][1-2\alpha(x-x_A)^2](z-z_A)\exp[-\alpha \mid \vec{r}-\vec{A} \mid^2] \quad (4.135)$$

$$\frac{\partial^2}{\partial x \partial z}\Phi_{D_{XZ}}(\vec{r}) = [1 - 2\alpha(x - x_A)^2][1 - 2\alpha(z - z_A)^2] \exp[-\alpha \mid \vec{r} - \vec{A} \mid^2] \quad (4.136)$$

$$\frac{\partial^2}{\partial y \partial z}\Phi_{D_{XZ}}(\vec{r}) = [-2\alpha(y - y_A)][1 - 2\alpha(z - z_A)^2](x - x_A) \exp[-\alpha \mid \vec{r} - \vec{A} \mid^2] \quad (4.137)$$

Second order derivative of D_{YZ} function:

$$\frac{\partial^2}{\partial x^2}\Phi_{D_{YZ}}(\vec{r}) = [1 - 2\alpha(x - x_A)^2](-2\alpha)(y - y_A)(z - z_A) \exp[-\alpha \mid \vec{r} - \vec{A} \mid^2] \quad (4.138)$$

$$\frac{\partial^2}{\partial y^2}\Phi_{D_{YZ}}(\vec{r}) = [3 - 2\alpha(y - y_A)^2](-2\alpha)(y - y_A)(z - z_A) \exp[-\alpha \mid \vec{r} - \vec{A} \mid^2] \quad (4.139)$$

$$\frac{\partial^2}{\partial z^2}\Phi_{D_{YZ}}(\vec{r}) = [3 - 2\alpha(z - z_A)^2](-2\alpha)(y - y_A)(z - z_A) \exp[-\alpha \mid \vec{r} - \vec{A} \mid^2] \quad (4.140)$$

$$\frac{\partial^2}{\partial x \partial y}\Phi_{D_{YZ}}(\vec{r}) = [-2\alpha(x - x_A)][1 - 2\alpha(y - y_A)^2](z - z_A) \exp[-\alpha \mid \vec{r} - \vec{A} \mid^2] \quad (4.141)$$

$$\frac{\partial^2}{\partial x \partial z}\Phi_{D_{YZ}}(\vec{r}) = [-2\alpha(x - x_A)][1 - 2\alpha(z - z_A)^2](y - y_A) \exp[-\alpha \mid \vec{r} - \vec{A} \mid^2] \quad (4.142)$$

$$\frac{\partial^2}{\partial y \partial z}\Phi_{D_{YZ}}(\vec{r}) = [1 - 2\alpha(y - y_A)^2][1 - 2\alpha(z - z_A)^2] \exp[-\alpha \mid \vec{r} - \vec{A} \mid^2] \quad (4.143)$$

Second order derivative of F_{XXX} function:

$$\frac{\partial^2}{\partial x^2}\Phi_{F_{XXX}}(\vec{r}) = [6-14\alpha(x-x_A)^2+4\alpha^2(x-x_A)^4](x-x_A)\exp[-\alpha\mid\vec{r}-\vec{A}\mid^2] \tag{4.144}$$

$$\frac{\partial^2}{\partial y^2}\Phi_{F_{XXX}}(\vec{r}) = [1-2\alpha(y-y_A)^2](-2\alpha)(x-x_A)^3\exp[-\alpha\mid\vec{r}-\vec{A}\mid^2] \tag{4.145}$$

$$\frac{\partial^2}{\partial z^2}\Phi_{F_{XXX}}(\vec{r}) = [1-2\alpha(z-z_A)^2](-2\alpha)(x-x_A)^3\exp[-\alpha\mid\vec{r}-\vec{A}\mid^2] \tag{4.146}$$

$$\frac{\partial^2}{\partial x\partial y}\Phi_{F_{XXX}}(\vec{r}) = [-2\alpha(y-y_A)][3-2\alpha(x-x_A)^2](x-x_A)^2\exp[-\alpha\mid\vec{r}-\vec{A}\mid^2] \tag{4.147}$$

$$\frac{\partial^2}{\partial x\partial z}\Phi_{F_{XXX}}(\vec{r}) = [-2\alpha(z-z_A)][3-2\alpha(x-x_A)^2](x-x_A)^2\exp[-\alpha\mid\vec{r}-\vec{A}\mid^2] \tag{4.148}$$

$$\frac{\partial^2}{\partial y\partial z}\Phi_{F_{XXX}}(\vec{r}) = 4\alpha^2(z-z_A)(y-y_A)(x-x_A)^3\exp[-\alpha\mid\vec{r}-\vec{A}\mid^2] \tag{4.149}$$

Second order derivative of F_{YYY} function:

$$\frac{\partial^2}{\partial x^2}\Phi_{F_{YYY}}(\vec{r}) = [1-2\alpha(x-x_a)^2](-2\alpha)(y-y_A)^3\exp[-\alpha\mid\vec{r}-\vec{A}\mid^2] \tag{4.150}$$

$$\frac{\partial^2}{\partial y^2}\Phi_{F_{YYY}}(\vec{r}) = [6-14\alpha(y-y_A)^2+4\alpha^2(y-y_A)^4](y-y_A)\exp[-\alpha\mid\vec{r}-\vec{A}\mid^2] \tag{4.151}$$

$$\frac{\partial^2}{\partial z^2}\Phi_{F_{YYY}}(\vec{r}) = [1 - 2\alpha(z - z_A)^2](-2\alpha)(y - y_A)^3 \exp[-\alpha \mid \vec{r} - \vec{A} \mid^2] \tag{4.152}$$

$$\frac{\partial^2}{\partial x \partial y}\Phi_{F_{YYY}}(\vec{r}) = [-2\alpha(x - x_A)][3 - 2\alpha(y - y_A)^2](y - y_A)^2 \exp[-\alpha \mid \vec{r} - \vec{A} \mid^2] \tag{4.153}$$

$$\frac{\partial^2}{\partial x \partial z}\Phi_{F_{YYY}}(\vec{r}) = 4\alpha^2(z - z_A)(x - x_A)(y - y_A)^3 \exp[-\alpha \mid \vec{r} - \vec{A} \mid^2] \tag{4.154}$$

$$\frac{\partial^2}{\partial y \partial z}\Phi_{F_{YYY}}(\vec{r}) = [-2\alpha(z - z_A)][3 - 2\alpha(y - y_A)^2](y - y_A)^2 \exp[-\alpha \mid \vec{r} - \vec{A} \mid^2] \tag{4.155}$$

Second order derivative of F_{ZZZ} function:

$$\frac{\partial^2}{\partial x^2}\Phi_{F_{ZZZ}}(\vec{r}) = [1 - 2\alpha(x - x_A)^2](-2\alpha)(z - z_A)^3 \exp[-\alpha \mid \vec{r} - \vec{A} \mid^2] \tag{4.156}$$

$$\frac{\partial^2}{\partial y^2}\Phi_{F_{ZZZ}}(\vec{r}) = [1 - 2\alpha(y - y_A)^2](-2\alpha)(z - z_A)^3 \exp[-\alpha \mid \vec{r} - \vec{A} \mid^2] \tag{4.157}$$

$$\frac{\partial^2}{\partial z^2}\Phi_{F_{ZZZ}}(\vec{r}) = [6 - 14\alpha(z - z_a)^2 + 4\alpha^2(z - z_A)^4](z - z_A) \exp[-\alpha \mid \vec{r} - \vec{A} \mid^2] \tag{4.158}$$

$$\frac{\partial^2}{\partial x \partial y}\Phi_{F_{ZZZ}}(\vec{r}) = 4\alpha^2(y - y_A)(x - x_A)(z - z_A)^3 \exp[-\alpha \mid \vec{r} - \vec{A} \mid^2] \tag{4.159}$$

$$\frac{\partial^2}{\partial x \partial z}\Phi_{F_{ZZZ}}(\vec{r}) = (-2\alpha)(x-x_A)[3-2\alpha(z-z_A)^2](z-z_A)^2 \exp[-\alpha \mid \vec{r}-\vec{A} \mid^2] \quad (4.160)$$

$$\frac{\partial^2}{\partial y \partial z}\Phi_{F_{ZZZ}}(\vec{r}) = (-2\alpha)(y-y_A)[3-2\alpha(z-z_A)^2](z-z_A)^2 \exp[-\alpha \mid \vec{r}-\vec{A} \mid^2] \quad (4.161)$$

Second order derivative of F_{XXY} function:

$$\frac{\partial^2}{\partial x^2}\Phi_{F_{XXY}}(\vec{r}) = [2-10\alpha(x-x_A)^2+4\alpha^2(x-x_A)^4](y-y_A) \exp[-\alpha \mid \vec{r}-\vec{A} \mid^2] \quad (4.162)$$

$$\frac{\partial^2}{\partial y^2}\Phi_{F_{XXY}}(\vec{r}) = [3-2\alpha(y-y)^2](-2\alpha)(x-x_A)^2(y-y_A) \exp[-\alpha \mid \vec{r}-\vec{A} \mid^2] \quad (4.163)$$

$$\frac{\partial^2}{\partial z^2}\Phi_{F_{XXY}}(\vec{r}) = [1-2\alpha(z-z_A)^2](-2\alpha)(x-x_A)^2(y-y_A) \exp[-\alpha \mid \vec{r}-\vec{A} \mid^2] \quad (4.164)$$

$$\frac{\partial^2}{\partial x \partial y}\Phi_{F_{XXY}}(\vec{r}) = [1-2\alpha(y-y_A)^2][2-2\alpha(x-x_A)^2](x-x_A) \exp[-\alpha \mid \vec{r}-\vec{A} \mid^2] \quad (4.165)$$

$$\frac{\partial^2}{\partial x \partial z}\Phi_{F_{XXY}}(\vec{r}) = (-2\alpha)(z-z_A)[2-2\alpha(x-x_A)^2](x-x_A)(y-y_A) \exp[-\alpha \mid \vec{r}-\vec{A} \mid^2] \quad (4.166)$$

$$\frac{\partial^2}{\partial y \partial z}\Phi_{F_{XXY}}(\vec{r}) = (-2\alpha)(z-z_A)[1-2\alpha(y-y_A)^2](x-x_A)^2 \exp[-\alpha \mid \vec{r}-\vec{A} \mid^2] \quad (4.167)$$

Second order derivative of F_{XXZ} function:

$$\frac{\partial^2}{\partial x^2}\Phi_{F_{XXZ}}(\vec{r}) = [2-10\alpha(x-x_A)^2+4\alpha^2(x-x_A)^4](z-z_A)\exp[-\alpha \mid \vec{r}-\vec{A} \mid^2] \quad (4.168)$$

$$\frac{\partial^2}{\partial y^2}\Phi_{F_{XXZ}}(\vec{r}) = [1-2\alpha(y-y_A)^2](-2\alpha)(x-x_A)^2(z-z_a)\exp[-\alpha \mid \vec{r}-\vec{A} \mid^2] \quad (4.169)$$

$$\frac{\partial^2}{\partial z^2}\Phi_{F_{XXZ}}(\vec{r}) = [3-2\alpha(z-z_A)^2](-2\alpha)(x-x_A)^2(z-z_A)\exp[-\alpha \mid \vec{r}-\vec{A} \mid^2] \quad (4.170)$$

$$\frac{\partial^2}{\partial x\partial y}\Phi_{F_{XXZ}}(\vec{r}) = [-2\alpha(y-y_A)][2-2\alpha(x-x_A)^2](x-x_A)(z-z_A)\exp[-\alpha \mid \vec{r}-\vec{A} \mid^2] \quad (4.171)$$

$$\frac{\partial^2}{\partial x\partial z}\Phi_{F_{XXZ}}(\vec{r}) = [1-2\alpha(z-z_A)^2][2-2\alpha(x-x_A)^2](x-x_A)\exp[-\alpha \mid \vec{r}-\vec{A} \mid^2] \quad (4.172)$$

$$\frac{\partial^2}{\partial y\partial z}\Phi_{F_{XXZ}}(\vec{r}) = (-2\alpha)(y-y_A)[1-2\alpha(z-z_A)^2](x-x_A)^2\exp[-\alpha \mid \vec{r}-\vec{A} \mid^2] \quad (4.173)$$

Second order derivative of F_{YYZ} function:

$$\frac{\partial^2}{\partial x^2}\Phi_{F_{YYZ}}(\vec{r}) = [1-2\alpha(x-x_A)^2](-2\alpha)(y-y_A)^2(z-z_A)\exp[-\alpha \mid \vec{r}-\vec{A} \mid^2] \quad (4.174)$$

$$\frac{\partial^2}{\partial y^2}\Phi_{F_{YYZ}}(\vec{r}) = [2-10\alpha(y-y_A)^2+4\alpha^2(y-y_A)^4](z-z_A)\exp[-\alpha \mid \vec{r}-\vec{A} \mid^2] \quad (4.175)$$

$$\frac{\partial^2}{\partial z^2}\Phi_{F_{YYZ}}(\vec{r}) = [3-2\alpha(z-z_A)^2](-2\alpha)(y-y_A)^2(z-z_A)\exp[-\alpha \mid \vec{r}-\vec{A} \mid^2] \quad (4.176)$$

$$\frac{\partial^2}{\partial x\partial y}\Phi_{F_{YYZ}}(\vec{r}) = (-2\alpha)(x-x_A)[2-2\alpha(y-y_A)^2](y-y_A)(z-z_A)\exp[-\alpha \mid \vec{r}-\vec{A} \mid^2] \quad (4.177)$$

$$\frac{\partial^2}{\partial x\partial z}\Phi_{F_{YYZ}}(\vec{r}) = (-2\alpha)(x-x_A)[1-2\alpha(z-z_A)^2](y-y_A)(z-z_A)\exp[-\alpha \mid \vec{r}-\vec{A} \mid^2] \quad (4.178)$$

$$\frac{\partial^2}{\partial y\partial z}\Phi_{F_{YYZ}}(\vec{r}) = [1-2\alpha(z-z_A)^2][2-2\alpha(y-y_A)](y-y_A)\exp[-\alpha \mid \vec{r}-\vec{A} \mid^2] \quad (4.179)$$

Second order derivative of F_{XZZ} function:

$$\frac{\partial^2}{\partial x^2}\Phi_{F_{XZZ}}(\vec{r}) = [3-2\alpha(x-x_A)^2](-2\alpha)(z-z_A)^2(x-x_A)\exp[-\alpha \mid \vec{r}-\vec{A} \mid^2] \quad (4.180)$$

$$\frac{\partial^2}{\partial y^2}\Phi_{F_{XZZ}}(\vec{r}) = [1-2\alpha(y-y_A)^2](-2\alpha)(z-z_A)^2(x-x_A)\exp[-\alpha \mid \vec{r}-\vec{A} \mid^2] \quad (4.181)$$

$$\frac{\partial^2}{\partial z^2}\Phi_{F_{XZZ}}(\vec{r}) = [2-10\alpha(z-z_A)^2+4\alpha^2(z-z_A)^4](x-x_A)\exp[-\alpha \mid \vec{r}-\vec{A} \mid^2] \quad (4.182)$$

$$\frac{\partial^2}{\partial x\partial y}\Phi_{F_{XZZ}}(\vec{r}) = (-2\alpha)(y-y_A)[1-2\alpha(x-x_A)^2](z-z_A)^2\exp[-\alpha \mid \vec{r}-\vec{A} \mid^2] \quad (4.183)$$

$$\frac{\partial^2}{\partial x \partial z}\Phi_{F_{XZZ}}(\vec{r}) = [1 - 2\alpha(x - x_A)^2][2 - 2\alpha(z - z_A)^2](z - z_A)\exp[-\alpha \mid \vec{r} - \vec{A} \mid^2] \tag{4.184}$$

$$\frac{\partial^2}{\partial y \partial z}\Phi_{F_{XZZ}}(\vec{r}) = (-2\alpha)(y - y_A)[2 - 2\alpha(z - z_A)^2](z - z_A)(x - x_A)\exp[-\alpha \mid \vec{r} - \vec{A} \mid^2] \tag{4.185}$$

Second order derivative of F_{XYY} function:

$$\frac{\partial^2}{\partial x^2}\Phi_{F_{XYY}}(\vec{r}) = [3 - 2\alpha(x - x_A)^2](-2\alpha)(y - y_A)^2(x - x_A)\exp[-\alpha \mid \vec{r} - \vec{A} \mid^2] \tag{4.186}$$

$$\frac{\partial^2}{\partial y^2}\Phi_{F_{XYY}}(\vec{r}) = [2 - 10\alpha(y - y_A)^2 + 4\alpha^2(y - y_A)^2](x - x_A)\exp[-\alpha \mid \vec{r} - \vec{A} \mid^2] \tag{4.187}$$

$$\frac{\partial^2}{\partial z^2}\Phi_{F_{XYY}}(\vec{r}) = [1 - 2\alpha(z - z_A)^2](-2\alpha)(y - y_A)^2(x - x_A)\exp[-\alpha \mid \vec{r} - \vec{A} \mid^2] \tag{4.188}$$

$$\frac{\partial^2}{\partial x \partial y}\Phi_{F_{XYY}}(\vec{r}) = [1 - 2\alpha(x - x_A)^2][2 - 2\alpha(y - y_A)^2](y - y_A)\exp[-\alpha \mid \vec{r} - \vec{A} \mid^2] \tag{4.189}$$

$$\frac{\partial^2}{\partial x \partial z}\Phi_{F_{XYY}}(\vec{r}) = (-2\alpha)(z - z_A)[1 - 2\alpha(x - x_A)^2](y - y_A)^2\exp[-\alpha \mid \vec{r} - \vec{A} \mid^2] \tag{4.190}$$

$$\frac{\partial^2}{\partial y \partial z}\Phi_{F_{XYY}}(\vec{r}) = (-2\alpha)(z - z_A)[2 - 2\alpha(y - y_A)^2](y - y_A)(x - x_A)\exp[-\alpha \mid \vec{r} - \vec{A} \mid^2] \tag{4.191}$$

Second order derivative of F_{YZZ} function:

$$\frac{\partial^2}{\partial x^2}\Phi_{F_{YZZ}}(\vec{r}) = [1-2\alpha(x-x_A)^2](-2\alpha)(z-z_A)^2(y-y_A)\exp[-\alpha\mid\vec{r}-\vec{A}\mid^2] \tag{4.192}$$

$$\frac{\partial^2}{\partial y^2}\Phi_{F_{YZZ}}(\vec{r}) = [3-2\alpha(y-y_A)^2](-2\alpha)(z-z_A)^2(y-y_A)\exp[-\alpha\mid\vec{r}-\vec{A}\mid^2] \tag{4.193}$$

$$\frac{\partial^2}{\partial z^2}\Phi_{F_{YZZ}}(\vec{r}) = [2-10\alpha(z-z_A)^2+4\alpha^2(z-z_A)^4](y-y_A)\exp[-\alpha\mid\vec{r}-\vec{A}\mid^2] \tag{4.194}$$

$$\frac{\partial^2}{\partial x\partial y}\Phi_{F_{YZZ}}(\vec{r}) = (-2\alpha)(x-x_A)[1-2\alpha(y-y_A)^2](z-z_A)^2\exp[-\alpha\mid\vec{r}-\vec{A}\mid^2] \tag{4.195}$$

$$\frac{\partial^2}{\partial x\partial z}\Phi_{F_{YZZ}}(\vec{r}) = (-2\alpha)(x-x_A)[2-2\alpha(z-z_A)^2](z-z_A)(y-y_A)\exp[-\alpha\mid\vec{r}-\vec{A}\mid^2] \tag{4.196}$$

$$\frac{\partial^2}{\partial y\partial z}\Phi_{F_{YZZ}}(\vec{r}) = [1-2\alpha(y-y_A)^2][2-2\alpha(z-z_A)^2](z-z_A)\exp[-\alpha\mid\vec{r}-\vec{A}\mid^2] \tag{4.197}$$

Second order derivative of F_{XYZ} function:

$$\frac{\partial^2}{\partial x^2}\Phi_{F_{XYZ}}(\vec{r}) = [3-2\alpha(x-x_A)^2](-2\alpha)(x-x_A)(y-y_A)(z-z_A)\exp[-\alpha\mid\vec{r}-\vec{A}\mid^2] \tag{4.198}$$

$$\frac{\partial^2}{\partial y^2}\Phi_{F_{XYZ}}(\vec{r}) = [3-2\alpha(y-y_A)^2](-2\alpha)(x-x_A)(y-y_A)(z-z_A)\exp[-\alpha\mid\vec{r}-\vec{A}\mid^2] \tag{4.199}$$

$$\frac{\partial^2}{\partial z^2}\Phi_{F_{XYZ}}(\vec{r}) = [3 - 2\alpha(z - z_A)^2](-2\alpha)(x - x_A)(y - y_A)(z - z_A)\exp[-\alpha \mid \vec{r} - \vec{A} \mid^2] \tag{4.200}$$

$$\frac{\partial^2}{\partial x \partial y}\Phi_{F_{XYZ}}(\vec{r}) = [1 - 2\alpha(x - x_A)^2][1 - 2\alpha(y - y_A)^2](z - z_A)\exp[-\alpha \mid \vec{r} - \vec{A} \mid^2] \tag{4.201}$$

$$\frac{\partial^2}{\partial x \partial z}\Phi_{F_{XYZ}}(\vec{r}) = [1 - 2\alpha(x - x_A)^2][1 - 2\alpha(z - z_A)^2](y - y_A)\exp[-\alpha \mid \vec{r} - \vec{A} \mid^2] \tag{4.202}$$

$$\frac{\partial^2}{\partial y \partial z}\Phi_{F_{XYZ}}(\vec{r}) = [1 - 2\alpha(y - y_A)^2][1 - 2\alpha(z - z_A)^2](x - x_A)\exp[-\alpha \mid \vec{r} - \vec{A} \mid^2] \tag{4.203}$$

A3. Basis set example for test H_2O molecule

The gaussian basis set used for calculations in the present thesis. The form of input is provided for an example molecule H_2O, for the *aug-cc-pvdz* basis set.

```
O    8.0       0.0000000000       0.0000000000       0.1135960000
   S       9
     1          11720.0000000000  0.00071000
     2           1759.0000000000  0.00547000
     3            400.8000000000  0.02783700
     4            113.7000000000  0.10480000
     5             37.0300000000  0.28306200
     6             13.2700000000  0.44871900
     7              5.0250000000  0.27095200
     8              1.0130000000  0.01545800
     9              0.3023000000 -0.00258500
   S       9
     1          11720.0000000000 -0.00016000
     2           1759.0000000000 -0.00126300
     3            400.8000000000 -0.00626700
     4            113.7000000000 -0.02571600
     5             37.0300000000 -0.07092400
     6             13.2700000000 -0.16541100
     7              5.0250000000 -0.11695500
     8              1.0130000000  0.55736800
     9              0.3023000000  0.57275900
   S       1
     1              0.3023000000  1.00000000
   S       1
     1              0.0789600000  1.00000000
   P       4
     1             17.7000000000  0.04301800
```

```
      2             3.8540000000  0.22891300
      3             1.0460000000  0.50872800
      4             0.2753000000  0.46053100
    P       1
      1             0.2753000000  1.00000000
    P       1
      1             0.0685600000  1.00000000
    D       1
      1             1.1850000000  1.00000000
    D       1
      1             0.3320000000  1.00000000


 H    1.0     0.0000000000      0.7535270000     -0.4543820000
    S       4
      1            13.0100000000  0.01968500
      2             1.9620000000  0.13797700
      3             0.4446000000  0.47814800
      4             0.1220000000  0.50124000
    S       1
      1             0.1220000000  1.00000000
    S       1
      1             0.0297400000  1.00000000
    P       1
      1             0.7270000000  1.00000000
    P       1
      1             0.1410000000  1.00000000

 H    1.0     0.0000000000     -0.7535270000     -0.4543820000
    S       4
      1            13.0100000000  0.01968500
```

```
  2              1.9620000000  0.13797700
  3              0.4446000000  0.47814800
  4              0.1220000000  0.50124000
S       1
  1              0.1220000000  1.00000000
S       1
  1              0.0297400000  1.00000000
P       1
  1              0.7270000000  1.00000000
P       1
  1              0.1410000000  1.00000000
```

The input described above contains the coordinates of O, H atoms of H_2O molecule. The Gaussian basis set is shown just below the coordinates. The type of function is mentioned along with the Gaussian exponent α and contraction coefficients.

A4. Movies of time-dependent electron densities and their properties

The time-dependent electronic wavefunctions in position space are obtained from the in-house package **ABELDYN**. The properites code **ABELDYNPROP** has been used to evaluate the TDMED and its properties. The time-dependent plots of intermediate steps are provided here in the following 2D figures. The 2D and 3D movies are provided through the weblink.

The Laser parameters in a.u. and SI are provided in the following table

Mol.	ω(a.u.)	ω(nm)	light	ϵ (a.u.)	ϵ (a.u.)	I (W/cm^2)	$T_{tot}(fs)$	α_o
HF	0.688	66.217	XUV	0.100	5.14$\times 10^8$	3.51$\times 10^{14}$	1.76	0.211
H_2O	0.546	83.496	XUV	0.100	5.14$\times 10^8$	3.51$\times 10^{14}$	2.22	0.336
CH_4	0.580	78.572	XUV	0.100	5.14$\times 10^8$	3.51$\times 10^{14}$	2.10	0.297
C_2H_4	0.419	108.69	XUV	0.100	5.14$\times 10^8$	3.51$\times 10^{14}$	2.90	0.569
Be	0.329	138.32	XUV	0.100	5.14$\times 10^8$	3.51$\times 10^{14}$	3.69	0.922
He	0.937	48.622	XUV	0.100	5.14$\times 10^8$	3.51$\times 10^{14}$	1.30	0.114
N_2	0.727	62.648	XUV	0.100	5.14$\times 10^8$	3.51$\times 10^{14}$	1.66	0.189
CO	0.636	71.62	XUV	0.100	5.14$\times 10^8$	3.51$\times 10^{14}$	1.91	0.247
C_6H_6	0.373	122.09	XUV	0.100	5.14$\times 10^8$	3.51$\times 10^{14}$	3.25	0.718
C_3H_6	0.4598	99.02	XUV	0.100	5.14$\times 10^8$	3.51$\times 10^{14}$	2.64	0.473

Mol.	Basis	N_{bas}
HF	aug-cc-pvdz	34
H_2O	aug-cc-pvdz	43
CH_4	aug-cc-pvdz	61
C_2H_4	aug-cc-pvdz	86
C_2H_4	aug-cc-pvdz	86
Be	aug-cc-pvdz	25
He	d-aug-cc-pvdz	35
N_2	aug-cc-pvdz	50
CO	aug-cc-pvdz	50
C_6H_6	aug-cc-pvdz	204
C_3H_6	aug-cc-pvdz	129

Weblinks of Time evolving 3D movies:

Helium Atom in Linearly Polarized LASER, parallel to Z-axis: 1. Time dependent Molecular Electron Densities, Laplacian, and Difference densities:

https://youtu.be/mlcuENC5d5s

2. Time dependent zero-Flux Surfaces, bond paths, basin boundaries, and critical points:

https://youtu.be/6UHD3PWjRRI

Hydrogen Fluoride in Linearly Polarized LASER, parallel to H-F bond: 1. Time dependent Molecular Electron Densities, Laplacian, and Difference densities:

https://youtu.be/MEeYCCf3kBk

2. Time dependent zero-Flux Surfaces, bond paths, basin boundaries, and critical points:

https://youtu.be/q4fzoIZN21g

Water in Linearly Polarized LASER along the Z-axis:

1. Time dependent Molecular Electron Densities, Laplacian, and Difference densities:

https://youtu.be/E1qkvEh3k-M

2. Time dependent zero-Flux Surfaces, bond paths, basin boundaries, and critical points:

https://youtu.be/Dmq9WdYoxkA

Water in Linearly Polarized LASER along the Y-axis:

1. Time dependent Molecular Electron Densities, Laplacian, and Difference densities:

https://youtu.be/hEkohvBdFog

2. Time dependent zero-Flux Surfaces, bond paths, basin boundaries, and critical points:

https://youtu.be/MAsuX_Kj8cs

Methane in Linearly Polarized LASER along the C_3-axis:

1. Time dependent Molecular Electron Densities, Laplacian, and Difference densities:

https://youtu.be/gQ_2c0ww_mU

2. Time dependent zero-Flux Surfaces, bond paths, basin boundaries, and critical points:

https://youtu.be/DahsH9pJF0E

Methane in Linearly Polarized LASER along the C_2-axis:

1. Time dependent Molecular Electron Densities, Laplacian, and Difference densities:

https://youtu.be/oAsVdKtlYtY

2. Time dependent zero-Flux Surfaces, bond paths, basin boundaries, and critical points:

https://youtu.be/3WadDwiNFk0

Ethylene in Linearly Polarized LASER along the Z-axis, parallel to C-C bond:

1. Time dependent Molecular Electron Densities, Laplacian, and Difference densities:

https://youtu.be/Lw7CjXNxQ84

2. Time dependent zero-Flux Surfaces, bond paths, basin boundaries, and critical points:

https://youtu.be/eycKki807Hg

Ethylene in Linearly Polarized LASER along the Y-axis, perpendicular to C-C bond:

1. Time dependent Molecular Electron Densities, Laplacian, and Difference densities:

https://youtu.be/wrXpPGuPcy0

2. Time dependent zero-Flux Surfaces, bond paths, basin boundaries, and critical points:

https://youtu.be/tJAg94zZxNA

Weblinks for 2D movies:

1. Helium atom in a linearly polarized LASER along Z: Time dependent atomic electron densities, gradients, Laplacian and difference densities on a 2D plane

https://youtu.be/UhHj95bvFp4

2. Beryllium atom in a linearly polarized LASER along Z: Time dependent atomic electron densities, gradients, Laplacian and difference densities on a 2D plane

https://youtu.be/6KtGtCQ2HNk

3. Hydrogen Fluoride in a linearly polarized LASER along Z: Time dependent MED, gradients, Laplacian and difference densities on a 2D plane

https://youtu.be/vlB69L89Yno

4. Water in a linearly polarized LASER along Z: Time dependent MED, gradients, Laplacian and difference densities on a 2D plane

https://youtu.be/Pd0sMU8dRTI

5. Water in a linearly polarized LASER along Y: Time dependent MED, gradients, Laplacian and difference densities on a 2D plane

https://youtu.be/tKgLH_Xg8Ig

6. Water in a linearly polarized LASER along Y: Time dependent MED, gradients, Laplacian and difference densities on a 2D plane

https://youtu.be/W1OYUgeHkis

7. Ethylene in a linearly polarized LASER along Y: Time dependent MED, gradients, Laplacian and difference densities on a 2D plane

https://youtu.be/W1OYUgeHkis

8. Ethylene in a linearly polarized LASER along Y: Time dependent MED, gradients, Laplacian and difference densities on a 2D plane

https://youtu.be/wAUztbgTZsk

A4.1 Movies of the time dependent QM vector current densities

Weblinks of movies for time-evolving QM vector current densities:

1. Helium Atom:

https://youtu.be/rmroZ_owc0Y

2. **Hydrogen Fluoride in Linearly Polarized LASER along Z:**

https://youtu.be/Uo73fGY8aYk

3. **Water in Linearly Polarized LASER along Z:**

https://youtu.be/fehoCk2SE2E

4. **Water in Linearly Polarized LASER along Y:**

https://youtu.be/CCrIXqLKdDg

5. **Ethylene in Linearly Polarized LASER along Z:**

https://youtu.be/uevLd1pNqSY

6. **Ethylene in Liearly Polarized LASER along Y:**

https://youtu.be/8pHPN54Pn4g

Example input and output to run ABELDYNPROP code

Prerequisite: The user should ensure the successful installation of ABELDYNPROP codes on local desktop or server computing machines with any Unix-based operating system. The machine should have Fortran, linear algebra library packages (BLAS and LAPACK), and MPI installed before running the code. The required source code and installation files are provided in the 'abeldynprop.zip' folder on a CD with the thesis physical copy.

The input files describe the input parameters required for calculating molecular electron density and related properties based on the input property keywords (for example, keywords: EDEN, EGRD, ELF, VDEN, ZEROFS, BDPARTSP, ...). The input file contains three sections called "SECTION-PROPERTY," "SECTION-PARAMETER," and "SECTION-TIMEFILE." The section "SECTION-PROPERTY" takes the input of the property keyword, atom-basis file, real/complex wavefunction information, and number of processors for the calculations. The parameters required for every property keyword may differ, which are specified in the "SECTION-PARAMETER." The "SECTION-TIMEFILE" should be present for a time-evolving wavefunction in the input file. The section takes the time file prefix name, start and end indices of time steps, and the time file step size.

To perform the calculation follow these steps in the working directory:

1. Create a folder named "inpdir". This folder should contain two files: 1. "input.dat", and 2. molecular information file (for example, "h2o.dat", See chapter 2). The molecular information file is a ".dat" extension file could obtained by running a single point energy job using GAMESS package.

2. If the card mentioned below in the "input.dat" file is COMPLEX, then the user should create a folder named "timefile".

```
MO_REAL_OR_COMPLEX        ::
```

All the wavefunction coefficient files at each time step are obtained from the solutions of TDSE and should be kept in the "timefile" folder. We use wavefunctions obtained from an in-house code ABELDYN, which solves time-dependent Hartree Fock for this case. Generally, the wavefunction coefficients obtained from TDSE solutions are complex. To use the code, the real-part and the imaginary-part part of the complex wavefunction coefficients should be written out in single column as separate files (N_{tot} = $\mathrm{N}_{bas} \times \mathrm{N}_{bas}$).

If the card mentioned in the "input.dat" file is "REAL", then "timefile" folder is not required.

3. The bash script "runscript.sh" would run the code for the specific job. After the completion of the run, a "result" folder is created. This folder would contain the output files of the calculations in specific keywords with timefile prefixes. For example, in the "result" folder, a job for the calculation of electron density (keyword-EDEN) for ten-time steps would contain 10 folders named "edenstep1", "edenstep2", "edenstep3", ... , "edenstep10".

Example-1: Input and output example for the calculation of molecular electron density over a 3D-grid for YZ-oriented water molecule in the presence of a Strong linearly polarized LASER field. The following is an input file format to be written in file named as "input.dat" for the calculation:

```
# SECTION-PROPERTY
PROPERTY_TO_CALCULATE     :: EDEN
ATOM_BASIS_FILE           :: h2o.dat
MO_REAL_OR_COMPLEX        :: COMPLEX
N_PROCS                   :: 4

# SECTION-PARAMETER
CART_GRID_XMIN_XMAX_NX    :: -8.000000000, 8.000000000, 101
CART_GRID_YMIN_YMAX_NY    :: -8.000000000, 8.000000000, 101
CART_GRID_ZMIN_ZMAX_NZ    :: -8.000000000, 8.000000000, 101
DATA_FILE_TYPE_CUBE/VTK   :: cube

# SECTION-TIMEFILE
TIMEFILE_PREFIX           :: tmcoef
TIMEFILE_START_INDEX      :: 1
TIMEFILE_END_INDEX        :: 921
TIMEFILE_STEP_SIZE        :: 1
```

Output: A successful run of the code using this input file would generate output files for each 921 time-step for water molecule in the "result" folder. The outputs will contain ".cube" data files for the three-dimensional rectangular grid.

Note: A similar input file description would be required to calculate gradients, hessian, laplacian, vector-current density, and electron localization function. Property keywords: EGRD, EHES, ELAP, VDEN, and ELF. The first card input in the "SECTION-PROPERTY" should be substituted with the appropriate keyword for the user to evaluate the desired property.

Example-2: Input and output examples for calculating critical points, zero-flux surfaces, gradient paths, and bond paths for water molecules in a Strong linearly polarized LASER field. The following is an input file format to be written in a file named "input.dat" for the calculation:

```
# SECTION-PROPERTY
PROPERTY_TO_CALCULATE    :: EDEN
ATOM_BASIS_FILE          :: h2o.dat
MO_REAL_OR_COMPLEX       :: COMPLEX
N_PROCS                  :: 4

# SECTION-PARAMETER
R_NR_NTHETA_NPHI         :: 8.000000, 11, 11, 11
MAX_NEWTON-RAPHSON_ITER  :: 50
CONVERGENCE              :: 1.0E-7
MINIMUM_DENSITY          :: 1.0E-6
ZFS_TOTAL_CIRCLE_POINTS  :: 50
ZFS_GRADIENT_STEP_SIZE   :: 0.05
ZFS_POINTS_ALONG_VECTOR  :: 100
BP_GVEC_STEP_SIZE        :: 0.00010
BP_MAX_POINTS            :: 100000
GP_PLANE_VECTOR_1        :: 0.00, 1.00, 0.00
GP_PLANE_VECTOR_2        :: 0.00, 0.00, 1.00
GP_PLANE_CIRCLE_POINTS   :: 32
GP_VECTOR_STEP           :: 0.001
GP_TOTAL_STEPS           :: 6000

# SECTION-TIMEFILE
TIMEFILE_PREFIX          :: tmcoef
TIMEFILE_START_INDEX     :: 1
TIMEFILE_END_INDEX       :: 921
```

```
TIMEFILE_STEP_SIZE        :: 1
```

Output: The results would create output files containing the information of all the types of critical points, zero-flux surfaces, gradient paths and bonds paths at each time step for water molecule in linearly polarized field.

The (3,-3), (3,-1), (3,+1), (3,+3) CPs will be written out in "cpm3.dat", "cpm1.dat", "cpp1.dat" and "cpp3.dat" respectively. The zero-flux surfaces can be visualized through "cp1.vtk" and "cp2.vtk" files. The output data of gradient paths and bond paths are present in files with suffixes as "grad" and "bondpatha"/"bondpathb."

Example-3: Input and output examples for calculating norm, charge, kinetic energies, moments, and dipole of all the atomic basins present in the molecular electron densities of water molecules in a Strong linearly polarized LASER field. The following is an input file format to be written in a file named "input.dat" for the calculation:

```
# SECTION-PROPERTY
PROPERTY_TO_CALCULATE    :: EDEN
ATOM_BASIS_FILE          :: h2o.dat
MO_REAL_OR_COMPLEX       :: COMPLEX
N_PROCS                  :: 4

# SECTION-PARAMETER
R_NR_NTHETA_NPHI         :: 8.000000, 11, 11, 11
MAX_NEWTON-RAPHSON_ITER  :: 50
CONVERGENCE              :: 1.0E-7
MINIMUM_DENSITY          :: 1.0E-6
BP_RMAX                  :: 10.000000
BP_NR_NTHETA_NPHI        :: 201, 30, 60
BP_R_STEP_INCREMENT      :: 20
BP_GRADIENT_SCALAR       :: 0.05
BP_ASCENT_MAX_SEARCH     :: 600
BP_BISECTION_ERROR       :: 1.0E-5
BP_INTEGRATION_TYPE      :: 1
BP_INTEGRATION_POINTS    :: 501

# SECTION-TIMEFILE
TIMEFILE_PREFIX          :: tmcoef
TIMEFILE_START_INDEX     :: 1
TIMEFILE_END_INDEX       :: 921
TIMEFILE_STEP_SIZE       :: 1
```

Output: The successful run of the abeldynprop code would create a set of data files containing the information on the total number of critical points and the BADER partitioning properties of all the basins present. The information on properties for each atomic basin is tabulated in the "bader.dat" file.

Electronic properties of molecules

The figures show plots of molecular electron densities, their gradient, laplacian, and difference densities in the presence of linearly polarized laser for various molecules. The plots are shown for time steps near the half and full cycles in the LASER pulse. These represent the plots for the same molecules discussed in the thesis chapters.

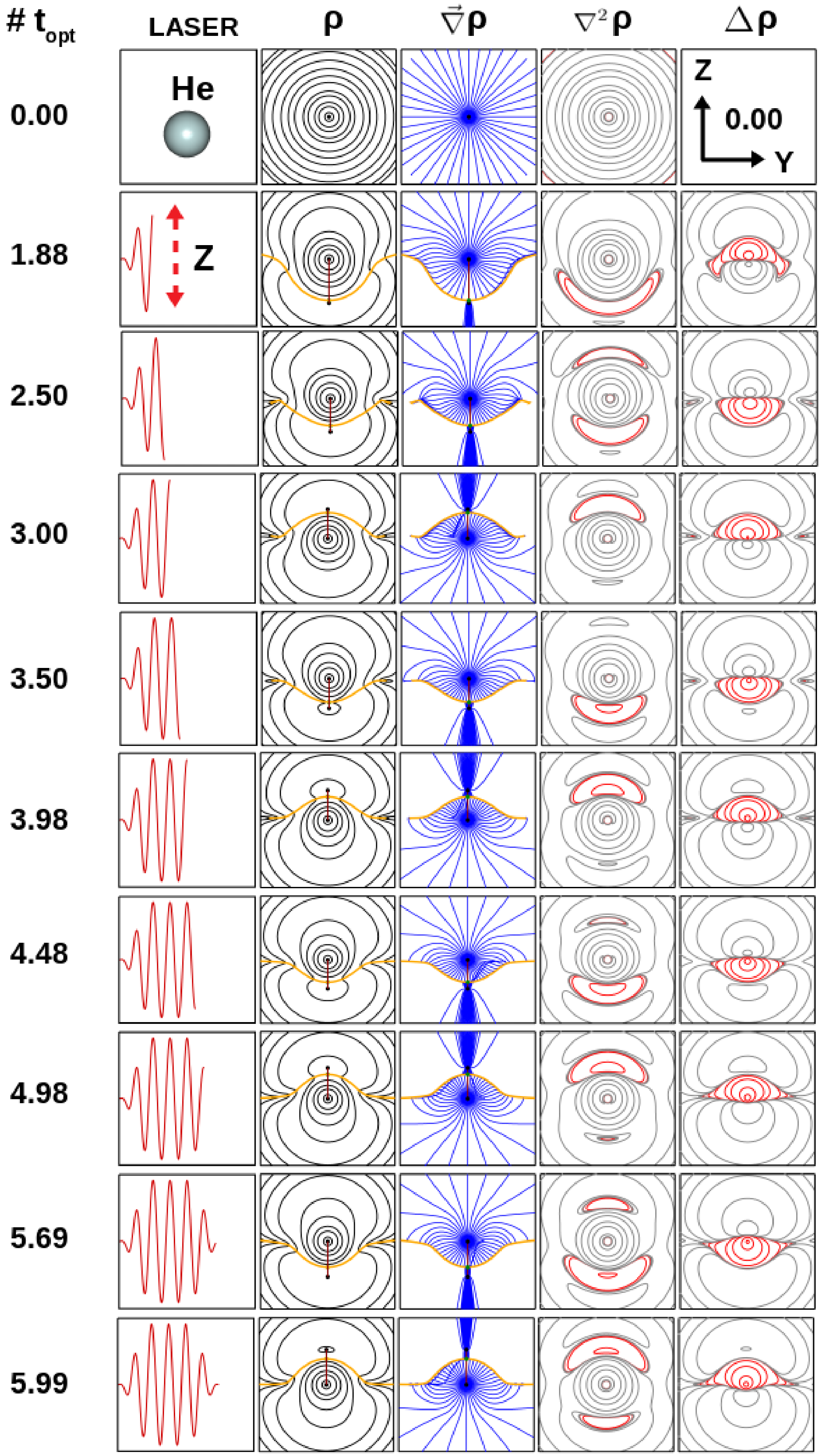

Figure 4.1: TDMED and its properties for ten time steps of Hellium atom in Z-polarized laser. Details described in Chapter 3.

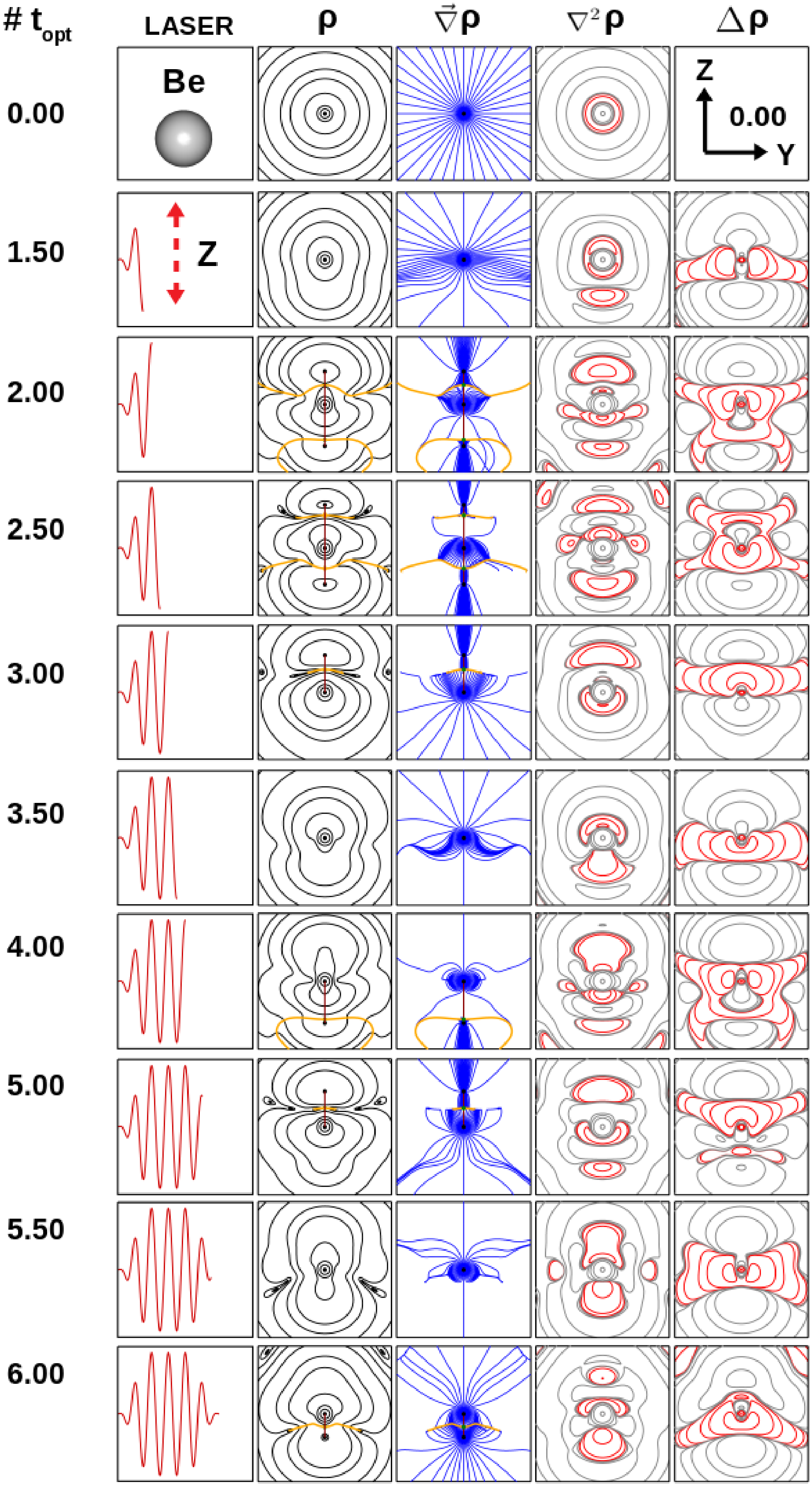

Figure 4.2: TDMED and its properties for ten time steps of Beryllium atom in Z-polarized laser. Details described in Chapter 3.

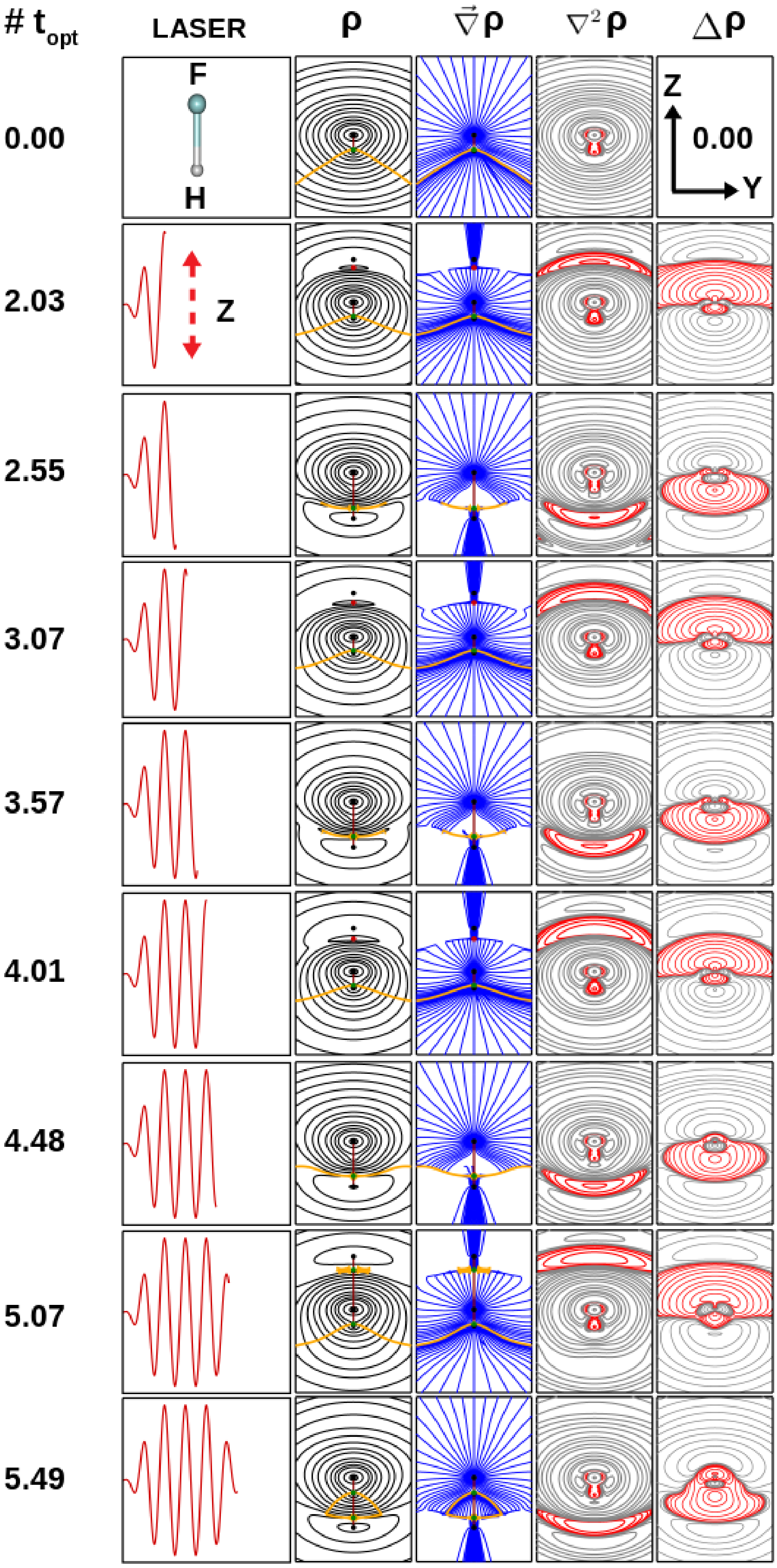

Figure 4.3: TDMED and its properties for nine time steps of Hydrogen Fluoride molecule in Z-polarized laser. Details described in Chapter 4.

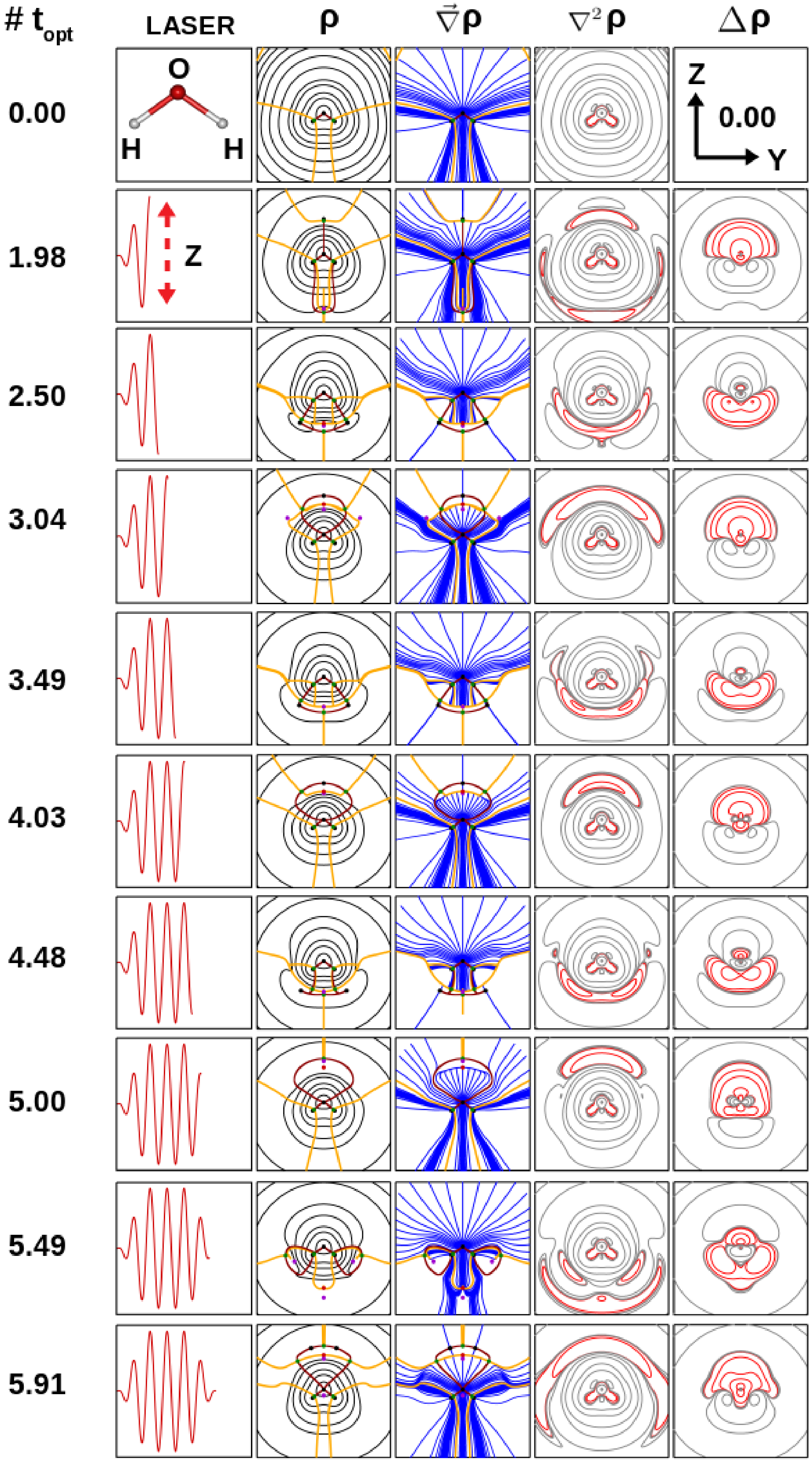

Figure 4.4: TDMED and its properties for ten time steps of Water molecule in Z-polarized laser. Details described in Chapter 4.

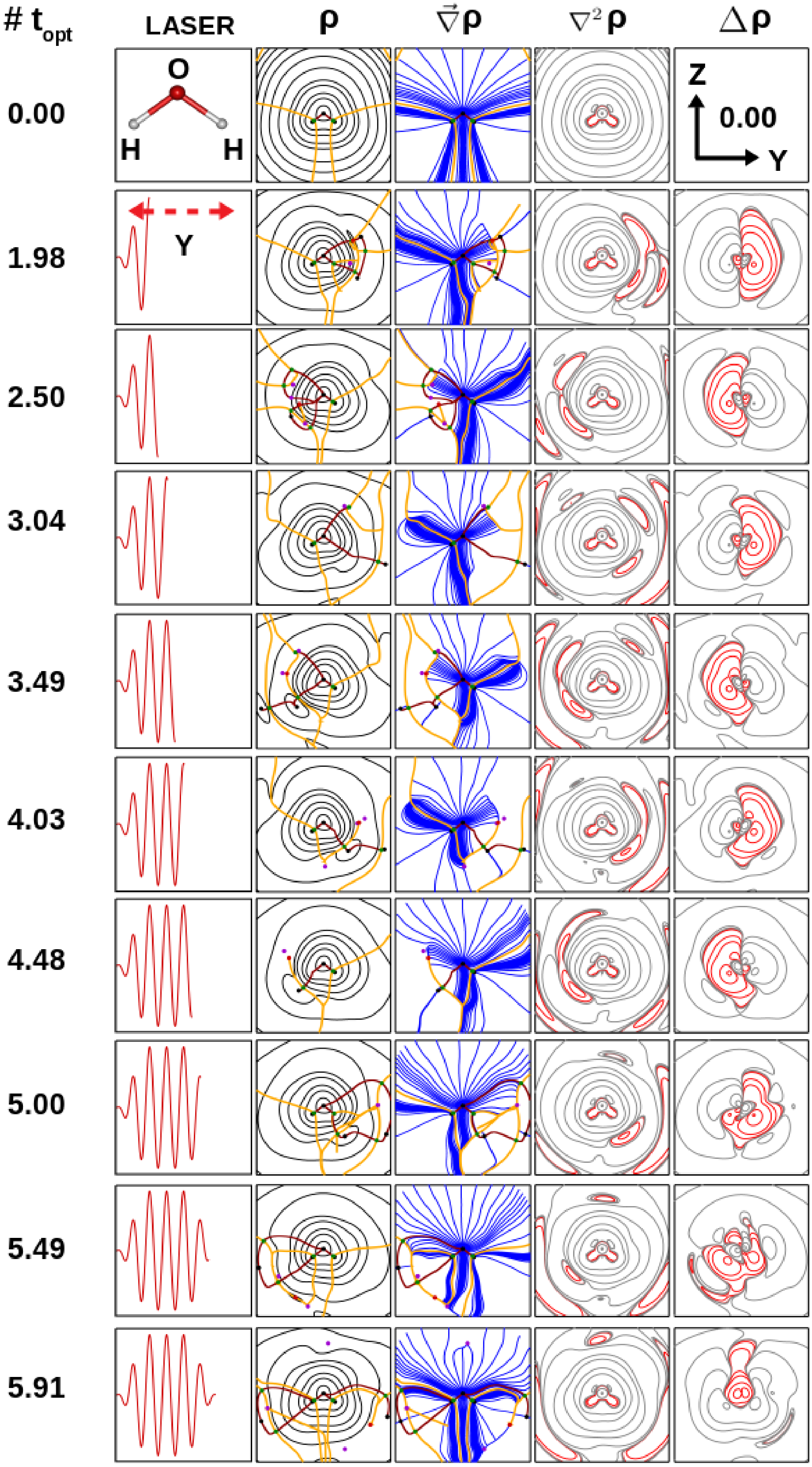

Figure 4.5: TDMED and its properties for ten time steps of Water molecule in Y-polarized laser. Details described in Chapter 4.

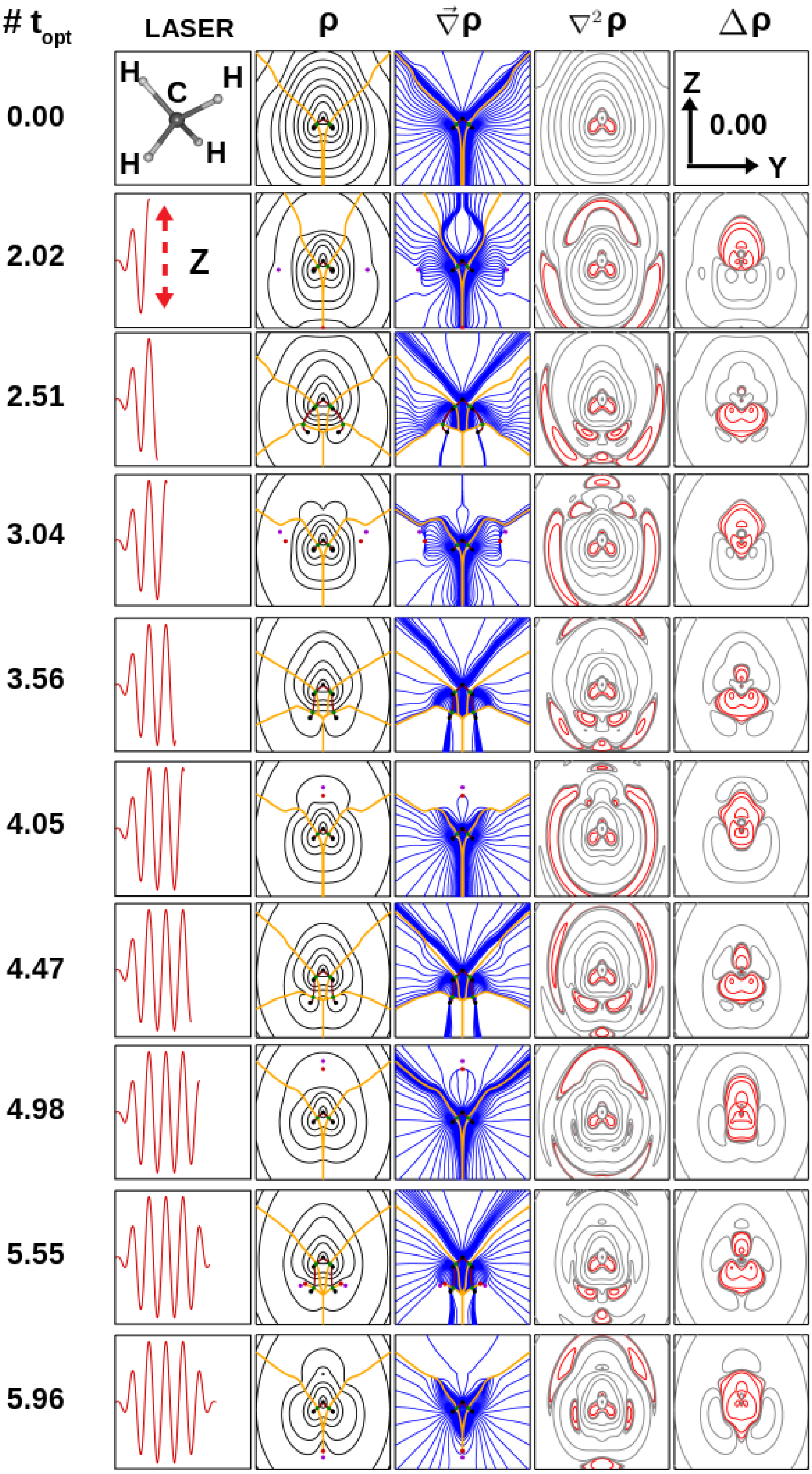

Figure 4.6: TDMED and its properties for ten time steps of Methane molecule in Z-polarized laser, parallel to C_2 axis. Details described in Chapter 4.

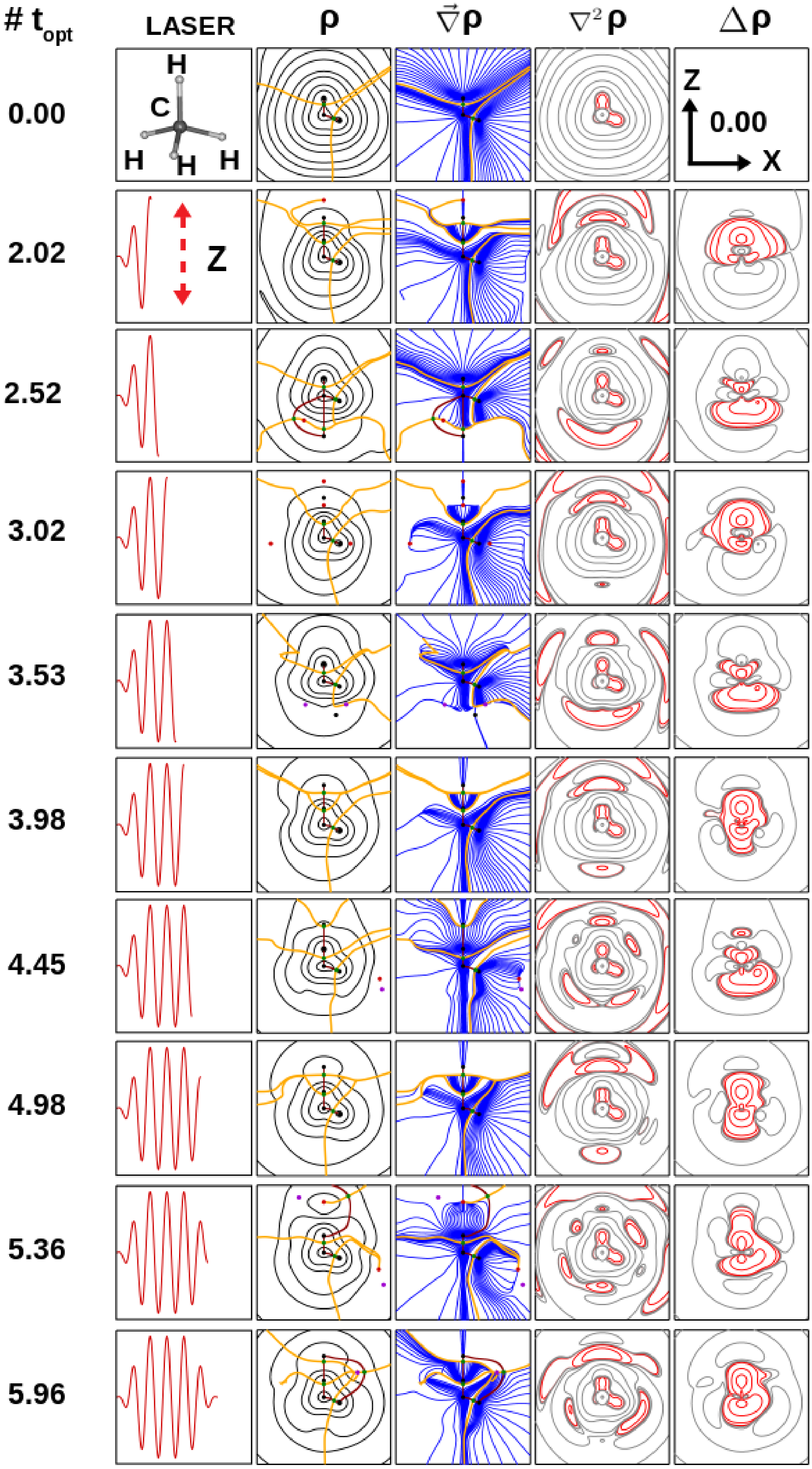

Figure 4.7: TDMED and its properties for ten time steps of Methane molecule in Z-polarized laser, parallel to C_3 axis. Details described in Chapter 4.

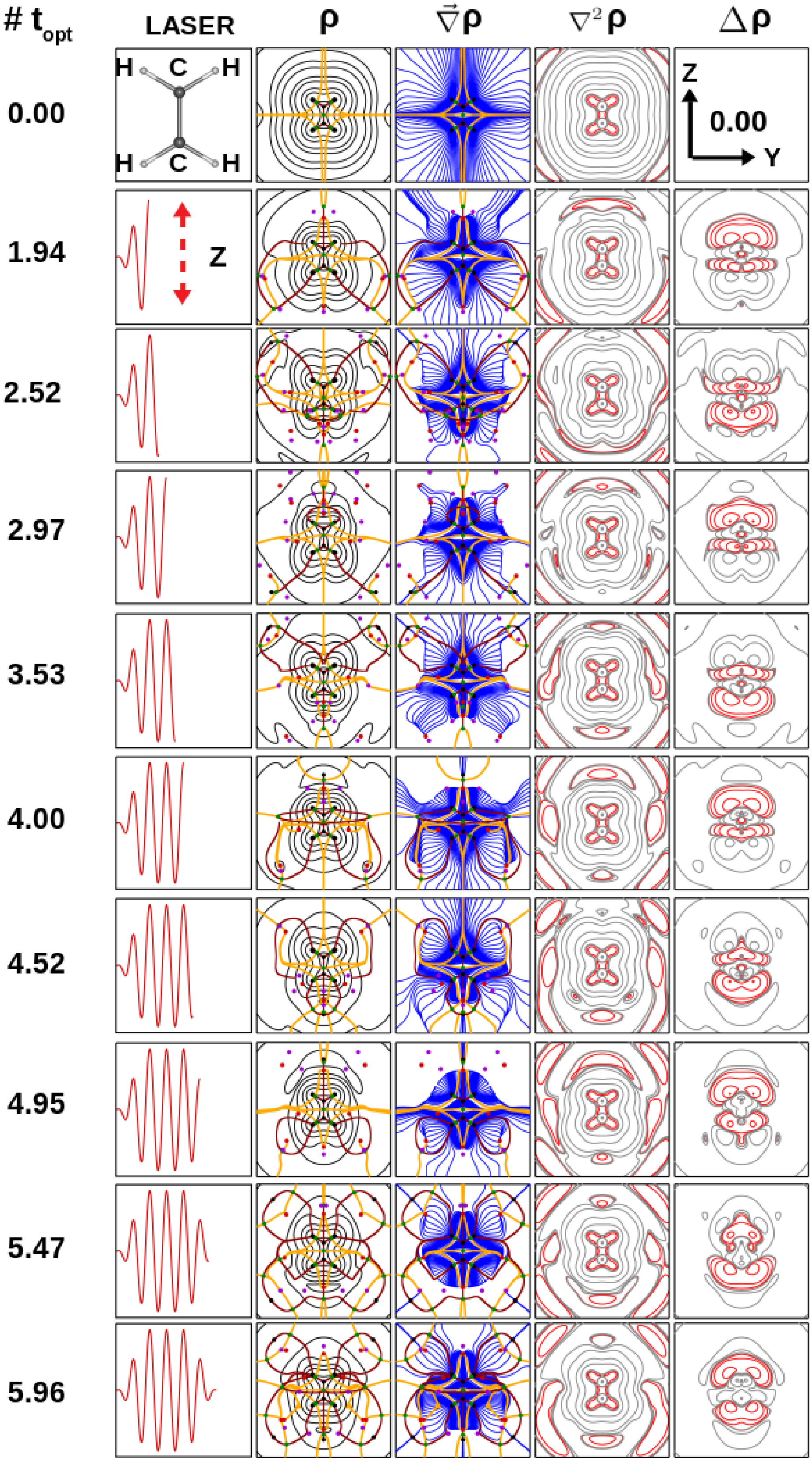

Figure 4.8: TDMED and its properties for ten time steps of Ethylene molecule in Z-polarized laser, parallel to $C - C$ bond. Details described in Chapter 4.

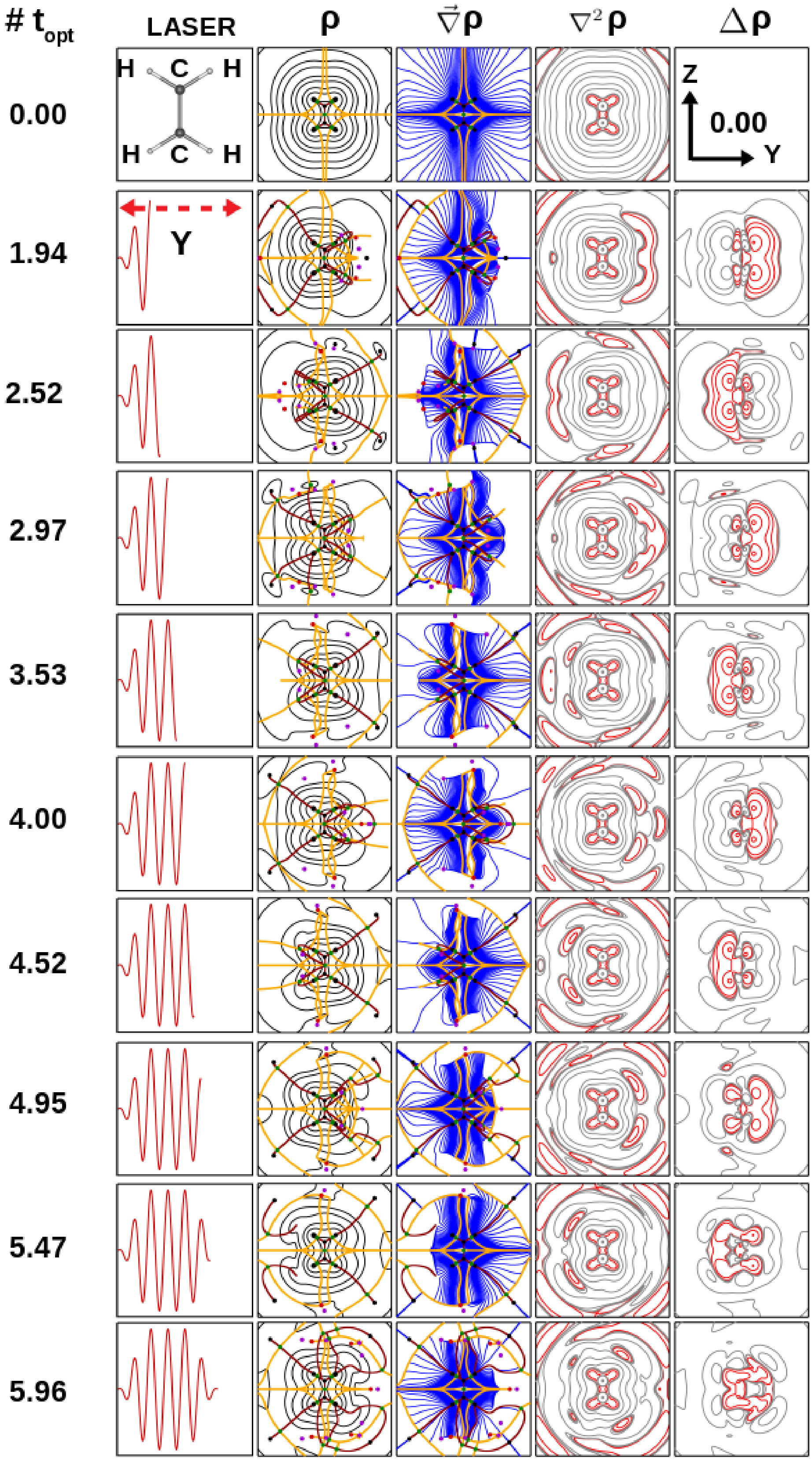

Figure 4.9: TDMED and its properties for ten time steps of Ethylene molecule in Z-polarized laser, perpendicular to $C - C$ bond. Details described in Chapter 4.